

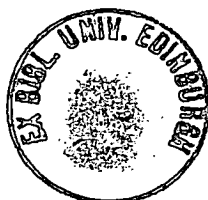
**THE OPTICAL CHARACTERISATION AND
KINETICS OF Ag PHOTODISSOLUTION
IN AMORPHOUS As-S FILMS.**

by
A. Zekak

**A thesis presented for the degree of Doctor of Philosophy
University of Edinburgh**

Department of Electrical Engineering

August 1993



DECLARATION

This work has been composed entirely by myself except where indicated otherwise and has not been submitted for any other degree.

ACKNOWLEDGEMENTS

The author wishes to express his gratitude to Dr. P.J.S. Ewen, Professor A.E. Owen, Dr. C.W. Slinger and Dr. A.P. Firth for their continuous help and encouragement throughout this project.

I would like to thank Gerry McDade and Paul Roger for their technical assistance and J. Craven of the Department of Geology for help with the SIMS measurements.

I am grateful to the Algerian Ministry of Higher Education for a studentship.

Finally, I would like to thank my family for their support and encouragement during the project.

ABSTRACT

The present work is concerned with a fundamental study of the metal photodissolution effect in chalcogenide glasses and in particular of those aspects which are relevant to one of the main application areas, the fabrication of diffractive optical elements for operation in the infrared. This study has dealt exclusively with glasses in the As-S system and has used mainly Ag as the source for photodoping.

The optical constants of undoped and photodoped As-S films of various compositions have been measured over a wide wavelength range. Pre-annealing the undoped As-S films produced an overall increase of about 3% in the refractive index, n , from the visible to the far-infrared region. The magnitude of the pre-annealing effect was found to increase with increasing As content, being most pronounced at $\text{As}_{40}\text{S}_{60}$. The maximum overall increase in n produced by photodoping was 20%. The single oscillator and dispersion energies, E_o and E_d , were obtained by fitting the measured dispersion relations using the Wemple-Didomenico model. The optical gap and E_o were found to decrease and E_d and the refractive index to increase with increasing Ag content. Regarding the dependence on As-S composition, for the most heavily Ag-doped films, n , E_o and E_d all exhibited a peak at ~ 30 at.% As but the change in the optical gap was similar to that of the undoped films.

The time dependence of the process was examined and found to be definitely linear for the conditions used. It was also found that the photodissolution process does not stop when the Ag is exhausted. Pre-annealing was found to decrease the rate of Ag photodissolution for all the As-S compositions investigated. The temperature dependence of the photodissolution rate was studied and the rate at 393 K was found to be a factor of 12 faster than at room temperature. Thermal dissolution was negligible at these elevated temperatures, which enabled a grating pattern to be fabricated at 383 K using the

photodissolution process. The rate was found to have a sublinear dependence on light intensity. Regarding the dependence on As-S composition, the maximum rate is obtained at $As_{30}S_{70}$ for both annealed and as-deposited films. The weak activation energy and linear time dependence observed suggest that the photodissolution process is a solid state chemical reaction and not a straightforward diffusion process. The results also emphasise the importance of both the doped/undoped and Ag/doped interfaces in the metal photodissolution process.

Secondary ion mass spectroscopy (SIMS) was used to probe the Ag distribution in the photodoped layer and showed that it had a uniform depth profile. The decrease in the Ag layer thickness at the surface of the double layer sample was found to have a linear time dependence.

Table of Contents

DECLARATION	1
ACKNOWLEDGEMENTS	2
ABSTRACT	3
CONTENTS	5
Chapter 1: INTRODUCTION	12
1.1 Introduction	12
1.2 The metal-photodissolution effect	13
1.3 Aims of the present work	14
1.3.1 Optical constants of undoped and photodoped As-S films	15
1.3.2 Kinetics of the Ag-photodissolution process in the As-S system	16
1.3.3 Secondary ion mass spectroscopy analysis	17
1.4 Organisation of the thesis	18
References	18
Chapter 2: PHOTO-INDUCED EFFECTS IN CHALCOGENIDE GLASSES	21
2.1 Introduction	21
2.2 The structure of As-S glasses	22

2.3 Irreversible photo-induced changes	23
2.3.1 Irreversible structural changes	24
2.3.2 Irreversible optical changes	25
2.4 Reversible photo-induced changes	29
2.4.1 Reversible optical changes (photodarkening)	29
2.4.2 Experimental evidence for the reversible photostructural changes	35
2.4.2.1 The direct experimental evidence	35
2.4.2.2 The Indirect experimental evidence	36
References	37
Chapter 3: PHOTO-INDUCED PHYSICO-CHEMICAL CHANGES IN CHALCOGENIDE GLASSES	43
3.1 Introduction	43
3.2 The photochemical effect	43
3.3 The metal-photodissolution effect	44
3.3.1 Photodissolution kinetics	45
3.3.1.1 The electrical method	46
3.3.1.2 Optical methods	47
3.3.1.3 Chemical methods	48
3.3.1.4 Other methods	49
3.3.2 Properties of the metal-photodoped material	49
3.3.2.1 Ag distribution after photodissolution	51
3.3.2.2 Chemical and structural properties	52
3.3.2.3 Electrical properties	54

3.3.2.4 Optical properties	54
3.3.3 Photodissolution models	55
3.3.3.1 Absorption in the undoped layer	55
3.3.3.2 Absorption in the metal	58
3.3.3.3 Absorption at the undoped/photodoped interface	58
3.4 Summary	61
References	62
Chapter 4: KINETICS OF THE PHOTODISSOLUTION PROCESS	68
4.1 Introduction	68
4.2 Chalcogenide photoresists	69
4.3 Fabrication of IR optical elements	71
4.4 Factors influencing the photodissolution rate	72
4.4.1 Composition dependence	73
4.4.2 Spectral dependence	74
4.4.3 Intensity dependence	77
4.4.4 The dependence on pre-history	78
4.4.5 Dependence on the metal-ion source	80
4.4.6 The effect of an applied electric field	82
4.4.7 The effect of temperature	83
4.4.8 The dependence on substrate material	84
4.4.9 The dependence on structure	84
4.5 Conclusions	85
References	86

Chapter 5: EXPERIMENTAL TECHNIQUES	91
5.1 Introduction	91
5.2 Sample preparation	92
5.2.1 Substrates	92
5.2.2 Film preparation	92
5.3 Film thickness measurement	94
5.4 Annealing pre-treatment	95
5.5 Kinetics measurements	95
5.6 Optical constant measurements	97
5.7 SIMS measurements	98
References	99
Chapter 6: OPTICAL CONSTANTS OF UNDOPED AND PHOTODOPED As-S FILMS	101
6.1 Introduction	101
6.2 Calculation of the refractive index	102
6.2.1 Refractive index of undoped and Ag-photodoped $As_{40}S_{60}$	104
6.2.2 Compositional trend of the refractive index in As-S and Ag-photodoped films	107
6.3 Optical absorption	110
6.3.1 Optical absorption coefficient of undoped and Ag-photodoped $As_{40}S_{60}$	111
6.3.2 Compositional trend of optical absorption in As-S and Ag-photodoped films	113

6.4 Dispersion and single oscillator energies	116
6.4.1 Dispersion and single oscillator energies of undoped and Ag-photodoped $As_{40}S_{60}$	116
6.4.2 Effect of composition on the dispersion and single oscillator energies in As-S and Ag-photodoped films	117
6.5 Summary	118
References	119
Chapter 7: KINETICS OF THE Ag-PHOTODISSOLUTION PROCESS IN THE As-S SYSTEM	123
7.1 Introduction	123
7.2 Experimental arrangement	124
7.3 Rate of Ag-photodissolution in $As_{40}S_{60}$ films	125
7.3.1 The effect of pre-annealing	125
7.3.2 The effect of temperature	126
7.3.3 The effect of light intensity	130
7.3.4 The effect of Cu as the metal ion source	131
7.4 Compositional dependence of the Ag-photodissolution rate	134
7.4.1 The effect of pre-annealing	134
7.4.2 The effect of temperature	135
7.5 Characteristics of the Ag-photodissolution process	135
7.6 The mechanism of the photodissolution process	138
7.7 Conclusions	139
References	140

Chapter 8: SECONDARY ION MASS SPECTROSCOPY ANALYSIS OF PHOTODOPED As-S FILMS	143
8.1 Introduction	143
8.2 The SIMS technique	144
8.3 Experimental procedure	145
8.4 Quantitative analysis of SIMS data	145
8.5 Ag depth profile in the photodoped layer	147
8.6 Time development of the Ag depth profile	148
8.7 Comparison of the SIMS and optical reflectivity kinetics results	150
8.8 Conclusions	151
References	152
Chapter 9: CONCLUSIONS AND SUGGESTIONS FOR FURTHER WORK	153
9.1 Introduction	153
9.2 Optical constants of undoped and photodoped As-S films	154
9.3 Kinetics of the Ag-photodissolution process in the As-S system	156
9.4 Secondary ion mass spectroscopy analysis	160
9.5 Suggestions for further work	161
9.5.1 Kinetics measurements	162
9.5.2 Sensitivity	162
9.5.3 Photoconductivity of the photodoped layer	163
9.5.4 Ag distribution in the photodoped layer	164
9.6 Summary	164

References	165
APPENDIX	168
LIST OF PUBLISHED WORKS	168

CHAPTER 1

INTRODUCTION

1.1. Introduction

Amorphous solids are characterised by the fact that, although structurally rigid, they possess no long-range order, as a result of which their optical, electrical and structural properties are generally "smeared out" in contrast to those of their crystalline counterparts. Additionally, from a thermodynamic point of view, an amorphous solid is in a non-equilibrium state, therefore, its structure and bond configuration are not fixed but can be altered, sometimes reversibly, not only by thermal treatment but also by light irradiation. This fundamental difference in the thermodynamics of amorphous and crystalline solids gives rise to many interesting properties and effects in amorphous materials.

Chalcogenide glasses are one of the most widely known families of amorphous materials and have been extensively studied over the past three decades, partly because of their fundamental properties and partly because of their applications. The chalcogenides are so called because they contain one or more of the chalcogen elements S, Se or Te. These elements can be combined with many others, for example As, Sb, P, Si and Ge, to form a wide variety of glass-forming systems, ranging from simple binary combinations to more complex multi-component systems such as As-Te-Ge-S-P. The As-S, As-Se and Ge-Se systems are among the most widely studied of the binary combinations and include the well-known compound glasses As_2S_3 , As_2Se_3 and $GeSe_2$. The chalcogenide glasses are relatively easy to prepare in either bulk or thin-film form.¹⁻⁴

The most important applications of chalcogenide glasses are currently in the field of optics and arise particularly from either their infra-red-transmitting properties or the many photo-induced effects they exhibit. These photo-induced effects range from reversible optical changes (e.g. photodarkening and photobleaching) caused by small changes in atomic rearrangements to more substantial modifications which completely change the physical and chemical nature of the material (e.g. photopolymerisation, photocrystallisation, photodissolution of metals etc.). The chalcogenide glasses have potential uses in many areas including integrated optics, optical imaging, holography, very large scale integration (VLSI) lithography, optical data storage, and infrared optics.

1.2. The metal-photodissolution effect

Of the various light-induced changes exhibited by chalcogenide glasses, the metal-photodissolution effect is probably the most important as far as applications are concerned because it produces the largest change in the properties of the chalcogenide, particularly the etch resistance and the refractive index. This effect, which is known also as "photodiffusion", "photodoping" or "photodissolution", occurs when a chalcogenide layer in contact with a metal layer is illuminated and is illustrated schematically in figure 1.1. In this effect metal ions dissolve into the glass and migrate through it in the direction of illumination, thereby altering the composition and structure of the glass and changing its physical properties, particularly its solubility and optical constants. The metal-photodissolution effect has been observed in many chalcogenide systems, e.g. As-S, As-Se, Ge-Se, As-S-Te and As-Se-Te glasses, and a variety of metals, metal compounds and alloys have been used as the metal-ion source, e.g. Ag, Cu, Zn, Ag₂S, Ag₂Se and alloys in the Ag-Cu system. Most investigations of this effect have been carried out on As-based chalcogenides or on Ge-Se glasses, using Ag metal as the source for photodoping.

ILLUMINATION

REFLECTED
LIGHT

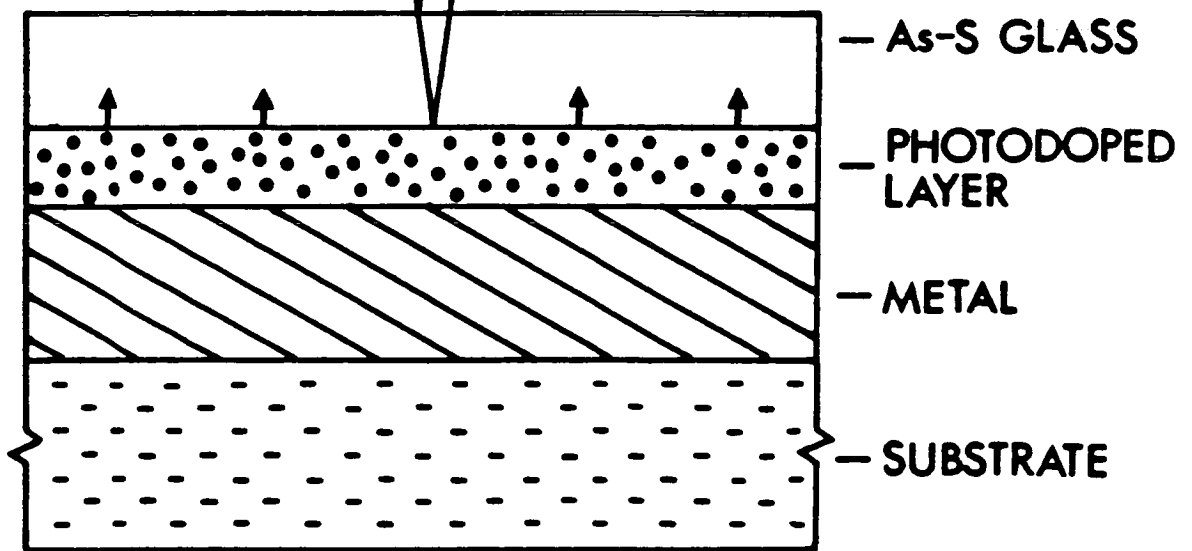


Figure 1.1. A schematic cross section through a sample during the photodissolution process.

Although the metal-photodissolution effect has been under investigation for over two decades, no completely satisfactory mechanism has been put forward. In addition, there are many inconsistencies in the experimental results reported in the literature. This is partly due to the variety of experimental techniques used and material systems examined, and partly due to the complexity of the effect and its dependence on many variables, such as light intensity and wavelength, temperature, chalcogenide composition, and film deposition conditions. For example, an important question is where is the light which effectively stimulates photodissolution absorbed? The conclusions in the literature differ considerably. Some investigators suggested that the actinic light is absorbed in the metal layer stimulating a solid-state chemical reaction⁵ or photoemission of electrons from the metal into the chalcogenide glass.^{6, 7} A number of experimental studies based on different techniques point to the active role of light absorbed in the doped region,^{8, 9} or near the interface between the doped and undoped glass.¹⁰⁻¹³ The range of different results obtained is reflected in a variety of models proposed for the effect. These models will be described in Chapter 3.

There is a need to reconcile these inconsistencies and to develop an accurate and comprehensive model of the process, not only for fundamental reasons, but also because the details of the mechanism are crucial to many of the applications. For example, the exposure time required in holographic or lithographic applications will be governed by the photodissolution kinetics.

1.3. Aims of the present work

The present work is concerned mainly with a fundamental study of the photodissolution effect and in particular of those aspects which are relevant to one of the application areas, namely the fabrication of diffractive optical elements operating in the infrared. The chalcogenide system chosen for investigation was the As-S system and

Ag was selected as the metal source for photodoping. These materials were chosen because they are the most widely studied, although despite extensive investigations, the photodissolution of Ag into As-S glasses is not fully understood. This work addresses three main areas: measurement of the optical constants of the Ag-photodoped and undoped As-S films; the kinetics of the photodissolution process; and finally the Ag depth profile in Ag-photodoped As-S films.

1.3.1. Optical constants of undoped and photodoped As-S films

A knowledge of the optical constants (absorption coefficient and refractive index) of both Ag-photodoped and undoped As-S films is important for both fundamental reasons and from the point of view of applications. In particular, it is necessary for measuring the kinetics of the photodissolution process using optical techniques and for detailed modelling of grating performance. It should also be noted that the characterisation of the photodissolution effect is mainly based on measurement of the changes that occur in the optical constants of the materials during illumination.

Although many reports have been published on the optical properties of the As-S system very few have investigated the effect of pre-treatment¹⁴⁻¹⁶ (e.g. pre-annealing) and Ag photodoping^{17, 18} on the optical characteristics of As-S films. In addition, these studies were either limited to one As-S composition (e.g. As₄₀S₆₀) or to a single wavelength. Because chalcogenide diffractive elements may have applications throughout the IR, particularly in either of the commonly used IR spectral bands (3-5 μm and 8-12 μm), it is important to obtain information on their optical properties over a wide range of wavelengths.

The effect of annealing on the optical and structural properties of as-deposited films was investigated by Deneufville et al.¹⁹ and Apling et al.^{20, 21} using diffraction techniques, and by Solin et al.²² using

Raman scattering. The general conclusion which can be drawn from the work of these authors is that the annealing of an as-deposited film near the glass transition temperature, T_g , causes a structural compaction and densification. This is due to the fact that the as-deposited film consists of molecules of the vapour species (particularly As_4S_4) embedded in a continuous random network, and annealing allows the molecular component to polymerise and combine with the original network to form a structure similar to that of the bulk glass. Deneufville reported²³ that the refractive index of an annealed film ($n= 2.51$) is approximately equal to that of the bulk material ($n= 2.528$). Annealed films may have advantages over as-deposited films as far as grating fabrication is concerned since they should have better adhesion to the substrate and should produce elements which are more stable under illumination. They will also yield a more controllable fabrication process. Pre-annealing is also known to affect the Ag-photodissolution rate and a knowledge of the optical constants of annealed As-S films is therefore needed for the analysis of photodissolution kinetics in such films and for modelling the performance of gratings made in annealed films.

The purpose of the optical constants study is therefore to extend this investigation over a wider wavelength range (from the visible to the far-IR region) and a wider range of As-S compositions. The effect of pre-annealing and Ag-photodoping on the optical properties of As-S films will be examined and in particular the extent to which they are affected by the amount of Ag introduced during photodoping.

1.3.2. Kinetics of the Ag-photodissolution process in the As-S system

A knowledge of the kinetics of the photodissolution process is essential both to understanding the mechanism of the effect and to exploiting its application, since the speed of image formation in the Ag/As-S system is mainly governed by the photodissolution rate. The photodissolution is influenced by many factors as will be reviewed in

Chapter 4. An attempt has been made to use some of these factors to speed up the image formation in the Ag/As-S system and has resulted in a significant improvement in the rate.

The kinetics study therefore focusses on the investigation of those factors which are most effective in improving the rate. Temperature, pre-annealing treatment, Ag film thickness, light intensity, metal source and As-S composition are the factors which have been investigated in order to increase the rate above that found by previous authors. The kinetics of the thermal dissolution of Ag in $\text{As}_{40}\text{S}_{60}$ films has also been investigated. In addition, the results of these experiments have been used to elucidate the nature of the Ag-photodissolution process in the As-S system.

1.3.3. Secondary ion mass spectroscopy analysis

Another aspect of the process which is important, both for fundamental reasons and as far as applications are concerned, is the distribution of Ag with depth into the photodoped film. In the case of grating applications, any change in Ag concentration with depth will be accompanied by a change in the refractive index and hence in the modulation. Therefore an investigation of the depth profile of the Ag photodissolved in the As-S structure, using the Secondary Ion Mass Spectroscopy (SIMS) technique, has been carried out in this work. The previous depth profile studies of the Ag/ $\text{As}_{40}\text{S}_{60}$ system^{24, 25} have revealed a step-like profile while in systems like $\text{Ag}_2\text{Se}/\text{GeSe}_2$ and $\text{Ag}_2\text{Se}/\text{GeSe}_9$, where the Ag is initially present as a compound, the Ag distribution is more like that expected from thermal diffusion.²⁶

The SIMS method has been shown by Polasko and co-workers²⁷ to provide useful information about Ag profiles in Ge-Se glasses. In the present study, information obtained from the SIMS method on two aspects of the photodissolution process will be reported: the nature of the Ag depth profile within the photodoped layer and the effect of

exposure time on the Ag depth profile. The latter will be compared to corresponding results obtained from an optical reflectivity technique.

1.4. Organisation of the thesis

Following this introductory chapter a review of previous work on photo-induced phenomena in chalcogenides and the photo-dissolution effect is presented in Chapters 2, 3 and 4. A description of the experimental methods employed in this study is then given in Chapter 5. The next three chapters present the results obtained in this work. The optical constants of undoped and Ag-photodoped As-S films are reported in Chapter 6, while, the results relating to the kinetics of the Ag-photodissolution process in the As-S system are described in Chapter 7. The secondary ion mass spectroscopy analysis of the Ag depth profile in the Ag photodoped films is presented in Chapter 8. Finally, the conclusions arrived at through this work and suggestions for future work are given in Chapter 9.

References

1. Elliot S.R., *Physics of Amorphous Solids*, 2nd edition, Longman, London, 1988.
2. Mott N.F. and Davies E.A., *Electronic processes in Non-Crystalline Materials*, Clarendon Press, 2nd edition, Oxford, 1979.
3. Madan A and Shaw M.P., *The Physics and Applications of Amorphous Semi-conductors*, Academic Press, Sandiego. CA, USA, 1988.
4. Zallen R., in *The Physics of Amorphous Solids*, ed. John Wiley, NY, USA, 1983.

5. Janai M., *Phys. Rev. Lett.*, vol. 47, p. 726, 1981.
6. Kostyshin M.T. and Minko V.I., *Fiz. Tekh. Poluprov.*, vol. 13, p. 809, 1979.
7. Lis S.A. and Lavine J.M., *Appl. Phys. Lett.*, vol. 42, p. 675, 1983.
8. Yamaguchi M., Shimizu I. and Inoue E., *J. Non-Cryst. Solids*, vol. 47, p. 341, 1982.
9. Kostyshin M.T., Kasyarum O.P. and Kudryavtsev A.A., *Ukrain. Fiz. Zh.*, vol. 29, p. 981, 1984.
10. Rennie J.H.S. and Elliot S.R., *J. Non-Cryst. Solids*, vol. 97/98, p. 1231, 1987.
11. Leung W., Cheung N. and Neureuther A.R., *Appl. Phys. Lett.*, vol. 46, p. 543, 1985.
12. Ewen P.J.S., Firth A.P., Zakery A. and Owen A.E., *J Non-Cryst Solids*, vol. 97/98, p. 1127, 1987.
13. Owen A.E., Firth A.P. and Ewen P.J.S., *Phil. Mag.*, vol. B52, p. 347, 1985.
14. Matsuda A. and Kikuchi M., *Proc. 4th Conf. on Solid State Devices (Suppl. to J. Japan Soc. of Appl. Phys. Vol.42 p.239 1973)*, Tokyo, 1972.
15. Yaji T. and Kurita S., *J. Appl. Phys.*, vol. 54, p. 647, 1983.
16. Chatani K., Shimizu I., Kokado H. and Inoue E., *Jap. J. Appl. Phys.*, vol. 16, p. 389, 1977.
17. Ewen P.J.S., Zakery A., Firth A.P. and Owen A.E., *Phil. Mag. B*, vol. 57, p. 1, 1988.
18. Zakery A., Zekak A., Ewen P.J.S., Slinger C.W. and Owen A.E., *J Non-Cryst Solids*, vol. 114, p. 109, 1989.

19. DeNeufville J.P., Moss S.C. and Ovschinsky S.R., *J. Non-Cryst. Solids*, vol. 13, p. 191, 1974.
20. Apling A.J., Leadbetter A.J. and Wright A.C., *J. Non-Cryst. Solids*, vol. 23, p. 369, 1977.
21. Leadbetter A.J., Apling A.J. and Daniel M.E., *J. Non-Cryst Solids*, vol. 21, p. 47, 1976.
22. Solin S.A. and Papatheodorou G.N., *Phys. Rev. B*, vol. 15, p. 2084, 1979.
23. DeNeufville J.P., Seguin R., Moss, S.C. and Ovshinsky S.R., *Proc. 5th Int. Conf. on Amorp. and Liquid. Semicond.*, p. 737, Garmish-Partenkirchen, Taylor and Francis, London, 1973.
24. Yamamoto Y., Itoh T., Hirose Y. and Hirose H., *J. Appl. Phys.*, vol. 47, p. 3603, 1976.
25. Goldschmidt D., Bernstein T. and Rudman P.S., *Phys. Stat. Sol. A*, vol. 41, p. 283, 1977.
26. Wagner A. and Barr D., *Proc. Electrochem. Soc.*, vol. 82, p. 281, Symp. Inorg. Resist. Syst., 1982.
27. Polasko K.J., Tsai C.C., Cagan M.R. and Pease R.F.W., *J. Vac. Sci. Technol.*, vol. B4, p. 418, 1986.

CHAPTER 2

PHOTOINDUCED EFFECTS IN CHALCOGENIDE GLASSES

2.1. Introduction

Photo-induced optical and structural changes have been observed in numerous chalcogenide glasses including a-Se, a-As₄₀S₆₀, a-As₂S₂Se₃, a-GeSe₂, and a-GeS₂. The key elements of these glasses, as far as photo-induced effects are concerned, are the chalcogen atoms,¹ S and Se. The photo-induced effects exhibited by As-S glasses are typical of those occurring in chalcogenides generally, and as this project is mainly concerned with the As-S system, the discussion will focus on these glasses.

This chapter gives an overview of photo-induced effects observed in both evaporated (or sputtered) thin films and melt quenched bulk glasses.²⁻⁴ These effects, which are induced by band-gap or above band-gap illumination are phenomenologically separated into two different categories, one being an irreversible photostructural change involving photopolymerisation, the other a reversible photostructural change accompanying a shift in the optical absorption edge (so called photodarkening). The latter is reversible in the sense that the initial state can be restored by thermal annealing near the glass transition temperature. The structure of the As-S glasses will be described briefly before proceeding to the details of these light-induced phenomena.

2.2. The Structure of As-S glasses

The glass forming region^{5, 6} in the As-S system extends approximately from As_5S_{95} to $\text{As}_{43}\text{S}_{57}$. It has been shown by several workers, e.g. Ewen,⁷ that the short-range order in stoichiometric $\text{As}_{40}\text{S}_{60}$ is similar to that in the corresponding crystal. This indicates that it has a network structure composed of AsS_3 pyramid units linked by As_2S bridges. Crystalline $\text{As}_{40}\text{S}_{60}$ has a monoclinic structure formed by 3-fold coordinated As and 2-fold coordinated S atoms.⁸ It involves two essentially different kinds of chemical bonds: strong covalent bonding between the As and S atoms and weak van-der-Waals-like bonding between layers. The nearest-neighbour coordination associated with the covalent bonds is essentially retained even in the disordered network of $\text{As}_{40}\text{S}_{60}$ glass, as confirmed by X-ray diffraction,⁹ Raman scattering¹⁰ and nuclear quadrupole resonance studies.¹¹

In contrast to the nearest-neighbour ordering there is less information on the second or third nearest-neighbour configurations. However, it is known that the absence of long-range order produces in the glassy network a small number of homopolar bonds, such as As-As or S-S bonds in the As-S glasses and at the same time, a much lower concentration ($10^{17} - 10^{18}/\text{cm}^3$) of bonding defects such as C_3^+ and C_1^- † centres.¹²⁻¹⁵ A characteristic feature of chalcogenide glasses is the electronic structure originating in the p-like lone pair electrons of the chalcogen atoms. A S atom has four outer p electrons, two of which form two covalent bonds (As-S bonds) with p electrons from neighbouring As atoms while the remaining two are localised on the chalcogen atoms as lone-pair electrons. It should be noted that there is essentially no difference in the basic band structure between crystalline and glassy $\text{As}_{40}\text{S}_{60}$. The top of the valence band is formed out of the lone-pair (LP) non-bonding p-states and the two bonding (σ) p-states are associated with defects: the valence-alternation-pair (C_3^+ and C_1^-) proposed by Kastner, Adler and Fritsche¹⁴ or charged dangling bonds (in terms of D^+ and D^-) suggested by Street and Mott.¹³

† C_3^+ is a S atom with 3 bonds and a positive charge. C_1^- is a S atom with 1 bond and a negative charge.

In the S-rich As-S glasses, for compositions with S content between 60 and 65 atomic% the extra S atoms were found to form non-planar As-S-S-As bridges and S₈ rings were also found in compositions more S-rich than As₃₇S₆₃. The As-As bonds in the As-S network were found to disappear rapidly as the S content is increased above 60 atomic%. As-S glasses more As-rich than As₄₃S₅₇ were found to consist of a glassy matrix into which crystallites of β-As₄S₄ were embedded. The glassy matrix had the same network structure as As₄₀S₆₀ glass, but there were no S-S bonds present, only As-As.

2.3. Irreversible photo-induced changes

Photo-induced changes are irreversible if, after illumination, the initial structural state cannot be regained by any simple combination of annealing or further illumination. For example, when As₄₀S₆₀ films are formed by thermal evaporation, their structure contains molecules of the predominant vapour species, which have been found to be^{16, 17} As₄S₃, As₄S₄ and S₂. As the film forms at room temperature it consists of molecular units, mainly bonded together by weak van-der-Waals forces. Illumination (or thermal annealing) of the film causes polymerisation of these molecular units, and its structure and optical properties are irreversibly changed, becoming similar to those of well-annealed films or bulk glassy samples.

2.3.1. Irreversible structural changes

Photostructural and thermostructural changes in $\text{As}_{40}\text{S}_{60}$ and As_2Se_3 have been studied by Deneufville et al.¹⁸ using X-ray diffraction, electron microscopy and optical techniques. They reported that the irreversible thermostructural and photostructural changes involved a kind of atomic rearrangement and suggested that a freshly evaporated film of $\text{As}_{40}\text{S}_{60}$ is composed of hard spheres of As_4S_6 molecules which when heated or illuminated undergo polymerization to form a structure characteristic of the bulk glass. This photo-induced irreversible process also involves volume contraction^{19, 20} and changes in UPS (ultra-high vacuum photoelectron spectroscopy) spectra²¹

Raman scattering and NQR (nuclear quadrupole resonance) results have given more detailed information on the structure of as-deposited $\text{As}_{40}\text{S}_{60}$ films. Solin and Papatheoderou¹⁷ studied the irreversible thermostructural transformation in $\text{As}_{40}\text{S}_{60}$ using the Raman scattering technique. The polarised spectra of as-deposited films consisted of several sharp molecular bands superimposed on a network-like continuum. Most of these sharp bands disappeared on annealing. The spectra from the annealed specimen, however, did not match the bulk glass spectra. They concluded that the photostructural and thermostructural transformation results from a polymerization of a partially cross-linked molecular glass as proposed by DeNeufville et al.¹⁸ Raman scattering results for the as-deposited, annealed, and bulk-glass forms of $\text{As}_{40}\text{S}_{60}$ have also been reported by Nemanich and co-workers.²² These results indicated that, after annealing just below the glass transition temperature, a gross structural change takes place. This irreversible change can also be partially induced by band-gap illumination. The results suggested the presence of As_4S_4 molecules in the as-deposited films.

Treacy and co-workers have carried out NQR studies of these phenomena.²³ According to their interpretation, $\text{As}_{40}\text{S}_{60}$ deposited on substrates at 300 K possesses AsS_3 pyramidal units, in addition to As_4S_4 molecular units, which lack the local two-dimensional order present in bulk $\text{As}_{40}\text{S}_{60}$. Therefore, it has been tentatively speculated

that irreversible photo-induced structural changes tend to produce an order similar to that which occurs in the bulk glass.

As₅₀Se₅₀ exhibits pronounced photo-induced changes. Recently, Elliot and Kolobov²⁴ showed in an EXAFS study of annealed and illuminated As₅₀Se₅₀ films, that the local structural changes within the first coordination sphere were relatively insignificant and the structure of an as-evaporated film, on annealing, does not approach that of the bulk glass, in contrast to the situation in As₄₀S₆₀. The authors stated that these photo-induced changes can be explained in terms of an increase in the bond angle subtended at the Se atom and in its fluctuation. They estimated the increase in the bond angle to be $\sim 10^\circ$, which is about twice that observed in As₄₀S₆₀.²⁵ This could be the main factor responsible for the fact that the structure of As₅₀Se₅₀ films, on annealing, does not approach that of the bulk glass.

2.3.2. Irreversible optical changes

The irreversible structural changes described above are always accompanied by optical changes, such as an increase in the refractive index and a red-shift of the optical absorption edge.^{1, 19} These changes are still not well understood. Deneufville et al.¹⁸ reported an irreversible increase in the refractive index of evaporated films with annealing at the glass transition temperature, T_g , or with band-gap illumination. Tanaka and Ohtsuka²⁶ studied photo-induced changes in the refractive index and thickness in evaporated As₄₀S₆₀ films by means of a prism coupling technique. The irreversible transformation was associated with an increase in refractive index of 0.113. They provided no structural interpretation to account for the increase in the refractive index.

Asahara and Izumitani²⁷ studied thermal relaxation processes in amorphous As-Se films. The transmission of as-deposited films increased and reached a certain maximum value in the visible region of

the spectrum. The transmission was also affected by heat treatment. As a result of heating at 175 °C over 50 min the optical gap increased from 1.67 to 1.80 eV. The change in the optical gap decreased with a decrease in the heat-treatment temperature. They explained the increase of transmission on the basis of structural relaxation. A high-temperature structure is considered to be frozen in the films during deposition. If these films are kept at a certain annealing temperature, the film structure will approach a certain stable glass structure. When annealed at high temperature, but below the glass transition temperature, the thermal energy is large enough to stabilize the high-temperature structure; while upon annealing at a temperature far below the glass transition temperature, the high-temperature structure tends to remain in the films. The kinetics studies revealed that the relaxation consisted of two first-order processes: the first is a rapid relaxation during the initial 5 minutes of heat treatment and was attributed to the disappearance of some structural defects, and the second is a slow relaxation which follows the first. The activation energies for the rapid and slow relaxations were 0.7 kcal mol⁻¹ and 9.2 kcal mol⁻¹ respectively. Kumar and White²⁸ studied the thermal ageing phenomenon in thin As₄₀S₆₀ thin films and their kinetics studies showed similar results to previous investigations.²⁷ They found that the rate of relaxation increases as the heat treatment temperature approaches the glass transition temperature. As a result of thermal ageing, there was a refractive index increase in the infra-red region of about 4%. They explained this increase on the basis of structural compaction. The inter-atomic distance will decrease and densification will occur during the ageing process.

Tanaka and Ohtsuka²⁹ investigated the compositional variation of the changes in the refractive index and in attenuation coefficients under illumination and on annealing for compositions between As₁₀S₉₀ and As₄₃S₅₇. Annealing was carried out in a slowly flowing stream of argon for 1 hr and at a temperature slightly below the glass transition temperature of the specimen. The films were illuminated in air at room temperature using an ultrahigh pressure 100 W Hg lamp with an infrared cut-off filter. The light intensity was of the order of 10² mW cm⁻². It had been previously reported^{1, 19} that an annealing treatment of As₄₀S₆₀ at about the glass transition temperature

determines the structural and optical properties of the films irrespective of their previous history. The results of Tanaka and Ohtsuka however, clearly indicated that this statement is only applicable to the composition $\text{As}_{40}\text{S}_{60}$ and not to others. They showed that generally the attenuation coefficient at 435 nm of annealed films and of annealed illuminated films are different, the magnitude of the attenuation coefficient for annealed illuminated films being slightly greater. They also showed that the changes between the illuminated annealed and the illuminated states are reversible on illumination and annealing for all the compositions. In addition, the irreversible changes have an anomalous minimum at the composition $\text{As}_{25}\text{S}_{75}$. Furthermore, the magnitude of the reversible change is about one-third of that of the irreversible change, but the time constant of the former is about twice as large as that of the latter. In qualitative agreement with the As-Se system,^{30, 31} the authors reported that the irreversible change for As-rich films is greater than that for $\text{As}_{40}\text{S}_{60}$. However the reversible change has a peak at $\text{As}_{40}\text{S}_{60}$. They explained this on the basis that evaporated films contain, in addition to As_4S_6 molecules, As_4S_4 molecules which can be polymerised by band gap illumination in chalcogen-deficient compositions. Furthermore, for the annealed illuminated specimens they interpreted the peak in terms of a decrease of the relative number of lone-pair electrons with decreasing S content in As-rich films. In the case of specimens with excess chalcogen, they speculated that these changes in optical properties depend mainly on transformation of As-S and S-S bonds. S-S bonds are transformed only on illumination, whereas As-S bonds are polymerised both on illumination and on annealing at slightly below the glass transition temperature.

Later, Tanaka and Ohtsuka³² also investigated photo-induced refractive index changes in $\text{As}_x\text{S}_{100-x}$ films as a function of composition in the range $15 \leq x \leq 45$. In contrast to their previous results,²⁹ the irreversible changes showed a maximum at $x = 40$, and they also noted that there are broad shoulders around $x = 20$ in both the irreversible and reversible changes. The behaviour of chalcogen-rich films was explained on the assumption that for these compositions some of the As atoms are included in molecular-like S_n rings and/or chains so that the number of As_4S_6 molecules is reduced in the

evaporated films.

Tanaka and Kikuchi have reported photobleaching in flash-evaporated $\text{As}_{57}\text{S}_{43}$ films^{33, 34} prepared at 80 nm/s. In this case the optical absorption edge of the sample is shifted towards shorter wavelengths after exposure to band-gap light and the initial state is never restored. In contrast to their interpretation of their results³⁵ for 77 K, they speculated that as the thermal energy kT carried by each atom is larger at room temperature than at 77 K, it may exceed some critical barrier for liberating the bonded As atoms from the network. The liberated As atoms can diffuse freely through the film and join with each other in clusters to form small As crystals. During the course of formation of these crystals the remaining network becomes relatively S rich, which is responsible for the edge-shifting to shorter wavelength at room temperature. This is essentially a photodecomposition of the sample into As microcrystals and the remaining $\alpha\text{-As}_{40}\text{S}_{60}$ network, and has been verified by detailed structural analysis.³⁵ In order to explain why the As atoms can escape easily from the network under illumination even at room temperature, they suggested that the quite high deposition rates they used might mean an effectively faster quenching of the material from the vapour to the solid compared with the deposition rates normally used. Therefore, it is likely that their films have a higher enthalpy than typical $\text{As}_{40}\text{S}_{60}$ films. The fact that their films are As rich with respect to $\text{As}_{40}\text{S}_{60}$ may be another reason. The same authors³⁶ studied the spectral response of the transmission edge-shift at room temperature and found it to have a broad peak near the absorption edge of the film. This result indicated that these irreversible optical changes are not thermally produced, but are directly induced by absorbed photons. They also reported that this edge-shifting depends only on the product of the incident light intensity and the exposure time.

2.4. Reversible photo-induced changes

Photo-induced changes are termed reversible if the initial structural state and optical properties are restored after an annealing treatment for some time at a temperature typically near the glass transition temperature, T_g , and higher than the illumination temperature. Reversible photodarkening and photostructural changes have been observed in well-annealed evaporated or sputtered films as well as melt-quenched bulk glasses.³ In this section the detailed experimental results obtained mainly for well-annealed evaporated $As_{40}S_{60}$ (EV- $As_{40}S_{60}$) and melt-quenched $As_{40}S_{60}$ (MQ- $As_{40}S_{60}$) are described.

2.4.1. Reversible optical changes (photodarkening)

Photodarkening consists of a nearly parallel shift of the absorption edge to lower energies³⁷⁻⁴⁰ and the reversible form has been reported for many chalcogenides.³⁸⁻⁴⁰ Figure 2.1 shows the reversible photodarkening² observed in EV- and MQ- $As_{40}S_{60}$ after repeated cycles of illumination/annealing at 170 °C. It is clear from the figure that both amorphous samples show a similar shift in the edge (0.05 eV) and there is no change in the case of crystalline $As_{40}S_{60}$. This indicates that photodarkening is unique to the amorphous state and must originate from the disordered structure. Furthermore, photodarkening is accompanied by a small increase in refractive index.^{19, 26, 29, 32}

Photodarkening is known to depend on various factors: the temperature at which the sample is illuminated, the light intensity, the illumination wavelength and the composition of the material. Generally, $|\Delta E_0|$, the magnitude of the shift of the optical absorption edge, increases with a decrease in the temperature at which the sample is exposed to light. Figure 2.2 shows the photodarkening in EV-

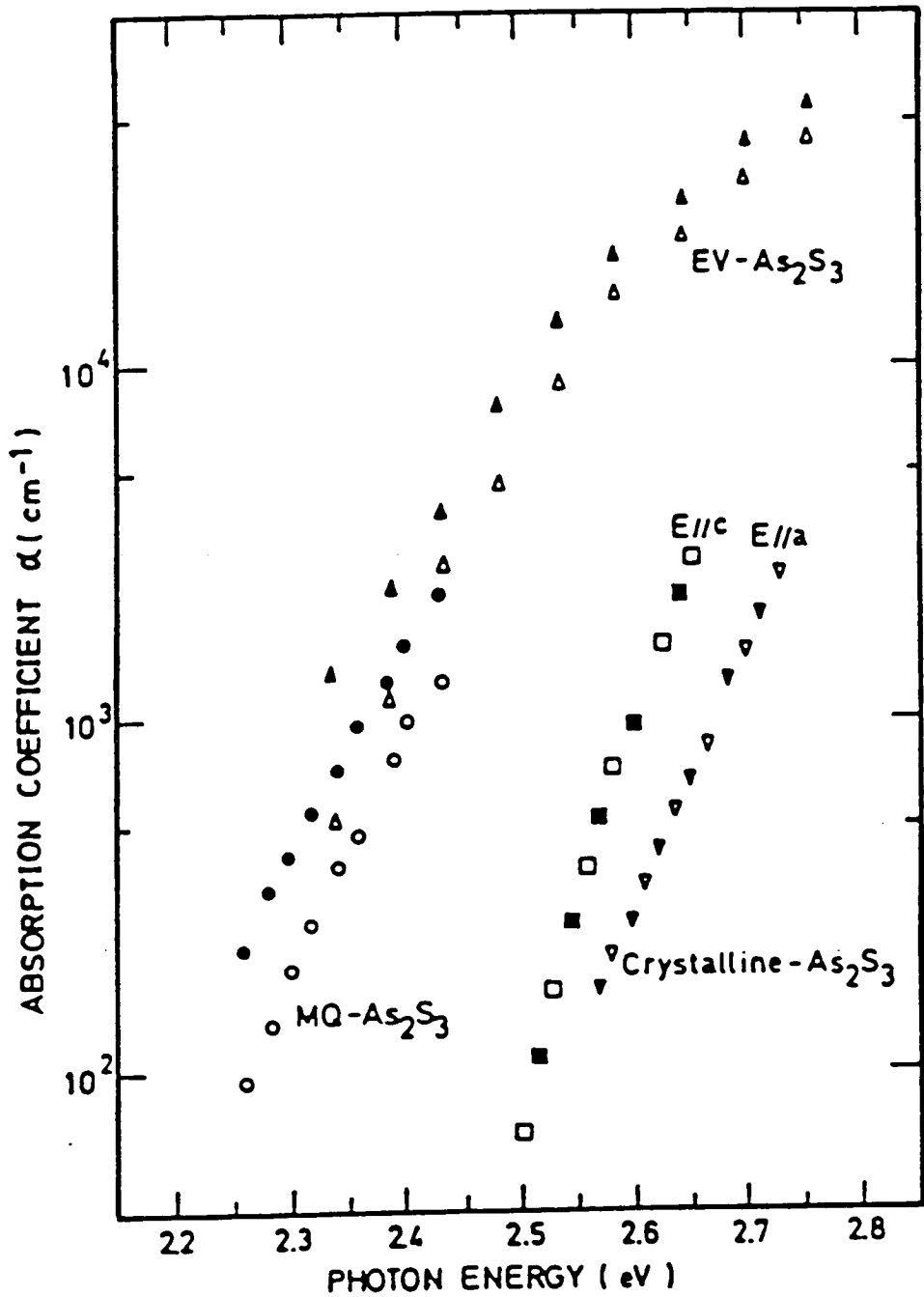


Figure 2.1. Optical absorption of EV-, MQ- $\text{As}_{40}\text{S}_{60}$ and crystalline $\text{As}_{40}\text{S}_{60}$ before (open symbols) and after band gap illumination (solid symbols). (EV = evaporated; MQ = melt quenched; E//c, E//a refer to the polarisation of the light relative to the a and c crystal axes).²

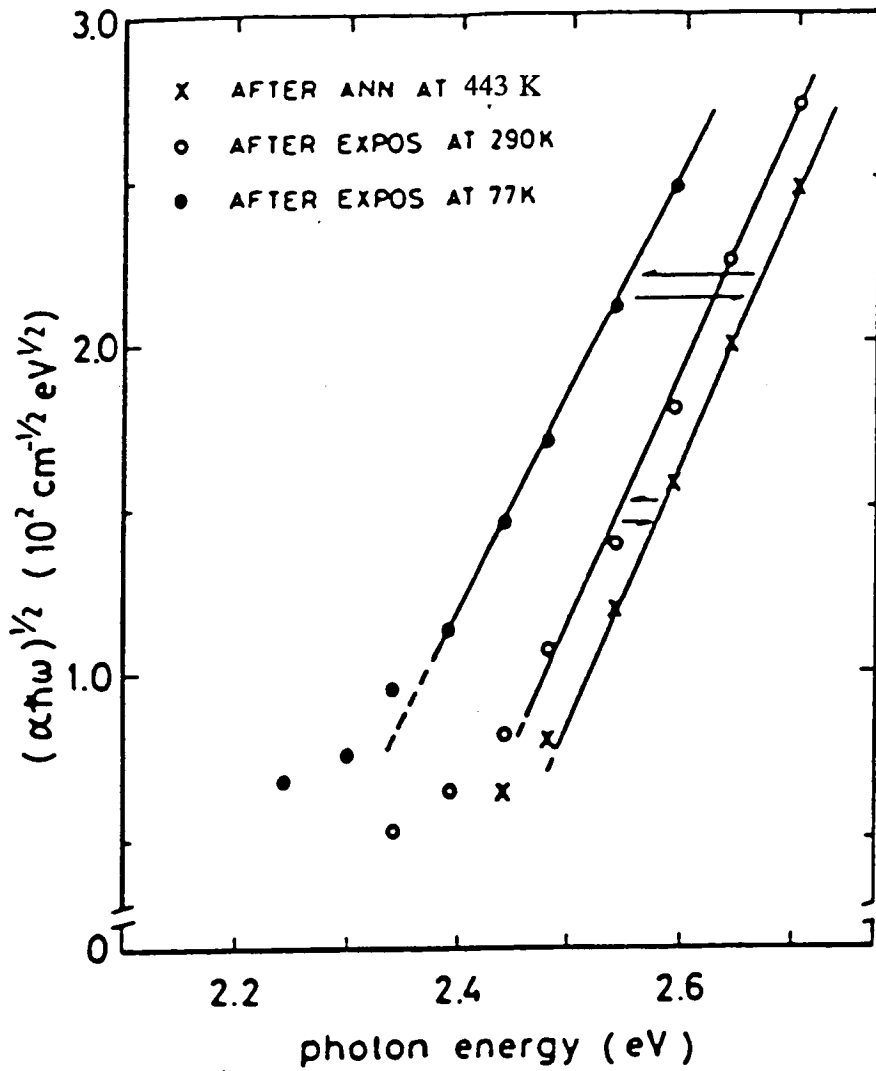


Figure 2.2. Photodarkening in EV-As₄₀S₆₀ for different exposure temperatures.⁴¹

As₄₀S₆₀ for different exposure temperatures.⁴¹ It should be noted that all the spectra were measured at room temperature, which implies that photodarkening involves some sort of nonlinear process. Such nonlinearity is reflected more clearly by the fact that the reciprocity law between incident photon flux, n , and exposure time, t , is not obeyed by this effect. It has long been believed³⁸ that ΔE_0 is affected only by the product, nt , but Tanaka⁴ observed that $|\Delta E_0|$ gets gradually larger with an increase in n under the condition of a constant nt product. The results⁴ for EV-As₄₀S₆₀, as shown in figure 2.3, indicate that the reciprocity law of n vs t does not precisely hold for the photodarkening process.

Hamanaka⁴² asserted that the intensity dependence does not originate from thermal effects but from pure photon effects. His argument is based on the experimental result that, even if photon doses are identical, a thermally relaxed film which has been illuminated with intense light exhibits greater photodarkening than a film illuminated with weak light.

Recently Tanaka⁴³ found that, when the sample is illuminated at room temperature, the photodarkening increases logarithmically with the light intensity. In addition, the magnitude of the photodarkening, induced by repeated pulsed illumination is governed by the time-averaged intensity. Therefore, they suggested that the intensity dependence originates from competition between a photo-effect and thermal relaxation. Their theoretical studies predicted that if the thermal effect can be suppressed, the photo-induced effects at room temperature can be enhanced by a factor of approximately two under intense illumination.

At low temperature, the photo-induced optical change involves two essentially different phenomena: a parallel shift of the absorption edge (photodarkening), and the appearance of a broad absorption band in the mid-gap region. The latter is caused by the formation of paramagnetic centres (similar to the D⁰ centres due to native defects) and is therefore always accompanied by ESR signals¹² (the density of centres $n_s = 10^{17} - 10^{18}/\text{cm}^3$). The photo-induced optical change in EV-As₄₀S₆₀ at 14 K for 488 nm excitation cannot be characterised by

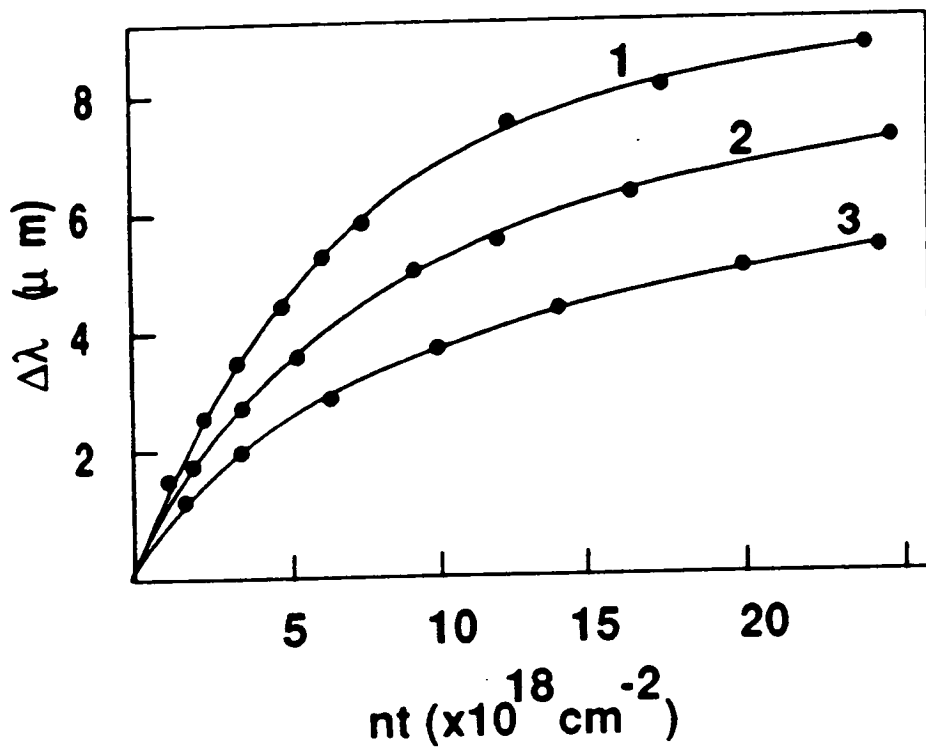


Figure 2.3. Wavelength shift between the annealed and photodarkened state as a function of the total number of photons absorbed for different photon fluxes $n[\text{cm}^{-2}\text{s}^{-1}]$. 1- $n= 8.28 \times 10^{16}$; 2- $n= 9.21 \times 10^{15}$; 3- $n= 1.03 \times 10^{15}$.⁴

a simple parallel shift of the absorption edge. The photo-induced absorption at lower photon energies can be removed not only by warming up to room temperature but also by irradiating the photodarkened film with light of photon energy lower than the band gap E_0 (e.g. 647.1 nm light from a Kr-ion laser). In contrast, part of the large shift that occurs in the absorption edge remains even after both procedures.⁴

Tanaka and Kikuchi³⁵ observed that their $As_{50}S_{50}$ films exhibited an increase in optical density after exposure to light at 77 K. They speculated that the incident photons absorbed by the film will excite valence electrons from their bonding states, in other words, the chemical bonds are being broken. Such broken or weakened bonds could cause the optical densification effect at 77 K, so that the recovery process induced by thermal annealing or illumination can reasonably be interpreted as a "re-tightening" of these bonds, corresponding to some kind of thermodynamic stabilization effect. They therefore ascribed the reversible optical densification effect at 77 K to photo-induced changes in the short-range order of the amorphous structure.

It was previously stated that light with energy close to the optical gap causes photodarkening. A more recent study of the spectral response of photodarkening has been carried out by Tanaka³ and the results are shown in figure 2.4. The photo-induced shift in absorption edge was measured at different photon energies, the results then being normalised to the number of absorbed photons. The response curve appears flat⁴⁴ for energies higher than 2.4 eV (the optical gap for $As_{40}S_{60}$) and thus it appears that photodarkening is induced by interband optical absorption.

The effect of composition on the magnitude of these photostructural changes can arise in one of two ways: the replacement of one type of chalcogen atom for another in an alloy of the same (stoichiometric) composition; or a change in composition away from stoichiometry. For the first case, it was found⁴⁵ that the S-containing glasses exhibit larger effects than do Se-based materials, which in turn exhibit larger effects than Te-based glasses. In the second case, the

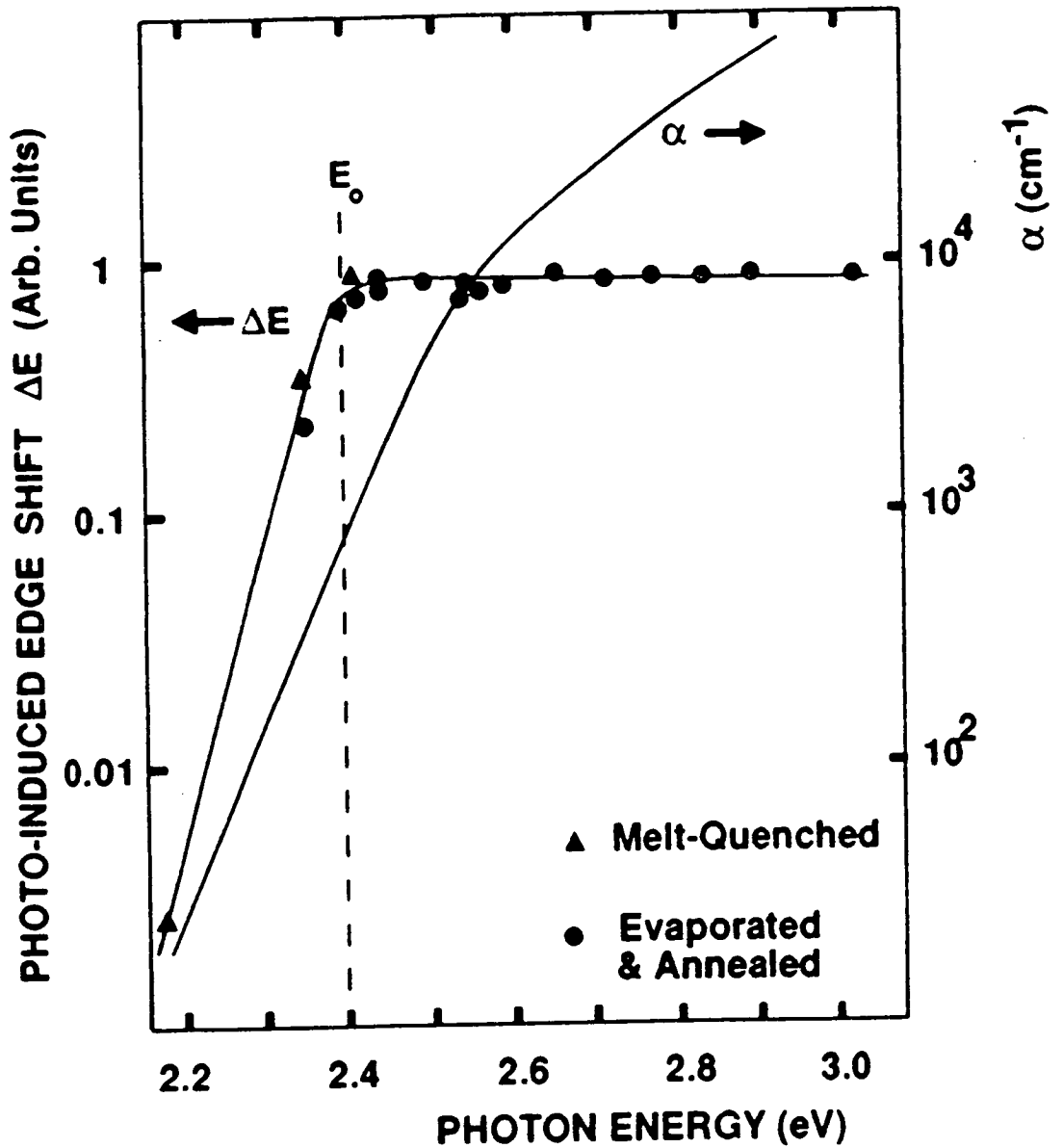


Figure 2.4. Photo-induced edge shift, ΔE , in $\text{As}_{40}\text{S}_{60}$ (normalised to the number of absorbed photons) as a function of the photon energy used to photodarken the sample.³

extent of the photodarkening is found to increase with an increase in As content in As-containing chalcogenide glasses.⁴⁶ Another compositional effect, reported by Liu and Taylor,⁴⁷ is the absence of photodarkening in bulk chalcogenide glasses alloyed with Cu. They speculated that this absence is probably due to the presence of tetrahedrally coordinated chalcogen atoms. They concluded, therefore, that a nonbonding chalcogen valence band, which is provided by two-fold coordinated chalcogen atoms, is necessary for the presence of photodarkening in the chalcogenide glasses.

Raman scattering studies on As-S films and thin bulk samples performed by Firth,⁴⁸ suggested that photodarkening is accompanied by an increase in As-As bond density. The author explained the increased photodarkening sensitivity of As-rich films by suggesting that As-As bonds are always present in As-rich films, even in well annealed films, and the probability that As atoms will be in neighbouring positions increases with As content. In contrast, in S-rich films As atoms are at a greater mean distance from each other since they are separated by $[S-S]_n$ chains. Consequently the probability that two or more As atoms will be in adjacent positions is lower, and therefore the photodarkening sensitivity is considerably reduced.

Several mechanisms have been proposed^{4, 16, 49-54} to account for various aspects of photodarkening. One of these is the double well potential model^{4, 16, 55} illustrated in figure 2.5 which shows a local bonding geometry that might be found in an $As_{40}S_{60}$ film. Positions A and A' represent a local bistable bonding configuration, and can be modelled by a "double well potential". The normal annealed condition of the film is state A, but by irradiating with bandgap light, the system gains enough energy to "flip" to state A', which is considered as the photodarkened state. The important feature of this model is that bonds are not broken. Instead there is a change in bond length and also in bond angle.

Keneman et al.⁵⁶ proposed another model which, in contrast to the above, does involve the breaking of bonds. These authors assumed that after initial evaporation an $As_{40}S_{60}$ film consisted mainly of As_2S_2 , S and As_2S_3 . Annealing at T_g converts the film to

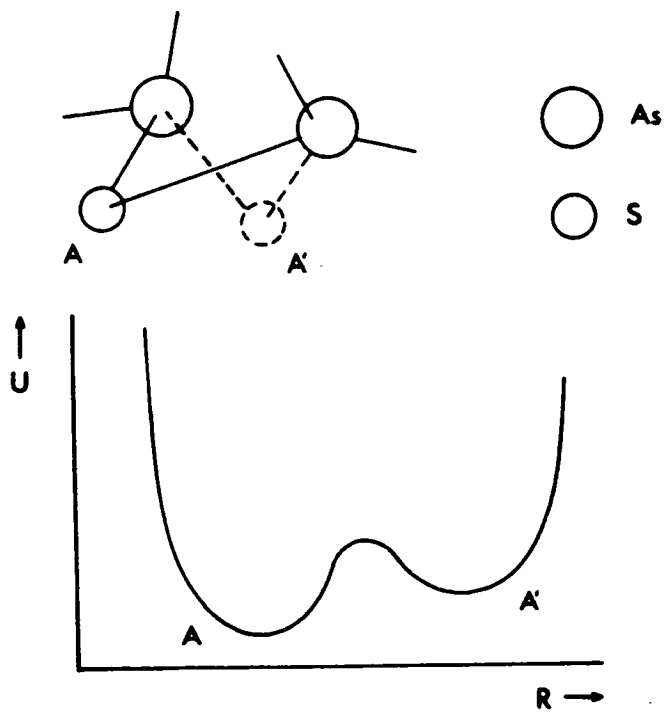
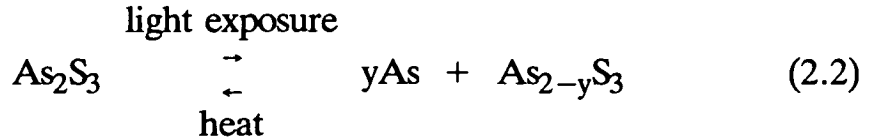


Figure 2.5. A schematic model of bistable local bonding geometries in $\text{As}_{40}\text{S}_{60}$ and the corresponding double-well potential.⁴

homogeneous $\text{As}_{40}\text{S}_{60}$ by the reaction



They ascribed the reversible photodarkening effect once the film is in the annealed state to As clustering according to the reaction



Another bond-breaking model is that based on the "self-trapped exciton" (STE) as suggested by Street.⁵¹ The exciton is an optically excited hole-electron pair with an energy, E_x . It is assumed that the energy of a defect pair ($\text{D}^+ \text{D}^-$) will be much lower than E_x , so that the exciton is unstable and will immediately form a $\text{D}^+ \text{D}^-$ pair. Originally the STE was suggested for the case of pure chalcogen glasses, but Elliot²⁵ has extended it to the case of chalcogenide alloys. The main difference between the two cases comes from the possibility of forming homopolar (like-atom) bonds in the latter case. According to Elliot,⁴⁹ in As_2Se_3 the formation of an STE will cause an As-Se bond to break and a Se-Se bond to form, the result being a pair of metastable defects, Se^{3+} and As^{2-} . In terms of bond redistribution, for every As-Se bond broken, 1 As and 2 Se bond-angles are lost and 3 Se bond angles are created. He assumed that the band gap is modified locally by the presence of photo-created homopolar bonds, with the result that the effective gap is changed from the value characteristic of the material containing only heteropolar bonds. Under this assumption, whether or not photodarkening or photobleaching occurs depends on the relative magnitude of the gaps for the alloy compared with those for the component elements. For example, the gap for a-As ($E_g \approx 1.4$ eV) is much smaller than for both a- $\text{As}_{40}\text{S}_{60}$ ($E_g \approx 2.4$ eV) and a- As_2Se_3 ($E_g \approx 1.8$ eV), whereas the gaps for a-Se and a-S are both larger ($E_g \approx 2.0$ and ≈ 3 eV, respectively). Photodarkening is therefore predicted in the case of formation of As homopolar bonds, and photobleaching for the formation of chalcogen homopolar bonds. The creation of As-As bonds in As-containing chalcogenides leads to the creation of a gap state in the lower half of the gap and a set of

states split off from the bottom of the conduction band. As a result, optical transitions can take place at a lower energy than in the case of material containing only heteropolar bonds, so that the overall absorption edge is therefore expected to shift to lower energies.

A further model suggested by Elliot⁴⁹ is one in which two As-Se bonds are broken simultaneously, and one As-As and one Se-Se bond are formed instead; in this way a chemically-ordered network (CON) is locally transformed into a random-covalent-network (RCN). This model predicts that the constituent atoms remain neutral, but that the short range order is partially destroyed.

In his latest model Elliot²⁵ asserted that the action of light in producing photostructural changes is to weaken and ultimately break bonds: not just the primary covalent bonds (intra-molecular bonds), but also the weaker "back-bonds" between non-bonded chalcogen atoms in neighbouring layers (inter-molecular bonds). In this model, he used an analogy that the effect of light is to act in the opposite direction to pressure, i.e. as a "negative pressure".

Elliot has also invoked the Dow-Redfield model⁵⁷ for the Urbach edge in terms of field-broadened exciton lines: he suggests that the photo-created defects increase the magnitude of the internal electric microfields and therefore cause an increase in the optical absorption at below-gap energies. One consequence of this latter mechanism for photodarkening is that the slope of the Urbach edge (on a plot of $\ln(\alpha)$ versus $h\nu$) should decrease in the photodarkened state, i.e when the density of charged defects, and hence internal microfields, is enhanced. Thus, in those instances where such a change in the slope of the Urbach edge has been observed,⁵⁸ the behaviour can be understood in these terms. However, it appears that more often a parallel red-shift of the Urbach edge accompanies photostructural change.⁴

Grigorovici and Vancu⁵² have proposed a model based on photo-induced polymerisation. For this model to be applicable it is necessary that discrete molecular units exist, even in well-annealed films. Illumination then causes these molecular units to join together in a more organised way. There are two main problems with this model. First, the annealing of the film, which erases the photodarkening,

would be connected with de-polymerisation but there is no evidence to support this. Secondly, the polymerisation model predicts densification and consequently a decrease in the thickness (volume) of the sample after illumination. This is in contradiction to the results already stated for $As_{40}S_{60}$.

2.4.2. Experimental evidence for the reversible photostructural changes.

2.4.2.1. The direct experimental evidence

The first direct evidence for the existence of photostructural change was obtained by X-ray diffraction measurements.⁴¹ Reversible changes have been observed for both EV- $As_{40}S_{60}$ and EV- $As_4Se_5Ge_1$.⁴⁰ The photostructural change was found to be characterised by an increase in randomness of the atomic configuration.

Utsugi and Mizushima observed a reversible change in the far-infrared absorption spectra of amorphous Ge-Se films and concluded that photoirradiation induces a large fluctuation in the Ge-Se bond angle.⁵⁹ Kumeda and co-workers have also suggested an increase in structural randomness as a result of an ESR study of the amorphous $As_2Se_3:Mn$ system.⁶⁰

2.4.2.2. The indirect experimental evidence

The indirect evidence for reversible photostructural changes has been mainly obtained by thin film dilatometry using a mechanical method⁶¹. Photo-induced thickness changes of EV and MQ-As₄₀S₆₀ samples for different exposure temperatures suggested that the fractional change, $\Delta d/d$, has almost no dependence on initial film thickness, d , which indicates that the change should be ascribed to a volume effect. It is noteworthy that $\Delta d/d$ for MQ-As₄₀S₆₀ nearly coincides with that of EV-As₄₀S₆₀ within experimental error. The value of $\Delta d/d$ is considered to be that due to a fractional volume change $\Delta V/V$, to a first approximation, since no discernible change in the area of sample surface was observed. Lower exposure temperature produces larger changes, as also observed by Tanaka.⁴¹ Elliot²⁵ has shown that the observed photo-induced volume increase can be accounted for quantitatively by both the inter-molecular bond breaking mechanism and by two of the intra-molecular bond-breaking processes which have been proposed, namely the self-trapped exciton model and the random-covalent network-transformation model. EXAFS measurements, performed by Yang et al.,⁶² showed that the change in the concentration of As-As bonds under illumination is only 0.5%, compared to 6% suggested by the bond-breaking model.⁶³ Therefore, they suggested that a rotation of adjacent AsS₃ pyramids about their shared S atom upon light soaking is the major cause of observed photo-dilation.

The surface roughness of thin films^{38, 64} of a-As₂Se₃ and a-Se has been observed to decrease on irradiation, indicating that the materials flow under the action of light. The glass transition temperature, T_g , another quantity related to flow, has also been observed to decrease on illumination⁶⁵ for the case of a-Se. In general the physical properties of chalcogenide glasses relax to the metastable equilibrium values at T_g . However, Tanaka and Ohtsuka³² reported for chalcogen-rich compositions in the As-S system that the reversible temperature,¹ T_{rev} , of heat treatment which produces metastable properties both in as-deposited and well-illuminated films was higher than T_g . Therefore, in the reversible processes, an annealing at the glass transition

temperature of the bulk glasses does not produce metastability in the evaporated chalcogenide-rich films. Tanaka and Ohtsuka also reported³² that the extent of the reversible processes is roughly correlated with As content. In addition, interatomic force constants have been observed to decrease after illumination, either when inferred indirectly from microhardness experiments⁶⁶ on a-Se and a-As₂Se₃, or more directly from the elastic moduli obtained from surface acoustic wave measurements⁶⁷ of a-As₄₀S₆₀. However, Lyubin⁶⁸ reported a reversible photo-induced increase in microhardness in amorphous As₃Se₂. Elliot²⁵ proposed that the photo-enhancement of viscosity and the reduction in T_g are due to a photo-induced reduction in intermolecular bonding.

References

1. Deneufville, J.P, *Optical Properties of Solids - New Developements*, p. 437, ed. Serapin B.O, North-Holland Pub. co., Amsterdam, 1975.
2. Hamanaka, H., Tanaka K. and Iijima S., *Solid State Comm.*, vol. 23, p. 63, 1977.
3. Tanaka K., *Proc. 7th Intern. Conf. Amorphous and Liquid Semiconductors*, p. 787, ed. Spear W.E., 1977.
4. Tanaka K., *Non-Cryst. Solids*, vol. 35&36, p. 1023, 1980.
5. Flashen, S., Pearson, A. and Northover, W.J., *Amer. Ceram. Soc.*, vol. 42, p. 450, 1959.
6. Myers, M.B. and Felty, E.J., *Mat. Res. Bull.*, vol. 2, p. 535, 1967.
7. Ewen P.J.S., Ph.D. Thesis, University of Edinburgh, 1978.
8. Zallen, R., *Optical and Electrical Properties*, 4, p. 231, D.Reidel Pub. co., Dordrecht, 1976.

9. Leadbetter, A.J., Apling, A.J., *J. Non-Cryst. Solids*, vol. 15, p. 250, 1974.
10. Lucovsky, G., Martin, R.M., *J. Non-Cryst. Solids*, vol. 8-10, p. 185, 1972.
11. Rubinstein, M. and Taylor, P.C., *Phys. Rev. Letters*, vol. 29, p. 119, 1972.
12. Bishop, S.G., Strom, U. and Taylor, P.C., *Phys. Rev. Letters*, vol. 34, p. 1346, 1975.
13. Street A. and Mott N.F., *Phys. Rev. Lett.*, vol. 35, p. 1293, 1979.
14. Kastner, M., Adler, D. and Fritzsche, H., *Phys Rev. Letters*, vol. 37, p. 1504, 1976.
15. Kastner, M., *Phys. Rev. B*, vol. 7, p. 5237, 1973.
16. Leadbetter A.J., Apling A.J. and Daniel M.E., *J. Non-Cryst Solids*, vol. 21, p. 47, 1976.
17. Solin S.A. and Papatheoderou G.N., *Phys. Rev.*, vol. 15(4), p. 2084, 1977.
18. DeNeufville J.P., Moss S.C. and Ovschinsky S.R., *J. Non-Cryst. Solids*, vol. 13, p. 191, 1974.
19. Kasai M., Nakatsui H. and Hajimoto Y., *J. Appl. Phys.*, vol. 45, p. 3209, 1974.
20. Kokado H., Shimizu I. and Inoue E., *J. Non-Cryst. Solids*, vol. 20, p. 131, 1976.
21. Takahashi T., Harada Y. and Hino S., *Solid State Comm.*, vol. 30, p. 635, 1979.
22. Nemanich R.J., Connell G.A.N., Hayes T.M. and Street R.A., *Phys. Rev. B.*, vol. 18, p. 6900, 1978.

23. Treacy D.J., Strom U., Klein P.B., Taylor P.C. and Martin T.P., *J. Non-Cryst. Solids*, vol. 35&36, p. 1035, 1980.
24. Kolobov A.V., Elliot S.R. and Taguirdzhanov M.A., *Phil. Mag. B*, vol. 41, p. 9913, 1990.
25. Elliot S.R., *J. Non-Cryst. Solids*, vol. 81, p. 71, 1986.
26. Tanaka K. and Ohtsuka Y., *J. Appl. Phys.*, vol. 49(12), p. 6132, 1978.
27. Asahara Y. and Izumitani T., *J. Appl. Phys.*, vol. 47(11), p. 4882, 1976.
28. Kumar B. and White K., *Thin Solid Films*, vol. 135, p. L13, 1986.
29. Tanaka K. and Ohtsuka Y., *Thin Solid Films*, vol. 48, p. 17, 1978.
30. DeNeufville J.P., Seguin R., Moss, S.C. and Ovshinsky S.R., *Proc. 5th Int. Conf. on Amorp. and Liquid. Semicond.*, p. 737, Garmish-Partenkirchen, Taylor and Francis, London, 1973.
31. Gurevich S.B., Ilyashenko N.N., Kolomiets B.T., Lyubin V.M. and Shilo V.P., *Phys. Stat. Sol. (a)*, vol. 26, p. K127, 1974.
32. Tanaka K. and Ohtsuka Y., *Thin Solid Films*, vol. 57, p. 59, 1979.
33. Tanaka K. and Kikuchi M., *Solid State Comm.*, vol. 11, p. 1311, 1972.
34. Mizuno H., Tanaka K. and Kikuchi M., *Sol. Stat. Commun.*, vol. 12, p. 999, 1973.
35. Tanaka K. and Kikuchi M., *Solid State Comm.*, vol. 13, p. 669, 1973.
36. Tanaka K. and Kikuchi M., *Proc. 5th Int. Conf. on Amorphous and Liquid Semiconductors*, p. 439, Taylor and Francis, London, Garmish-Partenkirchen, 1973.

37. Keneman S.A., *Appl. Phys. Lett.*, vol. 19, p. 205, 1971.
38. Berkes J.S., Ing S.W. and Hillegas W.J., *J. Appl. Phys.*, vol. 42, p. 4908, 1971.
39. Igo T. and Toyoshima Y., *Proc. 5th Int Conf. on Solid State Devices*, p. 106, Tokyo, 1973.
40. Tanaka K., Iijima S., Aoki K. and Minomura S., *Proc. 6th Int. Conf. Amorphous and Liquid semiconductors*, p. 442, ed. Kolomiets B.T., Leningrad, 1976.
41. Tanaka K., *Appl. Phys. Letters*, vol. 26, p. 243, 1975.
42. Hamanaka H., *J. Non-Cryst. Solids*, vol. 57, p. 401, 1983.
43. Tanaka K., *Thin Solid Films*, vol. 157, p. 35, 1988.
44. Mott N.F. and Davies E.A., *Electronic Processes in Non-Crystalline Materials*, p. Chap. 6, Oxford: Clarendon Press, First Edition, 1971.
45. Tanaka K., *Non-Cryst. Solids*, vol. 59/60, p. 925, 1983.
46. Kolomiets B.T. and Lyubin V.M., *Mat. Res. Bull.*, vol. 13, p. 1343, 1978.
47. Liu J.Z. and Taylor P.C., *Phys. Rev. Letters*, vol. 59, p. 1938, 1987.
48. Firth A.P., *Ph.D. Thesis*, University of Edinburgh, 1985.
49. Elliot S.R., *J. Non-Cryst. Solids*, vol. 59&60, p. 899, 1983, 1983.
50. Halpern V., *Phil Mag*, vol. 34, p. 331, 1976.
51. Street R.A., *Solid State Comm.*, vol. 24, p. 363, 1977.
52. Grigorovici R. and Vancu A., *J. Phys., Paris Colloq.*, vol. 42, p. 391, 1981.

53. Grigorovici R. and Vancu A., *J. Non-Cryst. Solids*, vol. 59&60, p. 909, 1983.
54. Frumar M., Firth A.P. and Owen A.E., *Phil. Mag. B*, vol. 50, p. 463, 1980.
55. Averjanov V.L., Kolobov A.V., Kolomiets B.T. and Lyubin V.M., *Phys. Stat. Sol.(a)*, vol. 57, p. 81, 1980.
56. Keneman S.A., Bordogna J. and Zamel J.N., *J. Appl. Phys.*, vol. 49(9), p. 4663, 1978.
57. Dow J.D. and Redfield D., *Phys. Rev. B1*, vol. 1, p. 3358, 1970.
58. Tsutsu H., Tamura K. and Endo H., *Solid state Comm.*, vol. 52, p. 877, 1984.
59. Utsugi Y. and Mizushima Y., *J. Appl. Phys.*, vol. 49, p. 3470, 1978.
60. Kumeda M., Nagaki Y., Suziki M. and Shimizu T., *Solide State co*, vol. 21, p. 717, 1977.
61. Hamanaka H., Tanaka K. and Iijima S., *Solide State Comm.*, vol. 19, p. 499, 1976.
62. Yang C.Y., Lee J.M., Paesler M.A. and Sayers D.E., *J. Non-Cryst. Solids*, vol. 97&98, p. 1119, 1987.
63. Frumar M., Firth A.P. and Owen A.E., *Phil. Mag. B*, vol. 50, p. 899, 1984.
64. Koseki H., Ueno T. and Oadjima A., *Jap. J. Appl. Phys.*, vol. 17, p. 1143, 1978.
65. Larmagnac G.P., Grenet G. and Michon P., *Phil. Mag. B*, vol. 45, p. 627, 1982.
66. Deryagin B.V., Toporov Yu.P., Merzhanov K.I., and Galvids N.M., Aleinikova I.N. and Burta-Gapanavich I.N., *Sov. Phys. Solid St.*, vol. 16, p. 1155, 1974.

67. Tanaka K., Kawakami N. and Oadjima A, *Jap. J. Appl. Phys.*, vol. 20, p. L874, 1981.
68. Lyubin V.M., "Structure and Properties of Non-Crystalline Semiconductors", *ed. by Kolomiets B.T.*, p. 415, Academy of Sciences of USSR, Leningrad, 1976.

CHAPTER 3

PHOTO-INDUCED PHYSICO-CHEMICAL CHANGES IN CHALCOGENIDE GLASSES

3.1. Introduction

In contrast to the photo-induced effects described in Chapter 2, illumination can also induce other types of photo-induced effects which produce very significant changes in the physical nature and chemical properties of chalcogenide glasses. The two most important photo-induced physico-chemical changes are described in this chapter: one is the photo-induced change in chemical durability (the photochemical effect) and the other is the photo-induced diffusion of metals (the photodissolution or photodoping effect). The properties of the metal-photodoped material and various models of the photodissolution effects are also presented in this chapter.

3.2. The photochemical effect

Whereas chalcogenide glasses are strongly resistant to acid solutions, they dissolve easily into alkaline solution. Illumination of the chalcogenide prior to immersion can cause a significant change in its solubility in alkaline solution,¹⁻³ the dissolution rate becoming either higher or lower depending on the composition of the chalcogenide glass. For example, according to Utsugi and Zembutsu,⁴ light-

irradiated $\text{As}_{10}\text{Se}_{67.5}\text{Ge}_{22.5}$ films dissolve more rapidly than unirradiated ones, while unirradiated $\text{As}_{40}\text{Se}_{15}\text{S}_{35}\text{Ge}_{10}$ films dissolve more rapidly than irradiated samples. Figure 3.1 shows the relationship between the etching time and the remaining thickness of the film. This photochemical effect is believed to be closely related to the photodarkening phenomenon described in the previous chapter, but the detailed nature of the effect as well as the mechanism underlying it, are not well understood.

3.3. The metal-photodissolution effect.

Kostyshin and co-workers (in 1966) were the first to observe⁵ that films of As chalcogenide semi-conductors, when brought into intimate contact with certain metals, are capable of giving a visible image after exposure to light. Since then a great deal of work has been done on this effect and this has been recently reviewed by Kolobov and Elliot.⁶ Initially this phenomenon was considered to be an interface reaction which was limited to a very thin interface region only. Further investigation showed, however, that relatively large amounts of the metal can migrate deep into the chalcogenide, and this effect is now termed "photodoping", "photodissolution" or "photodiffusion".

Photodissolution has been observed in many chalcogenide/metal combinations, including some where the metal is present in the form of a compound such as the sulphide or the selenide. The majority of this work has been done using Ag as the metal although Cu⁷ and Zn⁸ have also been shown to react with $\text{As}_{40}\text{S}_{60}$. The most widely used chalcogenide compositions in these studies are $\text{As}_{40}\text{S}_{60}$ and GeSe_2 although the effect has been observed in many other Ge and As chalcogenides.

Photodissolution was initially assumed to occur in a direction normal to the film surface and therefore was known as transverse photodissolution. However, Yamaguchi et al.⁹ showed that for an

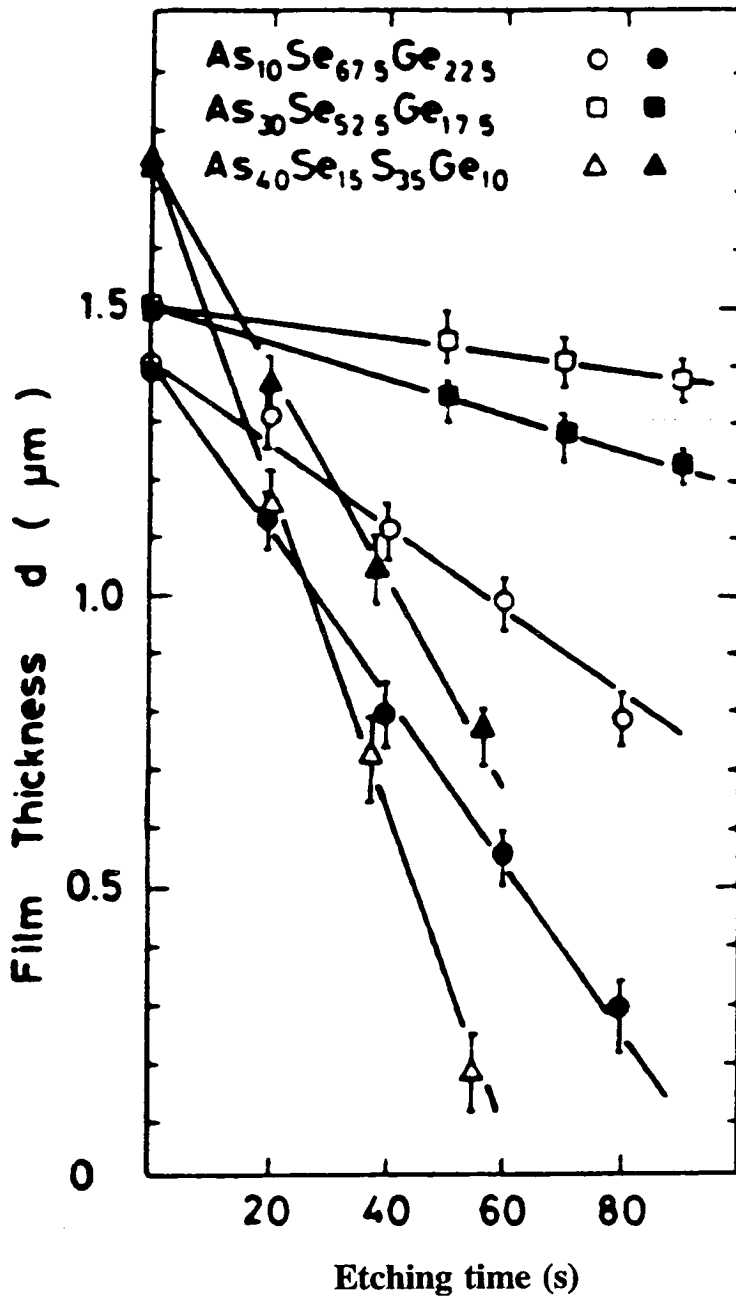


Figure 3.1. Thickness of various chalcogenide films as a function of etching time in NaOH solution (0.33M)⁴⁴.

glass structure under light excitation. The review of the kinetics studies presented below has been divided into four sections according to the technique used to study the kinetics.

3.3.1.1. The electrical method

Goldschmidt and Rudman¹¹ were the first in developing the method based on resistance measurement. They used samples consisting of about 30 nm of Ag under 50-250 nm of $As_{40}S_{60}$, illumination being from the $As_{40}S_{60}$ side. Their method was to measure the electrical resistance of the Ag, and from this to calculate its thickness as a function of illumination time. The authors noted that photodissolution proceeded in three stages. First there was an induction period during which very little reaction occurred. Following this there was a stage during which the reaction rate was constant, and finally a stage during which the reaction rate decreased to zero, as the Ag was exhausted. The induction period occurred only on initial illumination and was not repeated if the illumination was subsequently interrupted and then resumed.

Yaji and Kurita¹² also used the method of resistance measurement. It should be noted that this technique allows the decrease in the thickness of the Ag film to be determined as a function of time, but this does not necessarily reflect the increase in thickness of the photodoped layer. In their investigation, Yaji and Kurita also studied the latter by illuminating an Ag/ $As_{40}S_{60}$ sample with crossed laser beams to make a diffraction grating. The sample acts as a grating because some regions of the sample are photodoped while others are not, and when this grating is illuminated with a single light source the diffraction efficiency falls to zero as the remaining areas of Ag react. By measuring the reduction in diffraction efficiency the depth of the photodoped region can in principle be calculated. The authors found that during illumination the thickness of the photodoped region varied correspondingly with the decrease in the Ag film thickness. A similar

illuminated Ag film on an As_2Se_3 substrate, dissolution occurs first normal to the film surface, and then laterally at a much slower rate and this was termed lateral photodissolution.

The photodissolution of metals into chalcogenide glasses produces marked changes in many of their physical and chemical properties. In particular, it greatly reduces the solubility of the glass in alkalis, and increases its resistance to plasma etching,^{7, 8, 10} which enables these materials to be used as resists in photolithography. Although the technology of these resists has been extensively developed, no completely satisfactory mechanism has been proposed for the photodissolution effect itself. A description of the main features of the process and a review of the experimental work carried out to date in the field will be given in the following sections.

3.3.1. Photodissolution kinetics

Studying the reaction kinetics during illumination is an obvious way to obtain information about the process of photodissolution, but experimental difficulties mean that this is not a trivial undertaking. Various methods have been developed to monitor the kinetics and these usually involve measuring either the amount of Ag metal remaining on the surface (using chemical or electrical techniques), or the photodoped film thickness (using optical or spectroscopic techniques). The two most widely used techniques are optical probing which involves optical transmission and/or reflectivity monitoring, and the electrical methods (resistance monitoring). The samples in which photodissolution is observed normally consist simply of a layer of metal (usually Ag) in contact with a layer of chalcogenide glass. Samples can be made either with the Ag above the glass, or by depositing the Ag first and then the glass on top, and this bilayer combination can be illuminated from either the Ag or the chalcogenide side. The general aim of these kinetics studies is to determine the nature of the chemical reaction or other process by which the Ag is incorporated within the

experiment had been carried out some years before by Sharlandjiev et al.¹³ but these authors did not analyse their results in as much detail.

Konan et al.¹⁴ studied Ag photodissolution kinetics in the GeSe₃ system using a similar method to Goldschmidt. Their samples exhibited a photodissolution rate strongly related to the illumination wavelength, with a significant increase occurring for near UV light. They used the technique to study the intensity and spectral dependence of the photodissolution rate.

3.3.1.2. Optical methods

Firth et al.¹⁵ used a method based on optical reflectivity monitoring to investigate the growth of the photodoped layer in the Ag/As₄₀S₆₀ system. (This technique is described in detail in Chapter 5.) An As₄₀S₆₀ film was evaporated onto a thick Ag substrate and the reflectivity measured as a function of illumination time. At first the thickness of the doped layer was found to increase linearly with illumination time, but when all the As₄₀S₆₀ was used up a second phase appeared. This had a higher Ag concentration and was found to grow with a square root dependence on illumination time indicating that this second phase of the reaction is diffusion controlled. The same method was recently used by Konan et al.¹⁶ to determine the kinetics of the Ag photodissolution in GeSe₃ vitreous thin films.

Mizuno et al.¹⁷ used an optical transmission method to investigate the light-induced and thermal diffusion of Ag and Cu into 1mm thick As₄₀S₆₀ samples. In this case, the optical transmission of the metal layer was measured as a function of illumination time. Kolobov et al.¹⁸ have also used this technique to measure the dissolution of Zn into As₄₀S₆₀ samples.

Wagner et al.¹⁹ used X-ray diffractometry to monitor the changing thickness of the Ag film by measuring the change in the

integrated intensity of the 111 diffraction peak of Ag. This enabled them to obtain the rate of transverse photodissolution of the Ag. Lateral dissolution was measured in this study using a micrometric eyepiece under a microscope. In a prior investigation Rennie²⁰ used this X-ray diffraction (XRD) technique to study Ag photodissolution kinetics in GeSe₂ films.

3.3.1.3. Chemical methods

A third technique was used by Shirakawa et al.,²¹ who illuminated their Ag/glass samples and then developed them in an alkaline etchant. The remaining thickness after etching was plotted against illumination time. They found that for the Ag/As₄₀S₆₀ combination, photodoped layer thickness is proportional to the square root of the illumination time. However, if a small amount of Se or Te was added to the As₄₀S₆₀ the dependence of the photodoped thickness on illumination time became linear. From the square root relationship they concluded that the reaction is diffusion controlled. The method of developing exposed samples to determine the extent of the reaction relies on the large change in solubility in alkalis that it is produced by the incorporation of Ag into the glass, which has been mentioned earlier. However, the decrease in solubility is not simply dependent on Ag incorporation, and experiments like those performed by Shirakawa and co-workers are difficult to interpret. Hence investigations carried out using a developing or etching technique are really useful only for comparative studies. Yoshikawa et al.²² has also used this technique for the Ag₂Se/GeSe₄ system.

Lis and Lavine²³ illuminated samples consisting of Ag on top of As₄₀S₆₀, As₂Se₃ and GeSe₂ films, and developed these samples to measure the number of photons necessary to produce a relief image after developing. The authors plotted the reciprocal of the square root of the number of photons needed to produce a relief image against wavelength, and argued that the data was fitted by a straight line, thus

proving that photo-emission from the Ag was involved in the reaction. However this conclusion is possibly not valid, since the straight line fit obtained is very poor.

Buroff and Baeva²⁴ used a similar technique, but, after removal of both the unreacted $As_{40}S_{60}$ and the doped layer they estimated the amount of unreacted Ag by titration.

3.3.1.4. Other methods

Various other methods have been employed in investigating photodissolution kinetics. Rutherford backscattering spectroscopy (RBS) has been used by Wagner and Barr,²⁵ who studied $Ag_2Se/GeSe_2$ films and reported a cube root dependence of the photodoped thickness on illumination time. Leung et al.²⁶ also used RBS to study a slightly different system, $Ag_2Se/GeSe_9$, and reported that the depth of the photodoped Ag varied as the square root of illumination time.

Plocharski et al.²⁷ illuminated samples consisting of an Ag layer underneath an $As_{40}S_{60}$ layer and then etched off the unreacted glass. X-ray fluorescence was then used to measure the Ag, As and S content of the remaining photodoped layer. Results from this technique were found to be in general agreement with those from resistance measurements, but the scatter in the data was larger. No new results were obtained and the technique has not been developed further.

3.3.2. Properties of the metal-photodoped material

In the case of Ag photodissolution into As-S films the photodoped material is a three component Ag-As-S combination. A knowledge of

the structure of materials in the Ag-As-S system is thus useful in understanding the properties of the photodoped materials. Both crystalline and amorphous materials can be formed in the Ag-As-S system. The principal ternary crystalline compounds that form in this system are proustite (Ag_3AsS_3), smithite (AgAsS_2), a modification of smithite called trechmanite, and possibly Ag_7AsS_6 as reported by Blachnik and Wickel.²⁸

A detailed study of the glass-forming region in the Ag-As-S system has been made by Kawamoto et al.²⁹ Their results are shown in figure 3.2 and show clearly that the system contains two areas of glass formation. Similar results were obtained by Golovach et al.³⁰ One of the areas of glass formation is situated along the As-S edge and centred on the composition $\text{As}_{40}\text{S}_{60}$. This area is quite small with a maximum Ag content of about 4 atomic%. The other area of glass formation is an island region and extends along the $\text{As}_{40}\text{S}_{60}$ - Ag_2S tie-line from about 30 mole % to 70 mole % Ag_2S . It is suggested²⁹⁻³¹ that the area of glass formation centred on $\text{As}_{40}\text{S}_{60}$ is based on the AsS_3 pyramidal structural unit and that small amounts of Ag (< 4 atomic%) can be incorporated into the As-S network without significantly changing its structure. This was confirmed by Raman scattering experiments,³¹ which showed that an Ag-containing glass of composition $\text{Ag}_4\text{As}_{38}\text{S}_{58}$ had a similar structure to $\text{As}_{40}\text{S}_{60}$ glass. It is also suggested²⁹⁻³¹ that the larger island region is based on a structural unit found in the crystal smithite, AgAsS_2 . Evidence for this was again provided by Raman scattering experiments.³¹ It was deduced that glassy AgAsS_2 is formed from structural units found in smithite and that glassy $\text{Ag}_{30}\text{As}_{22}\text{S}_{48}$ contains structural units found in proustite.

As a result of metal photodoping some very marked changes take place in the optical, electrical, structural and chemical properties of the chalcogenide glasses. In the remainder of this section the properties of the metal-photodoped materials will be reviewed under four headings: the Ag distribution after photodissolution; chemical and structural properties; electrical properties; and optical properties.

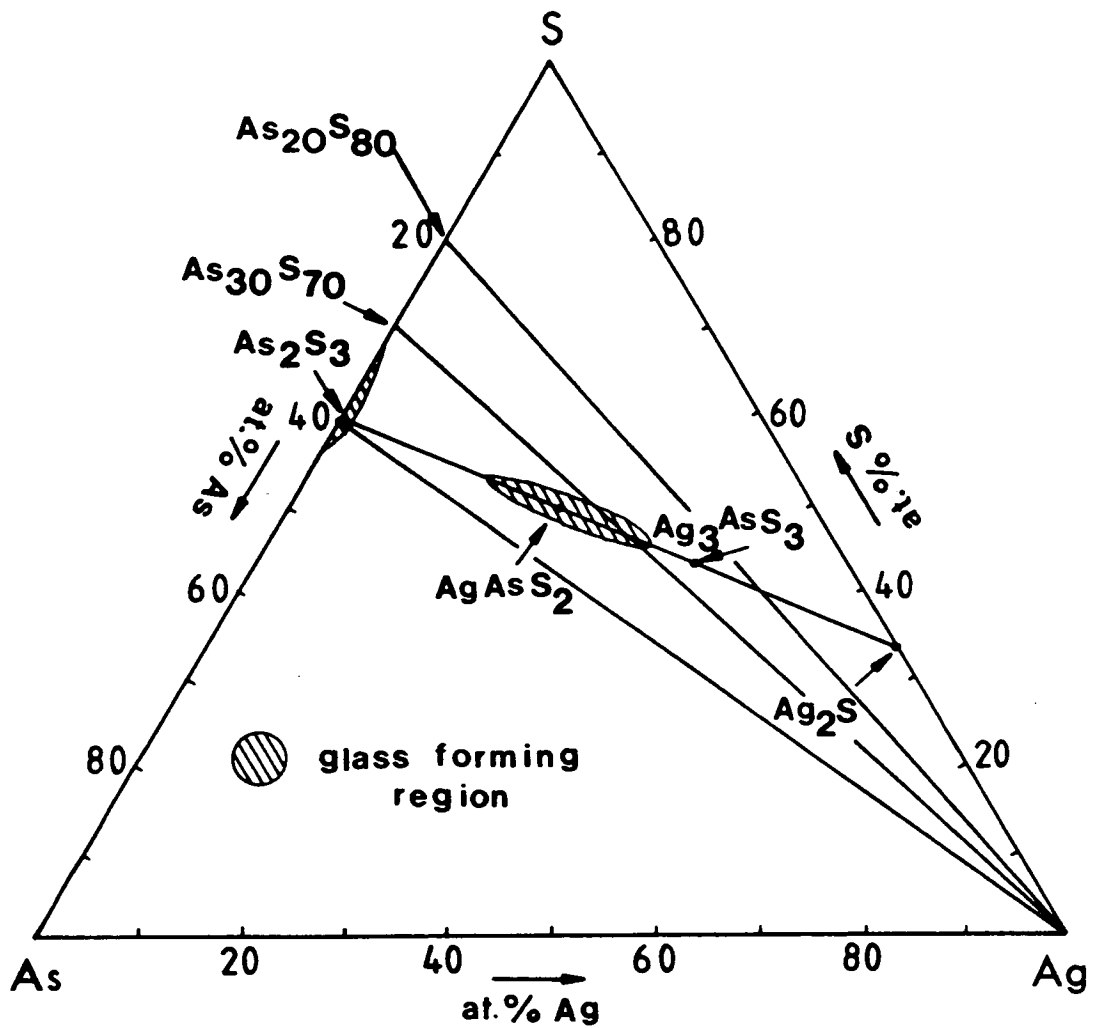


Figure 3.2. The glass forming region in the Ag-As-S system as determined by Kawamoto.²⁹

3.3.2.1. Ag distribution after photodissolution

The concentration of Ag in the photodoped region of a chalcogenide is uniform and falls abruptly to zero at the boundary with the undoped material. This step-like profile for the photodissolution front has been observed in Rutherford back-scattering experiments^{32, 33} and in electron microprobe studies.^{34, 35}

The maximum amount of Ag that will dissolve into an As-S film of a given thickness depends greatly on the composition. This has been determined by Yamaguchi et al.⁹ for a number of chalcogenide glasses. For films with formula As_2S_x the amount of photodissolved Ag appears to increase linearly with the S content, as is shown in figure 3.3. There is, however, a spread of values in the literature^{9, 27, 33, 36} for the amount of Ag which dissolves into $As_{40}S_{60}$: these range from 32 atomic% to 47 atomic%.

Buroff et al.³⁷ found that the thermal diffusion of Ag into $As_{40}S_{60}$ obeyed Fick's law. They measured an activation energy for diffusion of about 1 eV. Interestingly, when these authors studied the diffusion under the influence of an electric field³⁷ they found very different results. This time the Ag showed a step-like profile, with the Ag concentration being dependent on depth up to a certain point, after which it fell rapidly to zero. Yamamoto et al.³⁸ used Rutherford backscattering spectroscopy, to investigate the depth profile of Ag photodoped into $As_{40}S_{60}$. They reported that the depth profile was step-like, with the Ag constant up to a certain depth, but falling rapidly to zero beyond that point.

Suzuki et al.³⁹ reported that the first 3 nm of photodoped Ag/ $As_{40}S_{60}$ samples consisted only of Ag and S. However, the Auger depth profiling technique they used gives unreliable results for the first few tens of angstroms and their findings may not be significant.

In contrast with the Ag/ $As_{40}S_{60}$ system, the Ag depth profile in the $Ag_2Se/GeSe_3$ system was found to resemble a Fickian diffusion profile.^{40, 41}



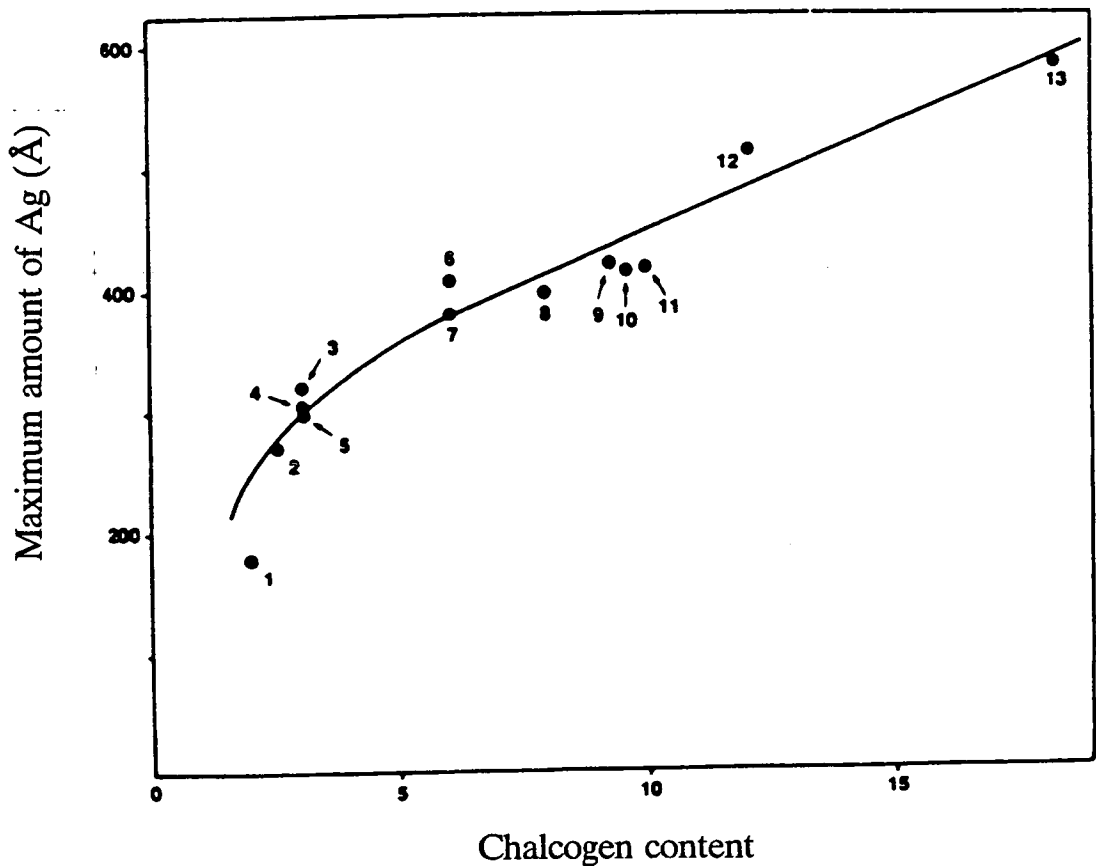


Figure 3.3. The maximum amount of Ag that can be photodissolved in various As chalcogenide films (50 nm thick) as a function of chalcogen content.⁹

1: $\text{As}_2\text{Se}_{1.9}\text{Te}_{0.12}$, 2: $\text{As}_2\text{S}_{2.6}$, 3: As_2Se_3 , 4: $\text{As}_2\text{S}_{2.9}\text{Te}_{0.1}$, 5: As_2S_3 , 6: As_2S_6 , 7: $\text{As}_2\text{Se}_{4.9}\text{Te}_{1.2}$, 8: As_2S_8 , 9: $\text{As}_2\text{S}_8\text{Se}_{1.3}$, 10: $\text{As}_2\text{S}_{9.6}$, 11: $\text{As}_2\text{S}_8\text{Te}_2$, 12: As_2S_{12} , 13: $\text{As}_2\text{Se}_{16}\text{Te}_2$.

3.3.2.2. Chemical and structural properties

In the case of the Ag/As₄₀S₆₀ system, photodissolution results in a well defined reaction product and several workers have investigated the nature of this product. The structure and composition of the product have been studied by Raman spectroscopy^{15, 31} and X-ray diffraction.⁴² Note, however that the X-ray diffraction studies were carried out not on photodoped samples, but only on bulk glasses made with differing amounts of Ag. The general conclusions were that the Ag seems to be co-ordinated to the chalcogen atoms, with the coordination number rising to four for large Ag concentrations. A number of XPS studies have been carried out,⁴³⁻⁴⁵ and these have concluded that the chemical shifts of the Ag and chalcogen atoms are consistent with Ag chalcogen bonds. No chemical shift is seen for the pnictogen atom, presumably indicating that its environment is little changed by photodissolution.

Matsuda³⁵ obtained the X-ray diffraction pattern for the surface of an As₄₀S₆₀ film into which Ag was photodissolved. Precise details of these experiments were not given, although it was stated that the As₄₀S₆₀ film was evaporated first, at a rate of 8.3 nm/sec, and that onto this was evaporated a film of Ag 20-100 nm thick, illumination during photodissolution being from the Ag film side. The surface was probed after the Ag film was etched off. Their results indicate the presence of faint traces of Ag₂S and As₂S₂ crystals in the photodoped material.

Contrary to these results the diffraction studies reported by DeNeufeville⁴⁶ and Salik⁴⁷ find no crystalline phases in Ag-photodoped As₄₀S₆₀ films. The samples investigated by Salik⁴⁷ were fabricated by evaporating the As₄₀S₆₀ on top of the Ag and the rate of evaporation was 2.5 nm per second.

Holmquist and Pask⁴⁸ used electron spectroscopy chemical analysis (ESCA) and electron microscopy analysis (EMA) to determine the reaction and diffusion characteristics of Ag in bulk As chalcogenide glass. They found that Ag diffusion from the metal or Ag₂Se in

$\text{As}_{40}\text{S}_{60}$ and As_2Se_3 at 175 °C is accompanied by the reduction of As from a valence of 3^+ or 2^+ to 1^+ to maintain the charge neutrality in the glass. Only Ag^+ diffuses at this temperature; all other ions were essentially immobile.

Shimizu et al.⁴⁹ suggested that the metals photodoped into chalcogenide glasses behave as structural modifiers, and that the density of states in the gap was increased by metal photodoping. This confirmed⁵⁰ that Ag is able to be homogeneously dissolved into $\text{As}_{40}\text{S}_{60}$ by photodoping, thereby maintaining an amorphous state. They suggested that Ag or Cu is bonded to the chalcogen (S) in $\text{Ag}_x(\text{As}_{40}\text{S}_{60})$ or $\text{Cu}_x(\text{As}_{40}\text{S}_{60})$ mixtures prepared by co-evaporation, which may cause an increase in the number of As-As bonds in order to satisfy bonding requirements. In addition to this they argued that the optical gap decrease accompanying Ag or Cu photodoping arises from the smaller binding energies of Ag-S, Cu-S or As-As bonds compared with As-S bonds.

Raman results obtained by Firth⁵¹ suggest that photodoped as-evaporated films of $\text{As}_{40}\text{S}_{60}$, $\text{As}_{38}\text{S}_{62}$ and $\text{As}_{20}\text{S}_{80}$ are phase separated whereas photodoped $\text{As}_{30}\text{S}_{70}$ films are homogeneous and have a structure similar to that of a bulk glass within the central region of glass formation and close to the Ag- $\text{As}_{30}\text{S}_{70}$ tie-line. Therefore compositions in the approximate range $\text{As}_{36}\text{S}_{64}$ to $\text{As}_{28}\text{S}_{72}$ would be expected to form a homogeneous Ag-photodoped phase since their tie lines to the vertex also pass through the central region of glass formation.

Steel et al.⁵² studied the structure of Ag photodoped films using EXAFS and demonstrated that the Ag-S environment in As-S films photodoped with Ag is very similar to that of the bulk Ag-As-S glasses. The structure of the films and glasses does not resemble any of the crystalline model compounds they examined, thus suggesting homogeneous dissolution of the Ag.

3.3.2.3. Electrical properties

The AC and DC conductivities of the metal-photodoped materials have been measured by several authors,^{49, 53-55} who agreed that metal-photodissolution causes the conductivity of the chalcogenide glasses to increase by several orders of magnitude. Shimizu et al.⁴⁹ studied the electrical conductivity of Ag and Cu photodoped glasses using a surface type cell. The chalcogenide glass compositions used in their experiment were $As_{40}S_{60}$, $As_{40}Se_{60}$ and $As_{16}S_{80}Te_4$. Their results implied that the conductivity was increased by Ag and Cu photodoping, and that, at the same time, the effective band gap, i.e. the "electrical band gap" was decreased. The conductivity, σ , is given by the following equation,

$$\sigma = \sigma_0 \exp^{\Delta E/kT} \quad (3.1)$$

where ΔE is the activation energy and is half of the effective band gap and σ_0 is the conductivity when $1/T$ tends to zero and is known as the pre-exponential factor. They observed that the decrease in the effective band gap caused by Cu photodoping was larger than that due to Ag.

In addition, a number of workers⁵⁶⁻⁵⁸ reported that on photodissolution an ionic component of the conductivity appears and that the ionic conductivity of the metal-photodoped materials is usually much greater than the electronic conductivity.

3.3.2.4. Optical properties

Several authors^{35, 51, 53, 59} found that the photodissolution of Ag into chalcogenides leads to a decrease in the optical transmission of the chalcogenide. Shimizu et al.⁴⁹ found that the optical absorption of chalcogenide glasses (e.g. As-S, As-S-Te, and As-S-Te) in the region of their absorption edges was increased by the photodoping of such metals as Ag or Cu. After illuminating an area of a binary layer

sample, they observed an increase in the overall transmittance of this area in the visible and infra-red regions. However, the tail of the absorption spectrum of the doped glass was found to have shifted to a longer wavelength than that of the undoped chalcogenide glass. In an experiment with $(As_2S_3)_{1-x}I_x$ samples, they found that the increase in the optical absorption caused by the photodoping of Cu was larger than that produced by Ag. Finally, they showed that the optical gap of the undoped glasses is decreased by metal photodoping. Shimizu et al.⁵⁰ also found that Cu altered the optical gap by a larger amount than Ag.

The optical transmissivity measurements carried out by Firth⁵¹ showed that if an As-S film were photodoped when Ag was in excess (i.e. Ag did not become exhausted during photodoping) the resulting photodoped film was optically much more absorbing than one formed when Ag was not in excess.

3.3.3. Photodissolution models

In the following discussion the various models of the photodissolution effect have been divided into three categories depending on where in the sample the actinic radiation is believed to be absorbed.

3.3.3.1. Absorption in the undoped layer

In this case the actinic light absorption is thought to occur in the undoped material adjacent to the already photodoped material. Kokado et al.⁶⁰ proposed that a potential barrier exists at the interface between the Ag and the chalcogenide and assumed this potential to have a minimum in the vicinity of the interface. When photons are

absorbed by the chalcogenide at the interface, photocarriers are generated (holes and electrons). These authors suggested that the holes will be captured by Ag atoms whereas the electrons will be repelled by the junction potential into the interior of the chalcogenide to be trapped. Assuming that the electron traps are associated with loosely bound chalcogen atoms, they speculate that the coulomb attraction between a negative chalcogen ion and a positive Ag ion is large enough for the Ag ion to be pulled into the chalcogenide. As the Ag enters the chalcogenide, a layer of a new composition rich in Ag is formed. The interface junction will move with the photodoped region and gradually form a hetero-junction. As photodoping continues, the junction region becomes wider and they state that the rate determining step for photodoping will be the diffusion of Ag ions through the photodoped region. They derived the following equation for the rate of growth of the doped region:

$$dx/dt = kI_{\text{abs}} + (k'/x)I_{\text{abs}} \quad (3.2)$$

where x is the depth of the photodoped layer, t the illumination time, I_{abs} is the number of absorbed photons per unit time and k and k' are constants. They state that the first term is for a photo-enhanced chemical reactivity with a short range influence and the second term describes the coulomb attraction between photogenerated ions (a negative chalcogen ion and a positive Ag ion) which drives the diffusion of Ag. At the beginning of photodoping (until a ~ 6 nm thick layer of Ag is dissolved) the second term is negligible, but in the later stages the first term can be neglected, giving the photodoped depth, x , a square root dependence on time

$$x = (2k'I_{\text{abs}}t)^{1/2} \quad (3.3)$$

This was consistent with their experimental results.

Ishikawa⁶¹ developed a model of photo-induced diffusion in terms of charged trapping centres⁶² (D^+D^-). According to Ishikawa the light deionises the charge centres of the undoped chalcogenide ($D^+ + D^- + h\nu \rightarrow 2D^0$) and the metastable D^0 traps electrons which are donated by Ag. As a result an ionised Ag^+ front is formed and then pulled by the D^- states into the chalcogenide. This model is capable of explaining why the Ag migrates as a step like concentration

profile as observed experimentally³³ and not in accordance with the usual Fickian diffusion profile, as was initially expected. However this model was contradicted by the following arguments advanced by Janai:^{63, 64}

a) The photodoping ceases when the metal is exhausted without further equalisation of the step-like metal concentration between the already doped and still undoped regions.

b) The number of D^+D^- centres of 10^{17} to 10^{18} cm^{-3} as suggested by the trapping centres model for the undoped chalcogenide cannot account for the observed maximum concentration of about 1.5×10^{22} Ag atoms/ cm^3 which occurs in photodissolution.

c) The spectral sensitivity of the photodissolution process extends much further into the long wavelength region than the absorption of the undoped chalcogenide.

Goldschmidt and Rudman¹¹ proposed that at short wavelengths, light absorbed in the chalcogenide glass leads to photodissolution. This idea was discussed by Malinowski and Buroff⁶⁵ who compared photodissolution to a tarnishing reaction and suggested that it is similar to the tarnishing of Ag in a S atmosphere. They proposed that in the photodoping process, illumination produces mobile holes in the $\text{As}_{40}\text{S}_{60}$ film, and if the photo-excitation is close enough to the Ag interface, then Ag-S bonds are formed. The illumination provides a supply of Ag ions which initially react at the Ag interface producing a layer of Ag_2S . They argued that the reaction is sustained because of the high electronic (e^-) and ionic (Ag^+) conductivity of the Ag_2S product layer.

3.3.3.2. Absorption in the metal

In the first report of photodissolution by Kostyshin et al.⁵ it was suggested that the light was absorbed in the layer of Ag metal, with the photo-emission of electrons and the consequent production of Ag ions. These ions were then thought to diffuse into $\text{As}_{40}\text{S}_{60}$ where they reacted. Goldschmidt and Rudman¹¹ agreed that light absorption at the Ag was important but at long wavelengths only. The observed spectral sensitivity together with the calculated spectral dependence of the reflectivity of the optical interfaces led Janai also to propose that the relevant light absorption is that occurring in the metal layer. This absorption triggers a solid state reaction at the metal-semiconductor interface, which results in a step-like profile.

Lis and Lavine²³ support Janai's proposal with the addition that the photodoping process is carried out by the internal photo-emission of hot electrons from the Ag into the chalcogenide. This conclusion is deduced from the observation that the reciprocal square root of the number of photons needed to produce a relief image varies linearly with wavelength.

3.3.3.3. Absorption at the undoped/photodoped interface

To this third group of models belong all those which consider the light absorption at the photodoped/undoped interface regions to be decisive for photodoping. For example, Yamaguchi et al.⁹ drew the conclusion that the photodoping process proceeds due to a light-enhanced diffusion of the Ag within the doped chalcogenide. The enhancement was believed to be caused by illumination-induced defects which can change places with the Ag atoms or ions, that is, which can give rise to atomic diffusion via defects.

Owen et al.⁶⁶ concluded from the so called "lateral" migration of Ag in a chalcogenide in contact with a conducting substrate that the

actinic radiation is absorbed within the photodoped layer close to the interface between the doped and undoped regions. This experiment indicated that electrons were an important factor in the process. They proposed a mechanism, based on a tarnishing reaction, in which the photodissolution occurs as a result of the photodeposition of Ag at the interface between the photodoped and undoped regions. The production of Ag at the interface will, however, be limited by the supply of electrons and can be represented by the equation



In As-S compounds the electronic properties are dominated by hole transport. It seems that free electrons are immediately trapped at defects, which in the case of S-rich films are likely to be 3-fold coordinated S atoms (referred to as C_3^+ centres). Therefore it is also likely that as soon as a positive Ag ion combines with an electron at a C_3^+ centre to form metallic Ag, it will spontaneously react with the S atom to form an Ag-S bond. Further reaction would probably then take place resulting in the formation of an homogeneous Ag-As-S compound. A similar experiment, carried out by Wagner et al.,⁶⁷ demonstrated also that the illumination at the undoped/photodoped interface controls the "lateral" photodissolution process.

Rennie et al.⁶⁸ noted that the spectral dependence of the observed doping rates and induction periods were closely related to the absorption spectrum of the Ag-containing chalcogenide and suggested that absorption in that part of the system is the limiting step for the photodoping rate. Their proposed mechanism for GeSe_2 samples was that there is a fast thermal reaction, independent of illumination which leads to a small amount of Ag metal being incorporated in the GeSe_2 . The dissolved Ag might, for example, occupy interstitial sites in the reaction product, instead of being incorporated substitutionally into the network, and is highly mobile. It is light absorbed by this interstitial Ag at the GeSe_2 /product interface that stimulates the reaction with the GeSe_2 , thus leading to photodissolution. They assumed that this thermal reaction is faster than photodissolution at room temperature but they did not know the nature of this reaction between the Ag metal and the Ag-photodoped product. To explain the effect of illumination, they proposed that the conduction and valence bands in

GeSe₂ are bent near the GeSe₂/product interface, as proposed by Kokado et al. for the Ag/As₄₀S₆₀ reaction. This band bending is shown schematically in figure 3.4. Light absorbed at the interface produces photo-carriers, which then separate due to the band bending. The photo-electrons move into the GeSe₂ where they are quickly trapped, while the holes stay in the product layer. This leads to a charge separation, which will increase until the electrostatic forces balance the band bending. The holes in the product layer react with the interstitial Ag to produce Ag ions, which are attracted towards the GeSe₂ where they react, thus increasing the size of the product layer. Note that light will of course be absorbed at sites other than the GeSe₂/product interface, but only at this point will the photo-carriers separate and cause efficient photodissolution.

Another model has been put forward by Kluge,⁶⁹ who considers the process as a radiation-enhanced solid state reaction. The reaction kinetics are believed to be governed by two physical processes: a) the generation of electrons and Ag (or Cu) ions at the Schottky barrier originating at the metal-chalcogenide interface and b) the transport of the electrons and metal ions through the Ag (or Cu) containing chalcogenide. According to Kluge the formation of this compound is a three dimensional intercalation reaction. The intercalation product possesses a high ionic conductivity after the Ag (or Cu) reaches a percolation threshold concentration. The percolation mechanism is responsible for the occurrence of the step-like doping profile. Both a) and b) are stimulated by absorption of light, which penetrates to the electrons and metal ions at the Schottky barrier. The light absorption within the bulk of the doped chalcogenide supplies free photo-electrons which have to maintain charge neutrality during the cation migration and which are necessary for insertion of the cation into the amorphous network. The insertion is based on the capability of the chalcogen to form C₁⁻ centres and the appearance of C₁⁻M⁺ (M=Ag or Cu) ionic bonds within the amorphous chalcogenide. As a result, a new compound, the intercalation product, is formed with new C₁⁻M⁺ bonds. The possible number of such bonds at thermodynamic equilibrium is much higher than the number of D⁺D⁻ centres and therefore the model can account for the observed maximum

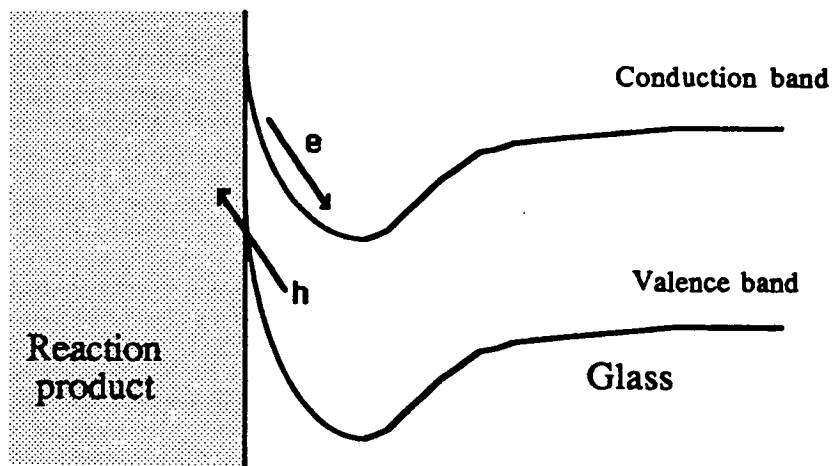


Figure 3.4. Bending of the conduction and valence bands in $As_{40}S_{60}$ near the $As_{40}S_{60}/Ag$ -photodoped interface, as proposed by Kokado et al.⁶⁰

concentration of about 1.5×10^{22} Ag atoms/cm³.

Recently, Elliot⁷⁰ proposed a theoretical model based on the combined transport of ionic and electronic charge carriers during the photodissolution process. The author suggested that the site of the absorption of the actinic light is determined by the sign of the dominant electronic (photo) carriers in the photodoped layer.

3.4. Summary

As seen from the present review, despite over two decades of investigation of the metal-photodissolution effect, no completely satisfactory mechanism has been put forward. In addition, there are many inconsistencies in the experimental results reported in the literature. This is partly due to the variety of experimental techniques used and material systems examined, and partly due to the complexity of the effect and its dependence on many variables, such as light intensity and wavelength, temperature, chalcogenide composition, and film deposition conditions. This range of different results obtained is reflected in a variety of models proposed for the effect. The two important fundamental questions which remain unresolved are: the location the actinic light which is efficient for producing the photodissolution effect is absorbed and the dissolution-limiting step. However, most of the authors agree on the following findings:

1- The reaction consists of three stages for the Ag/As₄₀S₆₀ system: an induction period, a period of constant rate and a period in which the rate falls to zero. There is also general agreement that the photodoping process consists of two stages for Ag₂Se/Ge-Se systems. The first stage is the photo-enhanced interface reaction, which has a rate proportional to the light intensity. The second stage is the photo-enhanced transport of Ag, which has a rate proportional to the cube root of the light intensity.³⁸

- 2- The concentration of Ag in the photodoped region of the chalcogenide is uniform and falls abruptly to zero at the boundary with the undoped material.
- 3- The amount of Ag which can be photodissolved into As-S films is large and >30 atomic%.
- 4- The Ag is co-ordinated to the chalcogen atoms in the photodoped product.
- 5- The amorphous state of the As-S film is maintained after photodoping.
- 6- Metal-photodissolution causes the conductivity of the As-S glasses to increase by several orders of magnitude.
- 7- Metal-photodissolution causes the optical transmission and the optical gap of the As-S glasses to decrease.

References

1. Gurevich S.B., Ilyashenko N.N., Kolomiets B.T., Lyubin V.M. and Shilo V.P., *Phys. Stat. Sol. (a)*, vol. 26, p. K127, 1974.
2. Nagai H., Yoshikawa A., Toyoshima Y., Ochi O. and Mizushima Y., *Appl. Phys. Lett.*, vol. 28, p. 145, 1976.
3. Vlcek M., Frumar M., Kubovy M., and Nevsimalova V., *J. Non-Cryst. Solids*, vol. 137-138, p. 1035, 1991.
4. Utsugi Y. and Zembutsu S., *Appl. Phys. Lett.*, vol. 27, p. 508, 1975.
5. Kostyshin M.T., Mikhailovskaya E.V. and Romenko P.F., *Sov. Phys. Solid State*, vol. 8, p. 451, 1966.

6. Kolobov A.V., Elliot S.R., *Advances in Physics*, vol. 40, p. 625, 1991.
7. Yoshikawa A., Ochi O. and Mizushima Y., *Appl. Phys. Lett.*, vol. 36, p. 107, 1980.
8. Hugget P.G., Frick K. and Lehman H.W., *Appl. Phys. Lett.*, vol. 42, p. 592, 1983.
9. Yamaguchi M., Shimizu I. and Inoue E., *J. Non-Cryst. Solids*, vol. 47, p. 341, 1982.
10. Chang M.S. and Chen J.T., *Appl. Phys. Lett.*, vol. 33, p. 892, 1978.
11. Goldschmidt D. and Rudman P.S., *J. Non-Cryst. Solids*, vol. 22, p. 229, 1976.
12. Yaji T. and Kurita S., *Jap. J. of Appl. Phy.*, vol. 22, p. 400, 1983.
13. Sharlandjiev P., Stoykova J. and Todorov T., *Opt. Commun.*, vol. 24, p. 67, 1978.
14. Konan K., Galibert G. and Calas J., *Phys. Stat. Sol.(a)*, vol. 107, p. 273, 1988.
15. Firth A.P., Ewen P.J.S. and Owen A.E., *J. Non-Cryst. Solids*, vol. 77/78, p. 1153, 1985.
16. Konan K., Elghrandi R.R., Galibert G. and Calas J., *J. Non-Cryst. Solids*, vol. 116, p. 63, 1990.
17. Mizuno H., Tanaka K. and Kikuchi M., *Sol. Stat. Commun.*, vol. 12, p. 999, 1973.
18. Kolobov A.V., Kolomiets B.T., Lyubin V.M. and Ioffe A.F., *Sol. Stat. Commun.*, vol. 54, p. 379, 1985.

19. Wagner T., Frumar M. and Benes L., *J. Non-Cryst. Solids*, vol. 90, p. 517, 1987.
20. Rennie J.H.S., Ph.D. Thesis, Jesus College, Cambridge, 1986.
21. Shirakawa T., Shimizu I., Kokado H. and Inoue E., *Photogr. Sci. Eng.*, vol. 19, p. 139, 1975.
22. Yoshikawa A., Ochi O., Nagai H. and Mizushima Y., *Appl. Phys. Lett.*, vol. 29, p. 677, 1976.
23. Lis S.A. and Lavine J.M., *Appl. Phys. Lett.*, vol. 42, p. 675, 1983.
24. Buroff A. and Baeva R., in *Proc. VI Int. Conf. Am. Semiconductors*, Leningrad, 1985.
25. Wagner A. and D.Barr D., in *Proc. Electrochem. Soc. (Symp. Inorg. Resist. Syst.)*, vol. 82, p. 281, 1982.
26. Leung W., Cheung N. and Neureuther A.R., *Appl. Phys. Lett.*, vol. 46, p. 543, 1985.
27. Plocharski J., Przyluski J. and Wycislik H., *J. Non-Cryst. Solids*, vol. 56, p. 325, 1983.
28. Blachnik R. and Wickel U., *z. Naturforsch*, vol. 85b, pp. 1268-1271, 1980.
29. Kawamoto y., Agata M. and Tsuchihashi S., *Yogyo-Kyokai-Shi*, vol. 82(9), p. 502, 1974.
30. Golovach I., Gerasimenko V.S., Silvka V.Y., Dovgoshei N.I., Bogdanova A. V. and Golovei M.I., *Fizika i Khimya Stekla*, vol. 3, p. 463, 1977.
31. Firth A.P., Ewen P.J.S. and Owen A.E., *J. de Phys. (Colloq. C4)*, vol. 42, p. 903, 1981.

32. Yamamoto Y. and Tadatsugu I., *J. Appl. Phys.*, vol. 47(8), p. 3603, 1973.
33. Goldschmidt D., Bernstein T. and Rudman P.S., *Phys. Stat. Sol. A*, vol. 41, p. 283, 1977.
34. Inoue E., Kokado H. and Shimizu I., in *Proc. 5th Int. Conf. on Solid State Devices (Suppl. to J. Japan Soc. of Appl. Phys. pp. 101 Vol. 43 1974)*, Tokyo, 1973.
35. Matsuda A. and Kikuchi M., *Proc. 4th Conf. on Solid State Devices (Suppl. to J. Japan Soc. of Appl. Phys. Vol.42 p.239 1973)*, Tokyo, 1972.
36. Kolwicz K. D. and Chang M.S., *J. Electrochem. Soc. Solid State*, vol. 127, p. 135, 1980.
37. Buroff A., Nebauer E. and Suptitz P., *Phys. Stat. Sol. A*, vol. 48, p. 109, 1978.
38. Yamamoto Y., Itoh T., Hirose Y. and Hirose H., *J. Appl. Phys.*, vol. 47, p. 3603, 1976.
39. Suzuki T., Hirose Y. and Hirose H., *Phys. Stat. Sol. A*, vol. 72, p. 165, 1982.
40. Balasubramanyam K., Chen L.J. Ruoff A.L. and Wolf E.D., *J. Appl. Phys.*, vol. 53, p. 5975, 1982.
41. Singh B. and Chopra K.L., *J. Appl. Phys.*, vol. 52, p. 428, 1981.
42. Bourne L.C., Rowland S.C. and Bienenstock A., *J. de Phys. Colloq, C4*, vol. 42, p. 951, 1981.
43. Ueno T., *Japan. J. Appl. Phys.*, vol. 22, p. 1469, 1983.
44. Ueno T. and Odajima A., *J. de Phys. Colloq. C4*, vol. 42, p. 899, 1981.

45. Zembutsu S., *Appl. Phys. Lett.*, vol. 39, p. 969, 1981.
46. DeNeufville J. P., "Amorphous and Liquid Semiconductors", in *Proc. 5th Int. Conf.*, ed. Stuke, J. and Brenig W., Taylor and Francis, London, Garmisch-Parkenkirchen, Germany, 1976.
47. Salik J. and Nadiv S., *Phys. Stat. Sol. (a)*, vol. 38, p. 177, 1976.
48. Holmquist G.A. and Pask J.A., *J. Americ. Ceram. Soc.*, vol. 62, p. 183, 1979.
49. Shimizu I., Sakuma H., Kokado H. and Inoue E., *Bull. Chem. Soc. of Japan*, vol. 46, p. 1291, 1973.
50. Shimizu I., Ikeda T. and Inoue E., *Preprint Int. Congress Photogr. Sci.*, p. 235, Rochester, New York, 1978.
51. Firth A.P., *Ph.D. Thesis*, University of Edinburgh, 1985.
52. Steel A.T., Greaves G.N., Firth A.P. and Owen A.E., *J. Non-Cryst. Solids*, vol. 107, p. 155, 1989.
53. Shimizu I., Sakuma H., Kokado H. and Inoue E., *Photogr. Sci. Eng.*, vol. 16, p. 291, 1972.
54. Plocharski J., Przyluski J. and Teodorczyk M., *J. Non-Cryst. Solids*, vol. 93, p. 303, 1987.
55. Hajto E., Belford R., Ewen P.J.S. and Owen A.E., *J. Non-Cryst. Solids*, vol. 137-138, p. 1039, 1991.
56. Kolobov A.V., Elliot S.R. and Taguirdzhanov M.A., *Phil. Mag. B*, vol. 41, p. 9913, 1990.
57. Danko V.A., Indutny I.Z. and Minko V.I., *Proc. of the Int. Conf. on Non-Cryst. Semicond.*, vol. 2, p. 234, Uzhgorod, 1989.
58. Kim D.Y., Onari S. and Arai T., *Jap. J. Appl. Phys.*, vol. 28, p. 965, 1989.

59. Ishikawa R. and Kikuchi M., *J. Non. Cryst. Solids*, vol. 35-36, p. 1061, 1980.
60. Kokado H., Shimizu I. and Inoue E., *J. Non-Cryst. Solids*, vol. 20, p. 131, 1976.
61. Ishikawa R., *Solid. Stat. Commun.*, vol. 30, p. 99, 1979.
62. Street A. and Mott N.F., *Phys. Rev. Lett.*, vol. 35, p. 1293, 1979.
63. Janai M., *Phys. Rev. Lett.*, vol. 47, p. 726, 1981.
64. Janai M., in *Proc. of the symposium on inorganic resist systems*, ed. Doane D.A. and Heller A. (The Electrochem. Soc., Inc.), p. 239, Montreal, 1983.
65. Malinowski J. And Buroff A., *Contemp. Phys.*, vol. 19, p. 99, 1978.
66. Owen A.E., Firth A.P. and Ewen P.J.S., *Phil. Mag.*, vol. B52, p. 347, 1985.
67. Wagner T., Frumar M. and Suskova V., *J. Non-Cryst. Solids*, vol. 128, p. 197, 1991.
68. Rennie J.H.S. and Elliot S.R., *J. Non-Cryst. Solids*, vol. 77/78, p. 1161, 1985.
69. Kluge G., *Phys. Stat. Sol. (a)*, vol. 101, p. 105, 1987.
70. Elliot S.R., *J. Non-Cryst. Solids*, vol. 130, p. 85, 1991.

CHAPTER 4

KINETICS OF THE PHOTODISSOLUTION PROCESS

4.1. Introduction

Photo-induced effects in chalcogenide glasses are of considerable technological importance, having applications in optical imaging, hologram recording and optical mass memories.¹⁻⁴ Photosensitive chalcogenide systems also have potential as photo-resists for microlithography in the fabrication of integrated circuits,⁵ and as some effects can be stimulated by X-rays and electron beams, as well as by light, very high resolution can be achieved. Of these effects, metal-photodissolution is probably the most useful since it produces the largest change in the properties of the chalcogenide, particularly the etch resistance and optical constants.

A knowledge of the kinetics of the photodissolution process is essential both to understanding the mechanism of the effect and to exploiting its application, since the speed of image formation in these systems is mainly governed by the photodissolution rate. In this chapter I will outline two of the main application areas for the effect (VLSI lithography and the fabrication of IR optical elements) and review the factors influencing the photodissolution rate.

4.2. Chalcogenide photo-resists

Interest in inorganic resist systems based on amorphous chalcogenide semiconductors was initially stimulated by their potential to extend photolithography into the submicron region.⁵ In terms of resolution capability and linewidth control the performance of these systems matches that of organic resists and they are compatible with industry-standard processing techniques, such as plasma-etching and spin-coating.⁶ They can be used as resists for X-ray, e-beam, ion-beam or deep-UV exposure, with an expected resolution capability of 0.3 μm in the last case. Because chalcogenide glasses can be deposited by vacuum evaporation very thin, uniform films are obtainable, which makes these materials particularly suitable for multilevel resist techniques for producing chromium photomasks and also for ion-beam lithography.

The most extensively studied chalcogenide resist system is $\text{Ag}_2\text{Se}/\text{Ge-Se}$ in which the basis of image formation is the metal photodissolution effect. The concept of using chalcogenide glasses, such as those in the Ge-Se system, as resists for microelectronics was first reported in 1976 by Yoshikawa et al.⁷ In a series of articles, they demonstrated that these inorganic resist systems have both high contrast and high resolution.^{8, 9} One micron features were well defined using optical contact printing methods, and submicron features were generated using e-beam exposure systems.⁹

Most studies of Ag/As-S resists have used amorphous $\text{As}_{40}\text{S}_{60}$ as the chalcogenide film. The compound $\text{As}_{40}\text{S}_{60}$ is commercially available in bulk glassy form and it has the additional advantage that as a prototype amorphous material it has been extensively studied, so that a considerable amount of information on its properties exists.¹⁰ Since 1978, Chang and co-workers have studied $\text{As}_{40}\text{S}_{60}$ resists extensively, using optical and X-ray exposure systems.¹¹⁻¹³ They were the first to report the dry development of an $\text{As}_{40}\text{S}_{60}$ -based resist using a CF_4 plasma process. A maximum etch rate ratio of 1.8:1 between the unexposed and exposed films was obtained prior to photodoping but Ag-photodoped $\text{As}_{40}\text{S}_{60}$ was found to have a much slower etch

rate in the CF_4 plasma. In an attempt to combine the Ag halide technology well known to the photographic industry with the newly developed chalcogenide resist technology to yield higher sensitivity and resolution, they overcoated their $\text{As}_{40}\text{S}_{60}$ films with AgCl and fabricated grating patterns of 12 μm period from both $\text{As}_{40}\text{S}_{60}$ and AgCl/ $\text{As}_{40}\text{S}_{60}$ samples.¹² The Ag-halide/chalcogenide-glass combination was also used as an X-ray resist and was found to be about twice as sensitive as PMMA for this type of exposure. An $\text{As}_{40}\text{S}_{60}$ film 300 nm thick was first evaporated, then a layer of AgCl 20 nm thick was evaporated on top of the $\text{As}_{40}\text{S}_{60}$ film. A pattern consisting of 6 μm lines was generated in this bi-layer sample by X-ray lithography.¹³ Chang has also used a pulsed electric field to enhance the sensitivity of these materials.¹⁴

To demonstrate the high resolution achievable with chalcogenide photoresists, a submicron (0.35 μm) optical grid was produced in $\text{As}_{40}\text{S}_{60}$ using a holographic illumination method.¹⁵ The thicknesses of Ag and $\text{As}_{40}\text{S}_{60}$ used were 30 nm and 500 nm respectively. The light intensity was $\sim 100 \text{ mW/cm}^2$ and the time of illumination 60-120 s, the illumination source being a cw-argon ion laser.

The structural studies carried out by Firth et al.¹⁶ using Raman spectroscopy indicated that for the best resolution the composition of the As-S film should be close to $\text{As}_{33}\text{S}_{67}$ since on photo-doping such samples will yield a single-phase homogeneous material. They also found that the Ag/ $\text{As}_{30}\text{S}_{70}$ system is compatible with both plasma and wet-chemical etching and produced a grating pattern using a conventional holographic technique¹⁷ with an Ar-ion laser as the illumination source. The thicknesses of the $\text{As}_{30}\text{S}_{70}$ and Ag films were 300 and 100 nm respectively. For generating test patterns, they also used a UV wafer stepper (Eaton Optimetrix 8010), typical exposure times for an incident intensity of 150 mW/cm^2 being 3-4 s.

The main disadvantage of these inorganic resists, compared with conventional organic resists, is that they are typically up to 5 times less sensitive,¹² the sensitivity of these resists being basically determined by the rate of the metal-photodissolution process. Various approaches, therefore, have been used to speed up image formation in these

materials (e.g. varying the glass composition or applying an electric field)¹⁸ but have produced only a small improvement in the rate. A detailed review of these approaches will be given in section 4.4.

4.3. The fabrication of IR optical elements

Chalcogenide glasses are well known IR transmitting materials, having pass bands (depending on composition) from the visible to beyond 15 μm , and have been employed in producing IR elements such as filters, windows and fibres.^{19, 20} By making use of the photo-induced effects mentioned in previous chapters, it is possible to produce embedded or surface-relief structures in chalcogenide films that can be used as IR diffractive elements. Such elements have several potential uses, for example in beam combining, filtering and spectral analysis, and also have advantages over conventional IR refractive elements (typically Ge lenses) as regards weight, cost and ease of manufacture.²¹ Photo-induced effects in chalcogenides (particularly photodarkening) have been used to fabricate holographic gratings (both phase and surface-relief types), so far for use at visible wavelengths.^{4, 22-24} Chang and Chen²⁵ applied a CF_4 plasma to produce grating patterns with a 6 μm linewidth in an $\text{As}_{40}\text{S}_{60}$ film 600 nm thick and measured the corresponding grating efficiencies as a function of etching time. The maximum grating efficiency was not more than 10%. As far as grating applications are concerned, the metal photodissolution effect is probably the most useful because it produces the largest change in the properties of the chalcogenide, particularly the refractive index²⁶ and etch resistance.¹⁶ Kostyshin et al.²⁷ were the first to report the fabrication of gratings using the metal-photodissolution effect. These gratings were recorded in $\text{Ag}/\text{As}_{40}\text{S}_{60}$ using argon-ion laser exposure at a wavelength of 488 nm. The diffraction efficiency was measured with a He-Ne laser at 632.8 nm and the best value obtained was 20%.

Zakery et al.²⁸ have carried out a theoretical analysis of transmissive gratings of the type likely to be produced by the metal photodissolution effect and have used this to predict diffraction efficiencies for devices made in the Ag/As₃₀S₇₀ system. For bulk diffractive devices with a rectangular modulation profile, predicted efficiencies in the multiwave regime were over 90% and in the volume regime could be as high as 100%, irrespective of the profile. Surface relief gratings with a rectangular profile yielded a maximum efficiency of at least 73%. Ewen et al.²⁹ fabricated bulk holographic gratings 1.5 μm thick, and reported a 30% diffraction efficiency at a wavelength of 1.5 μm for first diffraction orders.

For efficient operation IR elements must be relatively thick (of the order of several microns at least) and hence the depth to which the metal ions can photodope chalcogenide films is the main limitation for producing such IR elements. Inoue et al.³⁰ reported that in the case of the Ag/As₁₆S₈₀Te₄ combination, Ag penetrates at least 20 μm into the glass. This depth almost covers the range of thicknesses (6-23 μm) required for optimum performance of devices at 10.6 μm as predicted by Slinger et al.³¹ using coupled wave-theory. In the case of the Ag/As₄₀S₆₀ system, photodoping to a depth of 4 μm was observed by Ewen et al.²⁹ and the extrapolation of their results suggested that photodoping to a depth of at least 6 μm is possible. The maximum practicable depth is mainly governed by the rate of the photodissolution. There are various possibilities for improving the rate and these will be reviewed in the following sections.

4.4. Factors influencing the photodissolution rate

The speed of photodissolution is a crucial parameter for the applicability of the photodissolution process. Several avenues therefore have been tried to yield an increase in the photodissolution rate (e.g. varying the glass composition, applying an electric field or increasing the sample temperature during exposure). These avenues will be

reviewed in the following sections.

4.4.1. Composition dependence

The composition of the chalcogenide can affect the rate of photodissolution in one of two ways: the replacement of one type of chalcogen atom for another in an alloy of the same (stoichiometric) composition is one type of compositional change, and the change in composition away from stoichiometry is the other. For the first case, it has been observed by Yamaguchi et al.³² that for the As-S system, the photodoping rate is high compared to other chalcogenides. For the second case, Inoue et al.³⁰ have measured the dependence of the initial photodissolution rate on composition for As_2S_x films where $x=3$ to 18. The results show an increasing rate as x increases from 3 to 7, followed by a plateau region until $x=2$, after which the rate falls. The results show quite clearly that the initial part of the photodissolution process is strongly affected by the sulphur content of the As-S film.

Ewen et al.³³ showed that as the S content is increased above 60 atomic% the rate increases to a maximum around the composition $As_{33}S_{67}$ and then falls off. The maximum and minimum rates observed over the composition range studied differ by a factor of about two and the rate for $As_{33}S_{67}$ is clearly significantly higher than that for $As_{40}S_{60}$. They proposed that the peak in the photodissolution rate is due to a difference in the morphology of the photodoped product for compositions around $As_{33}S_{67}$ since these yield a homogeneous material on photodoping with Ag, in contrast to other compositions which yield a phase-separated mixture. The passage of electrons through the homogeneous product is likely to be faster than through phase-separated materials. Wagner et al.³⁴ found similar results. These authors studied the composition dependence in As-S samples containing from 60 atomic% to 80 atomic% S and found that the peak of the photodissolution rate occurs around $As_{30}S_{70}$.

4.4.2. Spectral dependence

Lavine et al.³⁵ have measured the wavelength dependence of the photodissolution process using an optical wedge technique. In this method a rectangular area of light is projected onto a sample, the horizontal axis of the rectangle being linear in wavelength whereas the vertical axis is a function of intensity. After a period of exposure a pattern is formed on the surface of the sample which represents the spectral sensitivity. Two sets of Ag/As₄₀S₆₀ film structures were used in the experiments, one consisting of 200 nm of Ag on 300 nm of As₄₀S₆₀ and the other, 5 nm of Ag on 50 nm of As₄₀S₆₀.

The sensitivity curves for the thinner sample are shown in figure 4.1 (a). Curve A is for illumination from the As₄₀S₆₀ side of the film and indicates that the photodissolution sensitivity is independent of the As₄₀S₆₀ absorption edge. The sensitivity curve is constant above 2.6 eV and only falls by an order of magnitude over the range 1.6-3 eV compared to a more than 3 orders of magnitude decrease in α over the same energy range. For illumination from the Ag side (curve B) the overall shape of the curve is the same, but the sensitivity is reduced by 1/2. The sensitivity curves for the thicker structure (200 nm Ag / 300 nm As₄₀S₆₀) are shown in figure 4.1(b). For illumination from the As₄₀S₆₀ side (curve A) the effect of optical absorption in the As₄₀S₆₀ film at energies above 2.6 eV is clearly seen. The As₄₀S₆₀ film is reducing the amount of light reaching the Ag/As₄₀S₆₀ contact area, which suggests that absorption of light within this interface region is important for photodissolution to occur. Illumination from the Ag side shows a similar sensitivity to the thinner sample (curve B, figure 4.1(a)) but there is a reduction in sensitivity due to the thicker Ag layer. It is clear from figure 4.1 (b), curve A, that when illumination is from the As₄₀S₆₀ side of the film the sensitivity is limited by the absorption edge of the chalcogenide. The As₄₀S₆₀ film thickness is therefore a useful parameter to vary to determine whether the dissolution rate is controlled by light absorbed in the bulk of the As₄₀S₆₀.

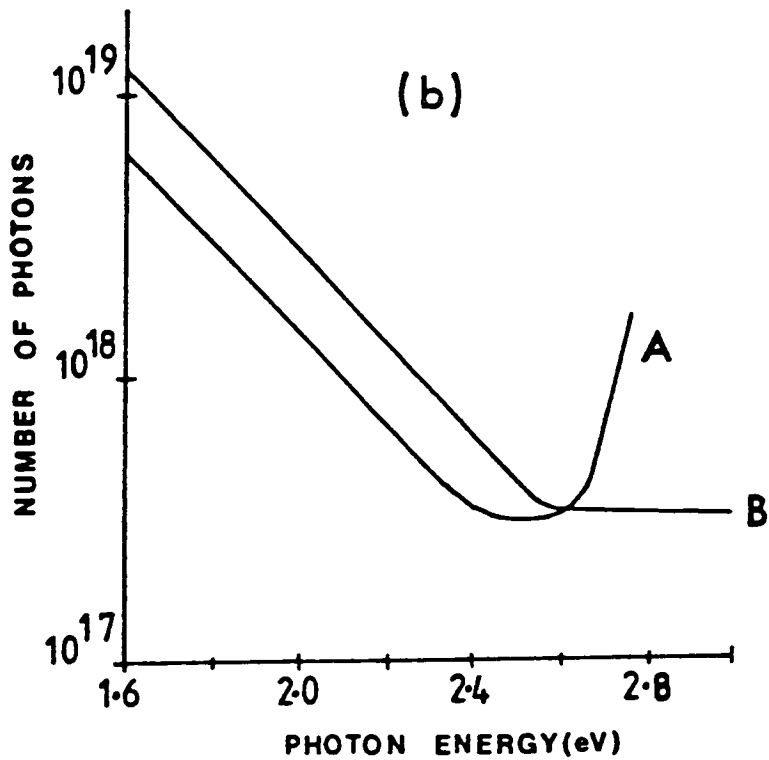
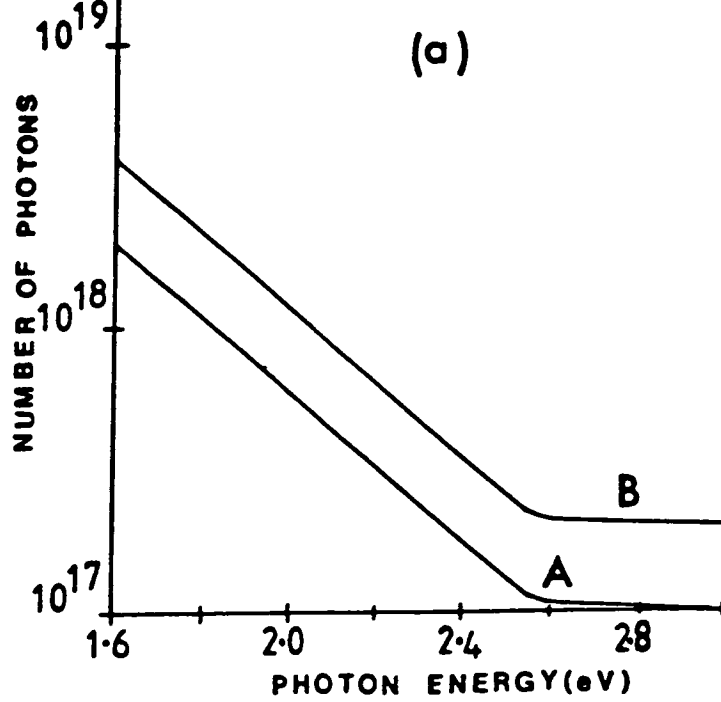


Figure 4.1. Number of photons required to generate a negative relief image as a function of photon energy. Figure (a) corresponds to 5 nm Ag on 50 nm As₄₀S₆₀ and figure (b) corresponds to 20 nm Ag on 300 nm As₄₀S₆₀. The curves A represents illumination from the As₄₀S₆₀ side and curves B from the Ag side.³⁵

Lis and Lavine³⁶ made extensive spectral measurements over the wavelength region 400-600 nm, that is from well above to well below the band gap of As₄₀S₆₀. While the sensitivity was greater at shorter wavelengths, they observed significant sensitivity at 800 nm where the absorption of As₄₀S₆₀ is negligible. In view of the fact that at small energies most of the photons were either reflected or transmitted through their samples, they prepared a three layer configuration to minimise the loss of photons. They deposited a relatively thick layer of Ag first, to act as a mirror and then tailored the thickness of the As₄₀S₆₀ to provide a minimum in the reflectivity, finally covering this with 10 nm of Ag. They obtained the highest sensitivity at 546 nm, whereas previously they always observed the peak sensitivity to be at higher energies. This suggested to them that absorption in the As₄₀S₆₀ was simply a loss mechanism and did not contribute at all to the photodoping. They concluded that the photons stimulating photodissolution are absorbed in the Ag and that only a few photons are responsible for the effect.

Goldschmidt and Rudman³⁷ have shown that if the effect is caused by light absorbed at the interface between the Ag and As₄₀S₆₀ then the rate of the initial part of the photodissolution process should be described by the rate equation

$$\text{rate} \propto I_0 e^{-\alpha d} \quad (4.1)$$

where α is the linear absorption coefficient, I_0 the light intensity at the As₄₀S₆₀ surface and d the thickness of the layer. Their experimental results do in fact show the dependence described by equation (4.1) and suggest that light absorbed in the vicinity of the Ag/As₄₀S₆₀ interface causes photodissolution.

Goldschmidt and Rudman³⁷ also measured the wavelength dependence of the linear part of the photodissolution kinetics (see stage 2 in figure 4.2) for two different As₄₀S₆₀ film thicknesses, 110 nm and 282.5 nm, deposited on top of a 30 nm thick Ag film. The results are shown in figure 4.3 and span the energy range 2.4 to 2.7 eV with a single measurement made at the He-Ne laser wavelength ($E = 1.96$ eV). Illumination was from the As₄₀S₆₀ film and the light

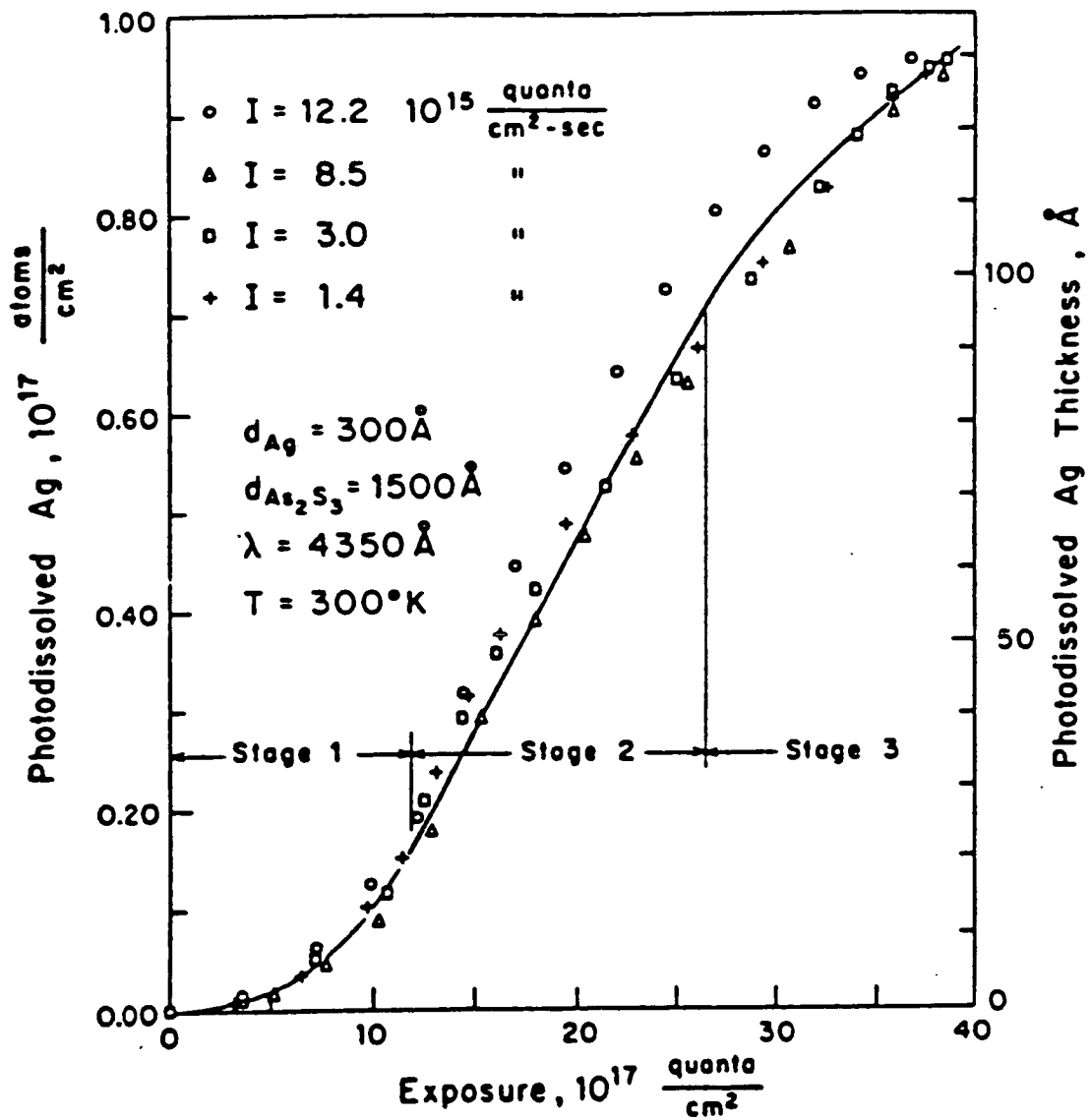


Figure 4.2. The exposure dependence of the amount of Ag photodissolved in $\text{As}_{40}\text{S}_{60}$ (exposure = intensity x time).³⁷

intensity was 10mW/cm^2 . For the thinner of the two samples the rate curve shows a steep rise from 2.4 eV to 2.7 eV, the value at 2.7 eV being 6 times the value at 2.4 eV. For the thicker sample, the curve peaks at ~ 2.7 eV, with the maximum value approximately half the value of the thinner sample at the same photon energy. The value for the photodissolution rate at the He-Ne laser energy was the same for both samples. The authors concluded that the photodissolution rate is proportional to the amount of light absorbed in the $\text{As}_{40}\text{S}_{60}$ film close to the $\text{As}_{40}\text{S}_{60}/\text{Ag}$ interface and that photo-electrons ejected from the Ag into the $\text{As}_{40}\text{S}_{60}$ play an important role.

Kokado et al.³⁸ have also measured the spectral sensitivity of the photodissolution process for different film thicknesses when illumination is from the chalcogenide side. Samples consisted of a combination of Ag and $\text{As}_{25}\text{S}_{75}$ and an optical wedge technique (described earlier) was used to measure the spectral sensitivity. Their results (figure 4.4) show that the short wavelength limit of the photodissolution sensitivity varies with the thickness of the chalcogenide. To analyse their results they used the following expression for the interband optical absorption coefficient, α

$$\alpha = k(h\nu - E_g)^2/h\nu \quad (4.2)$$

where k is a constant, $h\nu$ is the photon energy and E_g is the band gap of the $\text{As}_{25}\text{S}_{75}$ film. They suggest that if the photodissolution efficiency is independent of the incident photon energy then the intensity (I_{\min}) reaching the Ag/chalcogenide interface which produces the minimum detectable photodoping is given by

$$I_{\min} = I_0 e^{-k(h\nu^* - E_g)^2 d/h\nu} \quad (4.3)$$

where I_0 is the incident light intensity, d is the $\text{As}_{25}\text{S}_{75}$ film thickness, k is a constant and $h\nu^*$ is the short wavelength sensitivity limit. If the above suggestion is true then:

$$h\nu^* \propto (h\nu^*/d)^{1/2} \quad (4.4)$$

This was found to be the case, as shown in figure 4.5. These authors also considered the possibility that as photodissolution proceeds, a

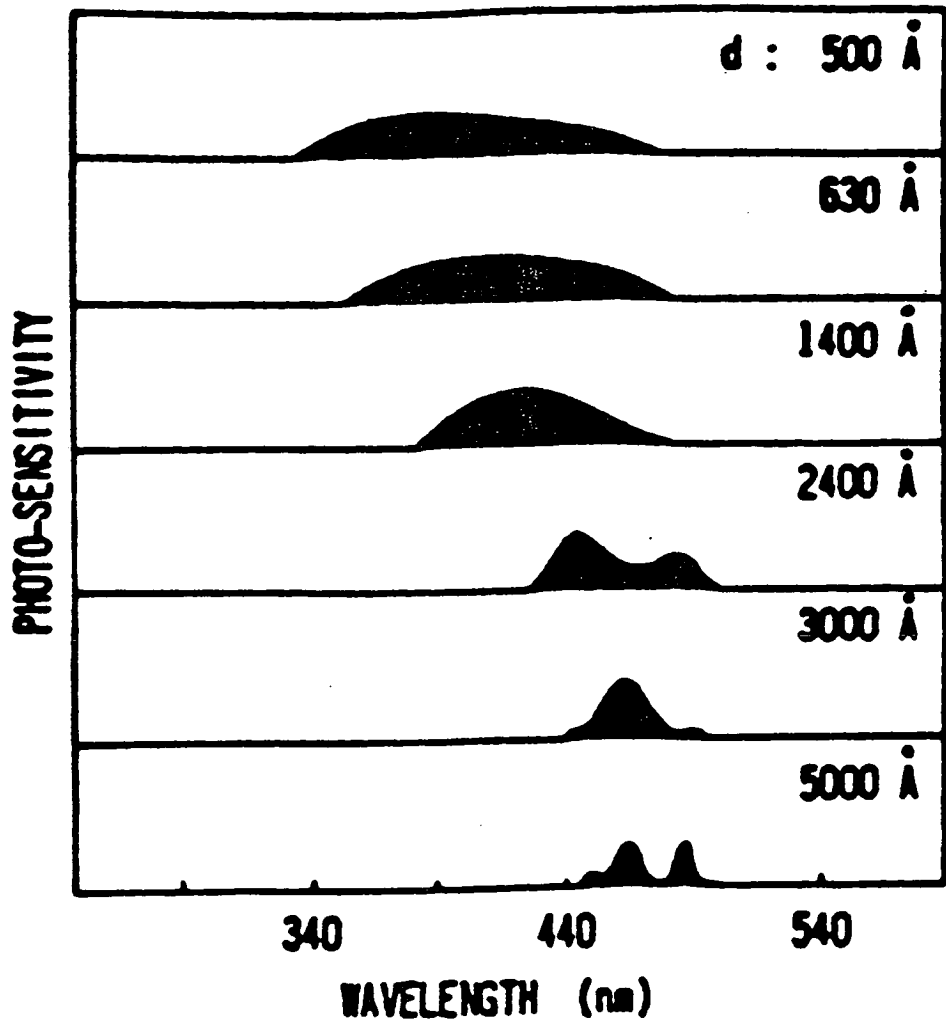


Figure 4.4. Spectral dependence of the photosensitivity in the case of the Ag/As₂₅S₇₅ system. The illumination is through As₂₅S₇₅ layers of thickness d . Multiple peaks seen in thick layers are due to interference and are not significant.³⁸

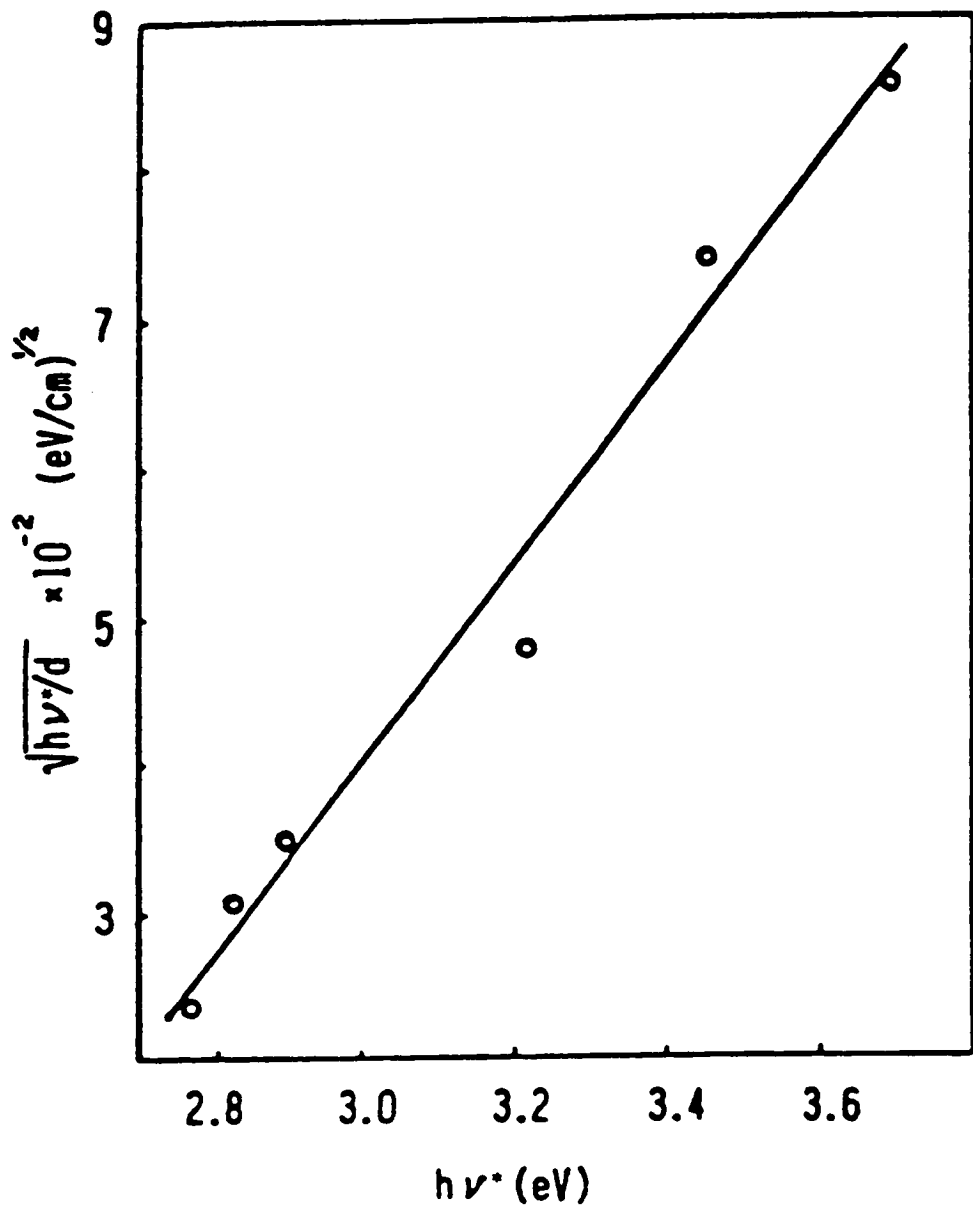


Figure 4.5. $(h\nu^*/d)^{1/2}$ versus photon energy, at the short-wavelength limit of photosensitivity shown in figure 4.4.³⁸

photodoped region is formed between the Ag and the chalcogenide, and furthermore that the photodoped region has an optical absorption edge which is shifted towards the red. They attempted to determine, using the optical wedge method, if absorption in the photodoped layer contributed to photodissolution. They measured the shift in the photosensitivity maximum with exposure (figure 4.6) and found it moved towards longer wavelengths. They concluded from these results that absorption in the Ag doped region contributes partly to further photodoping.

The sensitivity for the Ag/GeSe₂ system was found by Rennie and Elliot³⁹ to fall markedly for wavelengths longer than 600 nm. Although GeSe₂ is essentially transparent at 600 nm, the reaction is still fast at this wavelength. Since the absorption of photodoped GeSe₂ at 600 nm is significant, they suggested that the light stimulating photodoping is absorbed neither in the GeSe₂ nor in the Ag, but in the layer of Ag-photodoped GeSe₂.

4.4.3. Intensity dependence

Goldschmidt and Rudman³⁷ have studied the dependence of photodissolution rate on the intensity of the incident light. They reported that the induction period is inversely proportional to the illumination intensity and is observed independently of whether the sample is illuminated from the Ag or the As-S side.

Firth⁴⁰ studied the effect of light intensity on the photodissolution rate for the Ag-As₃₀S₇₀ combination. His results, plotted as the logarithm of reciprocal time (which represents the speed) versus the logarithm of incident light power, indicated a linear relation between intensity and photodissolution rate. The samples in these experiments were fabricated by first evaporating a Ag film 56 nm thick onto a glass slide and then an As₃₀S₇₀ film, with a thickness of 210 nm, on top of

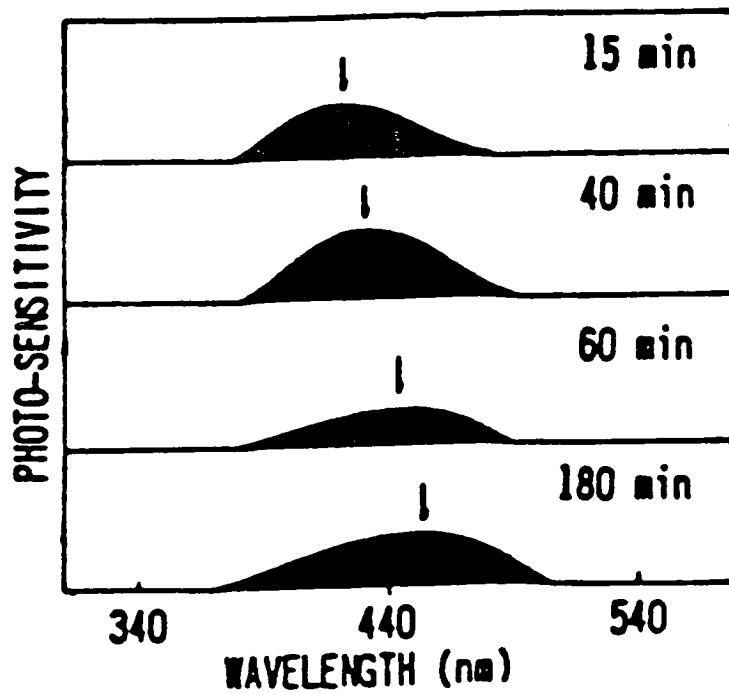


Figure 4.6. Shift of photosensitivity maximum (indicated by arrow) in the $\text{Ag}/\text{As}_{25}\text{S}_{75}$ system with exposure time. The sensitivity scale for the lower two spectrograms is reduced.³⁸

the Ag. The wavelength of the light used was 571.5 nm, with a power ranging from 4 - 50 mW.

Rennie and Elliot³⁹ studied the effect of light intensity on photodoping rate for the Ag/GeS₂ system. Light of wavelength 600 nm and varying in intensity from about 1 to 5mW/cm² was used in these experiments. The photodoping rate was found to have a sub-linear dependence on light intensity. A sub-linear dependence was also reported for the photodissolution of Zn into As₄₀S₆₀.⁴¹

Wagner and Frumar³⁴ found for the Ag/As₄₀S₆₀ combination that an increase in illumination intensity causes a decrease of the induction period and an increase in photodoping rate. The increase in intensity from 4 to 10 mW/cm² produced almost a factor of two increase in the photodoping rate. Their explanation was that the illumination provides the energy necessary for overcoming the thermodynamic barrier for the creation of the doped phase. In addition, intense illumination speeds up the polymerization and homogenisation which occurs in as-evaporated As₄₀S₆₀ layers.⁴²

4.4.4. The dependence on pre-history

Matsuda and Kikuchi¹⁸ have reported that if the As₄₀S₆₀ film is photodarkened prior to the deposition of the Ag film then the rate of photodissolution is enhanced. Lavine et al.³⁵ have measured the photodissolution rate of Ag into pre-annealed As₄₀S₆₀ films and found an increase of approximately an order of magnitude compared to the as-deposited film.

A more quantitative investigation has been carried out by Yaji and Kurita,²⁴ who compared the photodissolution rates for As₄₀S₆₀ films which were as-evaporated, annealed or pre-exposed. The method used to measure the photodissolution rates was to monitor the resistance change of a thin Ag strip as it photodissolved. In their

experiments the $\text{As}_{40}\text{S}_{60}$ films were annealed in the dark and in an N_2 atmosphere at $170\text{ }^\circ\text{C}$ for 1hr; the exposed films were produced by illumination with a 500 W high pressure Hg lamp through an IR-cut filter for half an hour. The samples consisted of 20 nm of Ag deposited on $1\text{ }\mu\text{m}$ of $\text{As}_{40}\text{S}_{60}$. The exciting light intensity was regulated at 5.8 mW/cm^2 and the illumination was through the Ag layer. They found that the largest dissolution rate occurred in pre-exposed annealed films and it was three times higher than the rate for as-deposited films. The value for the annealed film was approximately twice the value for the as-deposited film. They speculated that the photodissolution rate is dependent on the magnitude of the optical absorption in the film. This absorption increases with light exposure, so that more photocarriers are generated in the pre-exposed film than in the annealed or as-evaporated film.

Chatani et al.⁴³ reported that the photodoping rate depends very little on photo- or thermo-structural transformations in the film, and also that photo-oxidised $\text{As}_{40}\text{S}_{60}$ is insensitive to Ag doping. The sample configuration used in their experiments consisted of a thin Ag film 18 nm thick deposited on a 170 nm $\text{As}_{40}\text{S}_{60}$ film. The $\text{As}_{40}\text{S}_{60}$ film was annealed in vacuum (3×10^{-6} torr) at $170\text{ }^\circ\text{C}$ for 20 minutes. The pre-exposure of the film was carried out in vacuum for 14 hours using a high pressure Hg lamp and for one hour using a low pressure Hg lamp. Pre-exposure was also performed in air for 14 hours with a high pressure Hg lamp and for 50 minutes with a low pressure Hg lamp. The photo-oxidation of $\text{As}_{40}\text{S}_{60}$ was found to be enhanced more by illumination with the low pressure Hg lamp (using a wavelength of 254 nm) than with the high pressure lamp (using a wavelength of 366 nm). Ag was photodissolved into the $\text{As}_{40}\text{S}_{60}$ by illumination with monochromatic light (380 nm, 4.2 mW/cm^2) from the substrate side.

4.4.5. Dependence on the metal-ion source

Ewen et al.³³ investigated the effect on the photodissolution process in $\text{As}_{33}\text{S}_{67}$ of using Ag-Cu alloys as the metal source instead of pure Ag. They found that the rate increases gradually as the Cu content is increased, the rate for $\text{Ag}_{74}\text{Cu}_{26}$ being 12 % larger than that for pure Ag. They also observed that for a pure Ag source the photodissolution rate is dependent on the Ag layer thickness. Keeping the $\text{As}_{33}\text{S}_{67}$ film thickness constant at 400 nm, they varied the Ag film thickness from about 50 nm to 400 nm. Their results showed that below 140 nm the rate decreases significantly as the Ag layer thickness decreases, whereas above 140 nm the rate levels off as the Ag layer thickness is increased. They considered the possibility that this observation might be due to the changes which occur in the properties of metal films as their thickness is reduced below about 100 nm. In the case of Ag films, below about 40 nm the electrical conductivity starts to decrease and the optical constants change,^{33, 44} both of which effects may influence the photodissolution rate. For example, the decrease in the conductivity of the Ag film may affect the rate at which Ag ions or electrons are supplied for diffusion through the photodoped layer. However, it was concluded that such changes cannot account for these observations since the critical Ag thickness (~ 140 nm) is much greater than 40 nm.

In the case of Ag photodissolution into amorphous GeSe_2 films the rate has also been found to depend on Ag layer thickness³⁹ but in these experiments very thin Ag films were used and oscillatory behaviour was observed, which suggests an optical interference effect was responsible.

Mizuno et al.⁴⁵ observed that in the case of thermal-diffusion the diffusion rate of Cu atoms is larger than that of Ag atoms, while in the case of photo-diffusion the rate of Ag atoms is larger than that of Cu atoms.⁴⁶ They ascribed this observation to the difference in the transmission spectra between Cu and Ag films, since the transmittance of their Cu films decreased as the wavelength decreased below $0.57 \mu\text{m}$, whereas that for their Ag films increased. Thus in the case

of a Cu film, incident light in the wavelength region to which the photo-diffusion process is sensitive, is strongly absorbed and hardly reaches the interface between the Cu and the $\text{As}_{40}\text{S}_{60}$.

Kolobov and co-workers^{41, 47-49} showed that for illumination at elevated temperatures the photodoping of As-S samples with group II metals (Zn, Cd) is possible. They reported that Zn photodissolution is qualitatively similar to that of Ag but differs in several respects, in particular, it is characterised by a much greater value of the photodoping activation energy; it becomes faster as the arsenic content of the chalcogenide is increased; and it depends sublinearly on the light intensity.^{41, 48, 49}

Metal compounds can also be used as the metal-ion source, for example Chang and co-workers observed photodissolution in $\text{As}_{40}\text{S}_{60}$ samples overcoated with AgCl.¹² Lavine et al.³⁵ investigated the effect of using Ag_2S as an Ag source for photodoping $\text{As}_{40}\text{S}_{60}$ samples rather than pure Ag. The latter used evaporated Ag_2S films with thicknesses ranging from 10 to 40 nm, and observed two significant differences compared with the case for pure Ag: first, the speed with the Ag_2S source was slower by about an order of magnitude than that for pure Ag; secondly, at long wavelengths the $\text{Ag}_2\text{S}/\text{As}_{40}\text{S}_{60}$ combination exhibited an increase in sensitivity compared with $\text{Ag}/\text{As}_{40}\text{S}_{60}$. They explained these observations by assuming that short wavelength radiation is absorbed closer to the surface and only as the wavelength increases does the absorption occur within an interaction region at the $\text{Ag}/\text{As}_{40}\text{S}_{60}$ interface. These authors also studied another tri-layer system, consisting of 1 nm of Ag_2S evaporated on top of 50 nm of $\text{As}_{40}\text{S}_{60}$ with a further 10 nm of Ag evaporated on top of the Ag_2S layer. For this system they observed a spectral dependence similar to that for the $\text{Ag}_2\text{S}/\text{As}_{40}\text{S}_{60}$ system except that at the peak of the sensitivity the $\text{Ag}/\text{Ag}_2\text{S}/\text{As}_{40}\text{S}_{60}$ combination was about a factor of two faster than the $\text{Ag}_2\text{S}/\text{As}_{40}\text{S}_{60}$ combination.

Thin metallic coatings produced by dipping the chalcogenide into a solution of a metal compound are also effective sources. For example, Singh and co-workers⁵⁰ devised a chemical process, based on dipping thin films of $\text{As}_{40}\text{S}_{60}$ into an aqueous solution of Ag nitrate, to form a

thin layer of Ag_2S on $\text{As}_{40}\text{S}_{60}$. These authors used electron beam exposure to photodissolve the Ag_2S into the glass. This technique was later used by Petrova et al.⁵¹ who showed that it is possible to induce photodissolution of Ag_2S into $\text{As}_{40}\text{S}_{60}$ films with simple white light exposure.

4.4.6. The effect of an applied electric field.

Matsuda and Kikuchi¹⁸ found that the lateral photodissolution rate can be enhanced by an electric field. Their samples were prepared by first evaporating a film of SnO_2 over half of the surface of a glass slide and then evaporating an Ag strip along the central axis of the slide, spanning both the SnO_2 and glass areas. Finally, the whole surface was coated with $\text{As}_{40}\text{S}_{60}$ to produce the system shown schematically in figure 4.7. It was found that the enhancement occurs at the negative electrode side of the Ag strip, which is expected if the process depends on the transport of Ag^+ ions. Prior application of the electric field was also found to enhance subsequent photodissolution but the application of an electric field after photodissolution had finished produced no further effect.

Similar results have been obtained by Firth⁴⁰ but for transverse photodissolution. In these experiments the resistance method³⁷ was used for the rate measurement and a DC electric field was applied by using a transparent Au top electrode. The samples were fabricated with a first layer consisting of Ag strips 2 mm wide and 70 nm thick, on top of which was then deposited an As-S film, 250 nm thick, which was narrower than the substrate to allow electrical contact to be made to each end of the Ag strips. The top layer of the structure was a thin transparent film of Au. This was narrower than the As-S to prevent shorting of the Ag strips. It was found that applying a positive voltage to the top Au electrode slows down the process whereas applying a negative voltage speeds it up considerably (by a factor up to 2). It was also found that shorting the top Au electrode to the bottom Ag layer

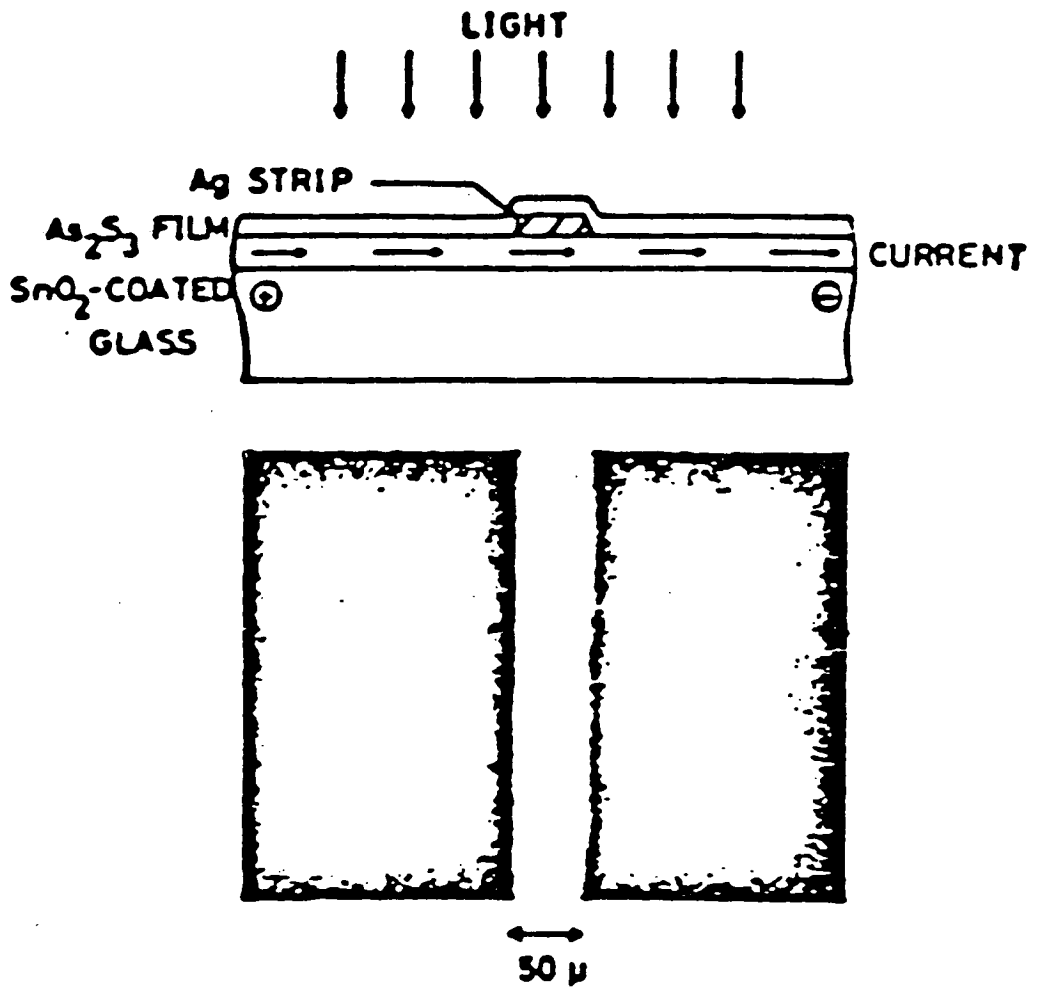


Figure 4.7. Sample configuration for electric field experiments and photograph showing the effect of the electric field on photodissolution.¹⁸

increased the speed of dissolution. The results are consistent with the contention that Ag^+ ions are mobile in photodoped films and play an important role in the photodissolution process. It was speculated that the increased dissolution rate that occurred when the sample was short circuited, is due to the supply of electrons, which would be kept constant by the short circuit.

4.4.7. The effect of temperature

It was established by Kostyshin and co-workers⁵² that the photodissolution process is highly sensitive to temperature. In one set of experiments²⁷ they heated $\text{Ag}/\text{As}_{40}\text{S}_{60}$ samples from room temperature up to 200 °C and found that the optimum sensitivity of their material was reached at approximately 80-100 °C. The difference between this optimum value and that at room temperature was approximately a factor of 2.

Mizuno et al.⁴⁵ studied the effect of temperature on the photodissolution of both Cu and Ag into disk samples of $\text{As}_{40}\text{S}_{60}$ with thicknesses in the range 0.6-1.0 mm. The temperature and light intensity used in these experiments were 120°C and 36mW/cm² respectively. From plots of the optical transmissivity of their sample at 0.8 μm versus time they showed that there is almost a factor of five difference between the photodoping rate at room temperature and that at 120 °C. They also found that at these higher temperatures Cu photodoping is faster by a factor of two than Ag photodoping.

Plocharski et al.⁵³ investigated the influence of temperature on the photodoping rate using the resistance method. The temperature range in this case was from 203 to 383 K and the illumination intensity was about 3.2mW/cm². Their results showed that there is approximately a factor of four difference between the photodoping rate at room temperature and that at 383 K. An Arrhenius plot for their data yields a straight line with a rather low value of 0.18 eV for the

activation energy which suggests a relatively weak temperature dependence for the process in the temperature range studied. However for the purely thermal doping process they obtained an activation energy of 1.5 eV.

Kolobov et al.⁴¹ studied the effect of temperature on the photodissolution of the second-group metal zinc. They found that the photostimulated dissolution of zinc is a thermally activated process, the activation energy being ~ 1.2 eV and practically independent of the light wavelength.

4.4.8. The dependence on substrate material

A series of experiments was carried out by Matsuda and Kikuchi¹⁸ in which they investigated the effect of a conducting substrate on the lateral photodissolution rate. The sample studied had the film structure described in section 4.4.6. Their results, reproduced in figure 4.8, show a significant lateral spreading of the Ag photodoped region when in contact with the conducting Au part of the substrate. Results for other conducting substrates are also shown in the figure. Firth⁴⁰ obtained the same result as Matsuda and Kikuchi,¹⁸ but noted that although the Au film plays a role in increasing the speed of photodissolution next to its surface, photodissolution normal to the film is not influenced by the Au layer.

4.4.9. The dependence on structure

Imura et al.⁵⁴ observed the photodoping of Ag into the cleaved surface of a single crystal of naturally occurring $\text{As}_{40}\text{S}_{60}$ (orpiment). These authors used both the resistance and Rutherford backscattering

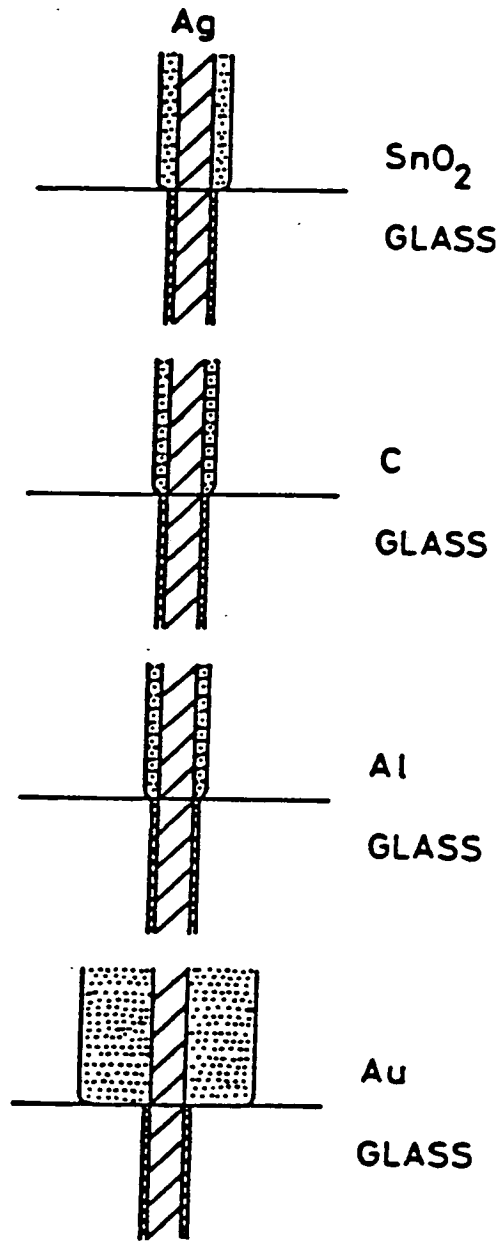


Figure 4.8. The dependence of the extent of lateral photodissolution dependence on different substrates.¹⁸

spectroscopy methods to monitor the photodissolution process. From their observations they deduced that the process does not require the photostructural changes observed uniquely in the amorphous phase. These photostructural changes, however, may exert an enhancing effect on the diffusion process, for the doping rate observed in the amorphous phase is larger by roughly two orders of magnitude than in the crystal. The difference in doping rate is not surprising because in general the diffusion coefficient in an amorphous semiconductor is larger by several orders of magnitude than in the crystalline form. On the other hand, the absorption coefficient of crystalline $As_{40}S_{60}$ is smaller than that of the amorphous phase by up to two orders of magnitude in the photon energy range from 2 to 3 eV.⁵⁵ Thus, if the crystal were to absorb photons as efficiently as the amorphous material, photodoping in it might proceed more quickly. Photodoping was not observed to occur in a film fabricated out of powdered orpiment even upon two month's illumination.⁵⁶ It was suggested that this was due to oxidation of the microcrystalline surface which was probably pronounced due to the grinding procedure used to produce the powdered crystal.

4.5. Conclusions

The review of factors influencing the photodissolution rate in the As-S system showed that the most effective factors in improving the rate are the As-S composition, temperature and light intensity. A detailed investigation of these factors might lead to a significant enhancement in the rate. The results of the present investigation into these factors are shown in Chapter 7 on the kinetics of the effect.

References

1. Shimizu I., Kokado H. and Inoue E., *Photogr. Sci. Engng.*, vol. 19, p. 136, 1975.
2. Shirakawa T., Shimizu I., Kokado H. and Inoue E., *Photogr. Sci. Eng.*, vol. 19, p. 139, 1975.
3. Asahara Y. and Izumitani T., *Phys. Chem. Glasses*, vol. 16, p. 29, 1975.
4. Bordogna J. and Keneman S.A., in *Holographic Recording Media*, ed. Smith H.M., p. 229, Berlin: Springer-Verlag, 1977.
5. Tai K.L., Ong E. and Vadimsky R.G., *Proc. Electrochem. Soc.*, vol. 9, p. 82, 1982.
6. Chern G.C. and Lauks, I., *J. Appl. Phys.*, vol. 54, p. 2701, 1983.
7. Nagai H., Yoshikawa A., Toyoshima Y., Ochi O. and Mizushima Y., *Appl. Phys. Lett.*, vol. 28, p. 145, 1976.
8. Yoshikawa A., Ochi O., Nagai H. and Mizushima Y., *Appl. Phys. Lett.*, vol. 29, p. 677, 1976.
9. Yoshikawa A., Ochi O., Nagai H. and Mizushima Y., *Appl. Phys. Lett.*, vol. 31, p. 161, 1977.
10. Mott N.F. and Davies E.A., in *Electronic processes in Non-Crystalline Materials*, Clarendon Press, Second Edition, Chap. 9, 1979.
11. Hou T.W. and Chang M.S., *Appl. Opt.*, vol. 18, p. 1753, 1979.
12. Chang M.S., Hou T.W., Chen J.T., Kolwicz K.D. and Zemel J.N., *J. Vac. Sci. Technol.*, vol. 16, p. 1973, 1979.
13. Kolwicz K. D. and Chang M.S., *J. Electrochem. Soc. Solid State*, vol. 127, p. 135, 1980.

14. Chang M.S., Hwang H.D. and Chen J.T., *9th Int. Conf. Proc. Electron and Ion Beam Sci. and Technol., ECS proceedings*, vol. 80-6, p. 407, 1980.
15. Hajto E. and Zentai G., *J. Non-Cryst. Solids*, vol. 90, p. 581, 1987.
16. Firth A.P., Ewen P.J.S., Owen A.E. and Huntley C.M., *Advances in Resist Technology and Processing II, SPIE 539*, p. 160, 1985.
17. Hariharan P., in *Optical Holography*, Chapter 12, Cambridge University Press, 1984.
18. Matsuda A. and Kikuchi M., *Proc. 4th Conf. on Solid State Devices (Suppl. to J. Japan Soc. of Appl. Phys. Vol.42 p.239 1973)*, Tokyo, 1972.
19. Savage J.A., in *IR Optical Materials and Their Antireflection Coatings*, p. 79, (Bristol: Adam Hilger), 1985.
20. Cimpl Z. and Kosek F., *J. Non-Cryst. Solids*, vol. 90, p. 577, 1987.
21. Close D.H., *Opt. Eng.*, vol. 14, p. 408, 1975.
22. Andreish A.M., Ponomar V.V., Smirnov A.V. and Mironos A.V., *Sov. J. Quantum Electronics*, vol. 16, p. 721, 1986.
23. Kase K., Chern G.C. and Lauks I., *Thin Solid Films*, vol. 116, p. L53, 1984.
24. Yaji T. and Kurita S., *J. Appl. Phys.*, vol. 54, p. 647, 1983.
25. Chang M.S. and Chen J.T., *Appl. Phys. Lett.*, vol. 33, p. 892, 1978.
26. Zakery A., Zekak A., Ewen P.J.S., Slinger C.W. and Owen A.E., *J Non-Cryst Solids*, vol. 114, p. 109, 1989.

27. Kostyshin M.I., Krashnojonov E.P., Makeev V.A. and Solobov G.A., *Appllication of Holography*, 1970. Eds.: Vienot J.C., Bulabois J. and Pasteur J. paper 11.7
28. Zakery A., Slinger C.W., Ewen P.J.S., Firth A.P. and Owen A.E., *J Phys. D: Appl. Phys.*, vol. 21, p. S78, 1988.
29. Ewen P.J.S., Slinger C.W., Zakery A., Zekak A., and Owen A.E., "Infrared and Optoelectronics Materials and Devices", in *SPIE Proc.*, vol. 1512, p. 101, 1991.
30. Inoue E., Kokado H. and Shimizu I., in *Proc. 5th Int. Conf. on Solid State Devices (Suppl. to J. Japan Soc. of Appl.Phys. pp. 101 Vol. 43 1974)*, Tokyo, 1973.
31. Slinger C.W., Zakery A., Ewen P.J.S. and Owen A.E., *Appl. Opti.*, vol. 31, p. 2490, 1992.
32. Yamaguchi M., Shimizu I. and Inoue E., *J. Non-Cryst. Solids*, vol. 47, p. 341, 1982.
33. Ewen P.J.S., Zakery A., Firth A.P. and Owen A.E., *Phil. Mag. B*, vol. 57, p. 1, 1988.
34. Wagner T. and Frumar M., *J. Non-Cryst. Solids*, vol. 116, p. 269, 1990.
35. Lavine J.M., Lis S.A., Goldberg G.M. and Masters M.I., *Proc. Electrochem. Soc.*, vol. 82, p. 265, 1982.
36. Lis S.A. and Lavine J.M., *Appl. Phys. Lett.*, vol. 42, p. 675, 1983.
37. Goldschmidt D. and Rudman P.S., *J. Non-Cryst. Solids*, vol. 22, p. 229, 1976.
38. Kokado H., Shimizu I. and Inoue E., *J. Non-Cryst. Solids*, vol. 20, p. 131, 1976.

39. Rennie J.H.S. and Elliot S.R., *J. Non-Cryst. Solids*, vol. 77/78, p. 1161, 1985.
40. Firth A.P., *Ph.D. Thesis*, University of Edinburgh, 1985.
41. Kolobov A.V., Kolomiets B.T., Lyubin V.M. and Ioffe A.F., *Sol. Stat. Commun.*, vol. 54, p. 379, 1985.
42. Nemanich R.J., Connell G.A.N., Hayes T.M. and Street R.A., *Phys. Rev. B.*, vol. 18, p. 6900, 1978.
43. Chatani K., Shimizu I., Kokado H. and Inoue E., *Jap. J. Appl. Phys.*, vol. 16, p. 389, 1977.
44. Heavens O.S., in *Optical Properties of Thin Solid Films*, Butterworth Scientific Publications, London, 1955.
45. Mizuno H., Tanaka K. and Kikuchi M., *Sol. Stat. Commun.*, vol. 12, p. 999, 1973.
46. Maruno S., Yamada T., Noda M. and Kondo Y., *Jap. J. Appl. Phys.*, vol. 10, p. 653, 1971.
47. Mizushima D. and Yoshikawa A., in *Amorphous Semiconductors Technologies and Devices*, ed. Hamakawa Y., p. 227, Tokyo-Amsterdam-N.Y. London, 1982.
48. Kolobov A.V. and Lyubin V.M., *Fiz. Tverd. Tela*, vol. 26, p. 2522, 1984.
49. Kolobov A.V. and Lyubin V.M., *Pisma v ZhTF*, vol. 11, p. 374, 1985.
50. Singh B., Beaumont S.P., Bower P.G. and Wilkinson D.W., *Appl. Phys. Lett.*, vol. 41(9), p. 889, 1982.
51. Petrova S., Simidchieva P. and Buroff A., in *Proc. of the Conf. "Amorphous Semiconductors"*, ed. Farhi-Vateva E. and Buroff A.T., p. 256, Gabiuro-Bulgaria, 1984.

52. Kostyshin M.T., *The Ukrainian Republican Conference on semiconductor thin films*, Udjgorod, "Naykova Dymka", Kiev, 1966.
53. Plocharski J., Przulski J. and Teodorczyk M., *J. Non-Cryst. Solids*, vol. 93, p. 303, 1987.
54. Imura T., Kubota K., Hiraki A. and Tanaka Ka., *J. Phys. Soc. Jap.*, vol. 52, p. 2459, 1983.
55. Mott N.F. and Davies E.A., in *Electronic processes in Non-Crystalline Materials*, p. 498, Clarendon Press, Seond Edtion, 1979.
56. Salik J. and Nadiv S., *Phys. Stat. Sol. (a)*, vol. 38, p. 177, 1976.

CHAPTER 5

EXPERIMENTAL TECHNIQUES

5.1. Introduction

This chapter describes the equipment and the different experimental procedures used to obtain the results in the present work. The experimental conditions and procedures can have a significant effect on the results obtained in these studies and it is likely that many of the inconsistencies in the literature arise from differences in experimental variables or sample preparation conditions.

The description of the experimental techniques has been divided into five main sections. The first two sections will be devoted to the procedures used in preparing the As-S, Ag and Cu films and the annealing pre-treatment of As-S films. The arrangements for measuring the photodissolution kinetics will be described in the third section. The fourth section is concerned with the methods used to obtain the optical constants and the final section deals with the SIMS technique.

5.2. Sample preparation

5.2.1. Substrates

The substrate is an important factor influencing the results and different substrates can be required for different types of experiment. Two different substrate materials (glass and NaCl) were used in this work depending on the type of experiment. Glass substrates, such as corning 7059 and microslides, were used for the measurements in the visible and near-IR spectral range and NaCl substrates for measurements in the middle/far-IR.

The cleanliness of the substrate affects the film thickness uniformity and the film adhesion to the substrate, therefore a thorough cleaning procedure was adopted: the substrates were initially rinsed in a solution of Teepol detergent and hot water and then, after rinsing in distilled water, were immersed in a solution of surface-active cleaning agent (Decon-90) and placed in an ultrasonic bath for a period of 30 minutes. Finally the substrates were rinsed in deionised water, dried with compressed nitrogen and placed in a dessicator for storage. The NaCl substrates were cleaned with a jet of compressed nitrogen.

5.2.2. Film preparation

As-S, Ag and Cu films were deposited by thermal evaporation. The evaporations were conducted in a vacuum chamber with an associated pumping system as shown in figure 5.1. The pumping system consisted of two pumps for two successive pumping stages: the rotary pump is used in the first stage to achieve a pressure of less than 10^{-2} torr and then the diffusion pump is used in the second stage to achieve a pressure of about 2×10^{-5} torr. The evaporation system was equipped with two boats: a tungsten boat was used to evaporate Cu

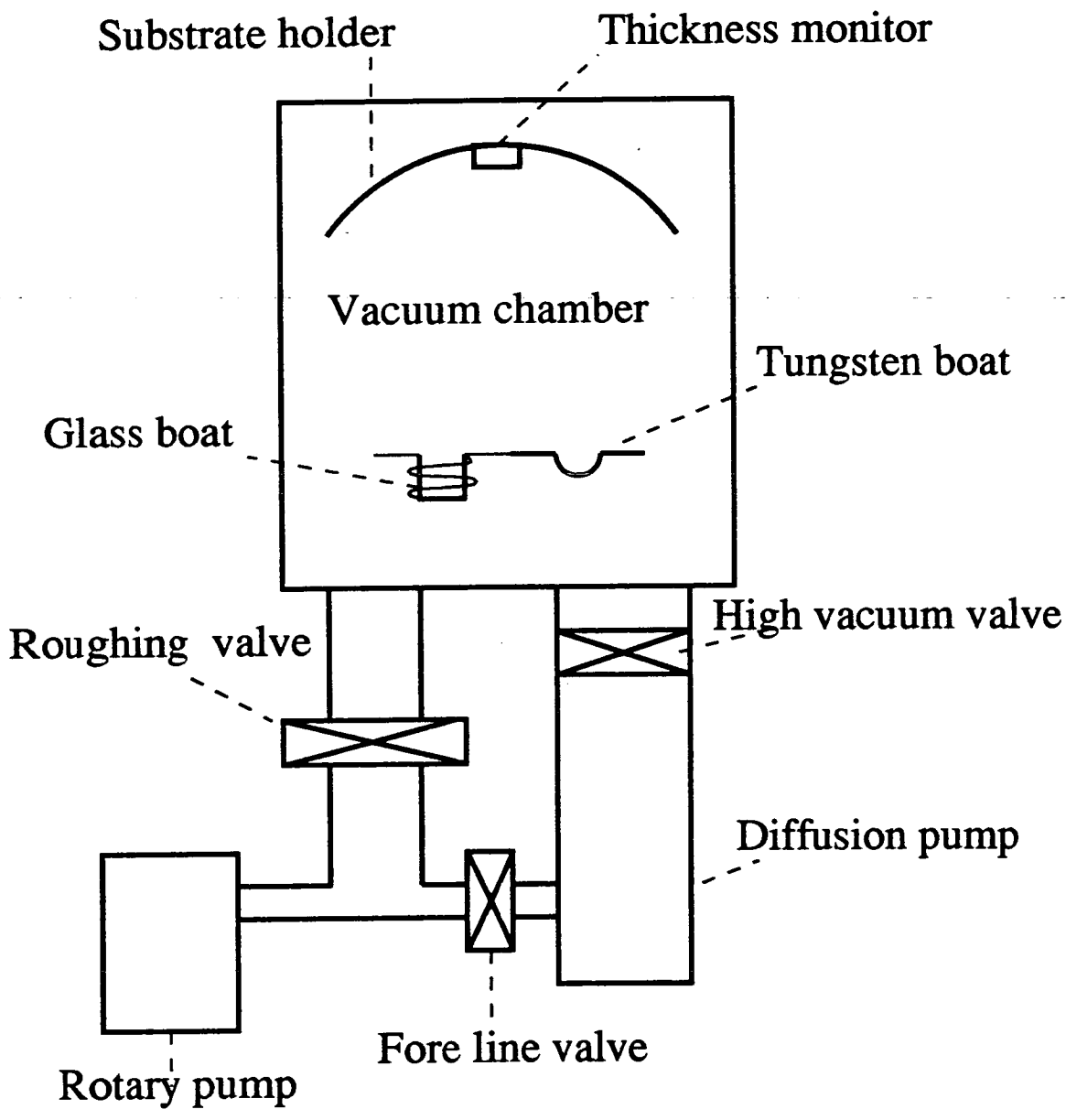


Figure 5.1: A schematic diagram of the evaporation system.

and Ag films and a quartz glass boat inside a helical tungsten filament for evaporating the As-S films. The boats were resistively heated by a high current produced by a step-down transformer controlled by a variac. The system was also equipped with a thickness monitor which will be described later on.

The As-S bulk material was made by melting appropriate amounts of the elements As and S in a 1 cm² bore quartz tube which was evacuated to a pressure of 10⁻⁴ torr. Because of the high vapour pressure of As and the consequent risk of explosion, the tube was placed partially inside the furnace and heated at 500 °C gradually for 2 hours to allow an initial reaction between As and S. The tube was then heated at 800 °C for 24 hours in a rocking furnace and then quenched in air. The material obtained was crushed into small fragments to be used later in the evaporation of the As-S films.

The evaporation rate of the As-S was kept within the range 0.1-0.6 nm/s. This low rate was adopted for the As-S films because it yields a stoichiometry close to that of the source.¹ (Compositional analysis of the As-S films in the present study confirmed that close agreement between the film and stoichiometric source is achieved at low deposition rates.) The evaporation sources used for Cu and Ag deposition were wires (99.998% pure) supplied from BDH Ltd. In contrast to the As-S evaporation rate, the Ag and Cu were evaporated at rates as high as 8 nm/s. The maximum thicknesses which could be obtained from a single evaporation were 800 nm for As-S films and 500 nm for Ag and Cu films. For thicknesses greater than these a multiple evaporations were performed.

The photodoped films and the samples used for studying the photodissolution process, were obtained by first evaporating the As-S layer on the glass substrate and then the Ag layer, or vice versa. The two layers were always deposited without breaking the vacuum except for samples in the annealing experiments; for these, the As-S film after deposition was annealed outside the vacuum chamber and the Ag layer then deposited on top.

5.3. Film thickness measurement

The film thickness measurements were carried out using a thickness monitor mounted within the evaporator, a mechanical stylus instrument (Taly-step), or a DekTak IIA surface profilometer. The film thickness monitor, based on a quartz crystal oscillator, was used to make measurements during the evaporation of the films whereas the Taly-step and the DekTak IIA were used after the films were fabricated as a check on the values obtained by the crystal monitor. The nearer the substrates are to the crystal monitor in the vacuum chamber the more accurate are the measured film thicknesses. The uncertainty in the film thickness measurements was about 2%.

The quartz crystals were thin discs, 14 mm in diameter, with thin film Au electrodes on each face having the geometries shown in figure 5.2(a). These crystals had a fundamental resonance frequency of 6 MHz and were purchased from Megatech Ltd. A small holder was made which exposed the circular deposition area as shown in figure 5.2 (b). Electrical contacts, made to the front and back electrodes of the crystal, were connected to an oscillator circuit. The oscillator output was fed to a frequency counter which could detect a change in frequency down to 1 Hz.

As a film of a given material is deposited on the crystal, the resonant frequency changes from its initial value, F_q , to a new value, F_c , for a given film thickness, d_f . An equation which relates the film thickness (in cm) to the frequency change is given by Lu and Lewis:²

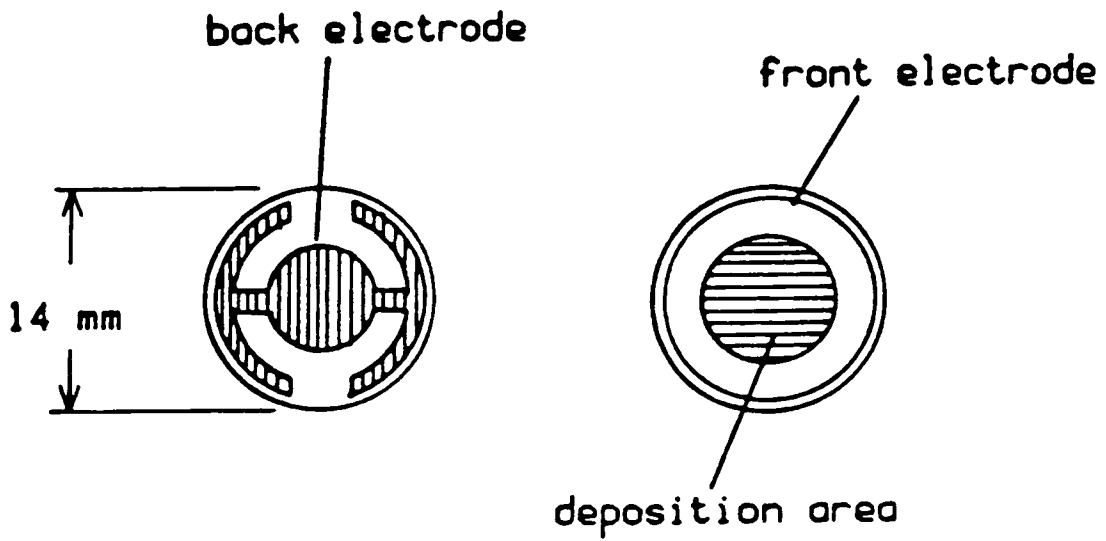
$$d_f = (1/C\rho_f)(F/F_q F_c) \quad (5.1)$$

where ρ_f is the film density (in g/cm^3) and $F = F_q - F_c$. C is a constant with a theoretical value of 2.26×10^{-6} (in $\text{cm}^2/\text{g Hz}$).

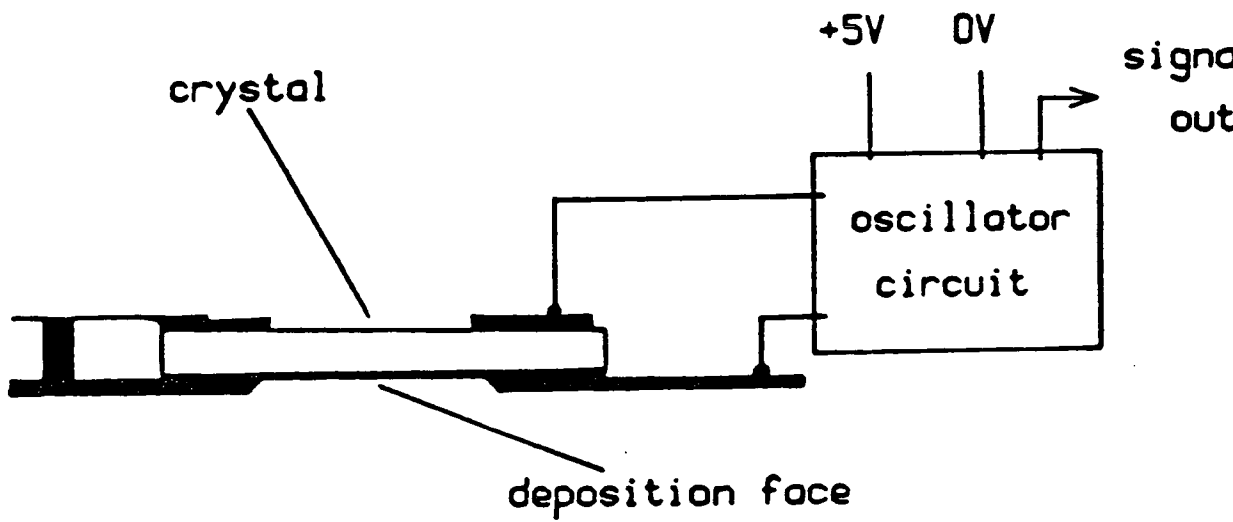
The densities of the As-S glasses were obtained using an empirical formula³ given by Tanaka and Minami:

$$\log(93.3 - W_{As}) = -0.3815d + 2.7190 \quad (5.2)$$

where W_{As} is the weight percentage of As in the compound and d is the density of the bulk glass. The Ag and Cu densities were taken as



(a)



(b)

Figure 5.2: The quartz-crystal thickness monitor. (a) quartz-crystal electrode geometry; (b) details of crystal holder.

10.5 and 8.93 g/cm³ respectively.

5.4. Annealing pre-treatment

This section describes the procedures used in the annealing pre-treatment for As-S films. The annealing was performed in a temperature-controlled vacuum oven (Gallenkamp Vacuum Oven OVL-570) for 1 hr in a nitrogen atmosphere. A schematic diagram of the annealing set up is shown in figure 5.3. The annealing temperature values (measured at $\pm 4^\circ\text{C}$) for different compositions in the As-S system were those obtained by Tanaka and Ohtsuka,⁴ and are listed in table 1:

Table 1: Annealing temperature for an As_xS_{100-x} specimen

As content, x (at.%)	40	37	33	30	25	20
Annealing temp., T (°C)	160	156	137	120	110	105

5.5. Kinetics measurements

Studying the reaction kinetics is an obvious way to obtain information about the photodissolution process, but there are experimental difficulties associated with such measurements. Various methods have been developed which usually measure either the amount of metal remaining in the metal source or the thickness of the photodoped layer generated by the photodissolution process.

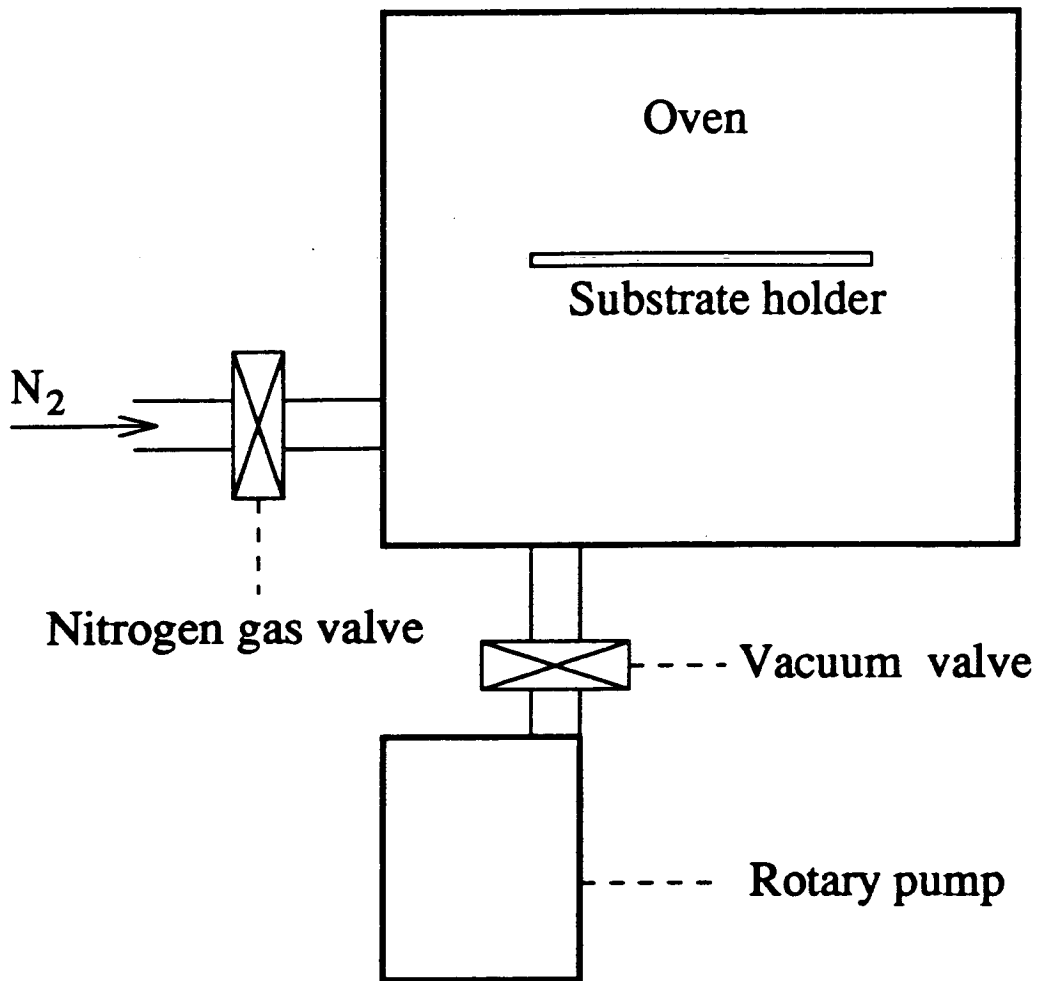


Figure 5.3: A schematic diagram of the annealing arrangement.

The main technique used in the present case to investigate the rate of photodissolution is optical reflectivity monitoring. A schematic diagram of the arrangement is shown in figure 5.4. A quartz halogen lamp (12V, 50W) provides the illumination, which is focussed onto the sample by means of microscope optics. Reflected light from the sample passes back through these optics and then, after passing through a right angle prism, is chopped at a frequency of about 80 Hz to minimise the effect of background irradiation. The reflected light is then focussed onto the aperture of the monochromator, in which the optics direct the selected wavelength onto a photodiode. A photocurrent proportional to the incident intensity is generated and converted to a photovoltage by means of a simple current-to-voltage converter. After passing this signal into a low-noise amplifier (Brookdeal 9453), the output is fed to a microcomputer. The data was collected by continuous time measurement software.

The optical reflectivity technique is based on the fact that the reflectivity of a weakly absorbing film varies periodically with its thickness due to interference between light reflected from the top and bottom surfaces of the film. Because photodissolution changes the thickness of the undoped As-S layer, as shown in figure 5.5, optical reflectivity monitoring is a suitable technique for investigating the development of these changes. The latter figure shows that there is a well defined interface between the doped and undoped regions of the film; the doped region is generally highly absorbing, so that as the photodoped layer expands towards the top surface of the film, a change in reflectivity will be observed due to the decreasing thickness of the undoped layer.

Some kinetics data based on optical transmissivity measurements has also been obtained. In contrast to the optical reflectivity measurements, the optical transmissivity data was collected in a discontinuous manner, i.e. the data was collected at specific fixed time intervals. The transmissivity was measured by a Perkin Elmer Lambda 9 spectrophotometer.

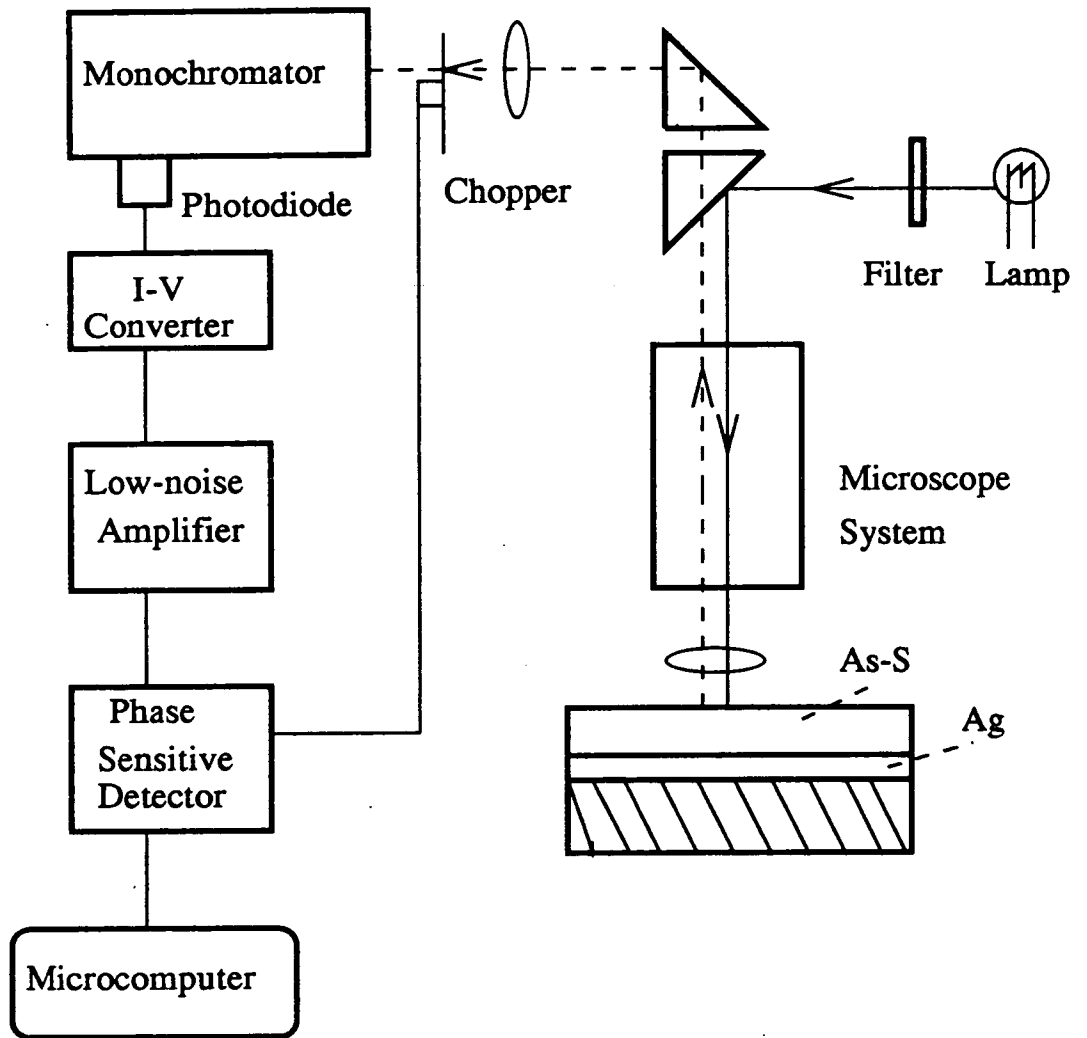


Figure 5.4: The experimental arrangement used to stimulate photodissolution and measure optical reflectivity as a function of time.

ILLUMINATION

REFLECTED
LIGHT

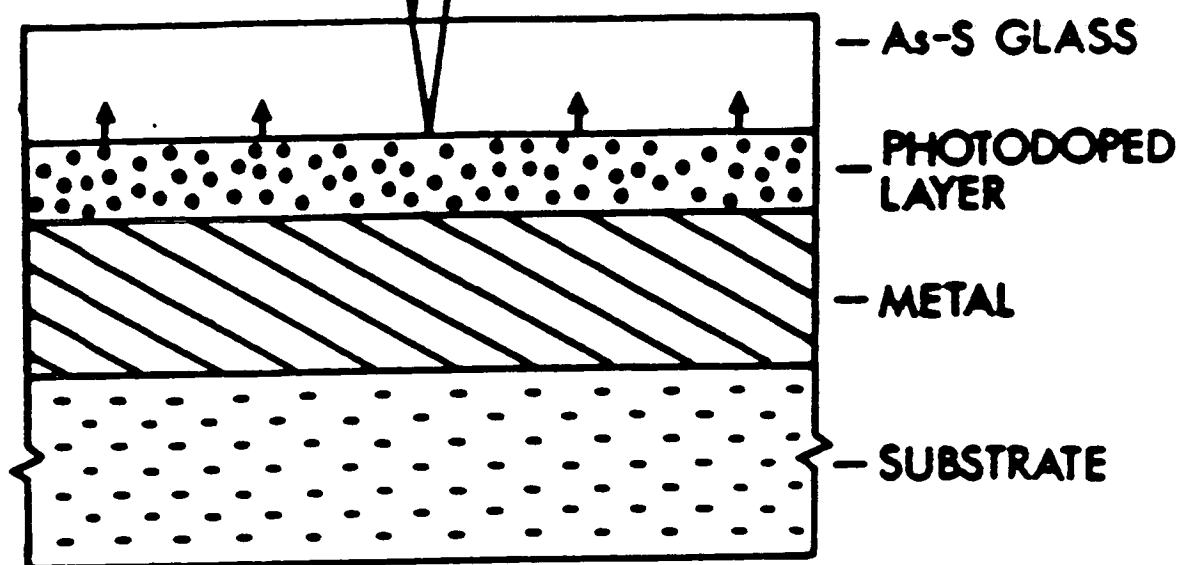


Figure 5.5: A schematic cross section through a sample during the photodissolution process.

5.6. Optical constant measurements

The optical constants were determined from the measurements of the transmission and reflection spectra. Two Perkin-Elmer spectrophotometers were used in this work depending on the wavelength range being investigated: in the visible and near IR range, a Lambda 9 model (185-3200 nm) was used and in the IR range, a model 1420 (2500-16000 nm) was used. The optical systems of the Lambda 9 and the 1420 are shown in figures 5.6 and 5.7 respectively. These two figures show that these spectrophotometers are dual beam instruments and therefore measurement was simply a matter of putting the sample to be measured in the compartment of the instrument. A reference substrate could also be placed in the reference chamber of the instrument if necessary. The data obtained was in the form of percentage transmission or reflection versus wavelength. To test the reproducibility of the spectra, five separate runs were made on one sample (area $\leq 1.5\text{cm}^2$) and the percentage transmission and reflection were found to agree to within 2% at all wavelengths.

In these spectrophotometers the slit width changes automatically as a function of spectral range, therefore manual selection of a suitable slit width is possible only at the beginning of the measurements. The selection of the slit width is very important since a wrong slit width may introduce a significant error in the transmission values.⁵ The selection of a slit width is based on the bandwidth of the fringes: a suitable slit width should be smaller than the bandwidth of the fringes and should be neither too narrow nor too wide. This is because a slit width that is too wide will decrease both the photometric accuracy and the resolution of the spectral detail and too narrow a slit width may increase noise. A good compromise between these two requirements is generally achieved with slit widths between one fifth and one tenth of the bandwidth of the fringes. The slit width used in the present work was about 2 nm in the visible and increased towards the IR region reaching a value of about 20 nm. This increase in the slit width is due to the increase in the bandwidth of the fringes in the IR region.

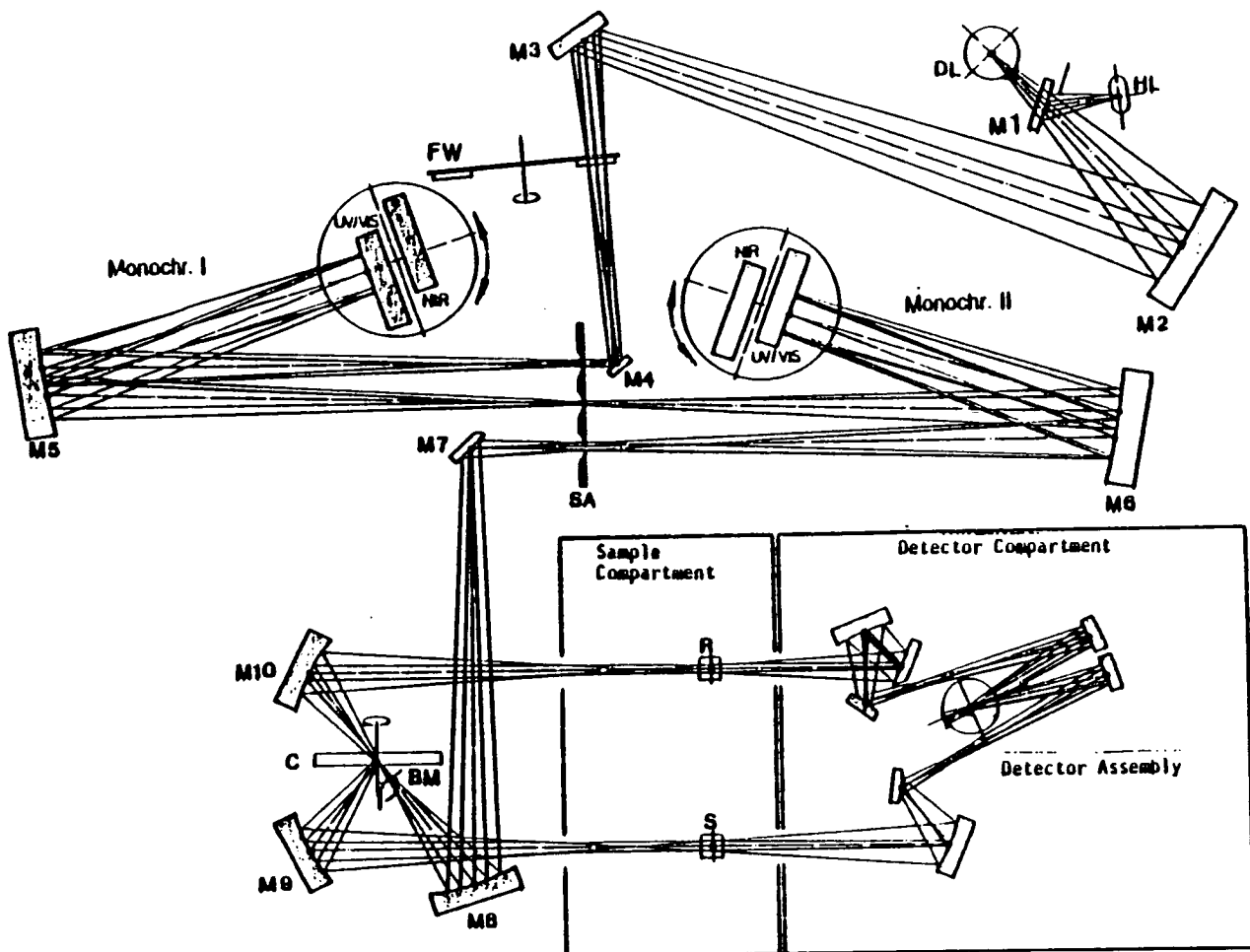


Figure 5.6: Optical schematic of the Lambda 9 spectrophotometer.

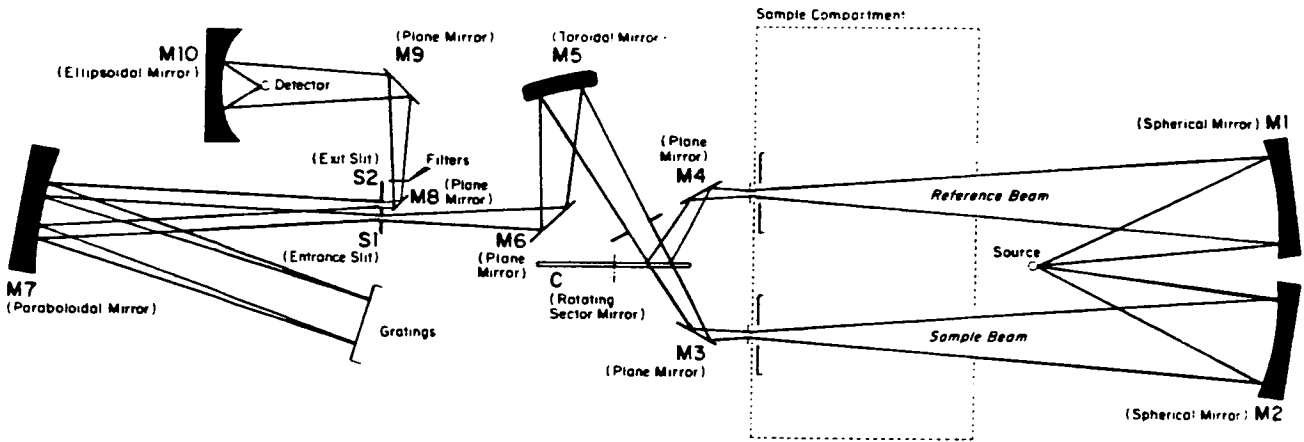


Figure 5.7: Optical schematic of the 1420 IR spectrophotometer.

The scanning speed is another parameter which might affect the results. The best results were obtained in the present work for a scanning speed between 60 and 120 nm/min. A scan speed that is too fast results in a loss of resolution and photometric accuracy.

The photodoped samples which were analysed with these instruments were obtained by illuminating As-S/Ag film combinations with UV light obtained from a mercury lamp (200 W) in a Karl Suss MJB-3 mask aligner. The intensity obtained from this source was not more than 1 mW/cm^2 , therefore for samples more than 800 nm thick simultaneous illumination (using a 150 W tungsten white light source) and heating was used to achieve a fast photodoping rate and fully photodoped samples. Note that the photodoped films obtained using either the mercury or tungsten lamps were similar in their optical properties. In case an Ag or As-S layer was left on top after full photodoping of the sample, it was subsequently etched to ensure that a single photodoped layer was investigated. Iron III nitrate ($\text{Fe}(\text{NO}_3)_3$) in methanol or water was used to etch any Ag left on top and a saturated solution of ammonia in methanol was used to remove any undoped As-S remaining.

5.7. SIMS measurements

The SIMS analysis was performed with a Cameca IMS-3f ion microanalyser using different primary beams such as Cs^- , O_2^- , and O_2^+ . The optical schematic of this instrument is shown in figure 5.8. The sample is inserted into a high vacuum chamber ($\sim 10^{-9}$ torr) and must be perfectly flat, fit within a 1 inch circular area, and be less than 10 mm thick. In SIMS analysis, the surface of the sample is bombarded with a finely-focussed beam of primary ions. The collision cascade generated by the impacting ions results in the ejection and ionisation of atoms from the surface of the sample. These secondary ions are then passed to a mass spectrometer for analysis. The general procedure for producing a SIMS depth profile is to monitor the secondary ion signal

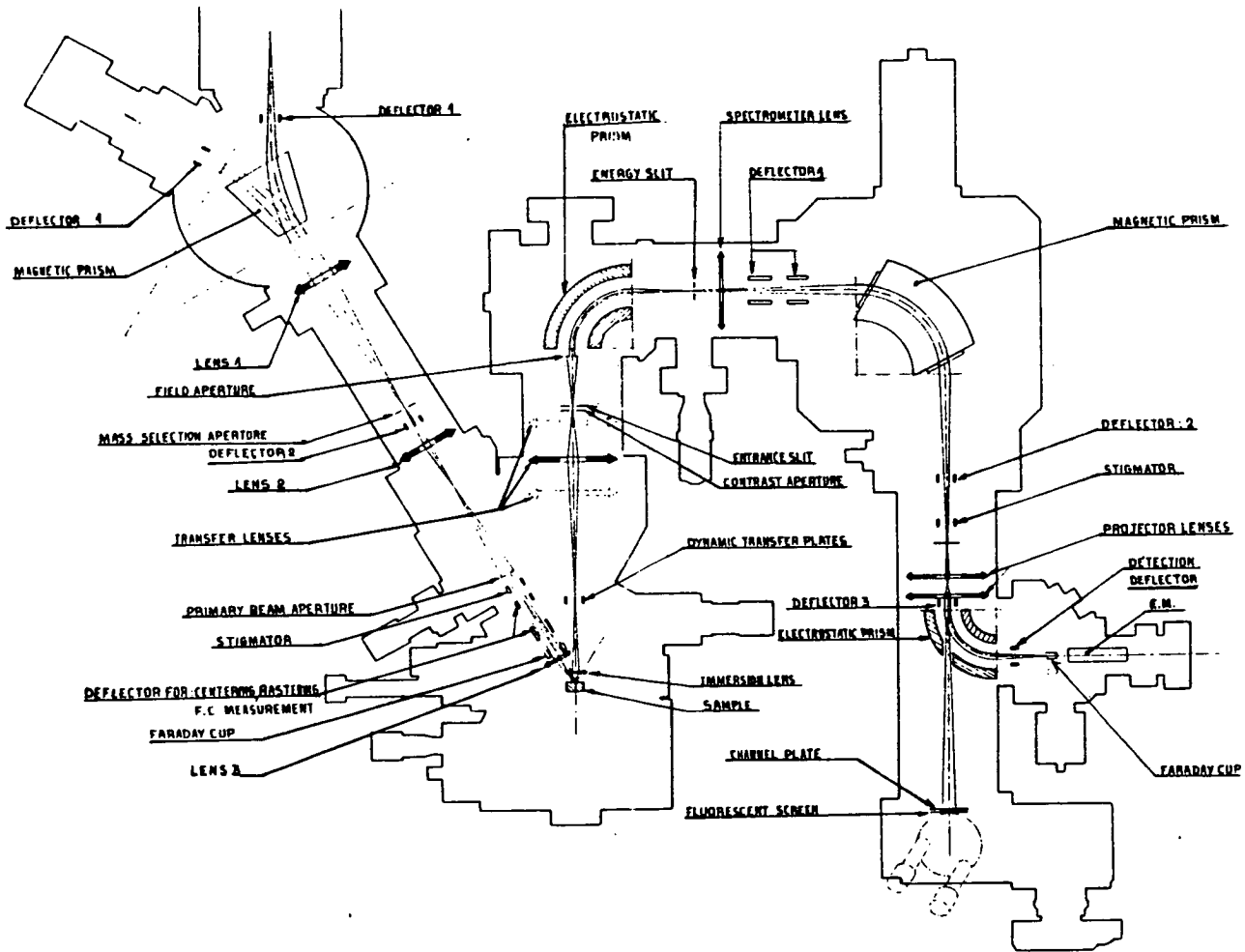


Figure 5.8: Optical schematic of the Cameca IMS-3f ion microanalyser.

of the element of interest as a function of sputter time.

This analysis was carried out to obtain the concentration depth profile for Ag and As in photodoped As-S films. The secondary ion species analysed were Ag_{109}^+ , As_{75}^+ and O_{16}^+ . The SIMS parameters such as raster size, primary beam species and depth resolution were varied in order to optimize the profiles, the best results being obtained using an O_2^- beam with a bombardment energy of 10.6 keV and a raster size of 150 μm . The surface area investigated was about $0.89 \times 10^{-3} \text{ cm}^2$. The double layer $\text{As}_{40}\text{S}_{60}/\text{Ag}$ samples were coated with a thin gold layer to avoid beam charging effects. In each sample, the measurements were repeated four times and the reproducibility was about $\pm 10\%$.

It is virtually impossible to extract meaningful depth profile information from SIMS data unless one maintains constant primary ion intensity and uniform primary ion current density over the secondary ion extraction area of the sample. In a stationary focused beam, the ion current density on the sample is not constant over the beam diameter, therefore, surface layer removal cannot be uniform. If the information zone for secondary ions extends over the total area of the incident beam, the contribution of ions from the crater edges will distort the profile of the subsurface layer. The broadening or skewing of a profile might also be caused by the diffusion of elements brought on or enhanced by ion damage to the solid, an increase in the local temperature of the bombarded area, and high electric field gradients produced from primary ion beam charging of the surface. The degree of surface charge buildup depends on the primary ion species, charge, energy and current density, the dimensions of the bombarded area and the conductivity and the thickness of the sample.

References

1. Goldschmidt D. and Rudman P.S., *J. Non-Cryst. Solids*, vol. 22, p. 229, 1976.

2. Lu C. and Lewis O.J., *Appl. Phys.*, vol. 43, p. 4385, 1972.
3. Tanaka M. and Minami T., *Japn. Appl. Phys.*, vol. 4, p. 939, 1965.
4. Tanaka K. and Ohtsuka Y., *Thin Solid Films*, vol. 57, p. 59, 1979.
5. Swanepoel R., *J. Phys. E: Sci. Instrum.*, vol. 16, p. 1214, 1983.

CHAPTER 6

OPTICAL CONSTANTS OF UNDOPED AND PHOTODOPED As-S FILMS

6.1. Introduction

A knowledge of the optical constants (absorption coefficient and refractive index) of both Ag-photodoped and undoped As-S films is important for both fundamental reasons and from the point of view of applications. In particular, it is necessary for measuring the kinetics of the photodissolution process using optical techniques and for detailed modelling of grating performance. It should also be noted that the characterisation of the photodissolution effect is mainly based on measurement of the changes that occur in the optical constants of the materials during illumination.

Although many reports have been published on the optical properties of materials in the As-S system very few have investigated the effect of pre-treatment¹⁻³ (e.g. pre-annealing) and Ag photodoping^{4, 5} on the optical characteristics of As-S films. In addition, these studies were either limited to one As-S composition (e.g. As₄₀S₆₀) or to a single wavelength. Because chalcogenide diffractive elements may have applications throughout the IR, particularly in either of the commonly used IR spectral bands (3-5 μm and 8-12 μm), it is important to obtain information on their optical properties over a wide range of wavelengths.

The effect of annealing on the optical and structural properties of as-deposited films was investigated by Deneufville et al.⁶ and Apling et al.^{7, 8} using diffraction techniques, and by Solin et al.⁹ using Raman

scattering. The general conclusion which can be drawn from the work of these authors is that the annealing of an as-deposited film near the glass transition temperature, T_g , causes a structural compaction and densification. This is due to the fact that the as-deposited film consists of molecules of the vapour species (particularly As_4S_4) embedded in a continuous random network, and annealing allows the molecular component to polymerise and combine with the original network to form a structure similar to that of the bulk glass. Deneufville reported¹⁰ that the refractive index of an annealed film ($n= 2.51$) is approximately equal to that of the bulk material ($n= 2.528$). Annealed films may have advantages over as-deposited films as far as grating fabrication is concerned since they should have better adhesion to the substrate and should produce elements which are more stable under illumination. They will also yield a more controllable fabrication process. Pre-annealing is also known to affect the Ag-photodissolution rate and thus a knowledge of the optical constants of annealed As-S films is needed for the analysis of the photodissolution kinetics and for modelling the performance of gratings made using annealed films.

The purpose of the work presented in this chapter is therefore to extend this investigation over a wider wavelength range (from the visible to the far-IR region) and a wider range of As-S compositions. The effect of pre-annealing and Ag-photodoping on the optical properties of As-S films will be compared and the dependence of the optical properties on the amount of Ag photodoped into the samples will be examined.

6.2. Calculation of the refractive index

The optical constants of undoped and photodoped As-S films can be calculated by considering the system shown in figure 6.1, which consists of an absorbing thin film on a thick, finite, transparent substrate. The film is of thickness d and has a complex refractive index $n^*=n-ik$, where n is the refractive index and k the extinction

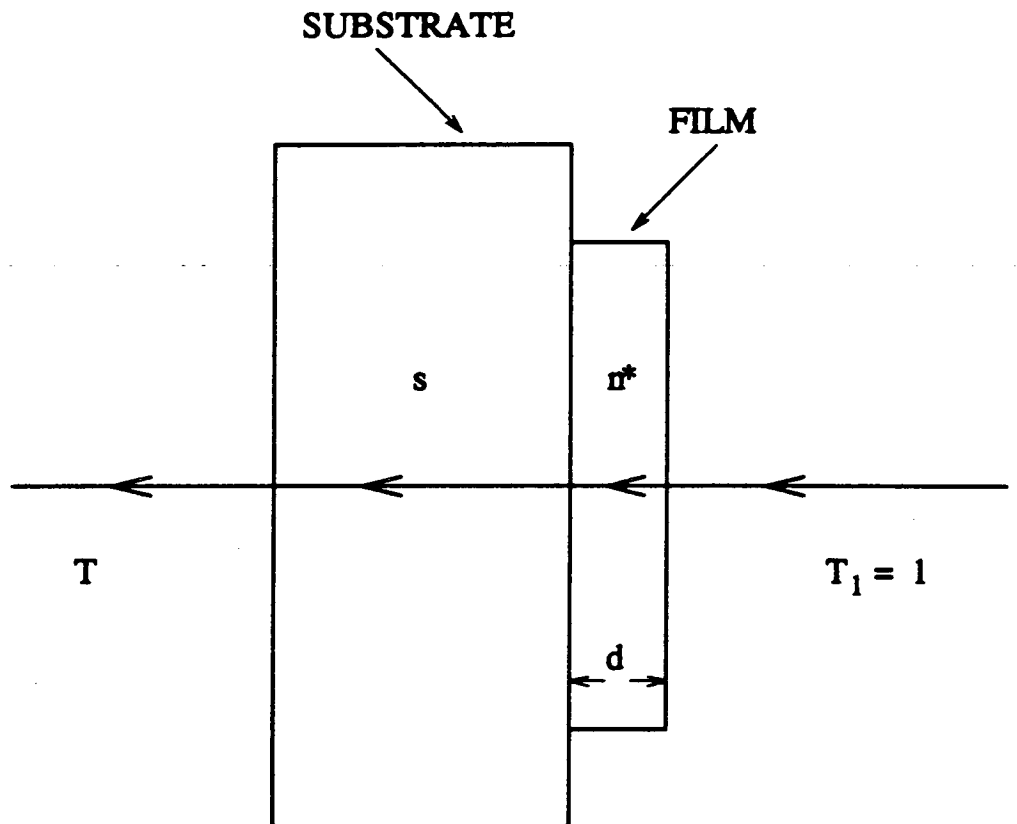


Figure 6.1. The system of an absorbing thin film on a thick finite substrate.

coefficient ($k = \alpha\lambda/4\pi$ where α is the absorption coefficient and λ the wavelength). The substrate is transparent and has a thickness several orders of magnitude larger than d , and index of refraction s . If the thickness d is not uniform or is slightly tapered, all interference effects are destroyed and the transmission as a function of wavelength is a smooth curve.

For the calculation of refractive index the transmittance spectra of the As-S films were used. A typical transmittance spectrum for an $As_{40}S_{60}$ film is shown in figure 6.2. This spectrum can be divided into three regions: a transparent region; a region of medium absorption; and a region of strong absorption known as the interference-free region. The refractive index was calculated using Swanepoel's method.¹¹ In the first region, where α is equal to zero, the refractive index is calculated using the following equation:

$$n = [M + (M^2 - s^2)^{1/2}]^{1/2} \quad (6.1)$$

where

$$M = [2s\sqrt{T_m}] - s^2 + 1/2 \quad (6.2)$$

T_m is the minimum transmission (see figure 6.2) and s is the substrate refractive index. In the second region, where α is different from zero, the refractive index is calculated using the relation:

$$n = [N + (N^2 - s^2)^{1/2}]^{1/2} \quad (6.3)$$

where

$$N = [2s\sqrt{T_m} - T_M] / [\sqrt{T_m} \sqrt{T_M}] + [s^2 + 1/2] \quad (6.4)$$

and T_M is the maximum transmission.

In the third region there are no fringes and the refractive index is determined by extrapolating the values calculated in the first and second regions of the spectrum. This extrapolation is carried out using the Wemple-DiDomenico relation¹²

$$n^2(\omega) = 1 + [E_d E_o / [E_o^2 - (h\omega)^2]] \quad (6.5)$$

where E_o is the single oscillator energy and E_d is the dispersion energy. In the present study, E_d and E_o were calculated using a least-squares

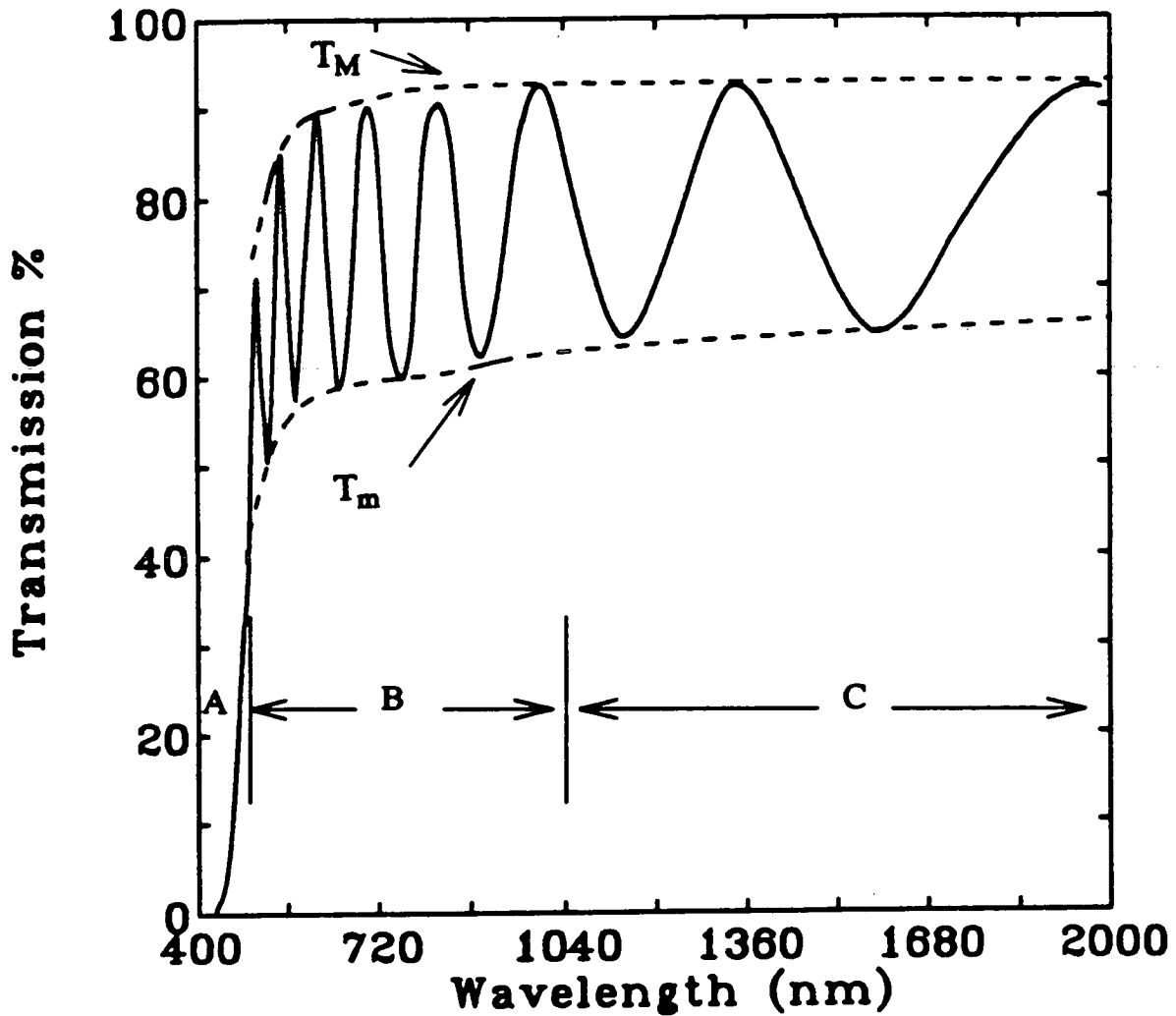


Figure 6.2. A typical transmission spectrum of an annealed $As_{40}S_{60}$ film. The film thickness in this case is about 800 nm. (A: transparent region, B: medium absorption region, C: strong absorption region, T_M : maximum transmission, T_m : minimum transmission).

fitting program based on the above equation. In this program the values of n from the first region and the corresponding energies are input in order to determine the values of E_d and E_o , which are then used to generate the refractive index in the third region. E_d and E_o will be discussed separately in a later section.

It was also possible to calculate the refractive index of the first and the second regions using the basic equation for interference fringes:

$$2nd=m\lambda \quad (6.6)$$

where m is an integer for maxima and half integer for minima. This method was used as a check on the results determined from Swanepoel's technique and the values of n obtained from both methods were in good agreement. The film thickness, d , was determined directly using either a quartz crystal monitor during deposition, a DekTak IIA surface profilometer or a Taly-step. The contribution to the uncertainty in the optical constant values obtained in the present work is mainly due to the error involved in the film thickness measurements. This error is evaluated to be typically around 2%.

6.2.1. Refractive index of undoped and Ag-photodoped $As_{40}S_{60}$

Annealing an as-deposited $As_{40}S_{60}$ film in an N_2 atmosphere at 160 °C for 1 hour was found to increase its refractive index by about 3% from the visible to the infra-red. Typical results are shown in figures 6.3(a) and 6.3(b). Figure 6.3(a) compares the dispersion of the refractive index over the range 400-2000nm for as-deposited and annealed $As_{40}S_{60}$ films 800 nm thick. Annealing also affects the refractive index further into the infra-red, as shown in figure 6.3(b), which compares the spectral dependence of n over the range 400-12000 nm for as-deposited and annealed $As_{40}S_{60}$ films 2000 nm thick. Note that the refractive index is almost constant from 2000 to 12000 nm.

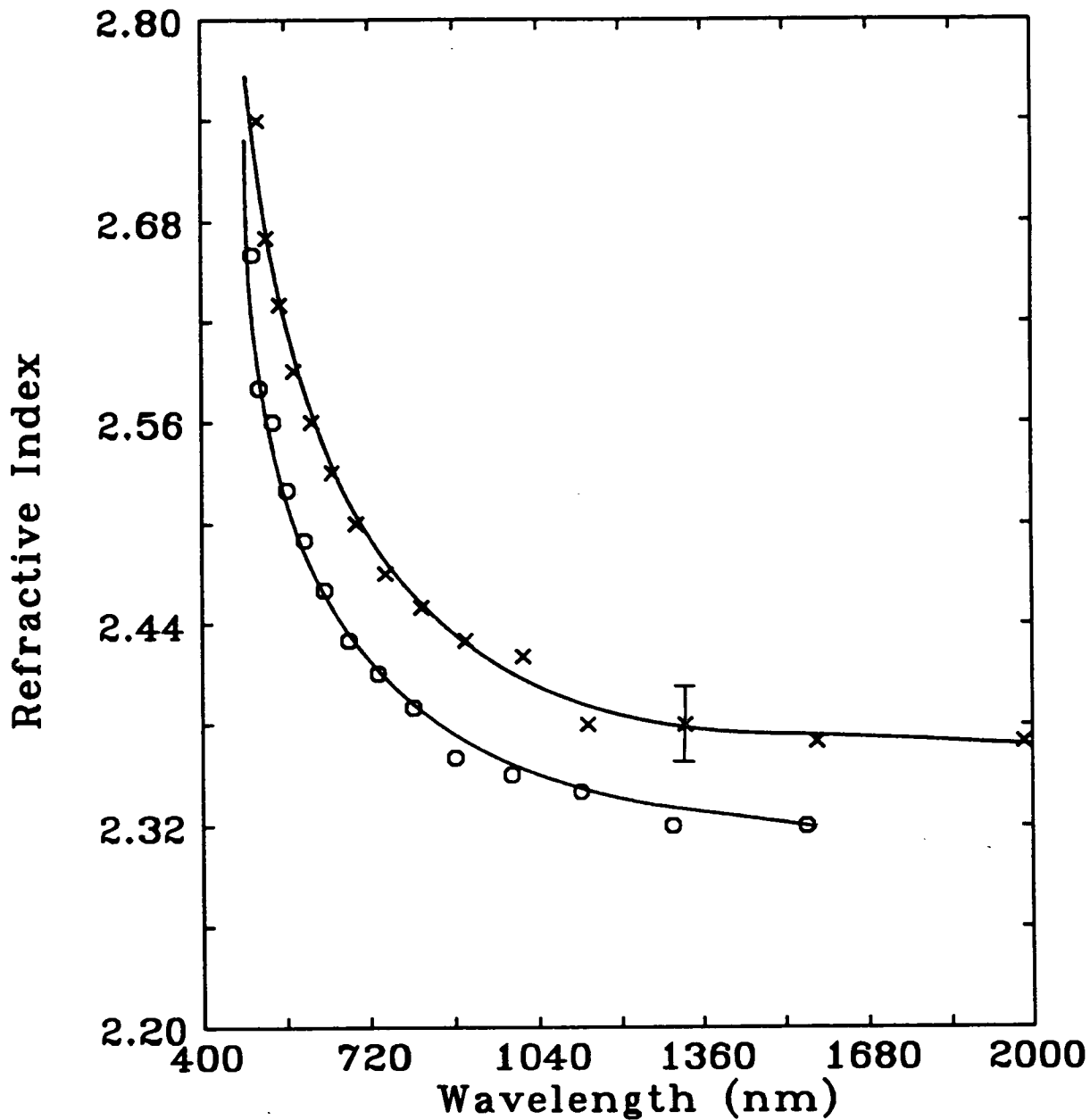


Figure 6.3(a). Spectral dependence of the refractive index for an annealed (x) and as-deposited (o) $As_{40}S_{60}$ film. The film thickness is about 800 nm.

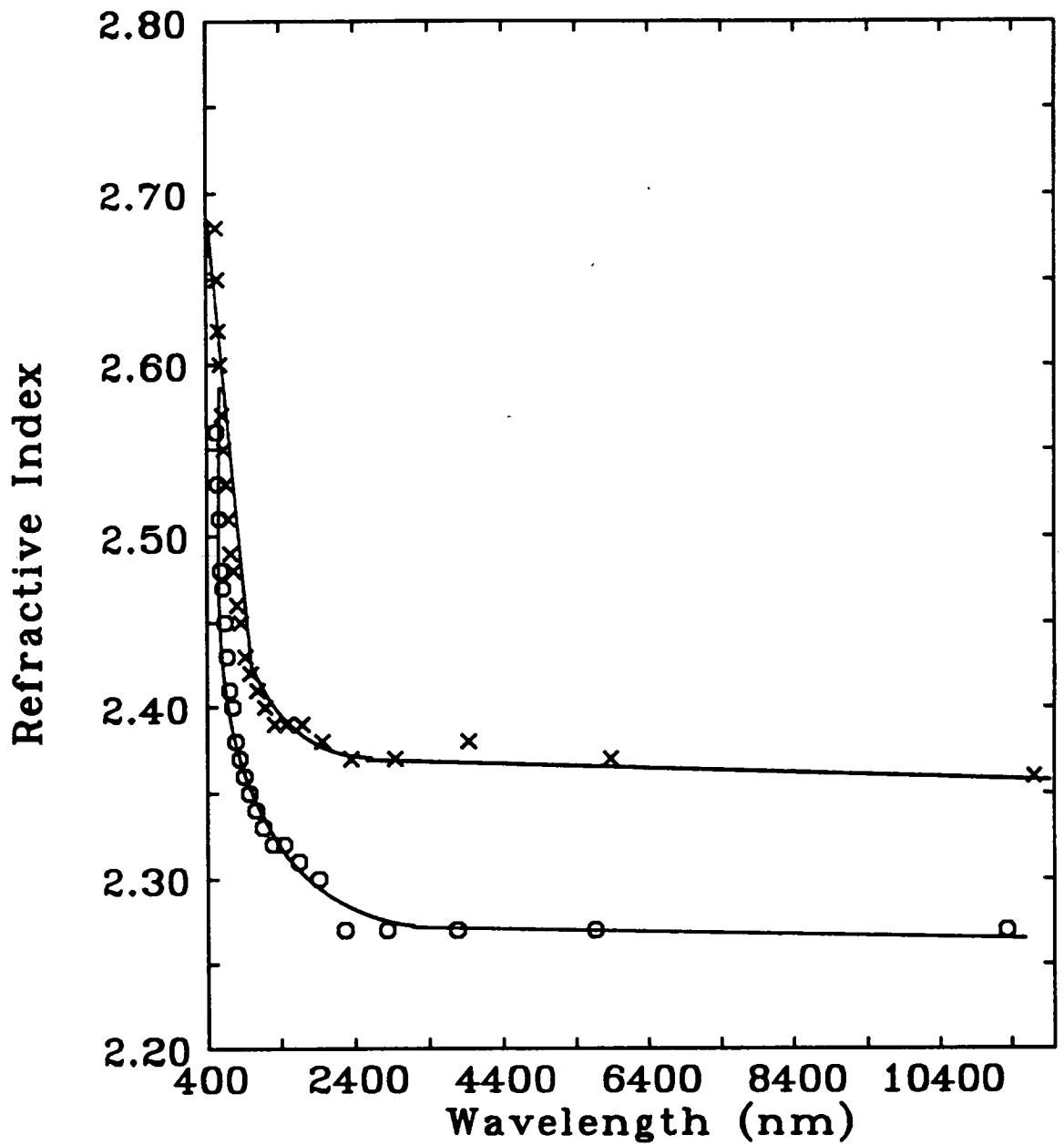


Figure 6.3(b). Spectral dependence of the refractive index for an annealed (x) and as-deposited (o) $As_{40}S_{60}$ film. The film thickness is 2000 nm.

A similar increase in refractive index was observed by Kumar et al.¹³ who reported that annealing $As_{40}S_{60}$ for 1 hour at 150 °C increases n in the IR from 2.34 to 2.43 (a 3.8 % increase). These results are also consistent with the findings of Tanaka and Ohtsuka,¹⁴ who measured the refractive index of $As_{40}S_{60}$ at a single wavelength, 633 nm, and found that annealing at 170 °C for 1 hour increased it from 2.45 to 2.55 (a 4.1 % increase). Deneufville et al.¹⁰ also measured the change in n at a single wavelength, 827 nm (1.5 eV), and found an increase from 2.42 to 2.51 (a 3.7 % increase). However, they annealed for 1 hour at 180 C, which is a higher temperature than used in the present study, and used a deposition rate higher than that used in this work (0.5 nm/s). The slight discrepancies between these studies are probably attributable to the different experimental conditions employed.

The refractive index of an undoped $As_{40}S_{60}$ film is also increased when Ag is introduced into it by photodoping. The magnitude of this increase is found to be strongly related to the amount of Ag incorporated into the structure, which can be as high as ~30-40 atomic%. Both as-deposited and annealed films exhibit the same kind of effect, which is illustrated in figure 6.4(a) for the case of annealed films. The Ag content in the samples was varied by changing the ratio of the Ag layer thickness to that of the $As_{40}S_{60}$ layer. Figure 6.4(b) compares the refractive index plots for the undoped, as-deposited and undoped, annealed material with those for the heavily doped, as-deposited and heavily-doped, pre-annealed samples, which had an Ag content of approximately 37 atomic%. The refractive index of the photodoped films is about 20 % higher than for the undoped films. In addition, the difference in n between annealed and unannealed samples is less for the heavily photodoped films, which indicates that the structure of the photodoped material may not be very dependent on the structure of the initial undoped film. A similar difference between the undoped and the most heavily doped material is found in the infra-red region, as shown in figure 6.5, which plots the refractive index out to ~12000 nm (12 μ) for an undoped, annealed film and a photodoped, annealed film, both of thickness ~2000 nm. Both films exhibit an essentially constant refractive index above ~2400 nm, the value of the photodoped material being about 16 % higher.

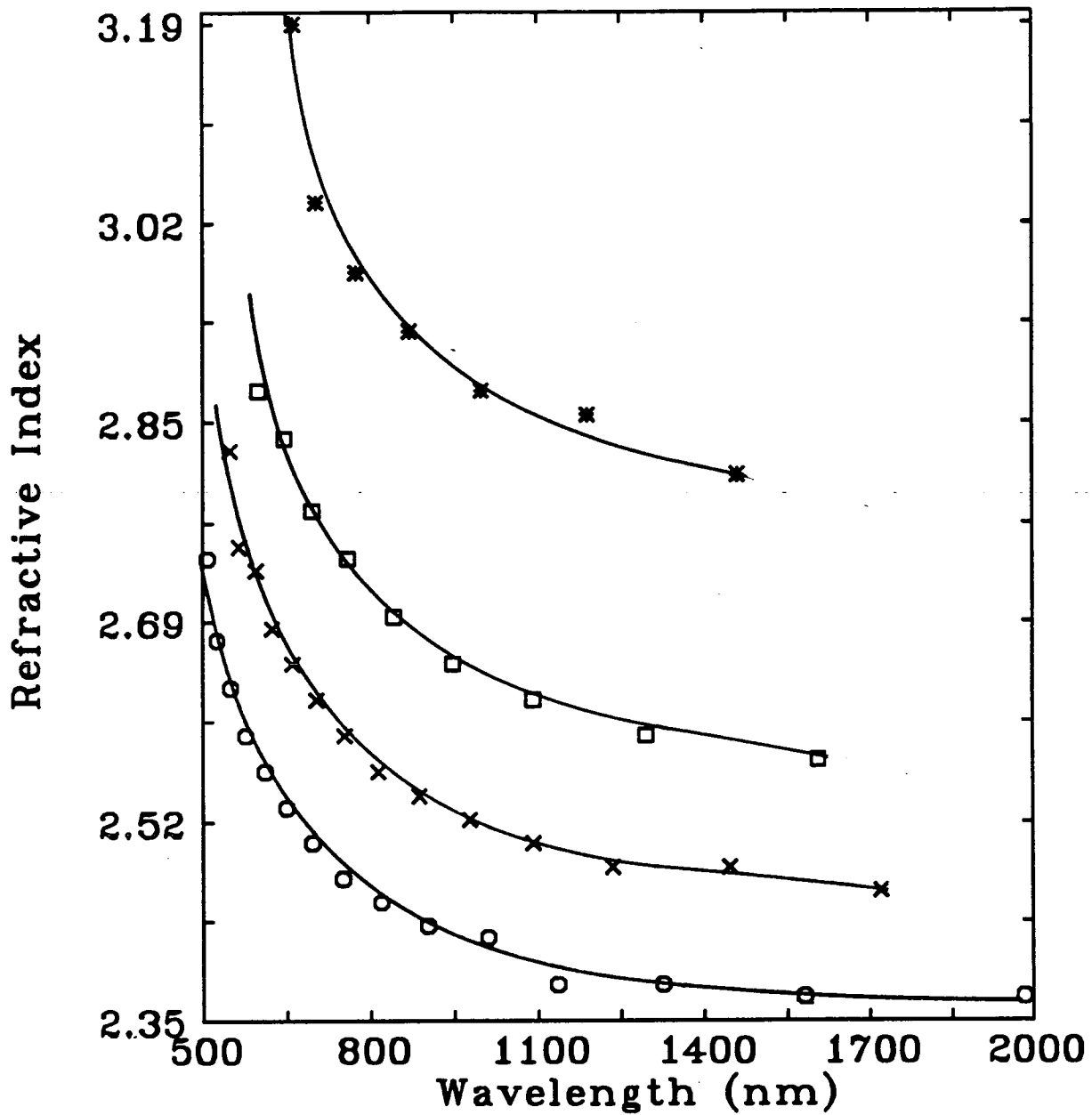


Figure 6.4(a). Spectral dependence of the refractive index of undoped and photodoped As₄₀S₆₀ films. Each curve corresponds to a different atomic% of Ag: 0 (o), 10 (x), 21 (□), 34.8 (*). The thicknesses of As₄₀S₆₀ films ranged from 500 to 800 nm, and the undoped films were pre-annealed at 160 °C for 1 hour.

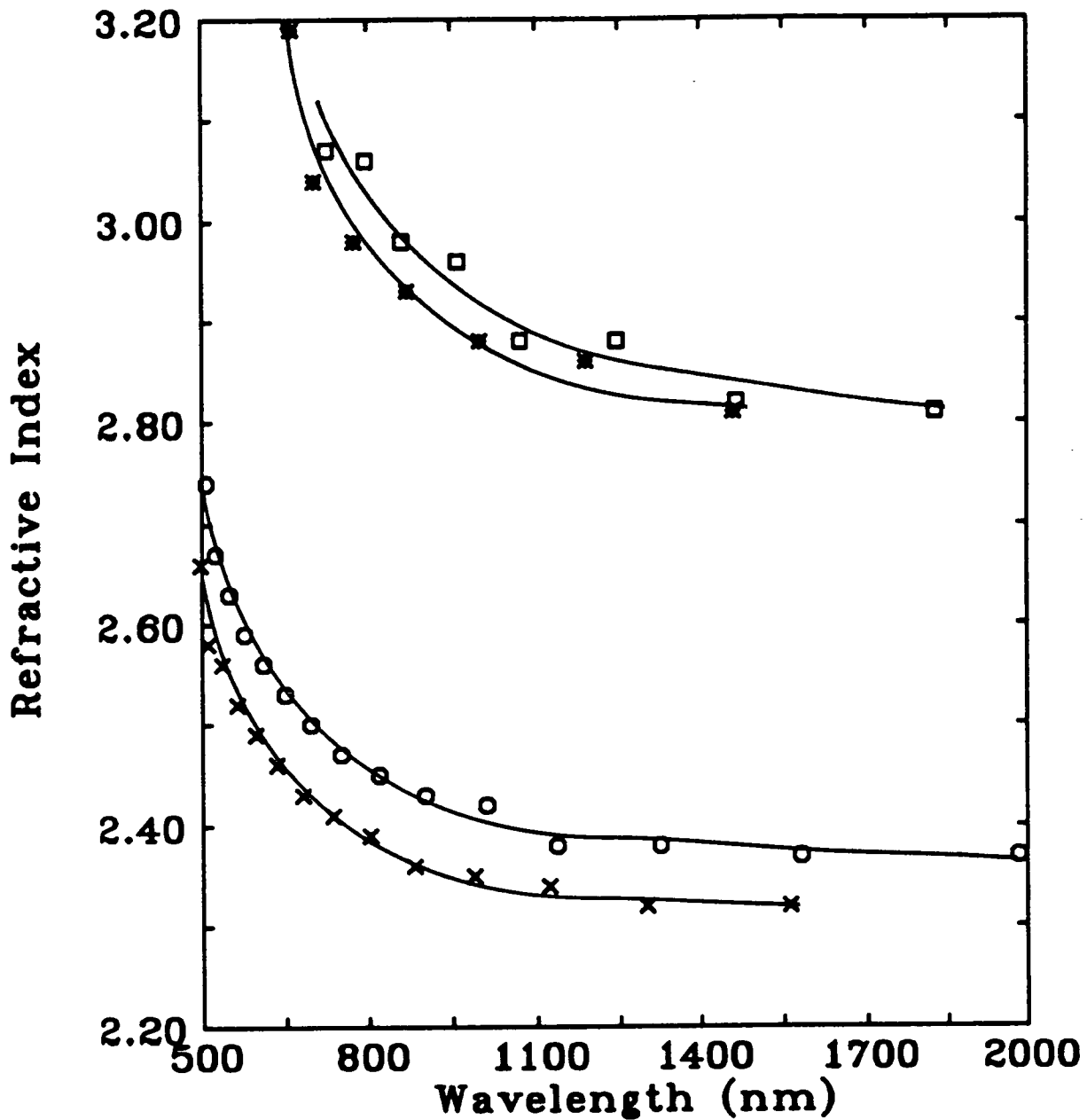


Figure 6.4(b). Spectral dependence of the refractive index of undoped and photodoped $As_{40}S_{60}$ films. The undoped films are represented by x for as-deposited films and o for annealed films. The photodoped films are represented by * for annealed and \square for as-deposited films. The Ag concentration in the photodoped films is 34.8 atomic%.

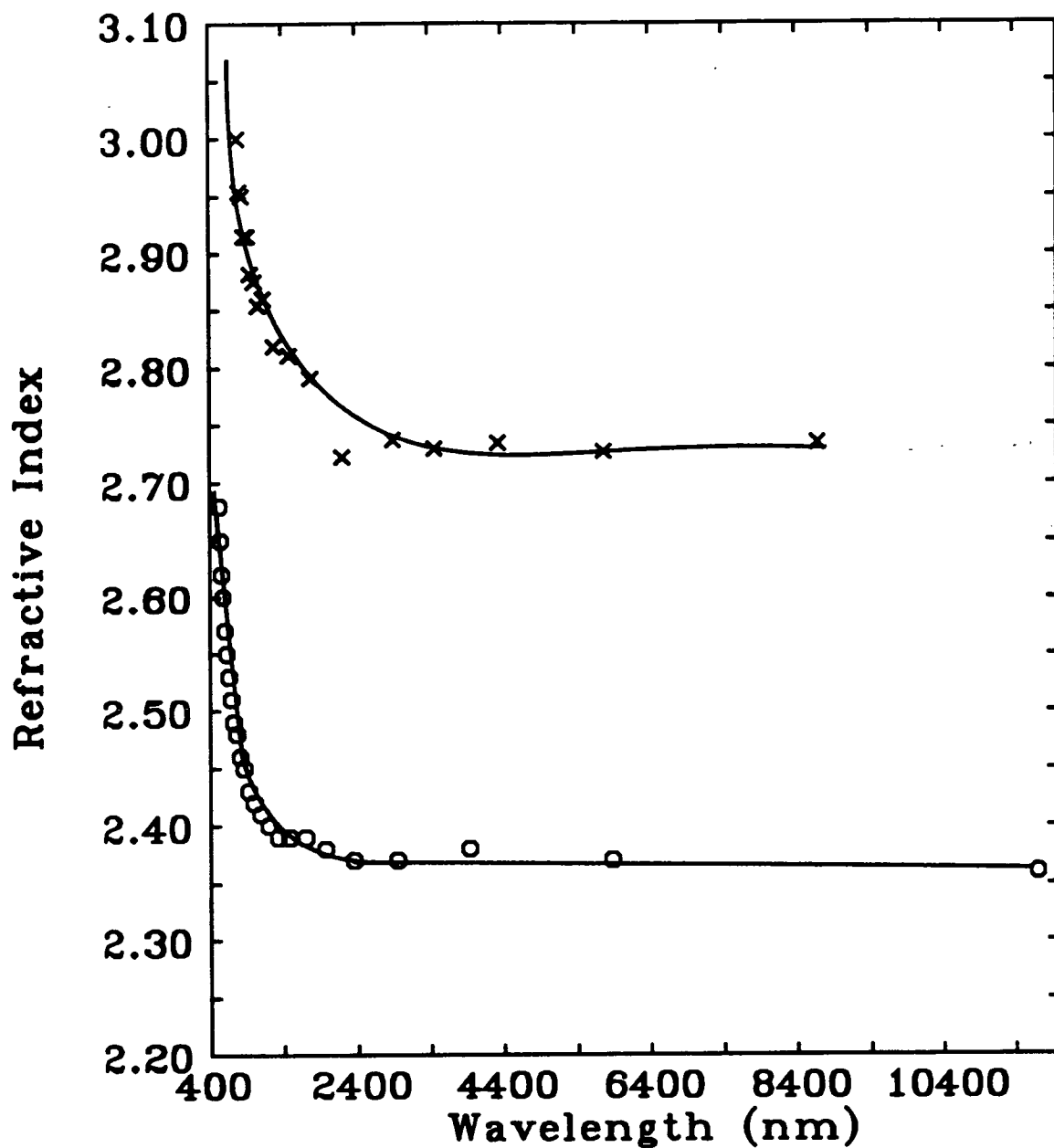


Figure 6.5. Spectral dependence of the refractive index of undoped (o) and photodoped (x) $As_{40}S_{60}$ films. The thickness of the films is 2000 nm for both cases. These results are for annealed films. The Ag concentration in the photodoped films is 34.8 atomic%.

To see the nature of the refractive index dependence on the Ag concentration at specific wavelengths, the refractive index values corresponding to 488, 514 and 633 nm are plotted in figure 6.6(a) versus Ag concentration for annealed films. These wavelengths were chosen because they correspond to widely used laser lines. This figure shows that the refractive index increases continuously as the Ag concentration increases, and this result is obtained for both annealed and as-deposited films. In addition, the trend of these plots above 12 atomic% Ag is not affected by annealing, as shown in figure 6.6(b), which compares the refractive index values at 633 nm versus Ag concentration for both annealed and as-deposited films. It appears, therefore that the annealing treatment affects the refractive index of only the undoped films and photodoped films containing less than 12 atomic% Ag. This suggests that the structure of the photodoped product containing more than 12 atomic% Ag does not depend on the details of the initial $As_{40}S_{60}$ structure.

Most of the Ag atoms photodoped into $As_{40}S_{60}$ form covalent bonds with S atoms although some are incorporated as interstitial Ag^+ ions. The fact that the initial structure formed by the annealing treatment disappears as the Ag content increases, shows that the presence of the Ag atoms changes the initial structure of the As-S film. Similar results were found by Yaji and Kurita¹⁵ for the effect of light exposure on photodoped layers containing different amounts of Ag. The authors found that the extent of the change produced by light exposure (photodarkening) decreased as the atomic% of Ag increased. They explained this by the fact that the presence of Ag atoms destroys the structural flexibility necessary for reversible photodarkening to occur, so this effect is not observed in heavily photodoped $As_{40}S_{60}$.

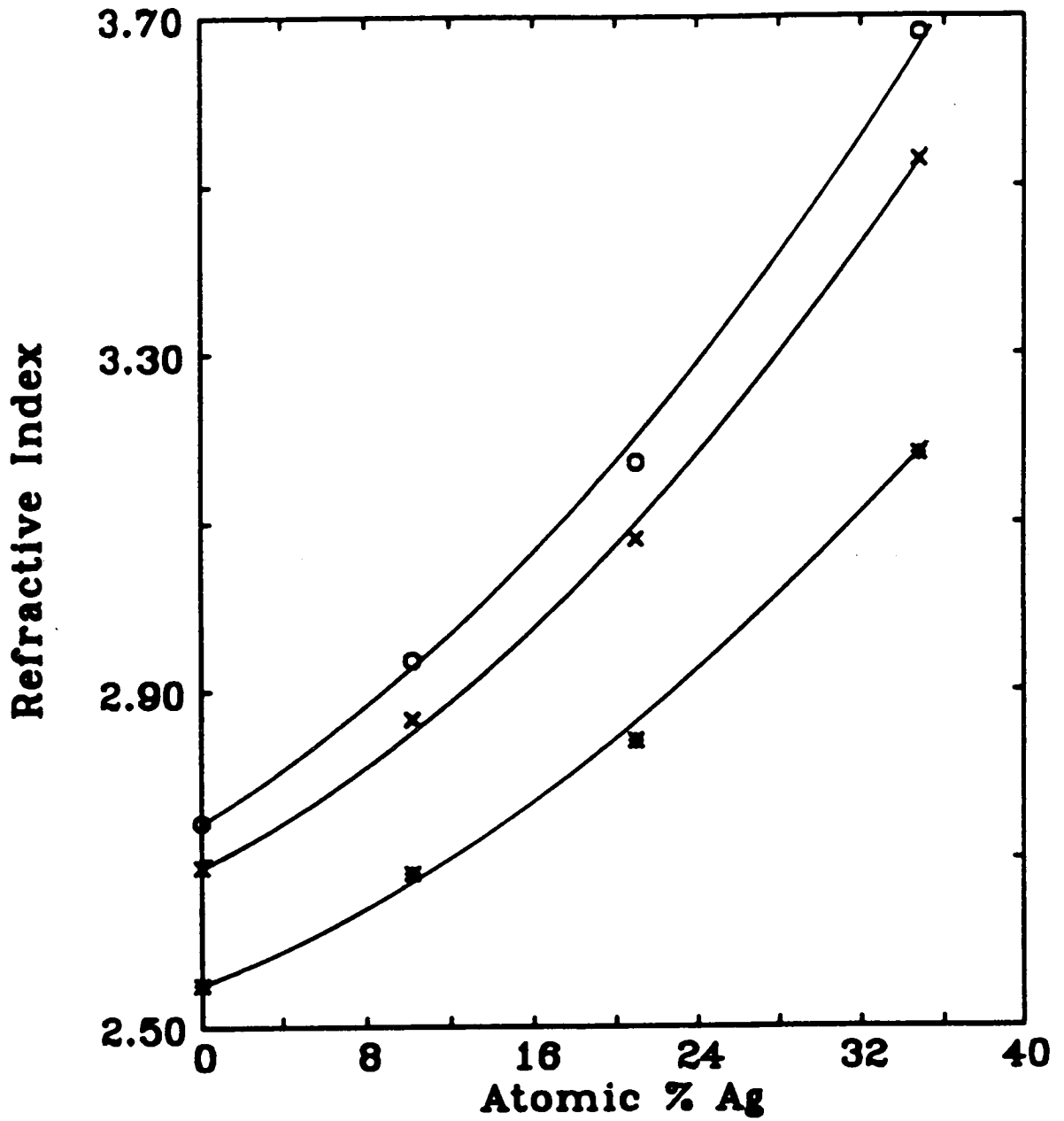


Figure 6.6(a). The effect of Ag content on the refractive index of annealed $As_{40}S_{60}$ films. Each group of data corresponds to a single wavelength: 488 nm (o), 514 nm (x) and 633 nm (*)

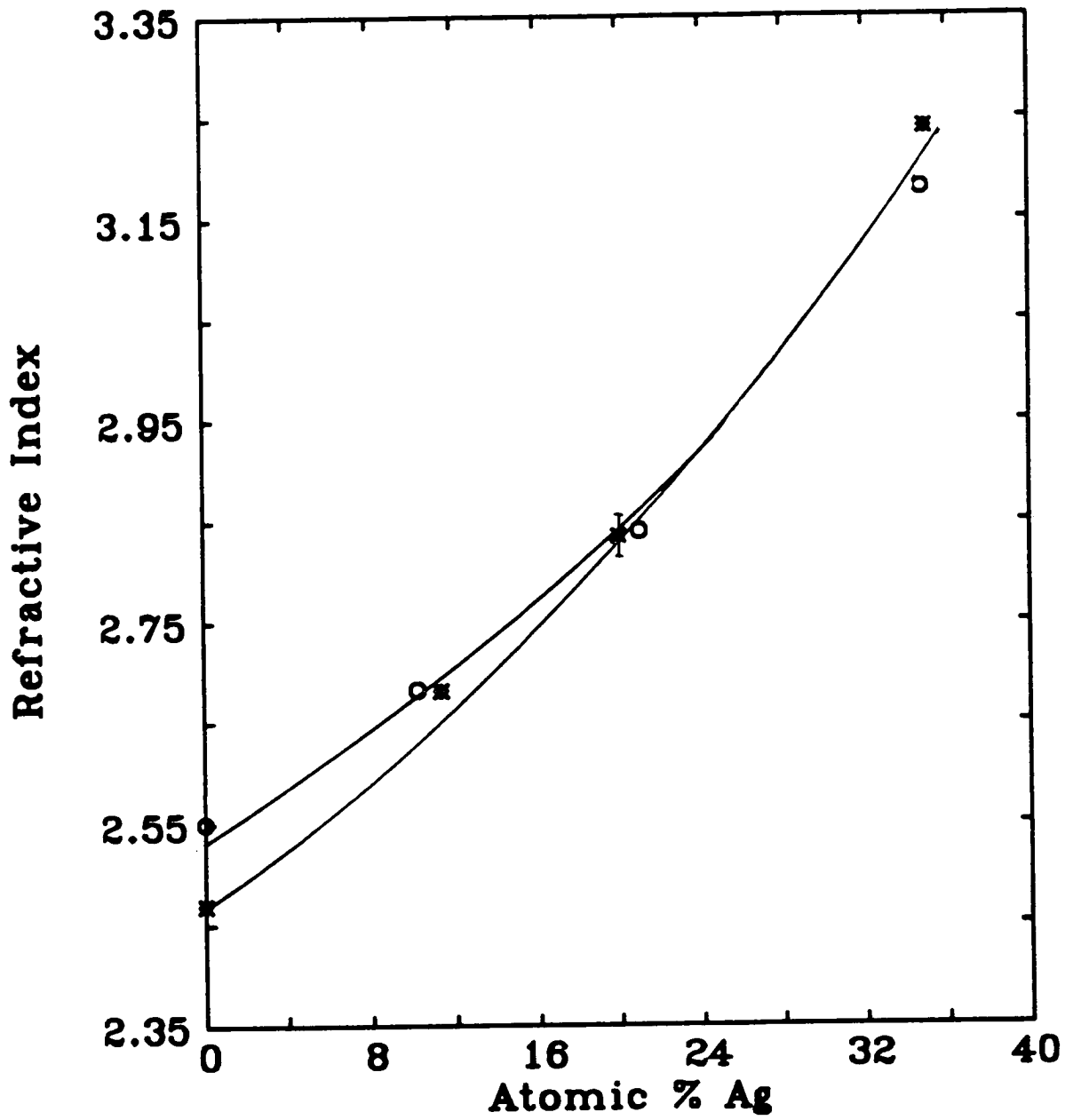


Figure 6.6(b). The effect of Ag content on the refractive index of annealed (o) and as-deposited (*) $\text{As}_{40}\text{S}_{60}$ films at a wavelength of 633 nm.

6.2.2. Compositional trend of the refractive index in As-S and Ag-photodoped films

Figure 6.7 shows the spectral dependence of the refractive index over the range 500 to 1400 nm for annealed, undoped films of various As-S compositions. Similar results were obtained for unannealed films. The figure shows that the refractive index increases as the As content increases. The refractive index at three wavelengths (488, 514 and 633 nm), determined from the results in figure 6.7, is plotted as a function of As content in figure 6.8. Clearly, n depends almost linearly on As content. This is in agreement with previous results obtained by Tanaka and Ohtsuka,^{14, 16} who measured n at a single wavelength (633 nm) and found it to vary linearly from 2.21 to 2.55 over the composition range 15 to 40 atomic% As.

The increase in n with As content may be due to the increase in density and compactness of the glass as its composition approaches $As_{40}S_{60}$. Tsuchihashi and Kawamoto¹⁷ reported that the structure of the glass tends towards that of plastic S as the As content is reduced below 40 atomic%, which results in an opening up of the structure.

In order to see the effect of annealing on the compositional dependence, figure 6.9 plots n at 633 nm as a function of As content for as-deposited and annealed films. This figure shows that annealing increases n and the magnitude of the increase becomes larger as the As content increases. Similar results were obtained by Tanaka and Ohtsuka,¹⁶ whose data are also plotted in this figure. The composition dependence of the change in n for the pre-annealing effect is similar to that produced by photostructural change, and in particular photodarkening,^{18, 19} the extent of which is found to decrease with decreasing As content. In the case of the irreversible photodarkening exhibited by as-deposited As-S films, the effect is due to light-induced polymerization of the molecular component of the film, particularly As_4S_4 molecules. As the As content is reduced below 40 atomic% the amount of molecular As-S in the film decreases, hence the extent of photodarkening is less. It is also possible that As-As bonds in the network structure may be contributing to the changes in n resulting

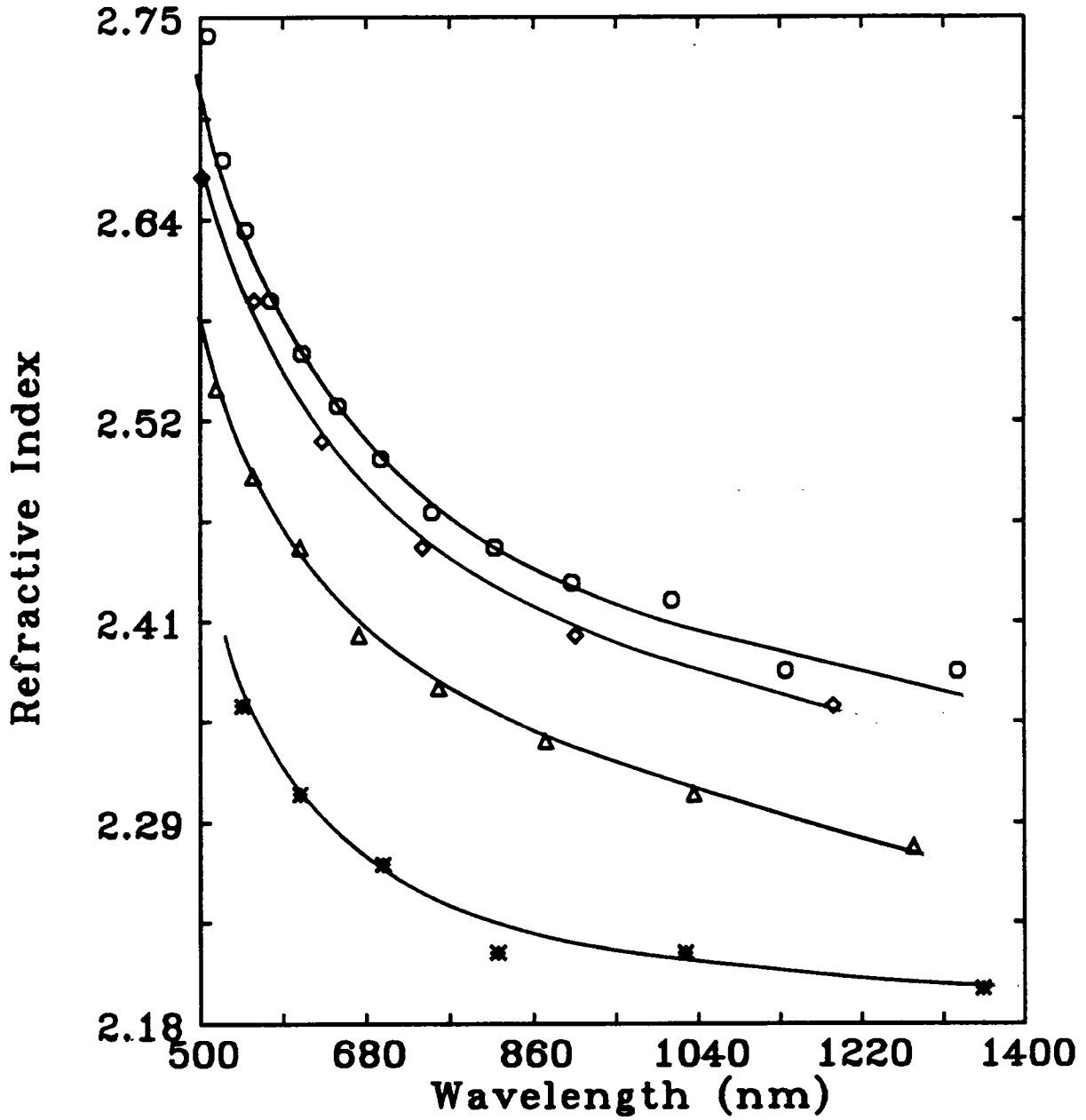


Figure 6.7. Spectral dependence of the refractive index for annealed As-S films. Each curve corresponds to a different composition: $As_{40}S_{60}$ (o), $As_{37}S_{63}$ (◊), $As_{30}S_{70}$ (Δ) and $As_{20}S_{80}$ (*).

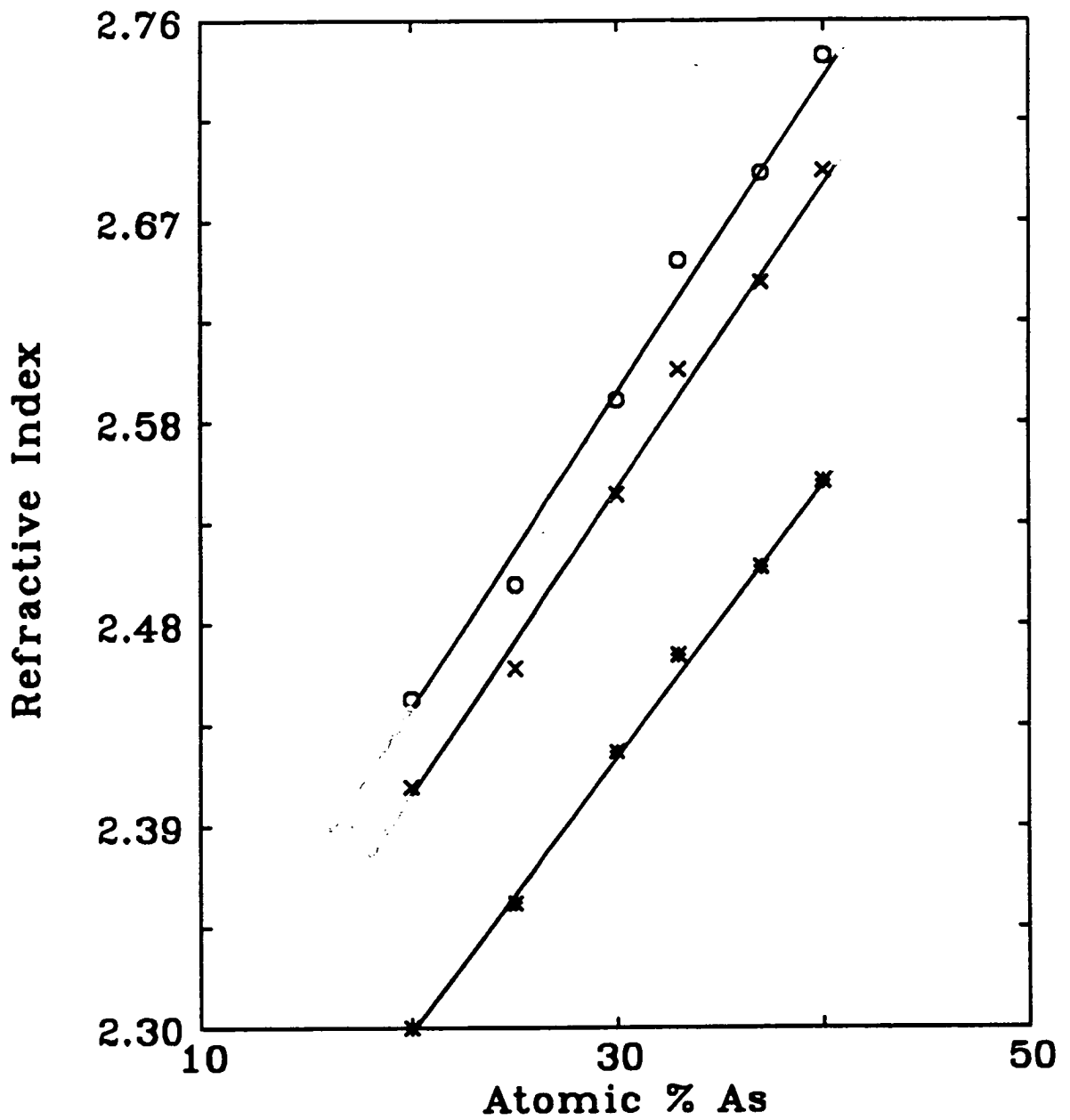


Figure 6.8. Variation of refractive index with As content for annealed As-S films. Each group of data corresponds to a different wavelength: 488 nm (o), 514 nm (x) and 633 nm (*).

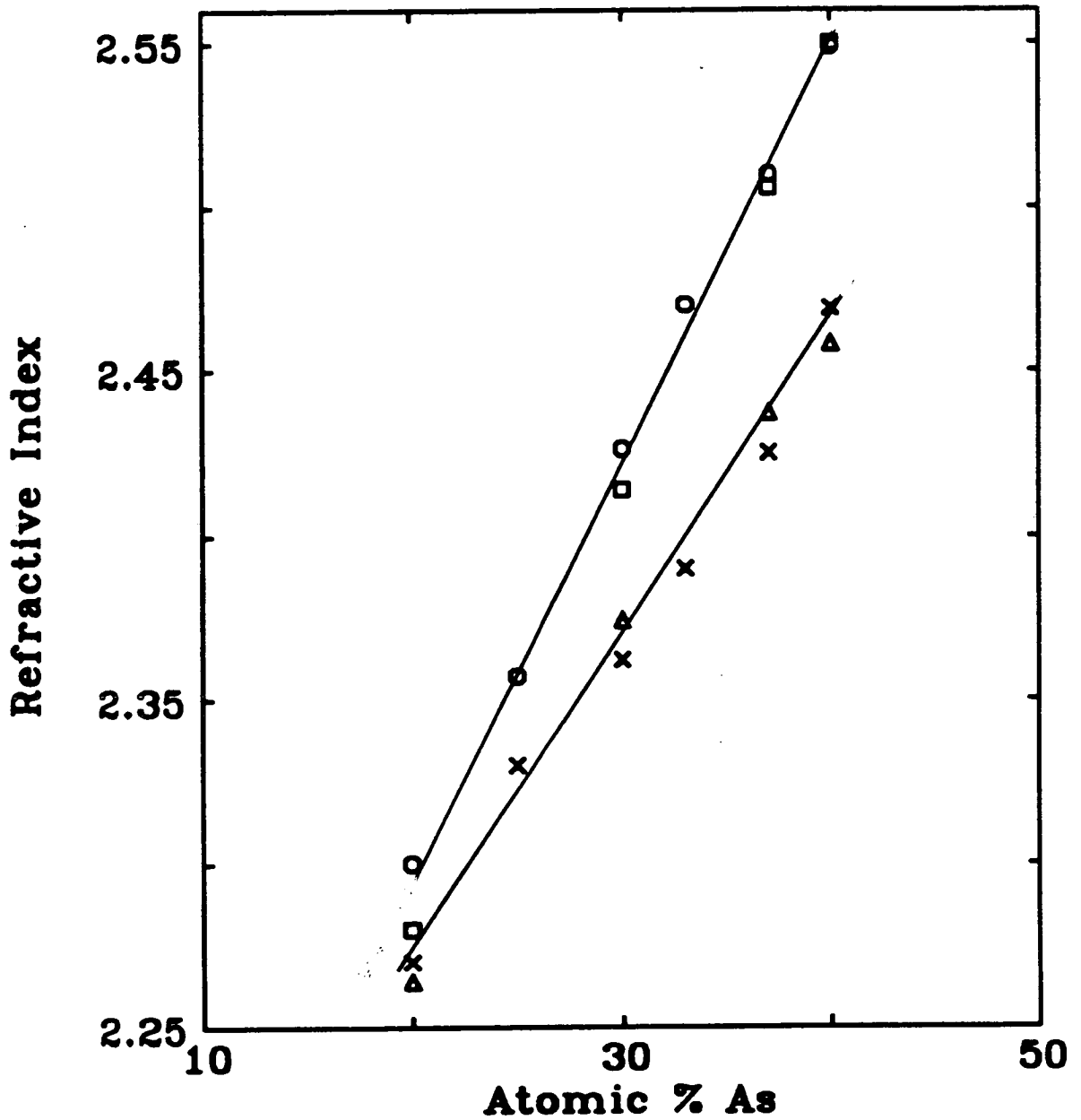


Figure 6.9. Variation of refractive index with As content for annealed (o) and as-deposited (x) As-S films. Tanaka's results¹⁶ are represented by □ for annealed and Δ for as-deposited As-S films.

from exposure to light, since the As-As bond density increases in $\text{As}_{40}\text{S}_{60}$ when it is photodarkened.²⁰ As the As content is reduced, the As-As bond density decreases, effectively dropping to zero below 40 atomic% As, so that again the effect is less pronounced for less As-rich films. Since the annealing treatment appears to have the same effect on n as light exposure, the above arguments can also be used to explain the effect of annealing on the composition dependence of n in As-S films.

The Ag-photodoped films used in this compositional study were prepared by photodoping different As-S compositions with the same amount of Ag, namely 27 atomic%. The films were illuminated for sufficient time to enable the Ag to traverse across the full thickness of the As-S film. This concentration is in the range which gives a homogeneous photodoped material for As-S compositions around $\text{As}_{30}\text{S}_{70}$. The compositional trend of the refractive index of these photodoped materials will be with respect to As concentration. Figure 6.10 shows the refractive index at 488, 514 and 633 nm versus As content for four photodoped films. These results exhibit a very interesting finding, which is the peak at 30 atomic% As for all these wavelengths. This peak might be due to the fact that $\text{As}_{30}\text{S}_{70}$ yields a homogeneous structure after photodoping, whereas glasses on either side of this composition become phase separated, which results in grain boundaries within the glass structure. This type of structure tends to be less dense and less compact which causes a decrease in the refractive index.

The compositional trend for undoped films is quite different from that for photodoped films, as shown in figure 6.11(a) which compares the corresponding plots for 633 nm. The refractive index of As-S films is a maximum at 40 atomic% As,¹⁴ whereas that for the photodoped material peaks at 30 atomic% As. The possible reasons for these observations have been explained above. The study of the composition dependence also yields quantitative information on the percentage change in refractive index as a result of photodoping. This is shown in figure 6.11(b), which indicates that the maximum change occurs at 30 atomic% As. The percentage refractive index change here is defined as the difference between the refractive indices of the undoped and

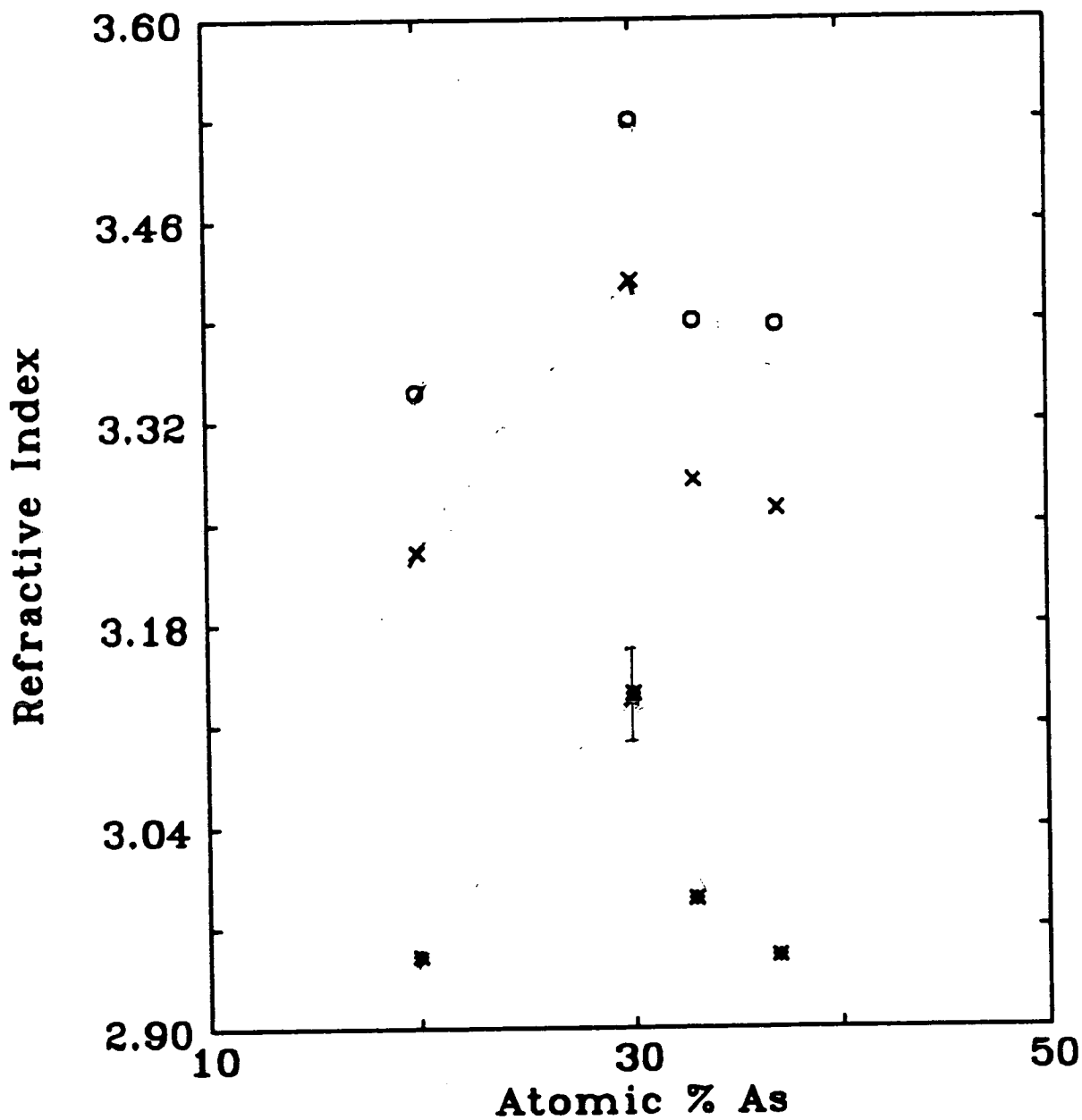


Figure 6.10. Effect of As content on the refractive index of photodoped, annealed As-S films. Each group of data corresponds to a different wavelength: 488 nm (o), 514 nm (x) and 633 nm (*). The Ag concentration is 27 atomic%.

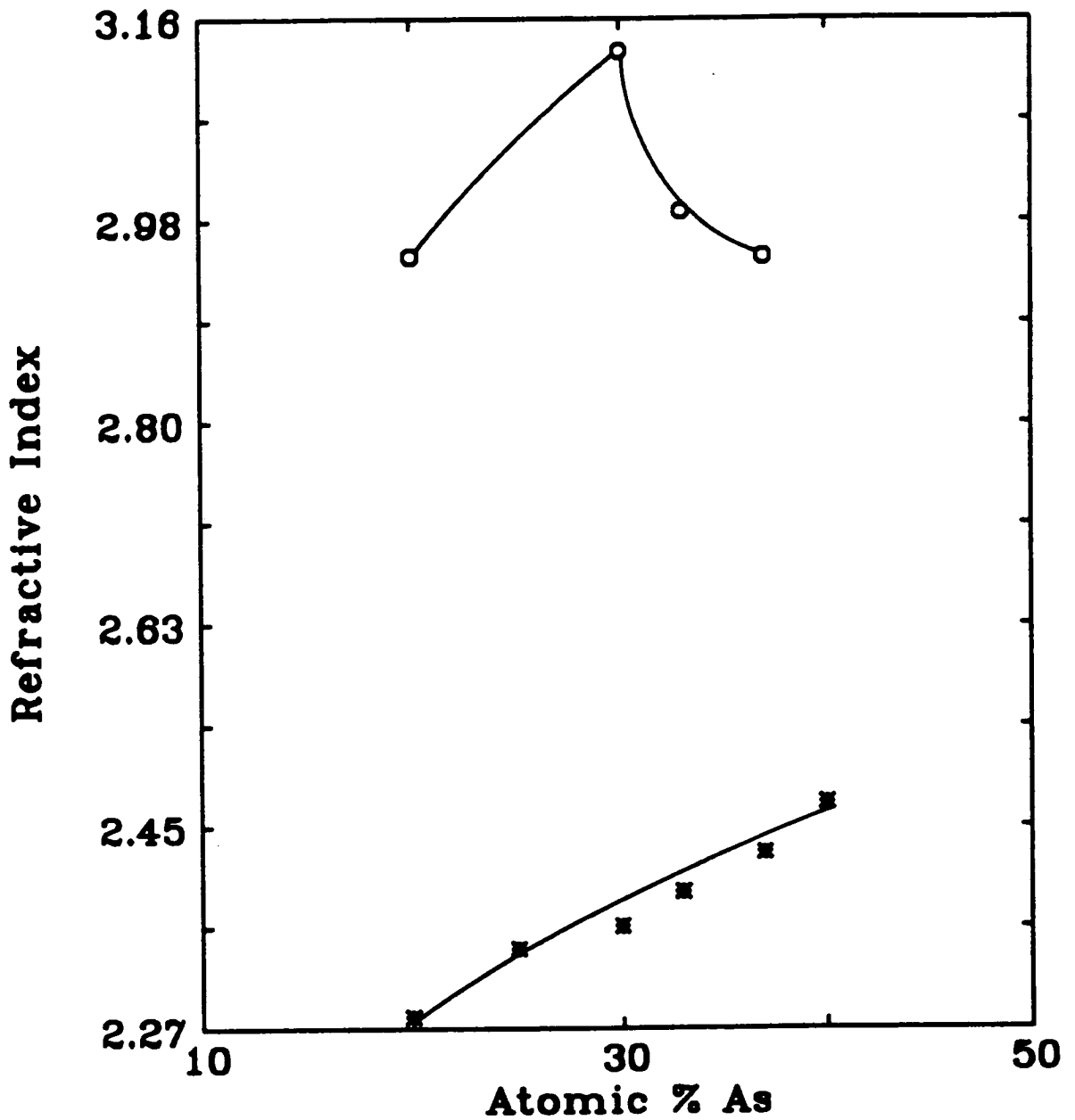


Figure 6.11(a). Comparison of the variation of refractive index with As content for undoped (*) and photodoped (o), annealed As-S films. The results are for a wavelength of 633 nm. The Ag concentration in the photodoped films is 27 atomic%.

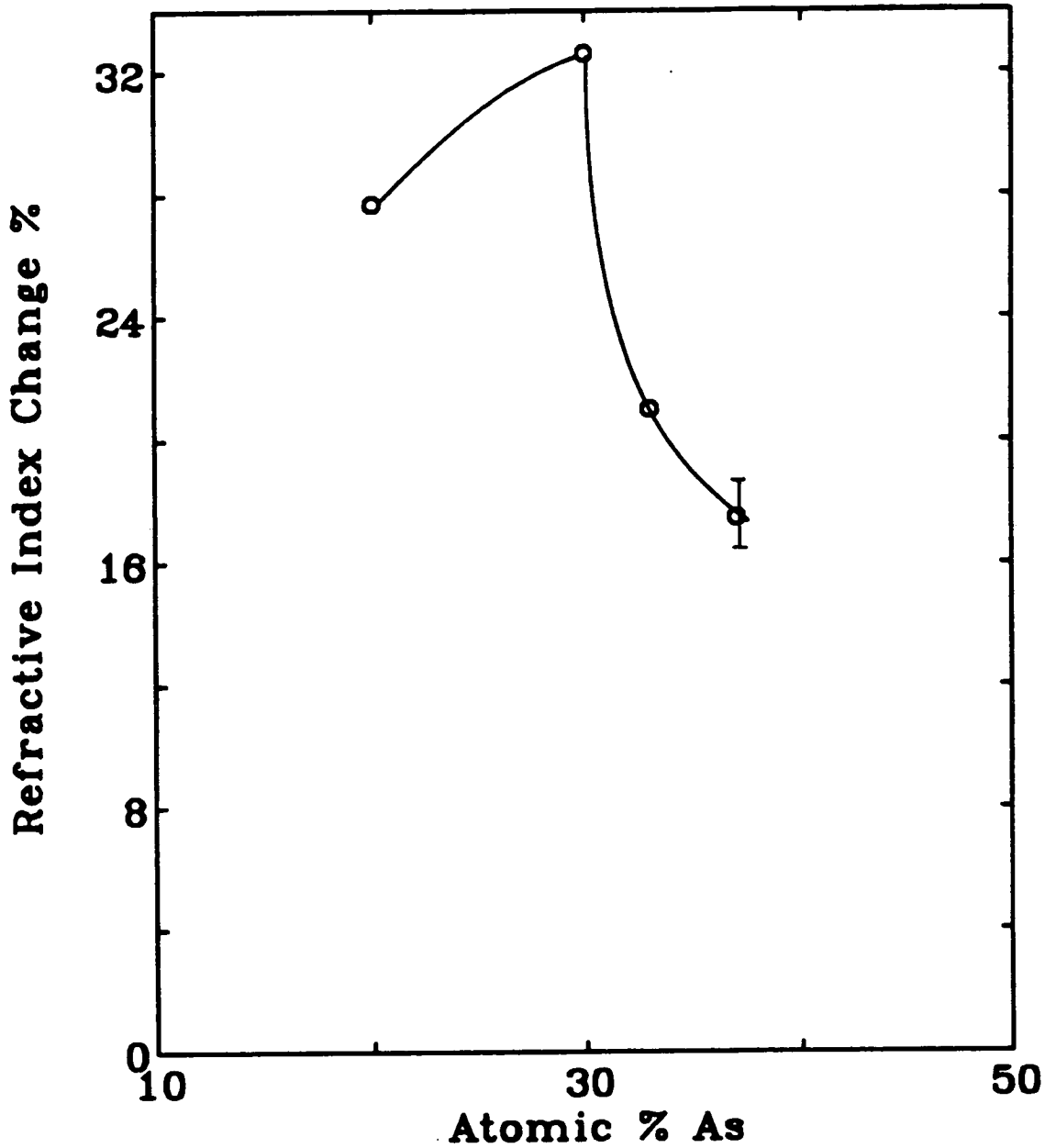


Figure 6.11(b). Effect of As content on the difference in refractive index between undoped and photodoped, annealed As-S films. The results are for a wavelength of 633 nm. The Ag concentration in the photodoped films is 27 atomic%.

photodoped films (n_u and n_{ph} respectively) divided by that of the undoped film:

$$(n_{ph} - n_u) \times 100 / n_u \quad (6.7)$$

This result is important from the point of view of applications, particularly with regard to grating technology, since grating efficiency depends on refractive index modulation. It would appear that compositions around $As_{30}S_{70}$ are the optimum for producing gratings by photodoping because they yield a homogeneous product, they exhibit minimum photodarkening, and they produce the largest change in refractive index.

Because the Ag-photodoping of $As_{30}S_{70}$ is believed to yield a homogeneous structure, it is worthwhile investigating the variation of refractive index with Ag concentration, as was done for $As_{40}S_{60}$. Figure 6.12 shows the spectral dependence of the refractive index for several Ag concentrations. In order to determine the refractive index dependence on Ag concentration, the values of n at 488, 514, 633 nm were derived from this data and plotted as a function of Ag concentration, as shown in figure 6.13. For Ag concentrations less than 12 atomic%, there is some curvature to these plots and n varies more slowly with Ag concentration, possibly because the low Ag concentrations do not result in a homogeneous photodoped product. Figure 6.14 compares the variation of n (at 633 nm) with Ag content for $As_{40}S_{60}$ and $As_{30}S_{70}$. It is apparent from this figure that the refractive index of $As_{40}S_{60}$ is larger than that of $As_{30}S_{70}$ at Ag contents less than 16 atomic%. However, above 16 atomic% Ag, the refractive index becomes larger than that of $As_{40}S_{60}$. This may be due to the fact that $As_{30}S_{70}$ yields a homogeneous structure after photodoping whereas $As_{40}S_{60}$ becomes phase separated, which results in grain boundaries within the glass structure. This type of structure tends to be less dense and less compact which causes a decrease in the refractive index. Similar results were found by Zakery et al. but for as-deposited $As_{30}S_{70}$ films.⁵

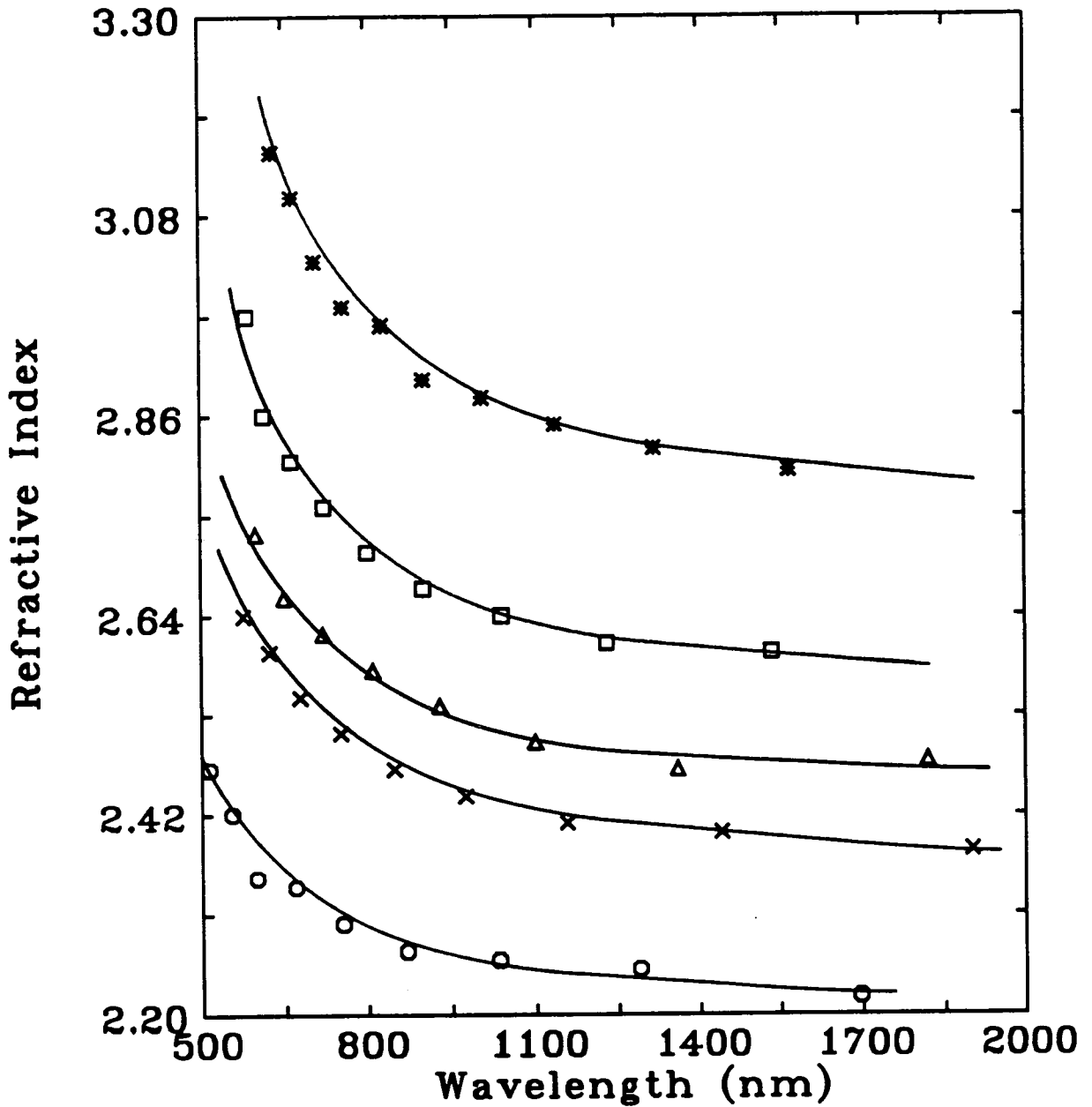


Figure 6.12. Spectral dependence of the refractive index of undoped and photodoped $As_{30}S_{70}$ films. Each curve corresponds to a different atomic% of Ag: 0 (o), 12 (x), 15 (Δ), 20 (\square), 27 (*). The thicknesses of the $As_{30}S_{70}$ films ranged from 500 to 800 nm. These results are for pre-annealed films.

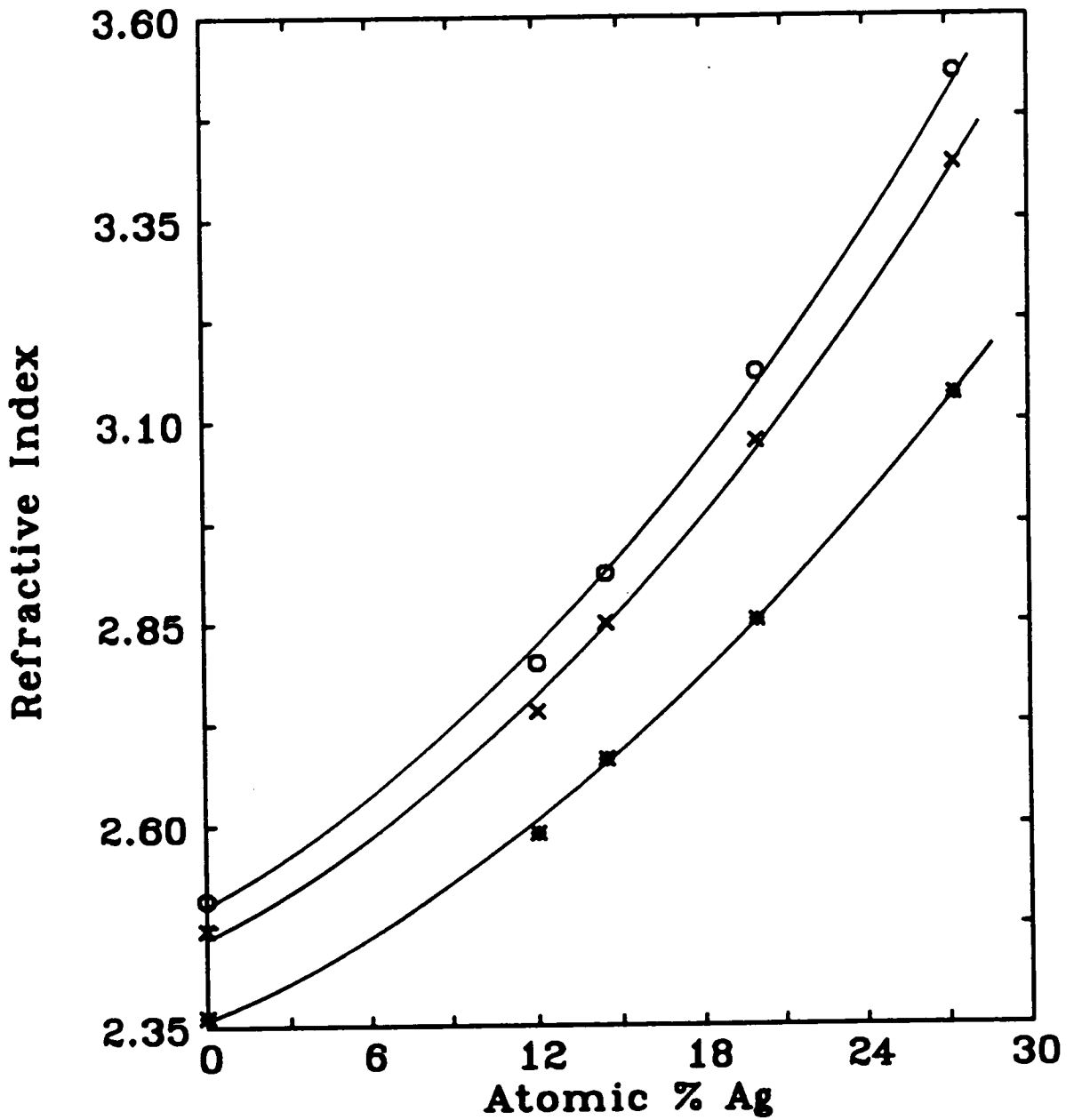


Figure 6.13. The effect of Ag content on the refractive index of annealed $As_{30}S_{70}$ films. Each group of data corresponds to a different wavelength: 488 nm (o), 514 nm (x) and 633 nm (*).

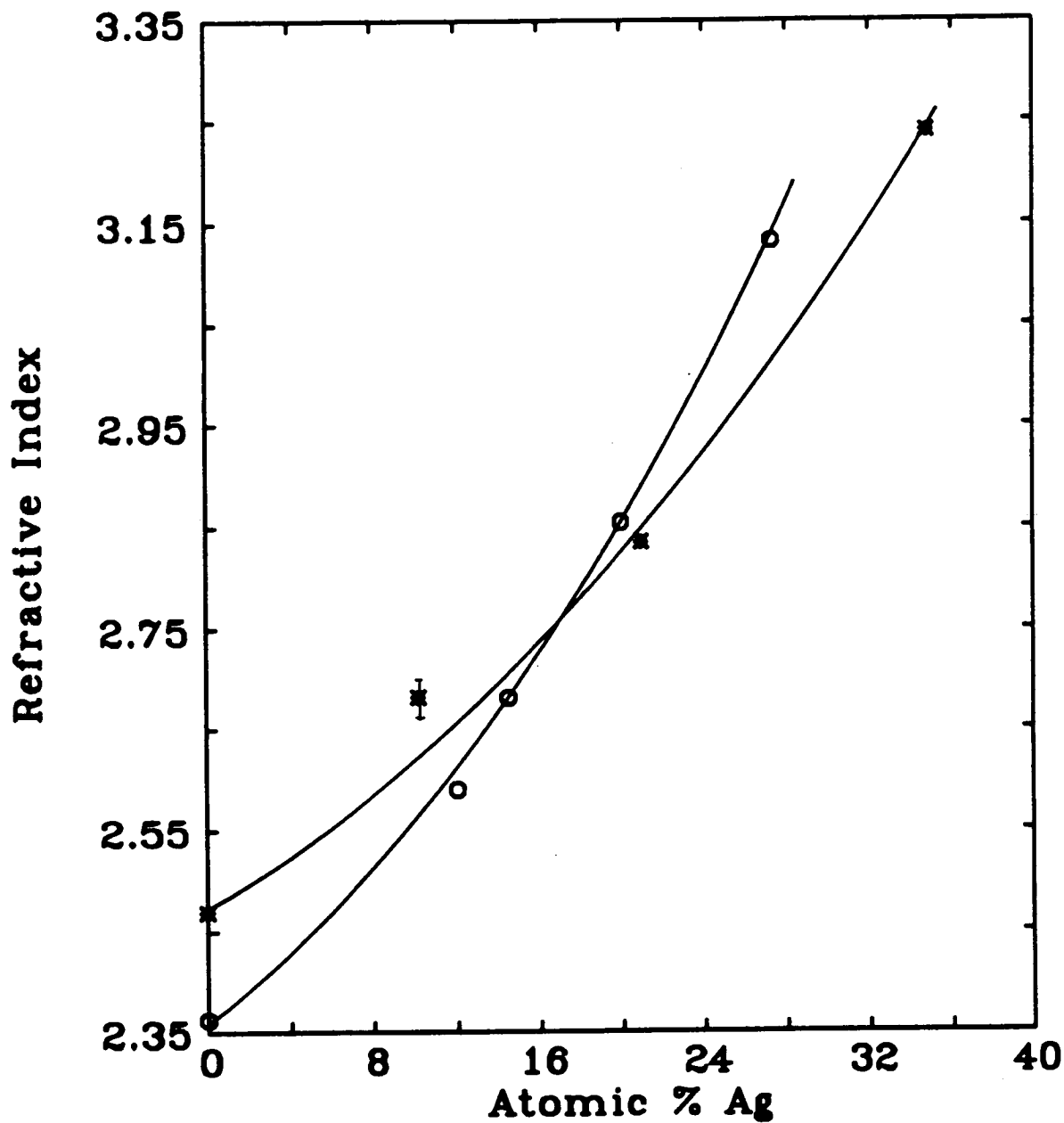


Figure 6.14. A comparison of the effect of Ag content on the refractive index of annealed $As_{30}S_{70}$ (o) and $As_{40}S_{60}$ (*) films. These results are for a wavelength of 633 nm.

6.3. Optical absorption

In this section, the measurements of the absorption coefficient, α , of the stoichiometric composition $As_{40}S_{60}$ will be presented for the visible region. The effect of the pre-annealing treatment and photodoping on the absorption coefficient will also be examined and the optical gap calculated.

According to Wood and Tauc,²¹ the optical absorption curve of an amorphous semiconductor typically consists of three parts, as described below.

a) A high absorption region ($\alpha \geq 10^4 \text{cm}^{-1}$) where, assuming parabolic band edges and energy independent matrix elements for interband transitions, the absorption coefficient is given by

$$\alpha(h\nu) = B(h\nu - E_g)^2 / h\nu \quad (6.8)$$

Here $h\nu$, E_g and B denote the photon energy, the optical gap, and a constant respectively. An optical gap E_g is then formally defined as the intercept of the curve of $(\alpha h\nu)^{1/2}$ versus $h\nu$.

b) An intermediate absorption range ($1 \text{cm}^{-1} < \alpha < 10^4 \text{cm}^{-1}$) in which absorption depends exponentially on photon energy:

$$\alpha(h\nu) = \alpha_0 e^{(h\nu/E_1)} \quad (6.9)$$

α_0 is a constant and E_1 a slope parameter which is usually between 0.05 and 0.08 eV.

c) A weak absorption tail at low absorption constants ($\alpha < 1 \text{cm}^{-1}$) whose shape and magnitude depend on the purity, thermal history and preparation conditions.

For the calculation of the absorption coefficient, the following formula will be used

$$x = e^{(-\alpha d)} \quad (6.10)$$

where x can have two different expressions depending on the spectral

region of interest (these regions were described earlier in section 6.2). In the first and second regions, where interference is present, x can be calculated using the following equation for the maximum transmissivity¹¹

$$T_M = Ax/(B - Cx + Dx^2) \quad (6.11)$$

where

$$A = 16n^2s \quad (6.12a)$$

$$B = (n+1)^3(n+s^2) \quad (6.12b)$$

$$C = 2(n^2-1)(n^2-s^2) \quad (6.12c)$$

$$D = (n-1)^3(n-s^2) \quad (6.12d)$$

In this region T_M has been chosen rather than T_m because the sensitivity of α to errors in the transmission is much lower for T_M than for T_m . In the third region, where there is no interference, T_M and T_m converge to a single curve T_0 known as the interference-free transmission. In this case, x can be expressed in terms of this interference-free transmission as

$$x = (n+1)^3(n+s^2)T_0/16n^2s \quad (6.13)$$

6.3.1. Optical absorption coefficient of undoped and Ag-photodoped $As_{40}S_{60}$

In contrast to the refractive index, the absorption coefficient was not significantly affected by the annealing treatment. Figure 6.15(a) shows the absorption coefficient versus photon energy over the range 380-540 nm for $As_{40}S_{60}$ before and after annealing (these measurements were made on a 800 nm thick film). The absorption

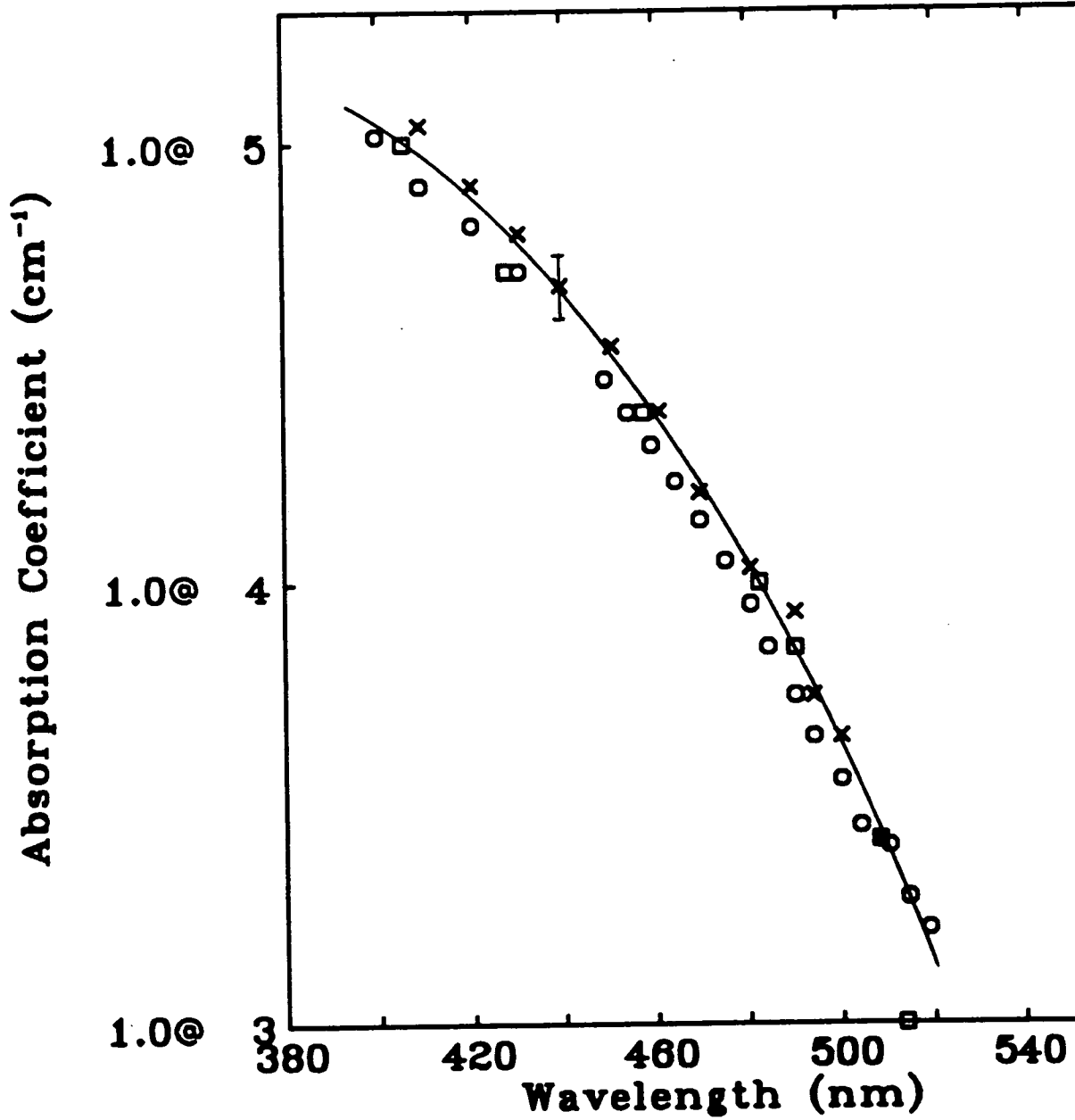


Figure 6.15(a). Spectral dependence of the absorption coefficient for annealed (x) and as-deposited (o) $\text{As}_{40}\text{S}_{60}$ films. The thickness is about 800 nm. Kosek's results²³ are represented by □.

coefficient of $As_{40}S_{60}$ has been measured by several authors.^{16, 22-24} The values obtained by Kosek²³ are also plotted in figure 6.15(a) and are in good agreement with the present results. The fact that annealing has little effect on the absorption coefficient might be due to the fact that it produces only a small change in the refractive index. The change in the refractive index must be large in order to produce a significant change in the absorption coefficient, as seen in the case of Ag-photodoping. Figure 6.15(b) compares the spectral dependence of α for undoped $As_{40}S_{60}$ with that for $As_{40}S_{60}$ heavily photodoped with Ag. Photodoping clearly produces a very significant change in α over this spectral range.

Using equation 6.8 for the high-absorption region the optical gap E_o for each sample can be determined from the intercepts of plots of $(\alpha h\nu)^{1/2}$ versus $h\nu$ such as that shown in figure 6.16 for annealed and as-deposited $As_{40}S_{60}$. The optical gap is about 2.39 and 2.42 eV for the annealed and as-deposited films respectively, and so is not significantly affected by the annealing treatment used in this work ($\Delta E_g = 0.03$ eV). A similar value of ΔE_g was reported by Deneufville et al.¹⁰ The values of the optical gap of $As_{40}S_{60}$ reported in the literature lie between 2.32 and 2.4 eV: Kosek²³ reported a value of 2.32 eV, whereas Kolomiets²⁵ obtained a value of 2.4 eV and Yamaguchi²⁴ 2.36 eV. These different values for the optical gap might be due to differences in the evaporation conditions used to deposit the films. The optical gap of an annealed film may be similar to that of an as-deposited film either because the annealing conditions used do not cause any important structural changes or because the optical gaps of these materials are not sensitive to the structural changes produced. Annealing treatment is known to shift the absorption edge of an *illuminated* $As_{40}S_{60}$ film towards higher energies.²⁶ This effect is related to the so-called reversible photodarkening phenomenon. However, in the present case annealing was carried out on an as-deposited (non-illuminated) film rather than illuminated one.

In contrast to annealing, the photodoping of $As_{40}S_{60}$ with Ag causes the optical absorption edge to be shifted significantly towards lower photon energies, as shown in figure 6.17, which compares the

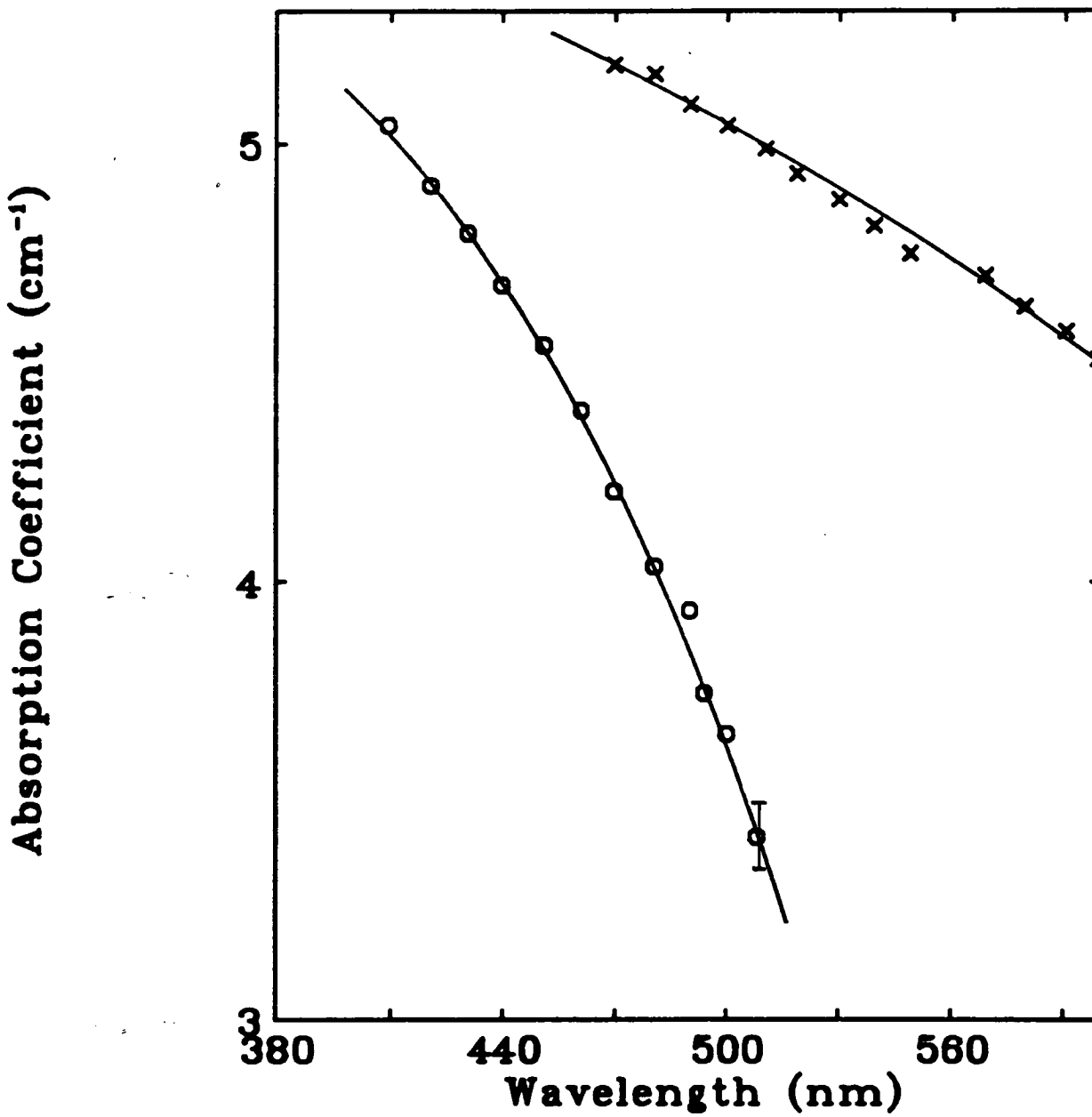


Figure 6.15(b). Spectral dependence of the absorption coefficient for annealed, undoped $As_{40}S_{60}$ films (o) and $As_{40}S_{60}$ films photodoped with the maximum amount of Ag (38.4 atomic %) (x). The film $As_{40}S_{60}$ thicknesses were about 800 nm.

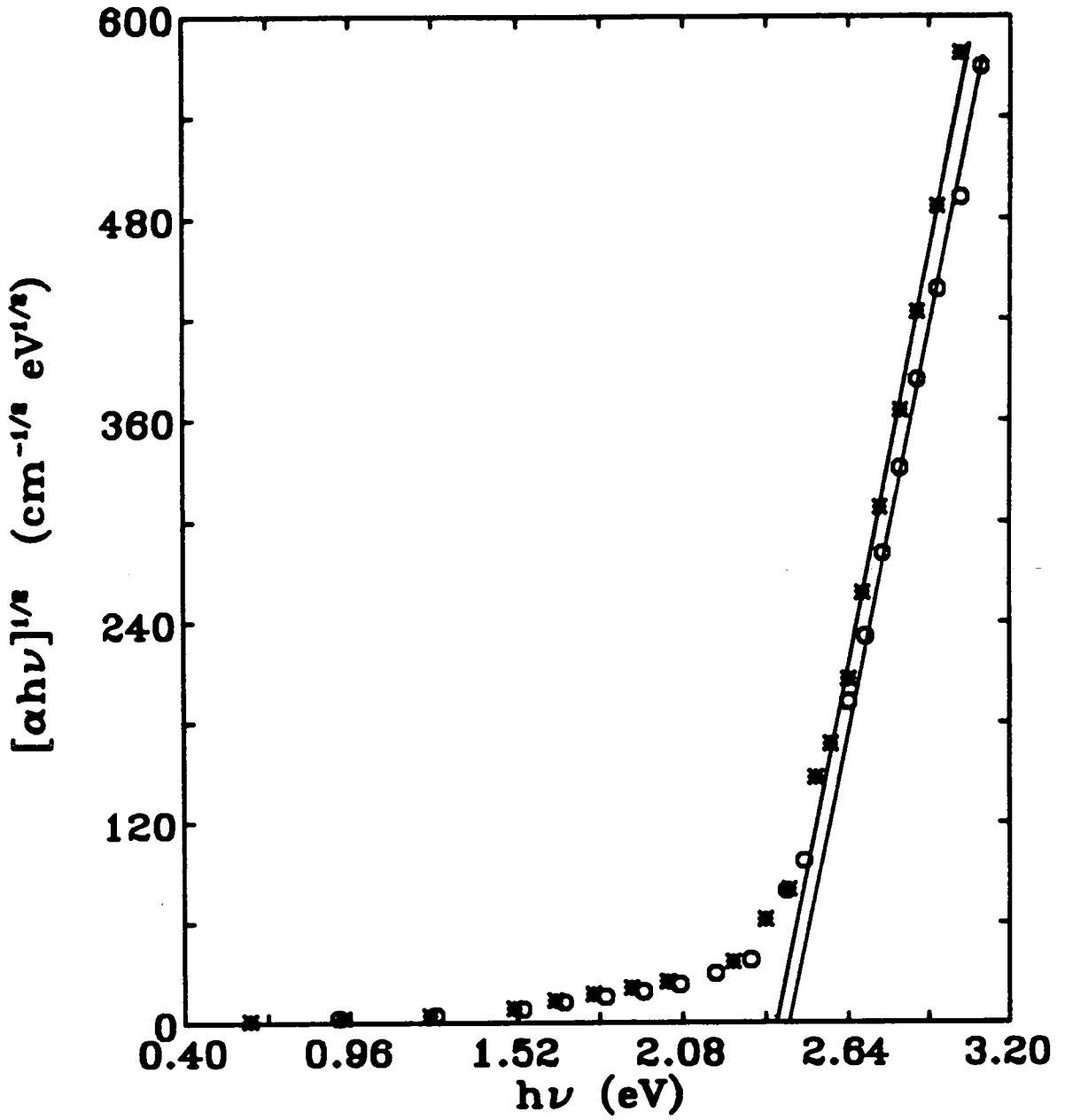


Figure 6.16. Optical absorption edge of annealed (*) and as-deposited (o) $\text{As}_{40}\text{S}_{60}$ films plotted as $(\alpha h\nu)^{1/2}$ versus $h\nu$.

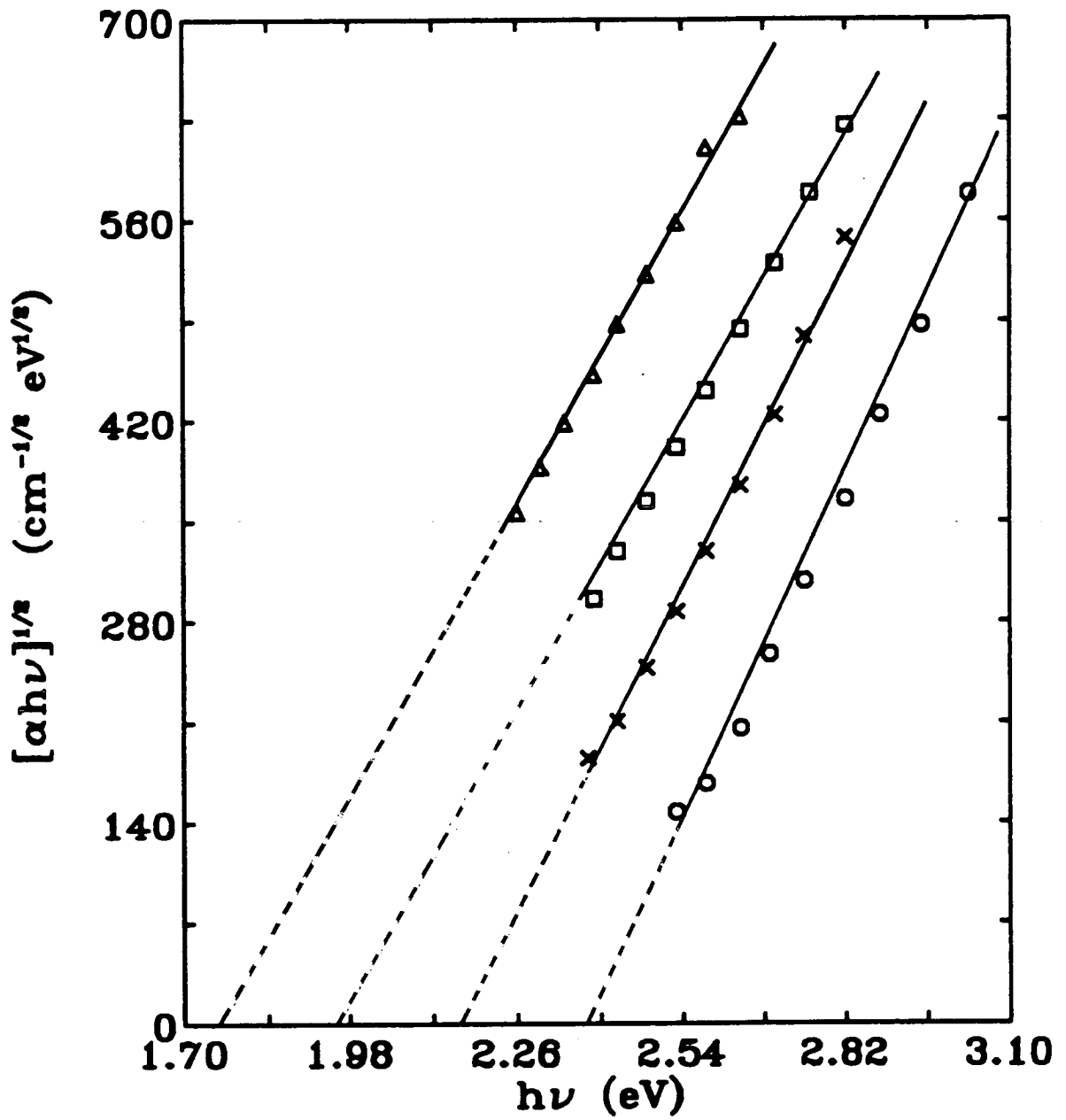


Figure 6.17. Optical absorption edge of annealed undoped (o) and photodoped $\text{As}_{40}\text{S}_{60}$ films. Each set of data corresponds to a different atomic% of Ag: 0 (o), 10 (x), 21 (\square), 34.8 (Δ).

$(\alpha h\nu)^{1/2}$ versus $h\nu$ plots for undoped $\text{As}_{40}\text{S}_{60}$ with those for three Ag photodoped samples. The optical absorption edge shift increases with increasing Ag concentration. This finding is clearly apparent in figure 6.18, where the optical gap determined from the plots in figure 6.17 is plotted directly versus Ag concentration for both as-deposited and pre-annealed films. This figure shows clearly that the Ag-photodoping causes a decrease in the optical gap. Similar results have been found for as-deposited films by Shimizu et al.,^{27, 28} whose data is also shown in this figure. It is possible that the decrease in E_g on incorporation of Ag arises from the smaller binding energy of Ag-S bonds compared to that of As-S bonds. The figure also shows that the optical gap of the photodoped $\text{As}_{40}\text{S}_{60}$ film is almost unaltered by the pre-annealing treatment. Again, this is probably because the structure of the photodoped product is not sensitive to the details of the initial structure of the $\text{As}_{40}\text{S}_{60}$ film.

The measurements of α , in this work, were limited to the visible spectrum because the absorption coefficient of As-S materials in the IR region is very small ($\alpha \leq 1\text{cm}^{-1}$).^{21, 22} Hence absorption coefficient measurements in the IR require thicker samples than used in this work. The sample thickness used to measure the absorption coefficient should satisfy the following relation:

$$\alpha d \approx 1 \quad (6.14)$$

The attempt made by Zakery et al.²⁹ to measure the absorption coefficient with thicknesses which did not satisfy the latter relation led to larger values of the IR absorption coefficient.

6.3.2. Compositional trend of optical absorption in As-S and Ag-photodoped films

The composition dependence of α at two wavelengths (488 and 514 nm) for annealed As-S films is shown in figure 6.19. Similar results were obtained for the as-deposited films. These results show

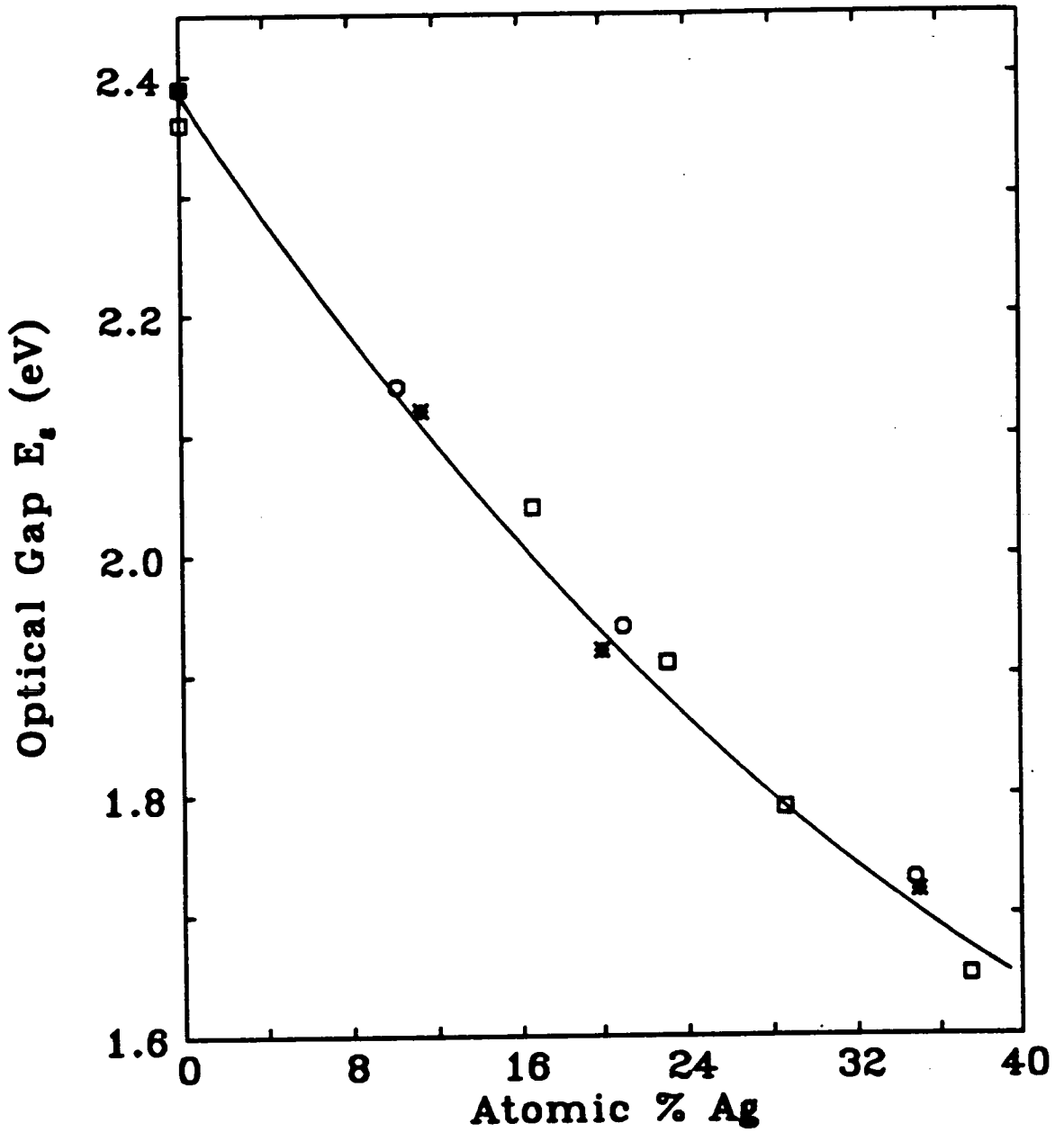


Figure 6.18. Effect of Ag content on the optical gap of annealed (o) and as-deposited (*) $As_{40}S_{60}$ films. the results of Shimizu et al.^{27,28} are also shown (□).

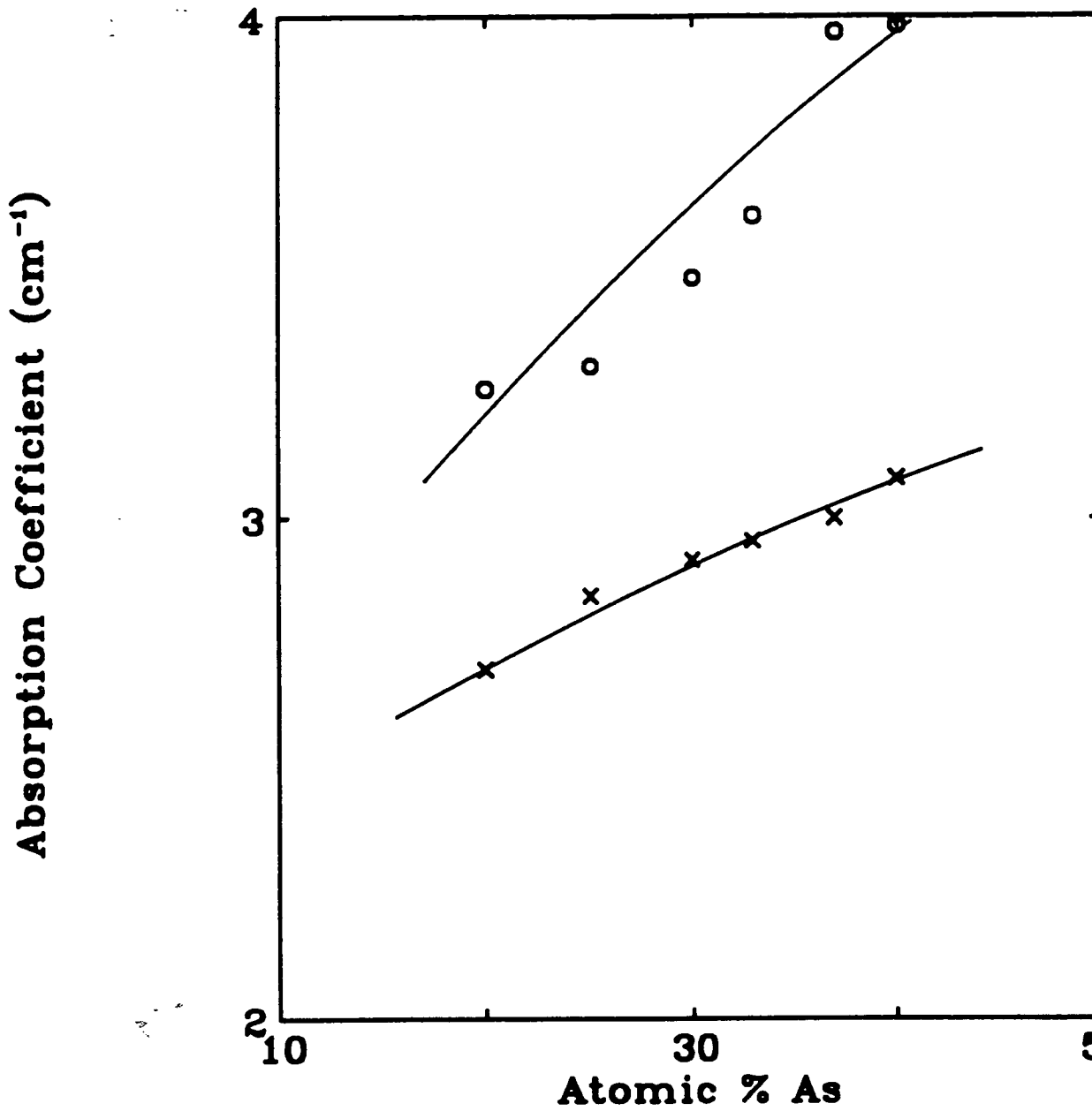


Figure 6.19. Effect of As content on the absorption coefficient of annealed As-S films. Each set of data corresponds to a different wavelength: 488 nm (o) and 514 nm (x).

that the absorption coefficient increases with increasing As content and that the slope of this trend increases at shorter wavelengths. The fact that the results for annealed samples are found to be similar to those for as-deposited, shows that the annealing treatment has little effect on the absorption coefficient for all the compositions investigated in this work. Similarly, Tanaka's¹⁶ results, obtained at 435 nm, showed that annealing produces only a very small increase in the absorption coefficient for all the As-S compositions. The magnitude of this increase in absorption coefficient was found to decrease as the S content is increased. This difference between his results and the present work might be due to the fact that the author used higher annealing temperatures (for each As-S composition investigated) than those used in the present study. For example, the annealing temperature he used for As₄₀S₆₀ was 180 °C.

Figure 6.20 shows that the plots of $(\alpha h\nu)^{1/2}$ versus $h\nu$ for annealed As-S undergo an almost parallel shift to lower photon energies as the As content decreases. The optical gaps determined from these plots are shown in figure 6.21 as a function of As content. The optical gap decreases as the atomic% of As increases. This finding is in good agreement with the work of Tanaka³⁰ whose results are also plotted in this figure. Similar results were obtained by Kosek,²³ who investigated As₂S_x samples with $3 \leq x \leq 5$. The decrease in E_g with decreasing S content is probably due to the fact that the bond strength of S-S bonds (229.9 kJ/mole) is greater than that of As-S (217.3 kJ/mole) or As-As (181.4 kJ/mole) bonds. As the S-S bond concentration decreases with decreasing S content, the average energy required to rupture a bond will therefore also decrease. The bonding energy values are taken from the work of Yamaguchi.²⁴

Plots of $(\alpha h\nu)^{1/2}$ versus $h\nu$ for various As-S compositions heavily photodoped with Ag are shown in figure 6.22. The optical edge is shifted towards lower photon energies as the As content increases in the photodoped films. This result is similar to that for undoped As-S films. This similarity is clearly apparent in figure 6.23, where the optical gaps of both Ag-photodoped and undoped As-S films are plotted versus As content.

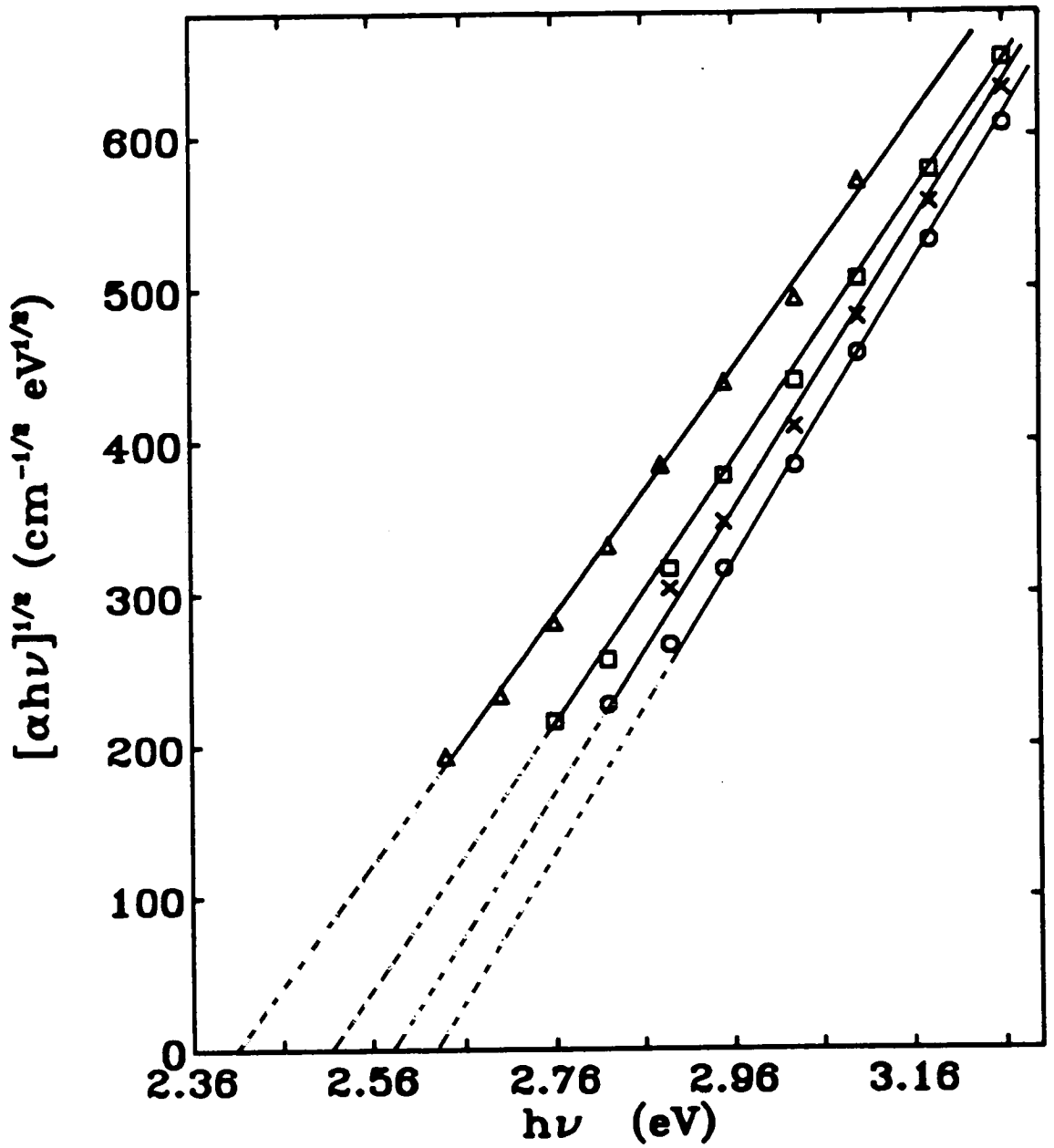


Figure 6.20. Optical absorption edges of annealed As-S films. Each set of data corresponds to a different composition: $\text{As}_{40}\text{S}_{60}$ (Δ), $\text{As}_{30}\text{S}_{70}$ (\square), $\text{As}_{25}\text{S}_{75}$ (x) and $\text{As}_{20}\text{S}_{80}$ (o).

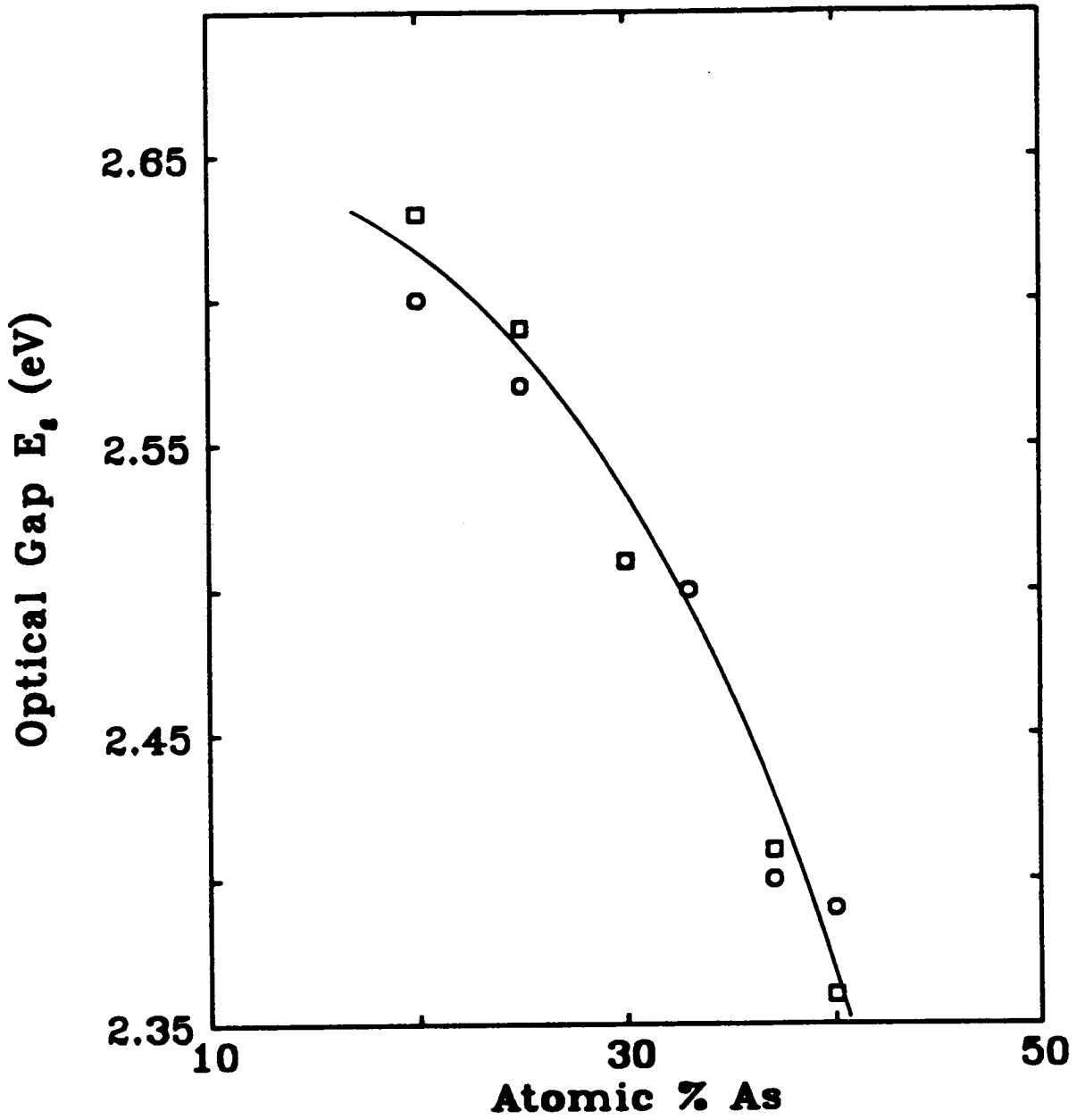


Figure 6.21. Effect of As content on the optical gap of annealed As-S films. Tanaka's results³⁰ are represented by □.

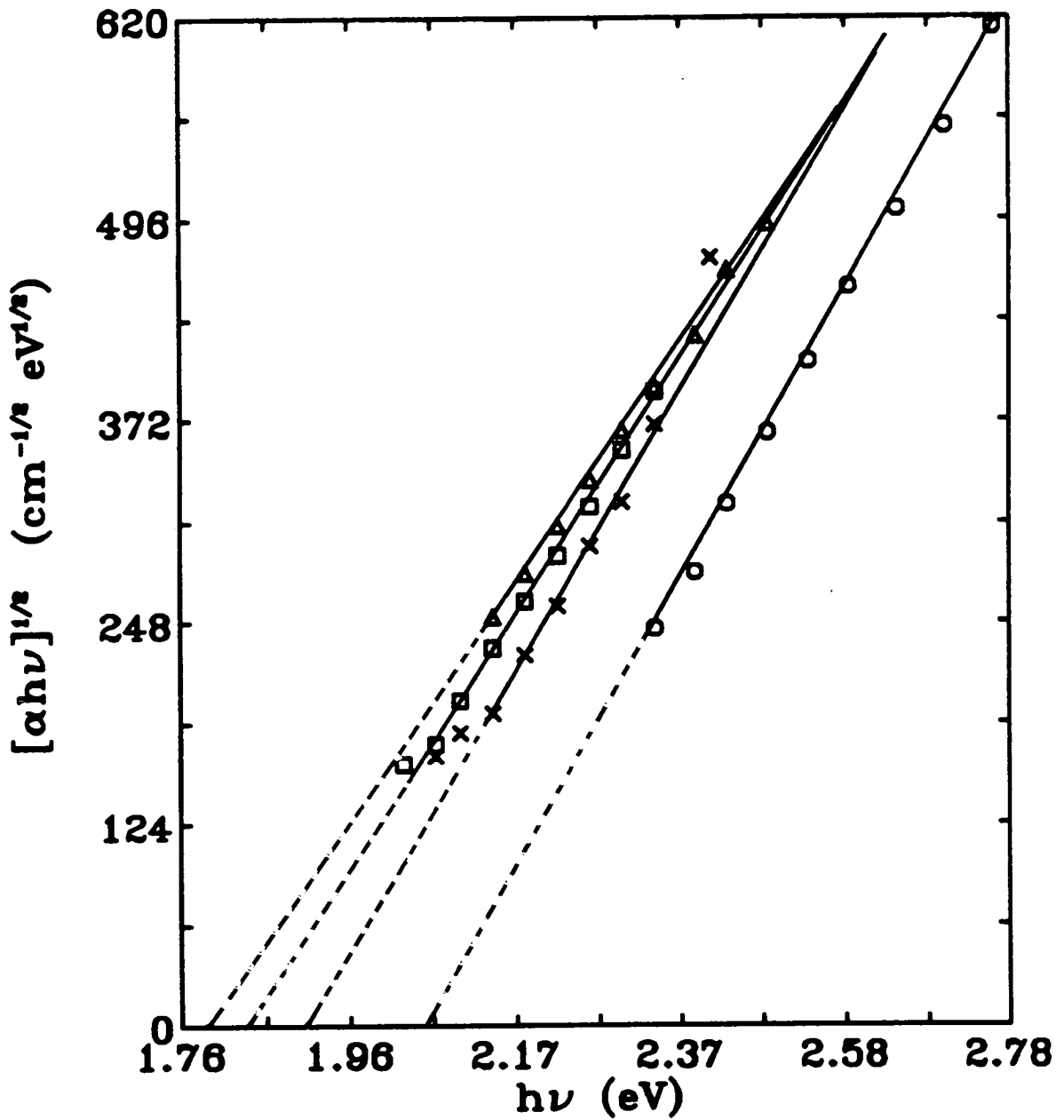


Figure 6.22. Optical absorption edge of photodoped, annealed As-S films. Each set of data corresponds to a different atomic% of As: 37 (Δ), 33 (\square), 30 (x) and 20 (o).

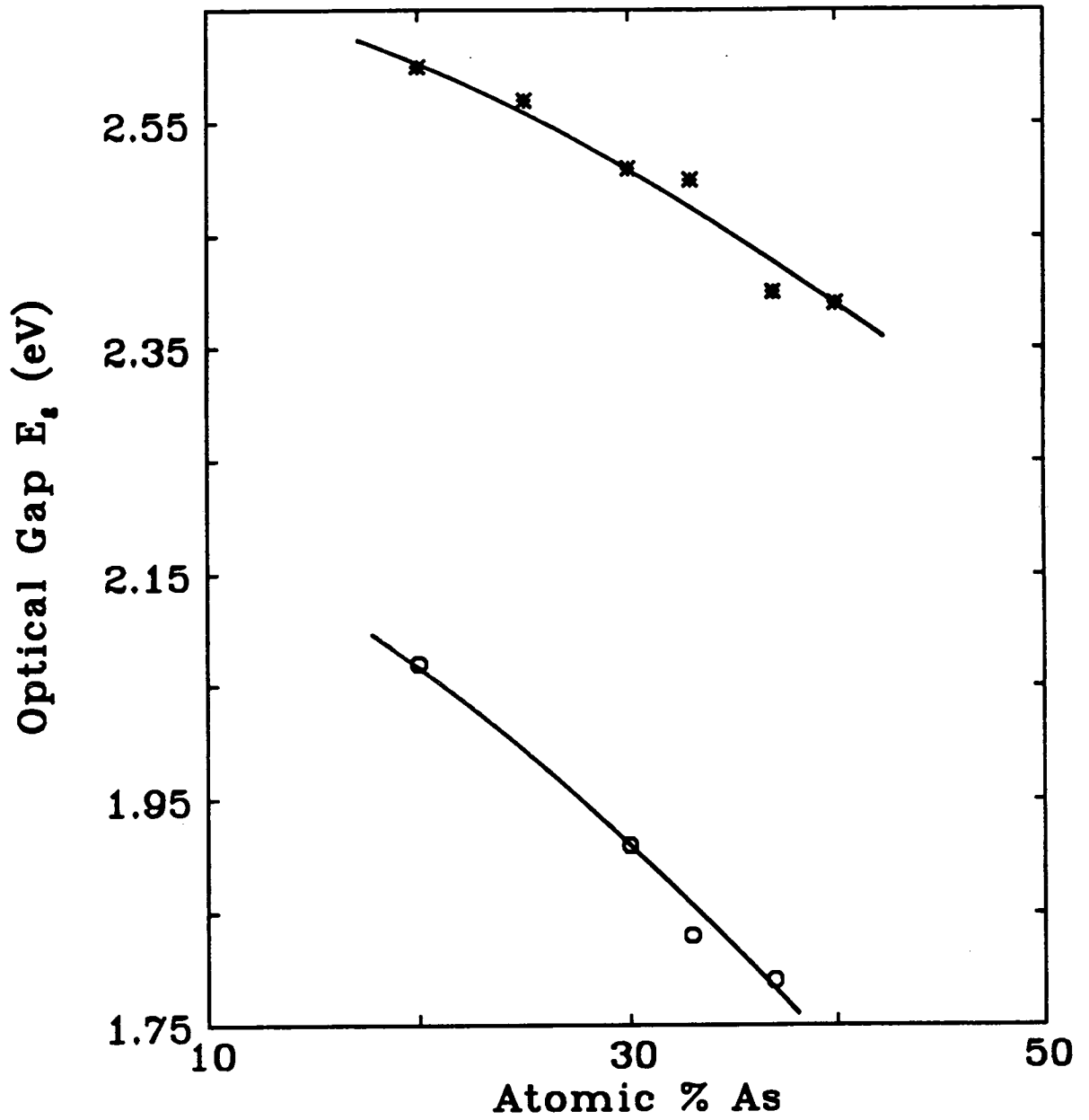


Figure 6.23. Effect of As content on the optical gap of undoped (*) and photodoped (o), annealed As-S films.

In figure 6.23 the slope of the plot for the undoped As-S samples is less than that for the photodoped films. This indicates that the presence of the Ag is affecting the S-S and As-S bond concentrations in such a way as to increase the influence of the relative concentration on E_g . Figure 6.24 shows the compositional trend of the change in the optical gap resulting from Ag-photodoping. The interesting feature of this figure is the peak around 33 atomic% As. The change in the optical gap here is defined as the difference between the optical gaps for the undoped and Ag-photodoped (E_{gu} and E_{gph} respectively) divided by that of As-S:

$$(E_{gu} - E_{gph})100/E_{gu} \quad (6.15)$$

The maximum change in the optical gap due to photodoping is about 27% and occurs for a composition around $As_{33}S_{67}$. This result is similar to that obtained for the refractive index (see section 6.2.2) and, again, may be due to the fact that compositions around this one yield a homogeneous product after photodoping. As stated earlier, $As_{30}S_{70}$ may be an important composition as far as applications are concerned and it is therefore of interest to investigate the dependence of optical absorption on Ag content for this material. Figure 6.25 shows that the optical edge is shifted towards lower photon energies as the Ag concentration increases, as in the case of Ag photodoped $As_{40}S_{60}$. The optical gaps for the photodoped $As_{30}S_{70}$ and $As_{40}S_{60}$ compositions studied are plotted versus Ag concentration in figure 6.26. Both types of film show a decrease in their optical gap as the Ag concentration increases. The results obtained by Shimizu et al.²⁷ are plotted in this figure showing a similar dependence to that for the $As_{40}S_{60}$ obtained in the present study. The variation in the optical gap for the photodoped $As_{30}S_{70}$ compositions is similar to that reported for photodoped $As_{30}S_{70}$ films which have not been pre-annealed.⁵

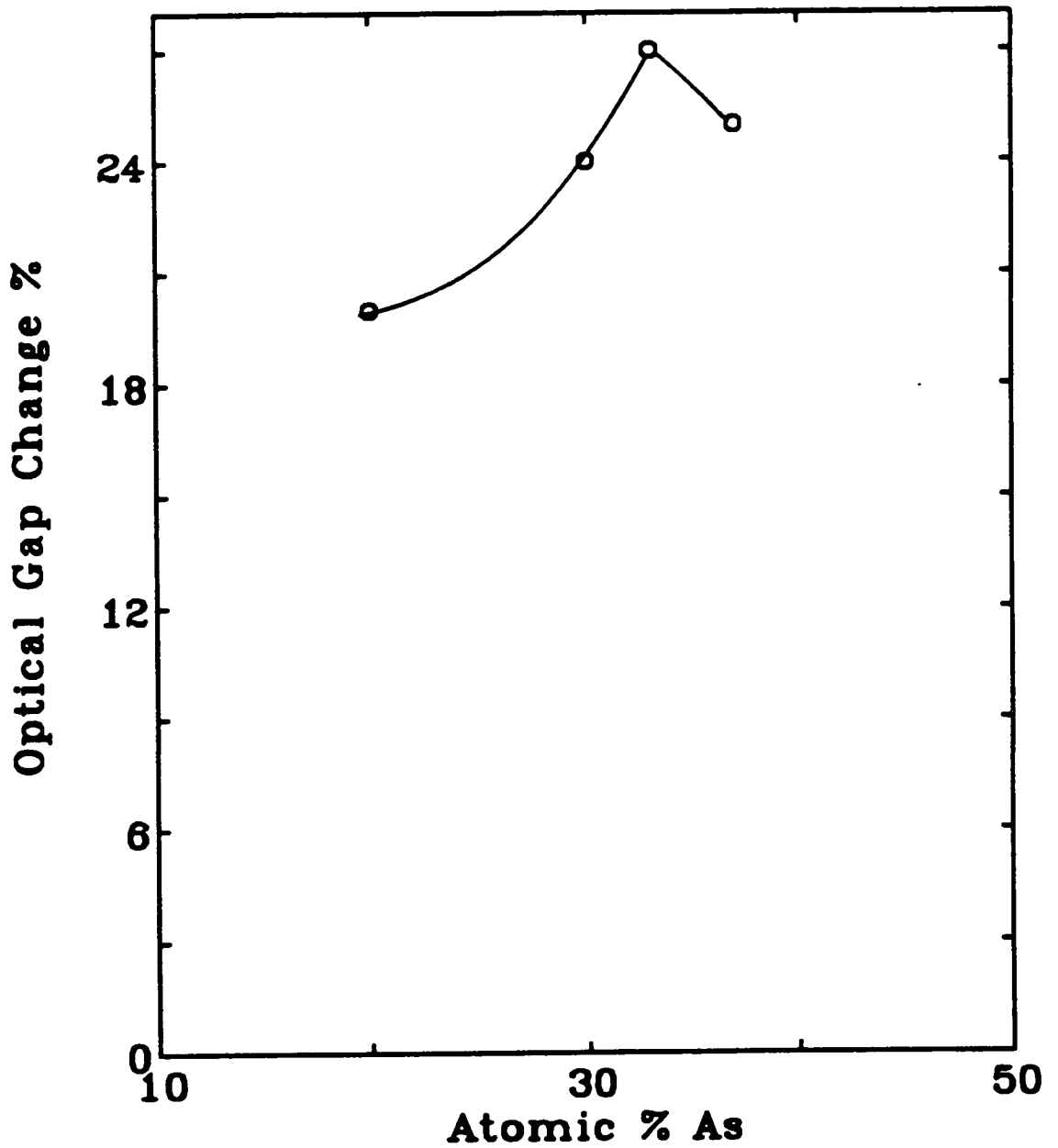


Figure 6.24. The effect of As content on the percentage difference in the optical gap between undoped and heavily doped, annealed As-S films. The heavily doped films contain 27 atomic% of Ag.

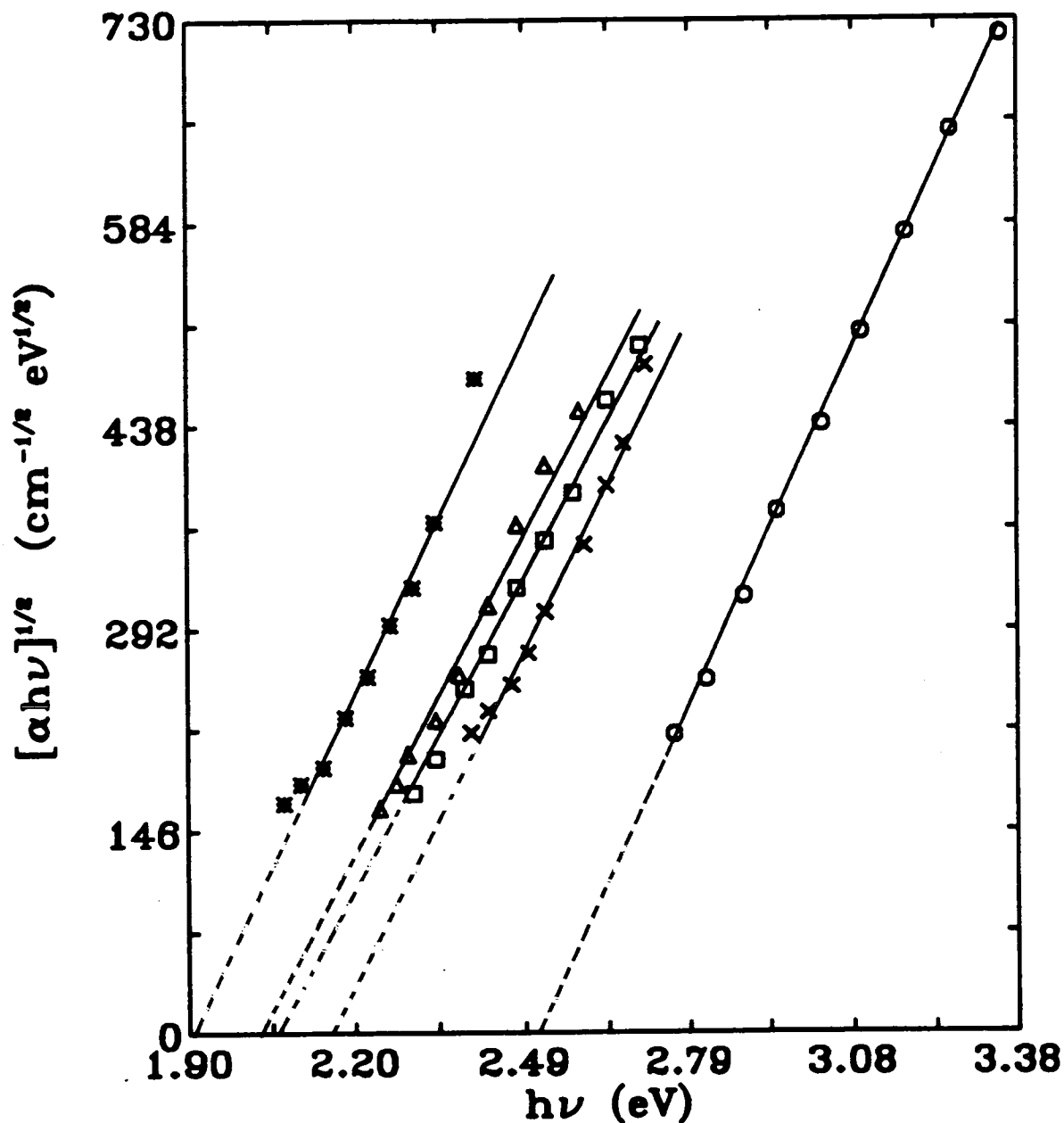


Figure 6.25. Optical absorption edge of annealed undoped (o) and photodoped $\text{As}_{30}\text{S}_{70}$ films. Each set of data corresponds to a different atomic% of Ag: 0 (o), 12 (x), 15 (\square), 20 (Δ), 27 (*).

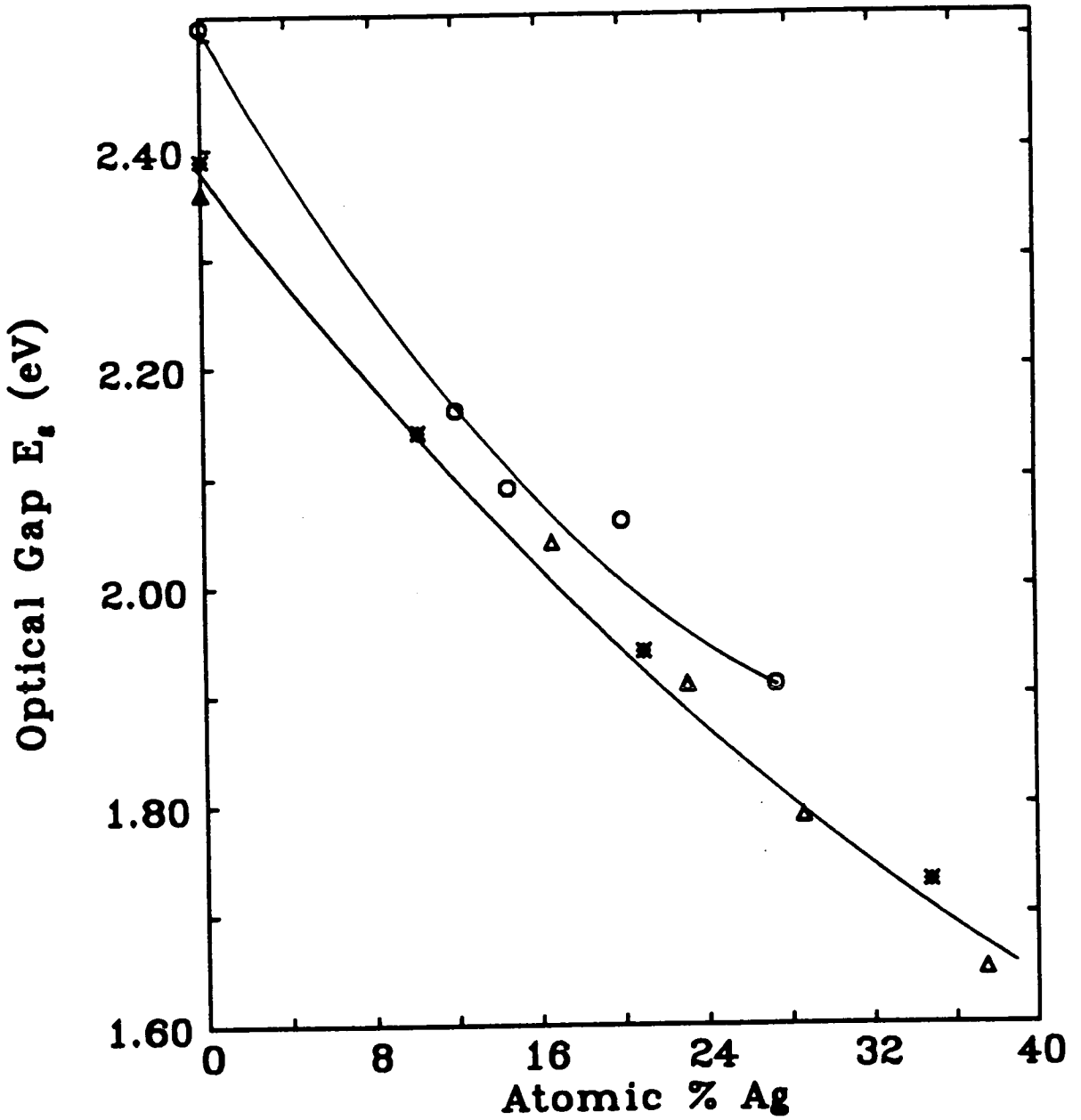


Figure 6.26. Effect of Ag content on the optical gap of annealed $As_{30}S_{70}$ (o) and $As_{40}S_{60}$ (*) films. Shimizu's results²⁷ are represented by Δ .

6.4. Dispersion and single oscillator energies

The dispersion of the refractive index of an amorphous material can be fitted by the Wemple-DiDomenico relation mentioned earlier and in this section this will be used to calculate, as explained in section 6.2, E_d and E_o for undoped and Ag-photodoped As-S films. Wemple has also pointed out that E_d obeys the simple empirical relation

$$E_d = \beta N_c Z_a N_e \text{ (eV)} \quad (6.16)$$

where β is equal to 0.37 eV for covalent materials (e.g. ZnS) and 0.26 eV for the more ionic materials (e.g. NaCl); N_c is the number of nearest neighbour cations to the anion (e.g. $N_c=6$ in NaCl); Z_a is the chemical valency of the anion (e.g. $Z_a=1$ in NaCl) and N_e is the total number of valence electrons per anion (e.g. $N_e=8$ in NaCl).

6.4.1. Dispersion and single oscillator energies of undoped and Ag-photodoped $As_{40}S_{60}$.

The effect of Ag on E_d and E_o for $As_{40}S_{60}$ and $As_{30}S_{70}$ will now be examined and these results will complement the earlier discussion of the refractive index and the optical gap. Figure 6.27(a) shows a plot of the dispersion energy, E_d , versus Ag concentration for annealed $As_{40}S_{60}$ and $As_{30}S_{70}$ films. E_d increases with increasing Ag content in the As-S structure. Similar to the refractive index results (figure 6.14 in section 6.2.2), this figure shows that there are two regions depending on the Ag content: in the first region, where the Ag content is below 12 atomic%, E_d is larger for $As_{40}S_{60}$ than for $As_{30}S_{70}$; however, the reverse is found in the second region where the Ag content exceeds 12 atomic%. A possible explanation of this behaviour was given in section 6.2.2.

The dependence of the single oscillator energies, E_o , on Ag concentration is shown in figure 6.27(b). In contrast to E_d , E_o

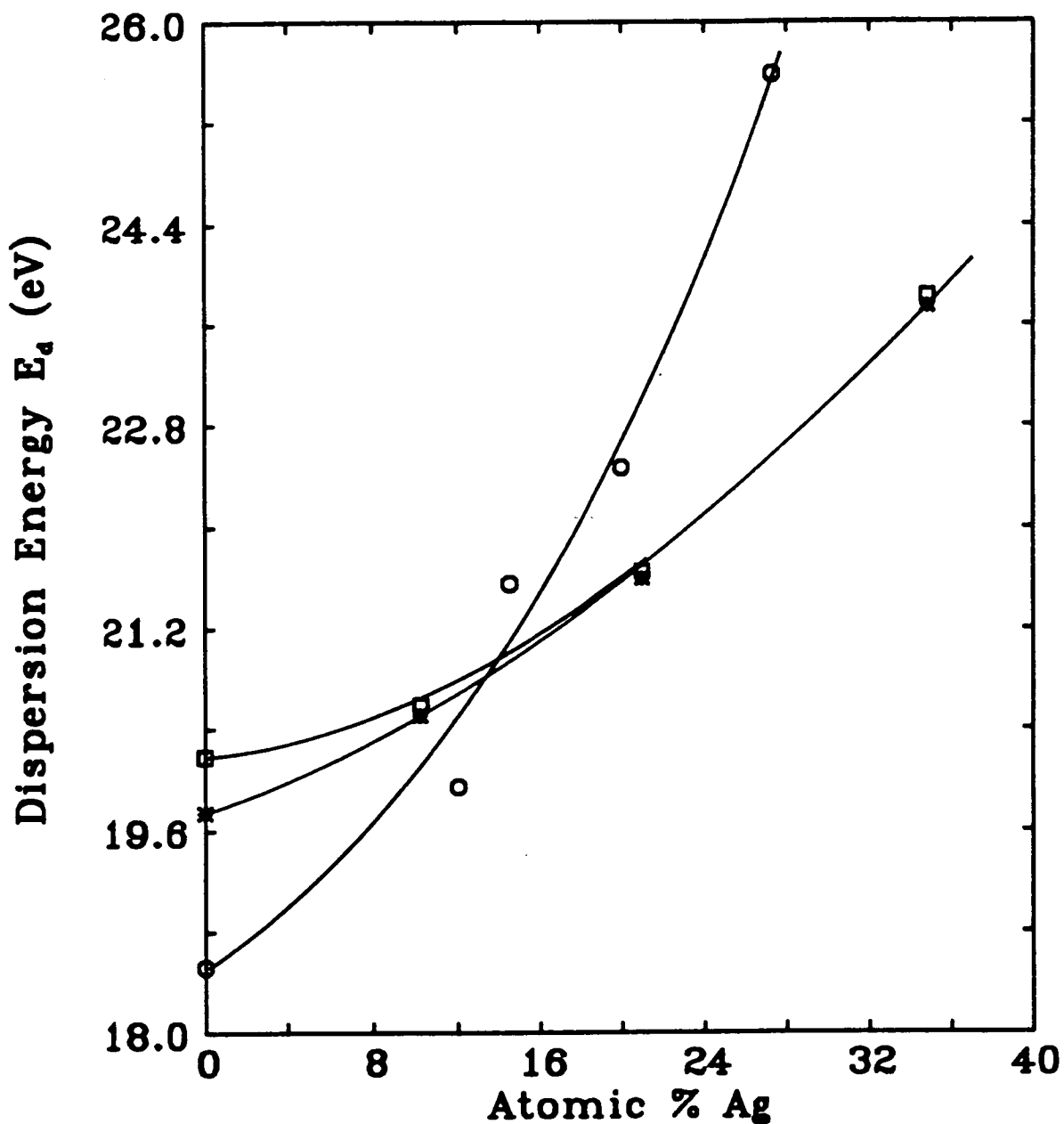


Figure 6.27(a). Effect of Ag content on the dispersion energy, E_d , of annealed $As_{40}S_{60}$ (\square), as-deposited $As_{40}S_{60}$ (*) and annealed $As_{30}S_{70}$ (o) films.

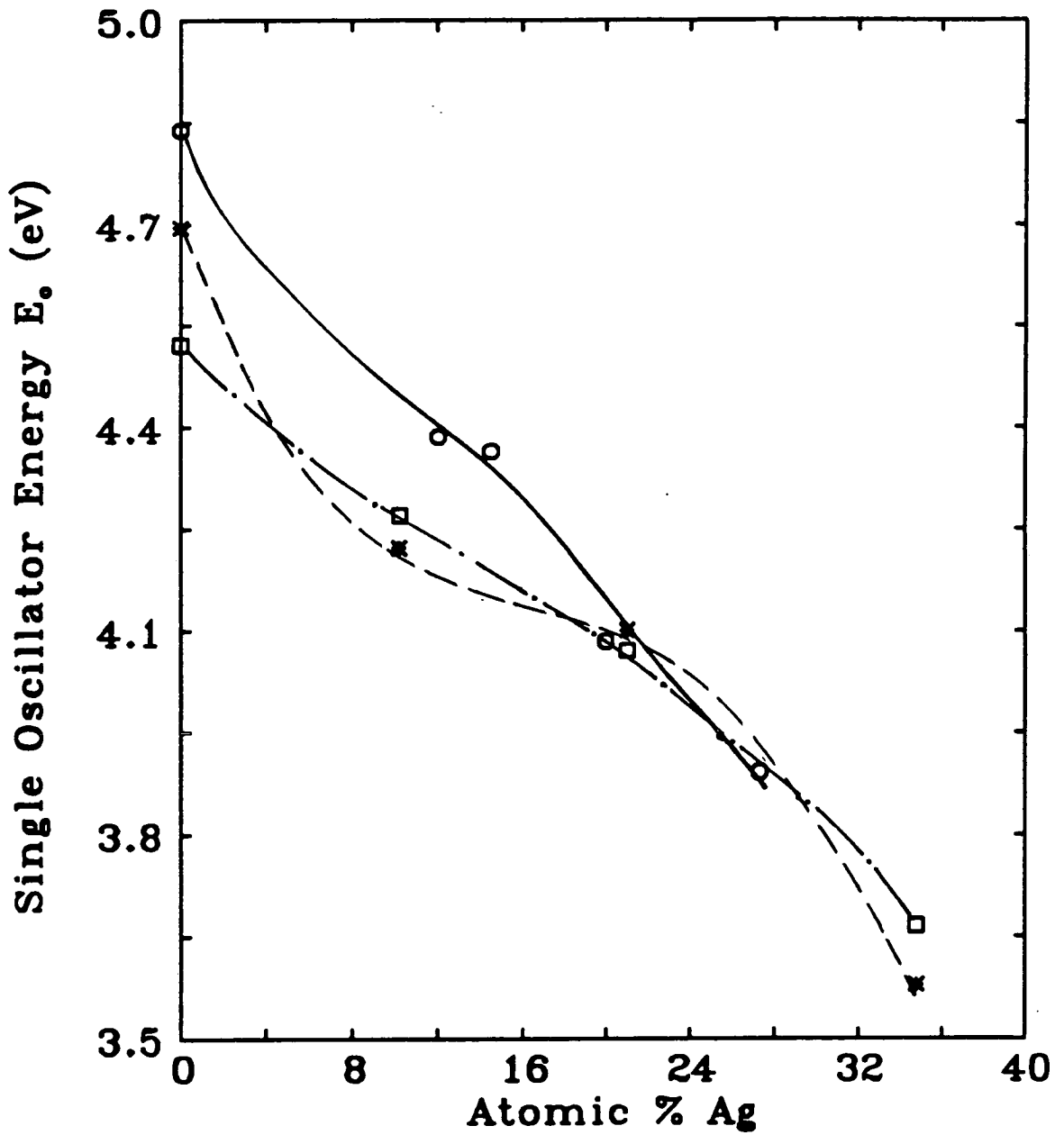


Figure 6.27(b). Effect of Ag content on the single oscillator energy, E_o , of annealed $As_{40}S_{60}$ (□), as-deposited $As_{40}S_{60}$ (*) and annealed $As_{30}S_{70}$ (o) films.

decreases with increasing Ag content in the As-S film. The inflection apparent in the plots around 16 atomic% Ag have also been observed in a recent study of $As_{33}S_{67}$.³¹

The results for as-deposited $As_{40}S_{60}$ are also plotted in the two figures to show the effect of annealing on these constants. In accord with previous observations for the refractive index and optical gap of the photodoped materials, the annealing treatment does not have any significant effect on E_d and E_o of the as-deposited films except at low Ag concentration. A possible explanation of these observations was given in section 6.2.1.

6.4.2. Effect of composition on the dispersion and single oscillator energies in As-S and Ag-photodoped Films

In this section the compositional dependence of E_d and E_o for both undoped and photodoped films will be investigated. Figures 6.28(a) and 6.28(b) show the compositional trend of the dispersion energy and the single oscillator energy respectively for both undoped and photodoped films. For the undoped films, while E_d increases with increasing As content, E_o decreases. The annealed films exhibited higher slopes than the as-deposited films and the difference between the slopes for these two types of film increased as the As concentration increased. This finding is consistent with the effect of annealing on the compositional trend of the refractive index. In the amorphous As-S system, it is reasonable to assume that E_d is proportional to N_c , which decreases from $N_c \sim 3$ for $As_{40}S_{60}$ to 2 for S. The present results agree closely with this quantitative prediction and this therefore confirms the validity of the Wemple-Didominico relation for the As-S system. Consequently, it can be concluded that the variation of E_d with composition in the As-S system is governed by the nearest-neighbour atomic configuration.

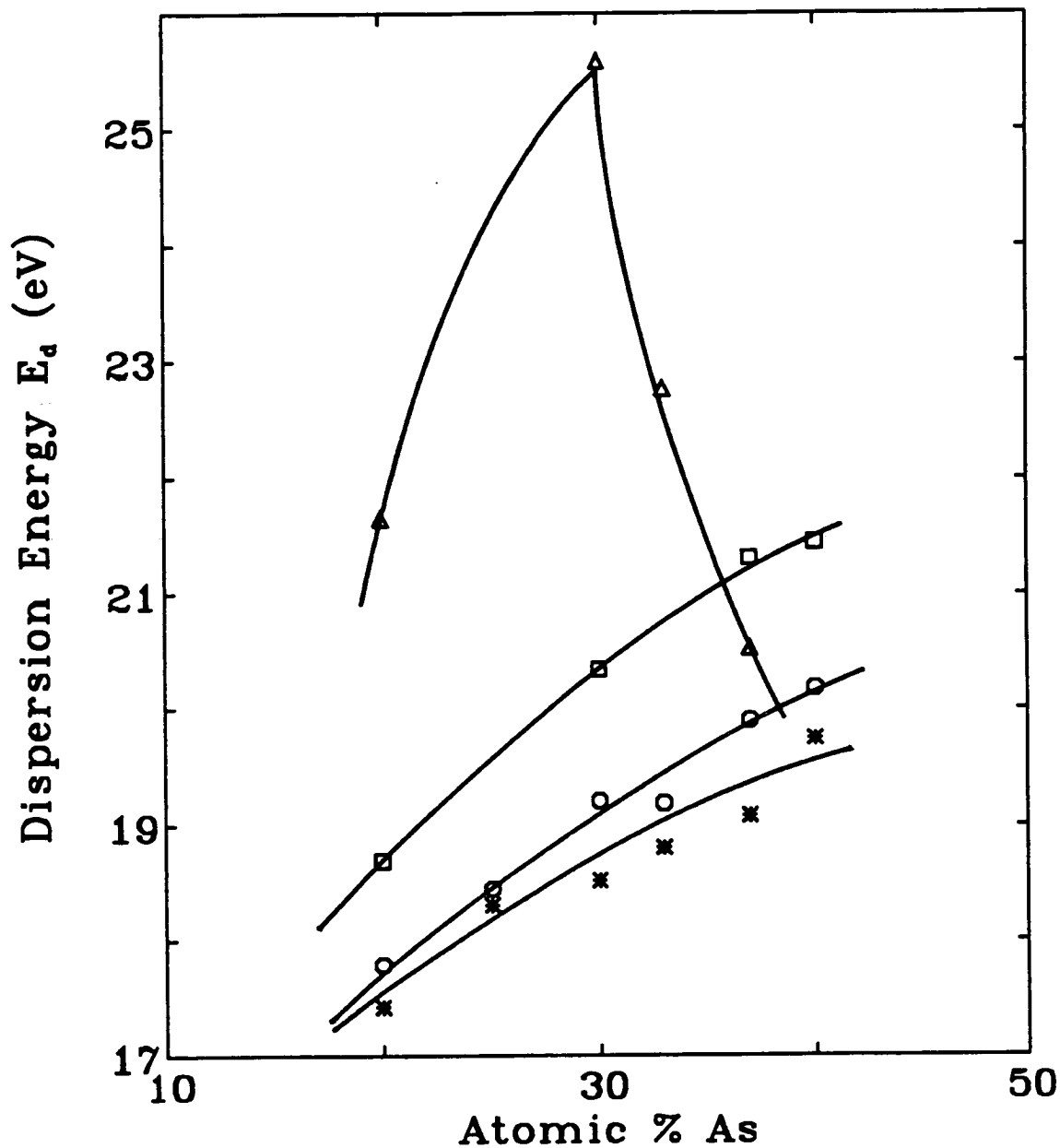


Figure 6.28(a). Effect of As content on the dispersion energy, E_d , of annealed As-S (o), as-deposited As-S (*) and annealed, heavily doped As-S (Δ) films. the Tanaka's results³⁰ are represented by \square . The heavily doped films contain 27 atomic% of Ag.

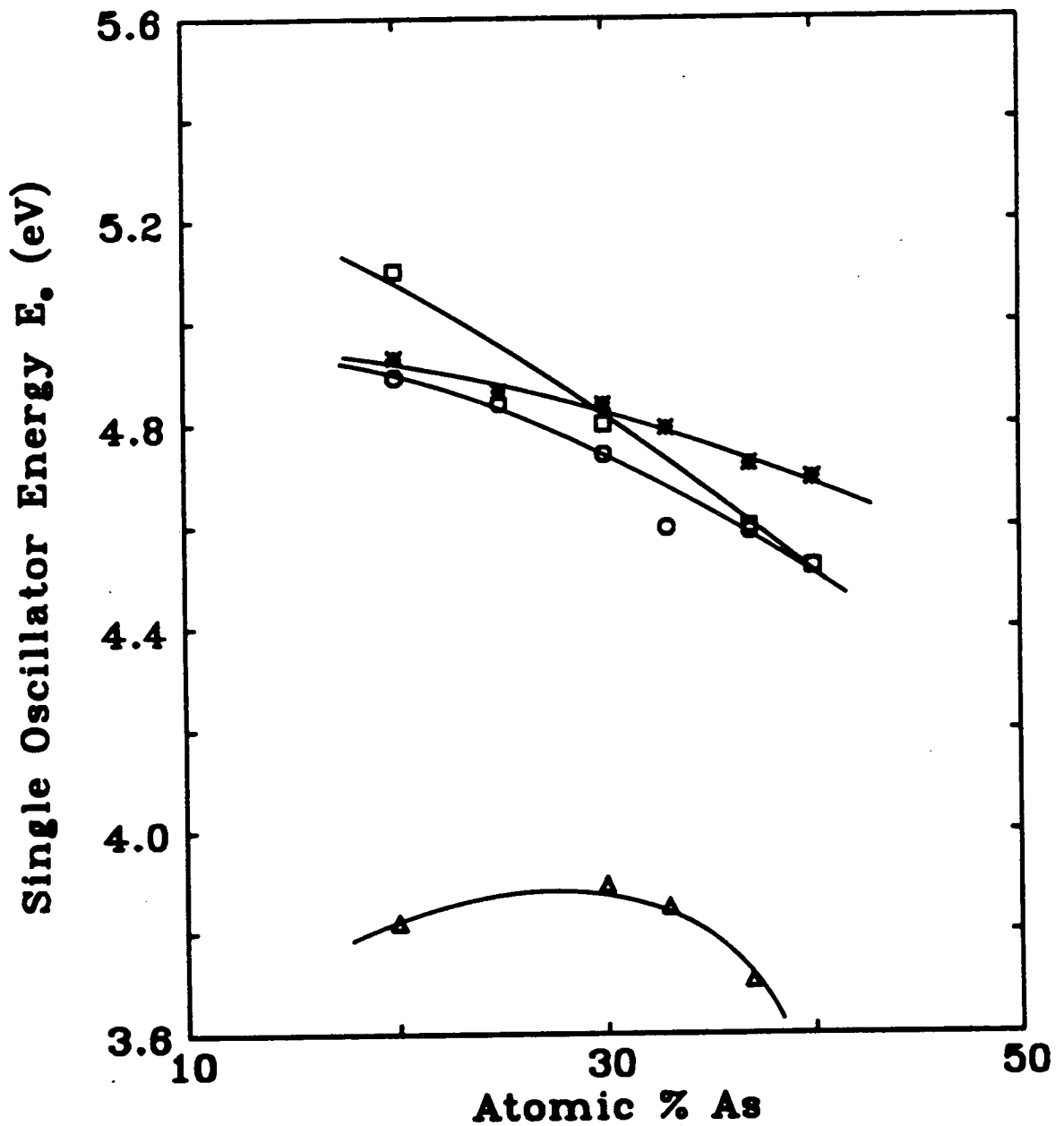


Figure 6.28(b). Effect of As content on the single oscillator energy, E_o , of annealed As-S (o), as-deposited As-S (*) and annealed heavily doped As-S (Δ) films. the Tanaka's results³⁰ are represented by \square . The heavily doped films contain 27 atomic% of Ag.

Tanaka³⁰ found a similar compositional trend for E_d and E_o and his results, for annealed As-S films, are also shown in figures 28(a) and (b). The values he reports for E_d are higher than those obtained in the present study. Analysis of his data¹⁴ suggests that the energy constants he obtained are too high to yield the refractive indices he himself measures.

The observation that E_d , E_o and the optical gap are a maximum or minimum at the stoichiometric composition and depend almost linearly on As content accords well with the compositional trends of other physical properties, such as glass transition temperature,¹⁷ dielectric constant³² and electrical conductivity.³³ This confirms that strong As-S bonds are favoured in these materials.

In contrast to the undoped films, the as-deposited or pre-annealed photodoped films exhibited different behaviour for E_d and E_o . In this case, the two constants have a maximum around 30 atomic% As rather than at 40 atomic% As, i.e. the stoichiometric As-S composition. This is consistent with the findings for the refractive index and optical gap reported in previous sections.

6.5. Summary

In summary, the investigation of the optical constants of undoped and photodoped As-S films, and the effect of annealing on these revealed the following:

1- Pre-annealing

The pre-annealing treatment of undoped As-S films produced an overall increase of about 3 % in their refractive index from the visible to the IR region. The single oscillator energy, E_o , for the undoped material was found to decrease by 3.9% as a result of annealing, and

the dispersion energy, E_d , to increase by 2 %. The magnitude of the pre-annealing effect was found to increase with increasing As content, being most pronounced at $As_{40}S_{60}$. The optical gap or the optical absorption edge were not altered significantly by the pre-annealing treatment applied to As-S films. It was also found that the pre-annealing did not alter the optical constants of photodoped films containing more than 12 atomic% Ag.

2- Photodoping with Ag

The photodoping of both as-deposited and annealed As-S films with Ag produced a much greater increase in the refractive index compared to the annealing effect. The maximum, overall increase, which extended from the visible to the IR, was found to be about 20%. The refractive index, the single oscillator energy, E_o , and the dispersion energy, E_d , were found to depend on the Ag content in the As-S structure. E_o and the optical gap were found to decrease and E_d to increase with the Ag content. The dependence on As-S composition for the most heavily doped films revealed that there is a peak around 30 atomic% As for the refractive index, and the single oscillator and dispersion energies. However, the composition dependence of the optical gap of the most heavily doped material exhibited similar behaviour to that of undoped films.

References

1. Matsuda A. and Kikuchi M., *Proc. 4th Conf. on Solid State Devices (Suppl. to J. Japan Soc. of Appl. Phys. Vol.42 p.239 1973)*, Tokyo, 1972.
2. Yaji T. and Kurita S., *J. Appl. Phys.*, vol. 54, p. 647, 1983.

3. Chatani K., Shimizu I., Kokado H. and Inoue E., *Jap. J. Appl. Phys.*, vol. 16, p. 389, 1977.
4. Ewen P.J.S., Zakery A., Firth A.P. and Owen A.E., *Phil. Mag. B*, vol. 57, p. 1, 1988.
5. Zakery A., Zekak A., Ewen P.J.S., Slinger C.W. and Owen A.E., *J Non-Cryst Solids*, vol. 114, p. 109, 1989.
6. DeNeufville J.P., Moss S.C. and Ovschinsky S.R., *J. Non-Cryst. Solids*, vol. 13, p. 191, 1974.
7. Apling A.J., Leadbetter A.J. and Wright A.C., *J. Non-Cryst. Solids*, vol. 23, p. 369, 1977.
8. Leadbetter A.J., Apling A.J. and Daniel M.E., *J. Non-Cryst Solids*, vol. 21, p. 47, 1976.
9. Solin S.A. and Papatheodorou G.N., *Phys. Rev. B*, vol. 15, p. 2084, 1979.
10. DeNeufville J.P., Seguin R., Moss, S.C. and Ovshinsky S.R., *Proc. 5th Int. Conf. on Amorp. and Liquid. Semicond.*, p. 737, Garmish-Partenkirchen, Taylor and Francis, London, 1973.
11. Swanepoel R., *J. Phys. E: Sci. Instrum.*, vol. 16, p. 1214, 1983.
12. Wemple S.H., *Phys. Rev B*, vol. 7, p. 3767, 1973.
13. Kumar B. and White K., *Thin Solid Films*, vol. 48, p. 135, 1986.
14. Tanaka K. and Ohtsuka Y., *Thin Solid Films*, vol. 57, p. 59, 1979.
15. Yaji T. and Kurita S., *Jap. J. of Appl. Phy.*, vol. 22, p. 400, 1983.
16. Tanaka K. and Ohtsuka Y., *Thin Solid Films*, vol. 48, p. 17, 1978.

17. Tsuchihashi S. and Kawamoto Y., *J. of Non-Cryst. Solids*, vol. 5, p. 286, 1971.
18. Kolomiets B.T. and Lyubin V.M., *Mat. Res. Bull.*, vol. 13, p. 1343, 1978.
19. Firth A.P., *Ph.D. Thesis*, University of Edinburgh, 1985.
20. Frumar M., Firth A.P. and Owen A.E., *Phil. Mag. B*, vol. 50, p. 463, 1984.
21. Wood D.L. and Tauc J., *Phy. Rev. B*, vol. 5, p. 3144, 1972.
22. Young P.A., *J. Phys. C: Solid St. Phys.*, vol. 4, p. 93, 1971.
23. Mott N.F. and Davies E.A., *Electronic Processes in Non-Crystalline Materials*, p. 347, Oxford: Clarendon Press, First Edition, 1971.
24. Yamaguchi M., *Phil. Mag. B*, vol. 51, p. 651, 1985.
25. Mott N.F. and Davies E.A., *Electronic Processes in Non-Crystalline Materials*, p. 335, Oxford: Clarendon Press, First Edition, 1971.
26. Hamanaka H., Tanaka K., Tsuji K. and Minomura S., *J. Phys., Paris Colloq.*, vol. 42, p. 399, 1981.
27. Shimizu I., Ikeda T. and Inoue E., *Preprint Int. Congress Photogr. Sci.*, p. 235, Rochester, New York, 1978.
28. Shimizu I., Sakuma H., Kokado H. and Inoue E., *Bull. Chem. Soc. of Japan*, vol. 46, p. 1291, 1973.
29. Zakery A., Ewen P.J.S., Slinger C.W., Zekak A. and Owen A.E., *J. Non-Cryst. Solids*, vol. 137&138, p. 1333, 1991.
30. Tanaka K., *Thin Solid Films*, vol. 66, p. 271, 1980.

31. Kosa T.I., Wagner T., Ewen P.J.S. and Owen A.E., *to be published in Phil. Mag.*, 1993.
32. Lucovsky G., Geils R.H. and Keezer R.C., in *Frishat (ed.), The Physics of Non-Crystalline Solids*, p. 299, Trens-Tech, Zellerfeld, 1977.
33. South R.B. and Owen A.E., in *Stuke. J and Brenig W. (eds.), Amorphous and liquid Sc.*, p. 305, Taylor and Francis, London, 1974.

CHAPTER 7

KINETICS OF THE Ag-PHOTODISSOLUTION PROCESS IN THE As-S SYSTEM

7.1. Introduction

A knowledge of the kinetics of the photodissolution process is essential both to understanding the mechanism of the effect and to exploiting its application, since the speed of image formation in the Ag/As-S system is mainly governed by the photodissolution rate. The photodissolution rate is influenced by many factors as reviewed in Chapter 4. Previous attempts to use these factors to speed up image formation in the Ag/As-S system have produced only a small improvement in the rate.

The work presented in this chapter focuses on the investigation of those factors which have been established to be most effective in improving the rate, namely, temperature, pre-annealing treatment, silver film thickness, light intensity, As-S composition and the type of metal used as the ion source. Data on the thermal dissolution of Ag in $As_{40}S_{60}$ films will also be reported. Finally, the results of this chapter will be used to gain further insight into the nature of the Ag-photodissolution process in the As-S system.

7.2. Experimental arrangement

The experimental details of the two techniques (optical reflectivity and optical transmissivity monitoring) used in the present case to investigate the rate of photodissolution were presented in Chapter 5. A typical plot of the reflectivity as a function of exposure time is shown in figure 7.1. The time between successive maxima and minima in the curve corresponds to the time required for the thickness of the undoped layer to decrease by $\lambda/2n$, where λ is the wavelength of the light and n the refractive index of the As-S glass. At the end of the photodissolution process the thickness of the undoped layer is zero so that the maxima and minima occur when the As-S layer thickness is an integer multiple of $\lambda/4n$, this integer being one for the last minimum, 2 for the last maximum, and so on. By noting the times corresponding to the maxima and minima it is thus possible to determine how the thickness of the undoped layer varies with time.

The thickness ranges of the As-S and Ag films used in these investigations are 300-2000 nm and 40-200 nm respectively. Both of the possible geometries (i.e. Ag above or below the As-S) were used in these experiments. Unless otherwise stated all the films examined were annealed, the procedures for the annealing pre-treatment for As-S films being presented in Chapter 5. The main contribution to the uncertainty in photodissolution rate values is due to the error involved in the thickness measurements which is $\sim 2\%$. Each value of the rate quoted is an average of 5 separate measurements and the resulting reproducibility is typically $\pm 3\%$. This good reproducibility was achieved because the measurements were limited to a sample area of 1 cm^2 over which the film is uniform.

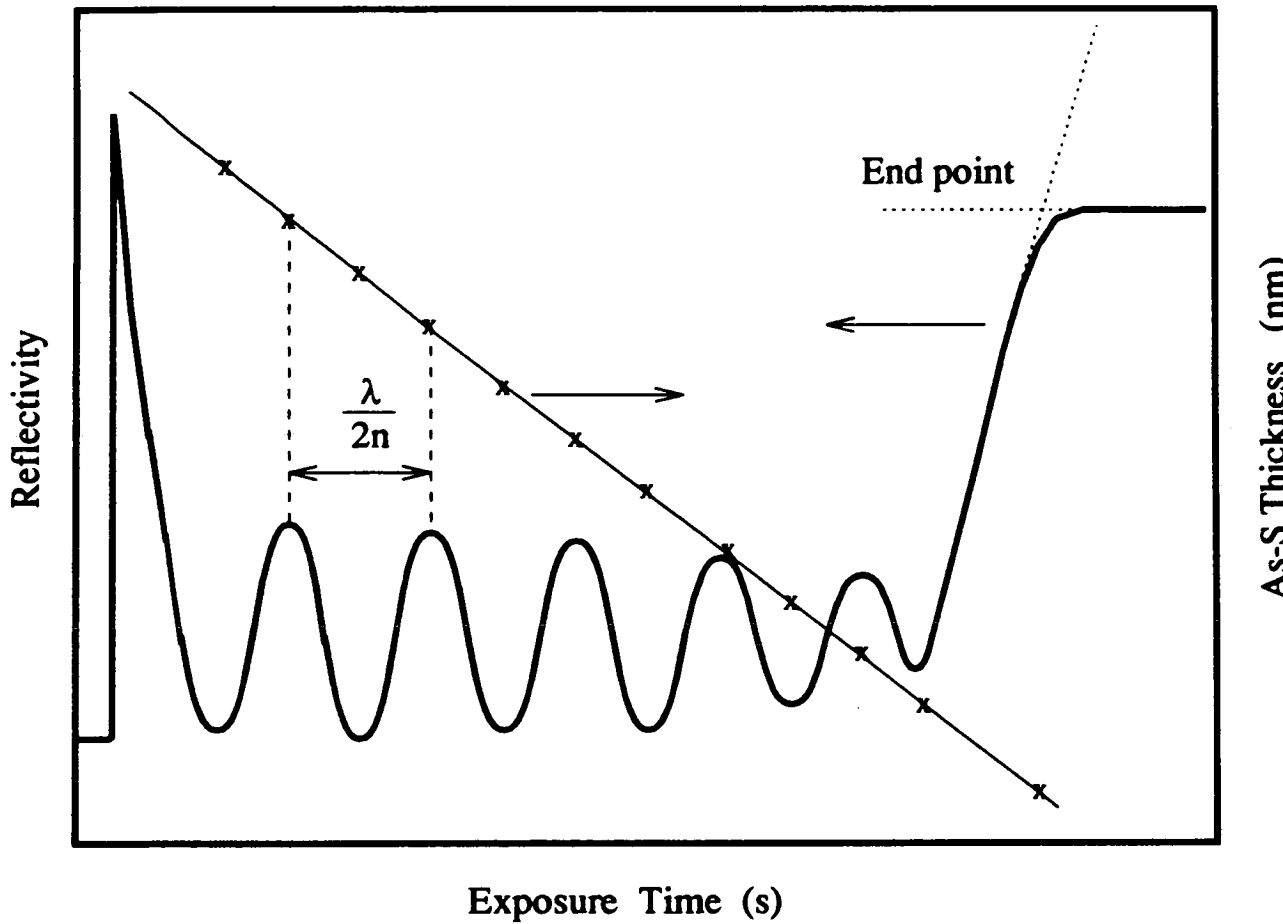


Figure 7.1. A typical plot (full curve) of the reflectivity as a function of exposure time for a sample undergoing photodissolution. The points show the thickness of the As-S film remaining at the peak and trough positions of the reflectivity curve.

7.3. Rate of Ag-photodissolution in $\text{As}_{40}\text{S}_{60}$ films

This section presents the results of the investigation into how the photodissolution rate in the stoichiometric composition $\text{As}_{40}\text{S}_{60}$ is affected by pre-annealing, temperature, light intensity and the type of metal used as the metal ion source.

7.3.1. The effect of pre-annealing

It was mentioned earlier, in section 4.4.4, Chapter 4, that there are conflicting reports on the effect of pre-annealing on photodissolution kinetics. Chatani et al. reported¹ that there is little change in the photodissolution sensitivity as a result of pre-annealing treatment. In contrast, Tamaki et al. observed² that pre-annealing produces a two orders of magnitude change in the photodissolution rate. Clearly, it is necessary to investigate the influence of this factor on the photodissolution sensitivity in a more detailed way.

Figure 7.2 compares the change in As-S thickness versus time for annealed and as-deposited $\text{As}_{40}\text{S}_{60}$ and shows that the annealing treatment has little effect, decreasing the rate of photodissolution rather than increasing it as reported by Tamaki et al..² Our results agree with those of Chatani et al. in that the pre-annealing treatment induces only a small change in the rate. The results obtained by Tamaki et al. might be due to the high As-S/Ag thickness ratio (20) they used in their experiment compared with the ratio of 2.5 used in the present case.

To verify this, the effect of the thickness ratio $d_{\text{As-S}}/d_{\text{Ag}}$ on the annealing behaviour was investigated. Figure 7.3 shows the photodissolution rate versus the As-S/Ag thickness ratio for annealed and as-deposited $\text{As}_{40}\text{S}_{60}$ films. These results show that the annealing treatment has little effect on the rate irrespective of the thickness ratio, although the magnitude of the effect does increase slightly as this

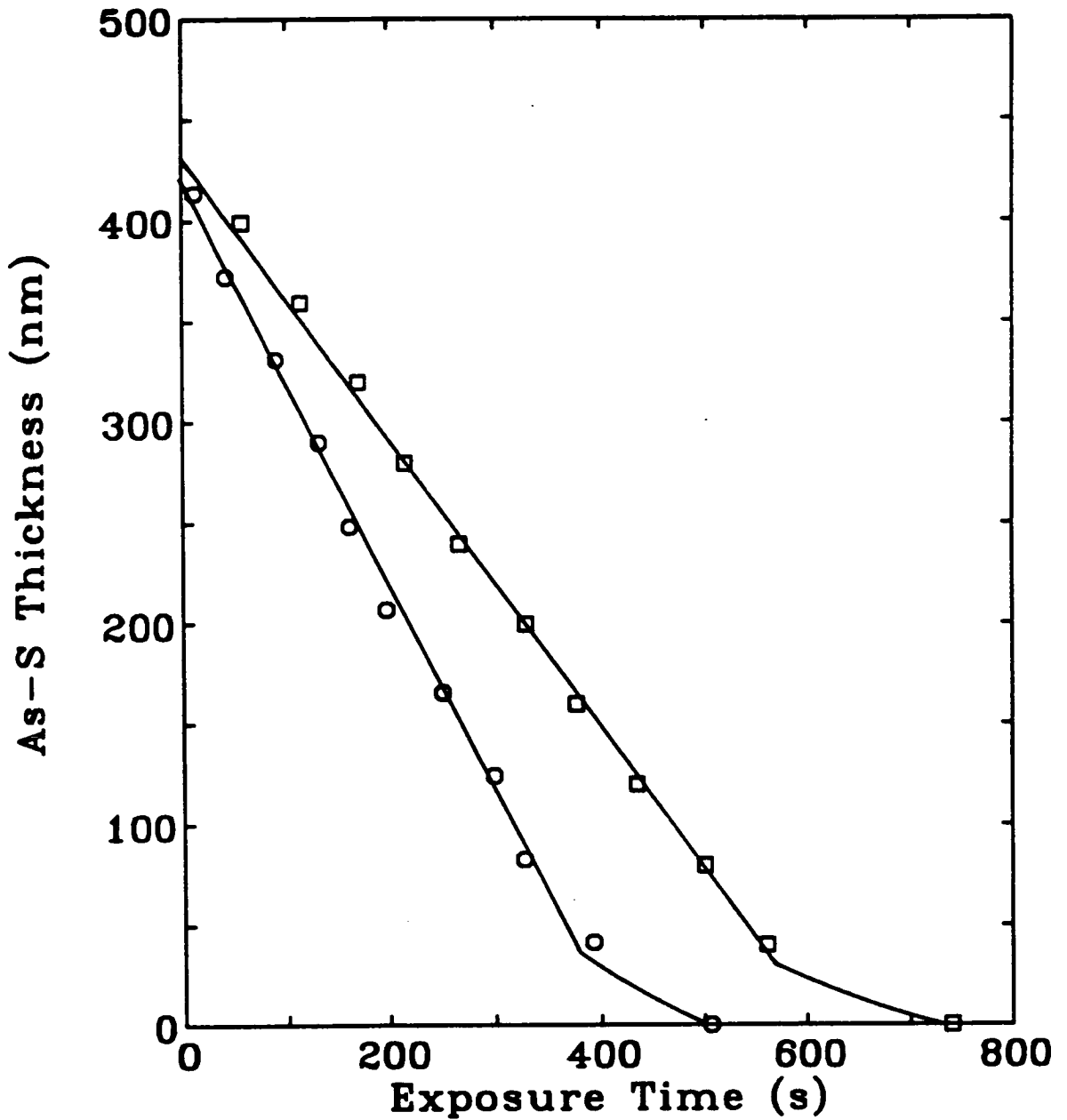


Figure 7.2. Decrease of the $As_{40}S_{60}$ layer thickness during white light exposure for both as-deposited (o) and annealed (\square) films. The initial thicknesses are 430 and 172 nm for the $As_{40}S_{60}$ and Ag films respectively.

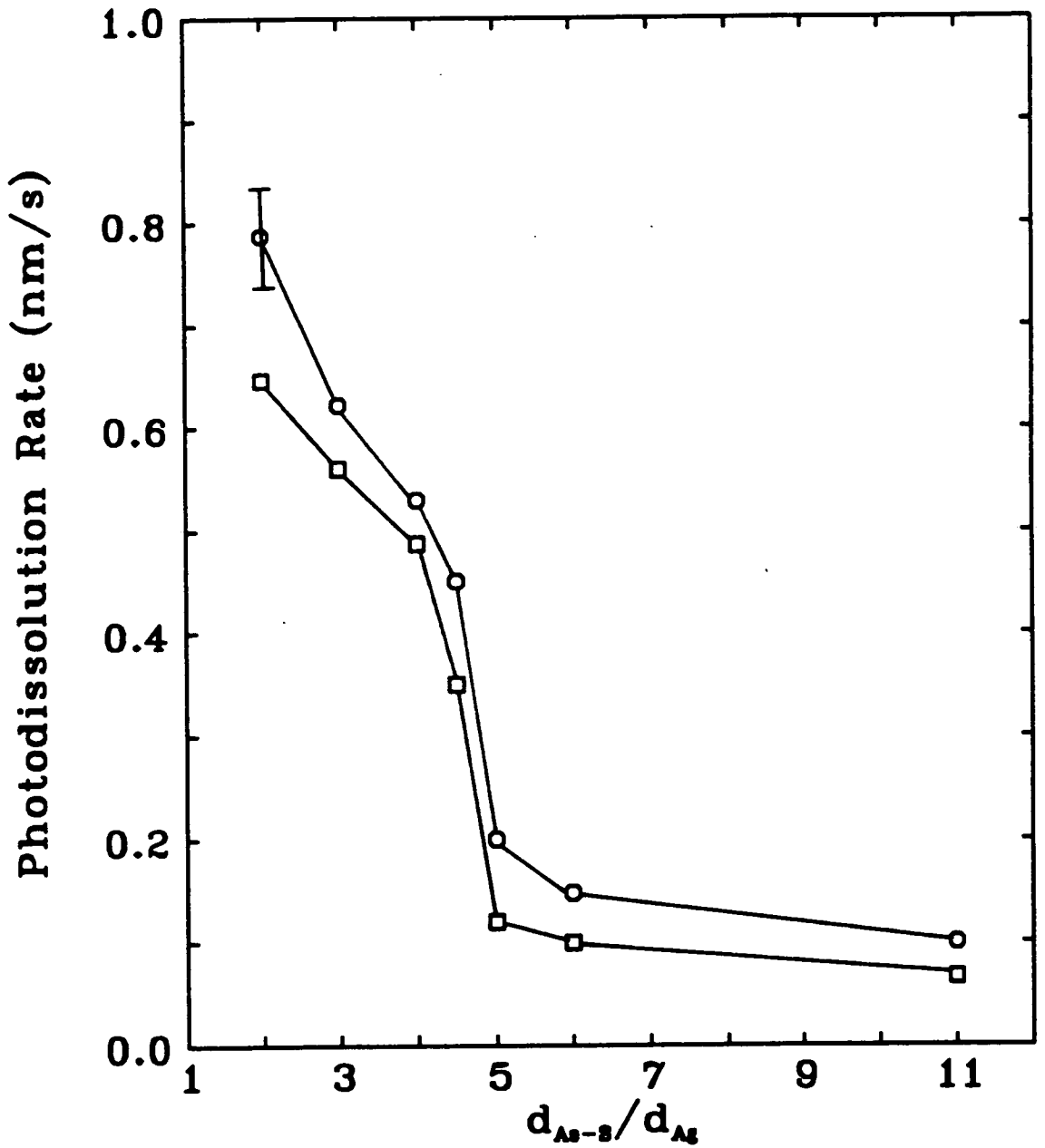


Figure 7.3. Ag photodissolution rate versus the ratio of the As₄₀S₆₀ to Ag film thicknesses ($d_{As_40S_60}/d_{Ag}$) for as-deposited (o) and annealed films (□). The As₄₀S₆₀ film thickness is 430 nm.

ratio decreases. Clearly, even for higher ratios the pre-annealing effect is still very small.

Another factor which might be responsible for these conflicting observations is sample preparation technique. The fact that there is little difference between the photodissolution rates of annealed and as-deposited films in the present case may imply that the structure of the as-deposited samples, made by our preparation method, is closer to that of the annealed films (and therefore to the bulk materials). The effect of annealing on film structure was discussed in detail in Chapter 2. The small rate decrease due to pre-annealing might be due to the fact that annealing an as-deposited film increases its density and compactness, which may limit the diffusion of Ag in the As-S structure.

A noticeable feature of the results in figure 7.3 is the abrupt change in the rate at around a ratio of 4-5. This feature might be connected with the amount of Ag incorporated in the $As_{40}S_{60}$ structure, since the Ag content determines the type of transport which takes place during the photodissolution process.³ For low concentrations (high thickness ratios) the process is dominated by electronic transport and the photodoped material can be considered as a doped semiconductor. For high concentrations (low thickness ratios) the process involves both ionic and electronic transport and this combination may yield a faster rate because both ions and electrons must be transported across the photodoped region. It is also important to note that the Ag film was exhausted for all As-S/Ag thickness ratios higher than or equal to three.

7.3.2. The effect of temperature

It has already been observed by other workers^{4, 5} that raising the temperature of the Ag/As-S sample will increase the speed of image formation, the reported magnitude of the increase being a factor of 3-4

at temperatures of ~ 400 K. Also, it was believed that significant thermal migration of the metal ions would occur above room temperature. The details of other studies concerning the effect of temperature were presented in Chapter 4. In the present case we observe an improvement in the rate by a factor of 10 at a similar temperature and negligible thermal diffusion. Hence heating the Ag/As-S combination during exposure will significantly enhance its sensitivity without degrading its resolution capability. Under these conditions the sensitivity of the Ag/As-S system is comparable with that of conventional organic resists, which were earlier reported as being typically 5 times more sensitive.⁶

The study of the effect of temperature on the photodissolution rate was carried out using a constant light intensity (70 mW/cm^2). The magnitude of this intensity is much higher than that ($\leq 10 \text{ mW/cm}^2$) used by other authors,^{4, 5} which may explain the larger increase in rate obtained in the present work compared with that observed by these authors. Typical results showing the effect of temperature on the photodissolution rate are presented in figure 7.4 for three temperatures: room temperature, 323 K and 393 K. Clearly, the slopes of the thickness versus time plots are significantly affected by temperature. Photodissolution rates at various temperatures are plotted in figure 7.5. The rate here is defined as the ratio of the initial As-S film thickness to the time required to completely photodeposit it with Ag. These results show that the rate at 393 K is a factor of 10 higher than at room temperature. In order to determine the activation energy of the photodissolution process within the temperature range of figure 7.5 (i.e. 300-400 K), an Arrhenius plot of the rate versus the reciprocal temperature was drawn and this is shown in figure 7.6. This figure yields a small activation energy of ~ 0.24 eV which implies a relatively weak temperature dependence for the process in the temperature range studied. Plochanski et al. found similar results.⁵

It is well known that the $\text{As}_{40}\text{S}_{60}$ film thickness itself is an important parameter in limiting the photodissolution rate and this represents a major obstacle in making devices with deep structures. The $\text{As}_{40}\text{S}_{60}$ film thicknesses used in obtaining the above results were ~ 390 nm. To determine whether a similarly large increase in the

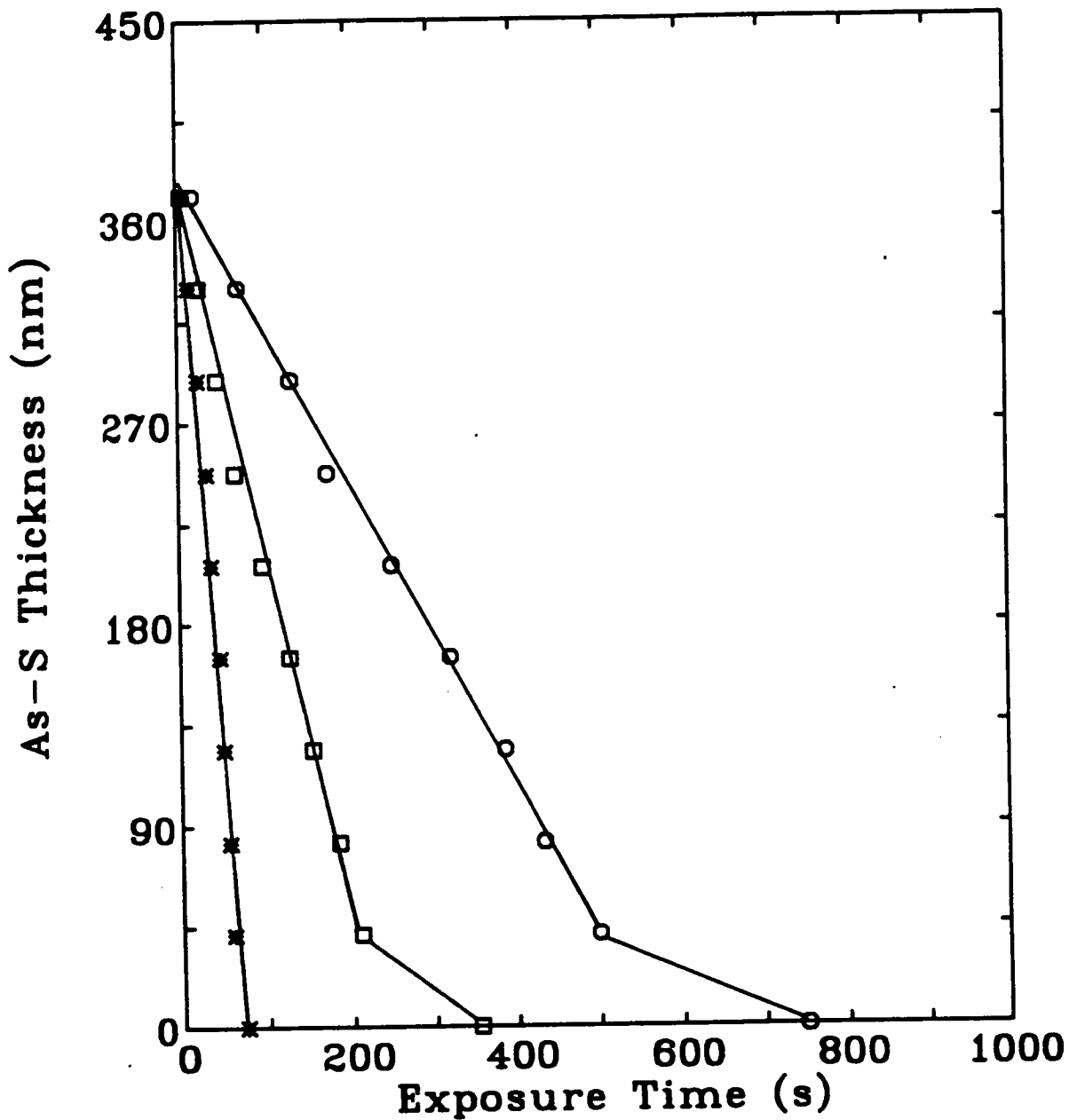


Figure 7.4. Decrease of the $As_{40}S_{60}$ film thickness during Ag photodissolution at various temperatures: room temperature (o), 323 K (□) and 393 K (*). The $As_{40}S_{60}$ and Ag film thicknesses are 372 and 89 nm respectively.

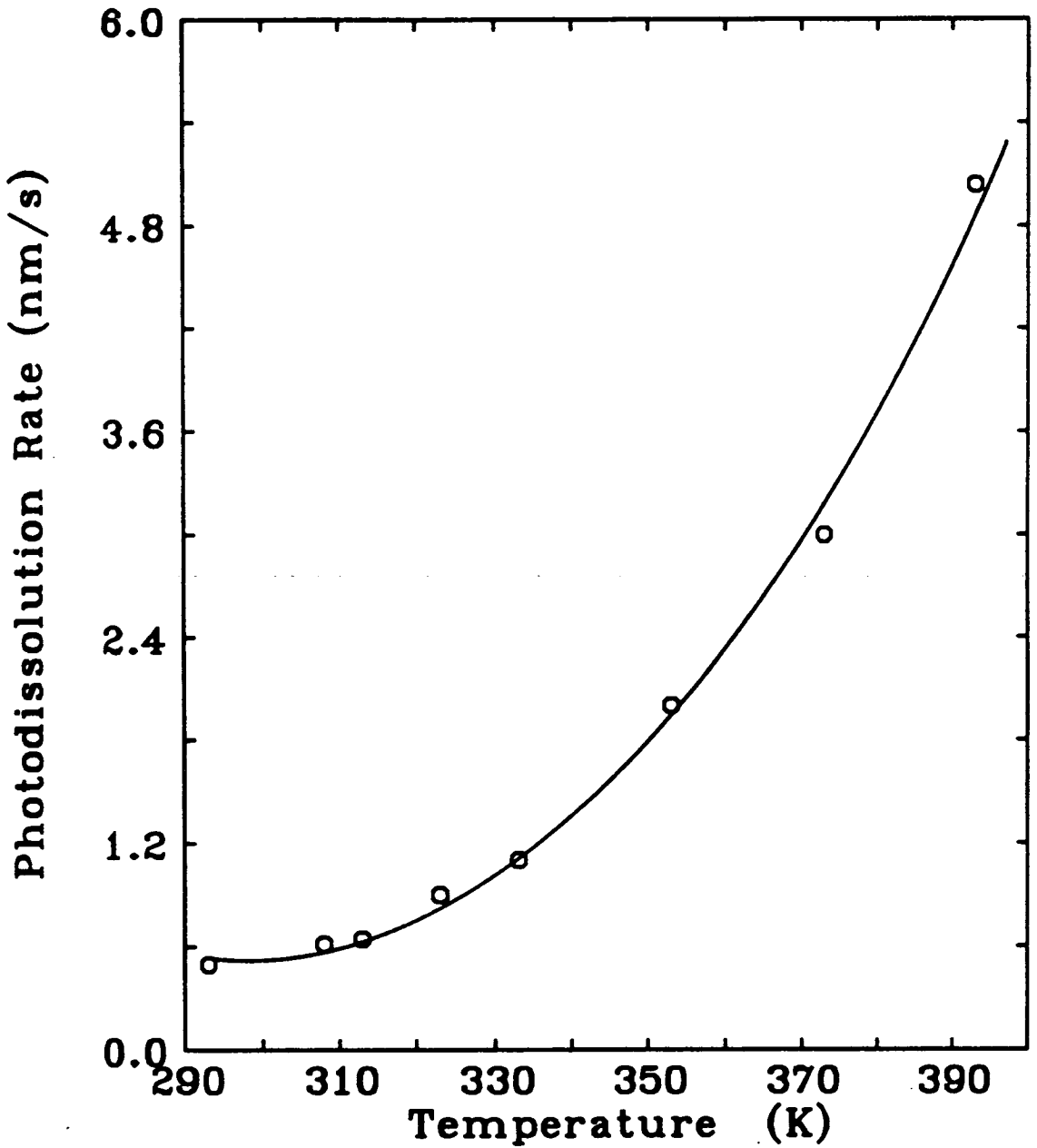


Figure 7.5. Temperature dependence of Ag photodissolution rate for the composition $\text{As}_{40}\text{S}_{60}$. The film thicknesses used in this experiment are similar to those in figure 7.4.

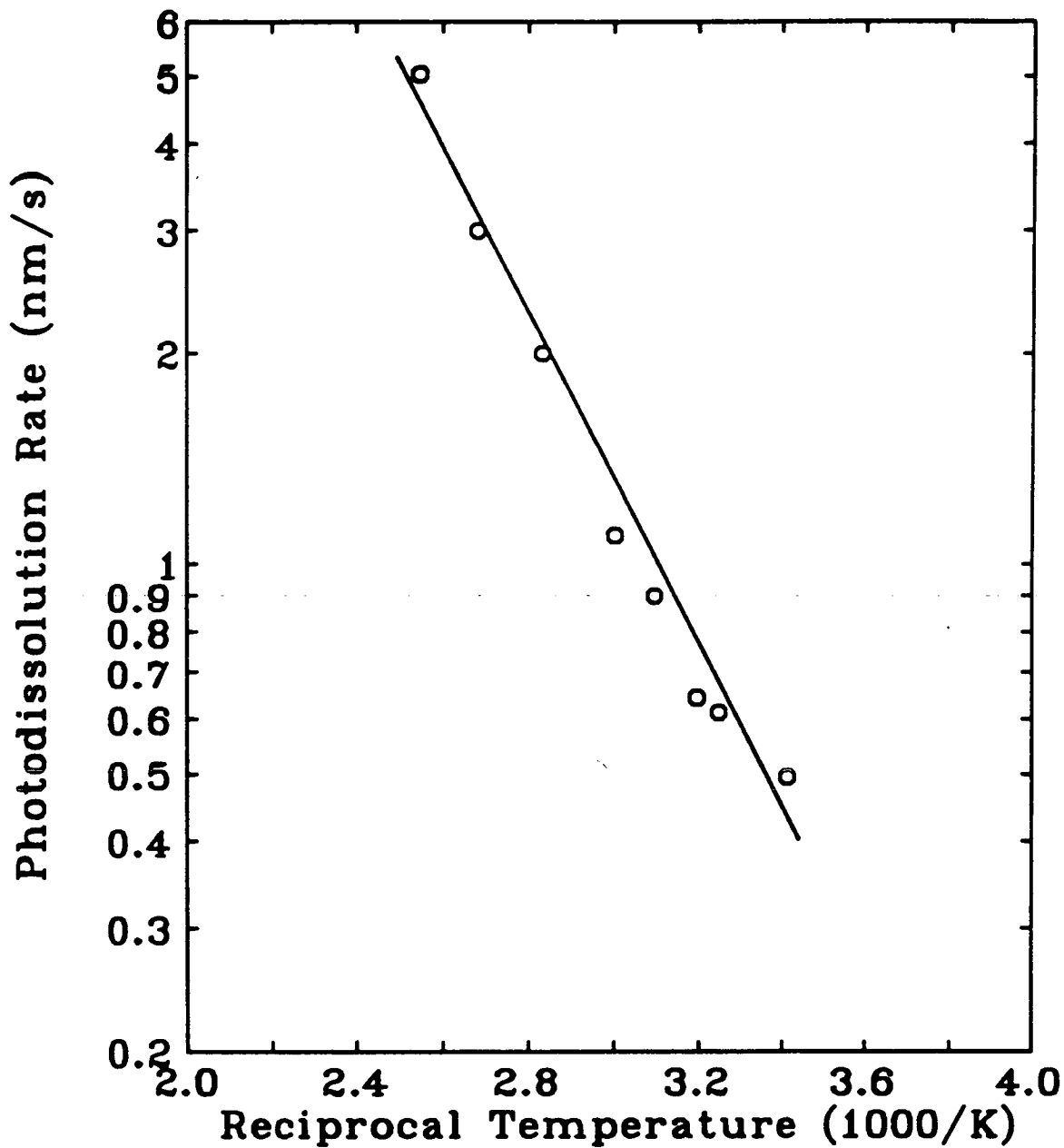


Figure 7.6. Arrhenius plot of photodissolution rate versus reciprocal temperature. The data of this figure were derived from that of figure 7.5.

photodissolution rate could also be obtained for much thicker $\text{As}_{40}\text{S}_{60}$ films, a sample with $d_{\text{As-S}} = 1710$ nm was examined. Figure 7.7 compares the As-S thickness versus time plots for this thicker sample at room temperature and 393 K; the photodissolution rate is a factor of 12 higher at 393 K. This finding confirms that with simultaneous illumination and heating of the $\text{Ag}/\text{As}_{40}\text{S}_{60}$ samples it is possible to overcome the thickness limitation of the photodissolution process and hence the fabrication of devices with deep structures is possible using this process.

In addition to the reflectivity method, transmissivity monitoring was also used to investigate the effect of temperature on the photodissolution rate. Although this technique is less accurate than reflectivity monitoring, it showed similar results. Figure 7.8 shows the transmission through the $\text{Ag}/\text{As-S}$ film combination as a function of exposure time at room temperature, 338 and 383 K. The time required for the transmission to reach saturation at its final value of $\sim 87\%$ is 40 min at room temperature but only 4 min at 383 K, again indicating a speeding up of the process by a factor of ~ 10 .

Although increasing the rate by a factor of 10 is an important achievement, it will only be of practical value in grating fabrication if there is no isotropic thermal dissolution of the Ag, since any lateral movement of the metal ions will make it difficult to control the profile and will affect the resolution capability. It is expected that significant thermal dissolution of the metal ions will occur above room temperature and it is known that such dissolution occurs in all directions, in contrast to photodissolution which proceeds mainly along the direction of illumination.

The evaluation of the magnitude of the thermal dissolution rate at 383 K was achieved using the transmissivity method. Figure 7.9 shows the transmissivity of a $\text{Ag}/\text{As}_{40}\text{S}_{60}$ film combination at 383 K as a function of annealing time. The increase in transmissivity is due to the thermal dissolution of Ag into the $\text{As}_{40}\text{S}_{60}$ film and the end of the process is marked by saturation of the transmissivity at its final value of $\sim 87\%$. The time corresponding to the onset of saturation in this figure is about 480 min, which yields a thermal dissolution rate of

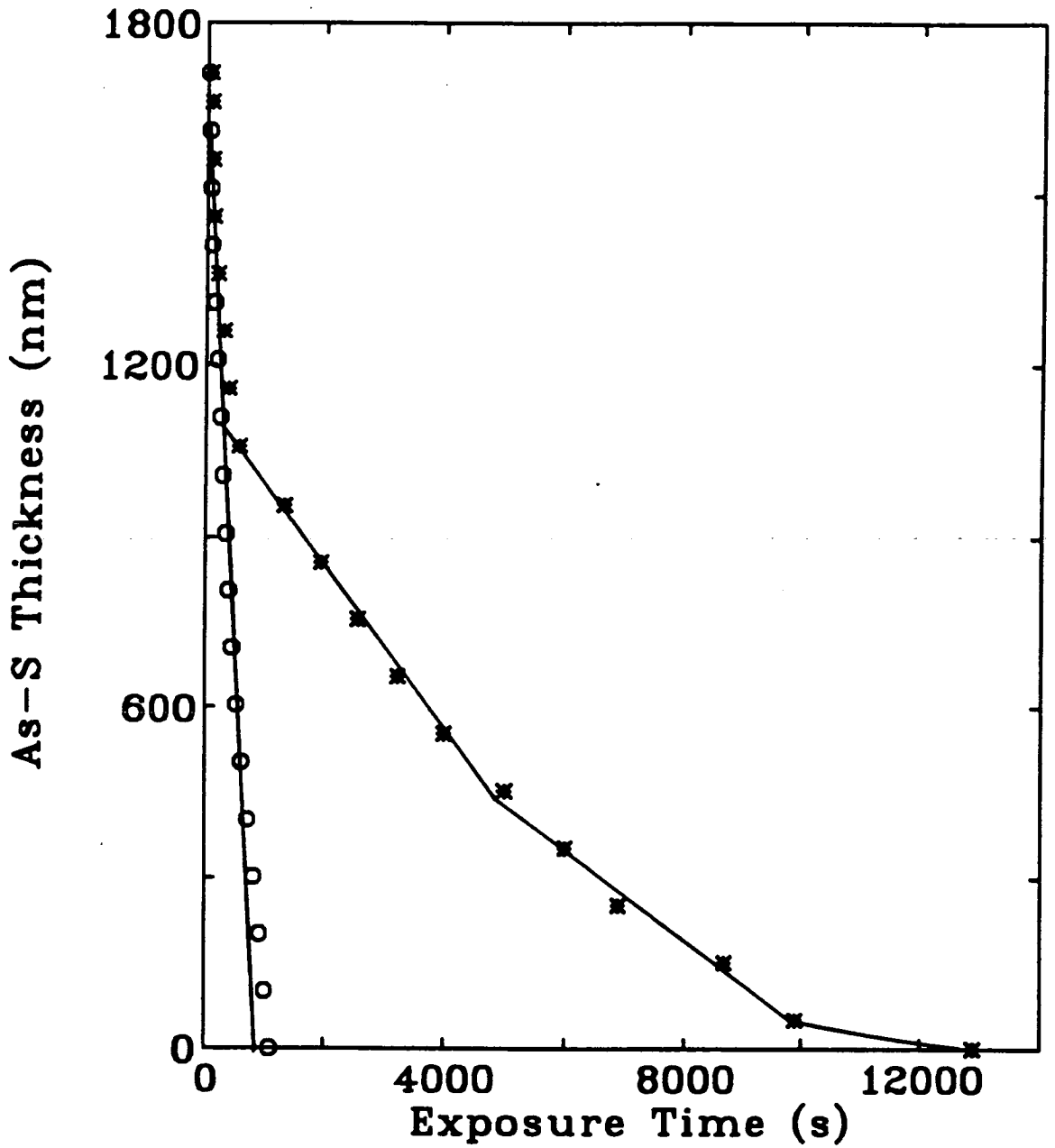


Figure 7.7. Decrease of $As_{40}S_{60}$ film thickness as a function of exposure time at room temperature (*) and 393 K (o). The $As_{40}S_{60}$ and Ag film thicknesses were 1710 and 210 nm respectively. (Light intensity = 70 mW/cm²).

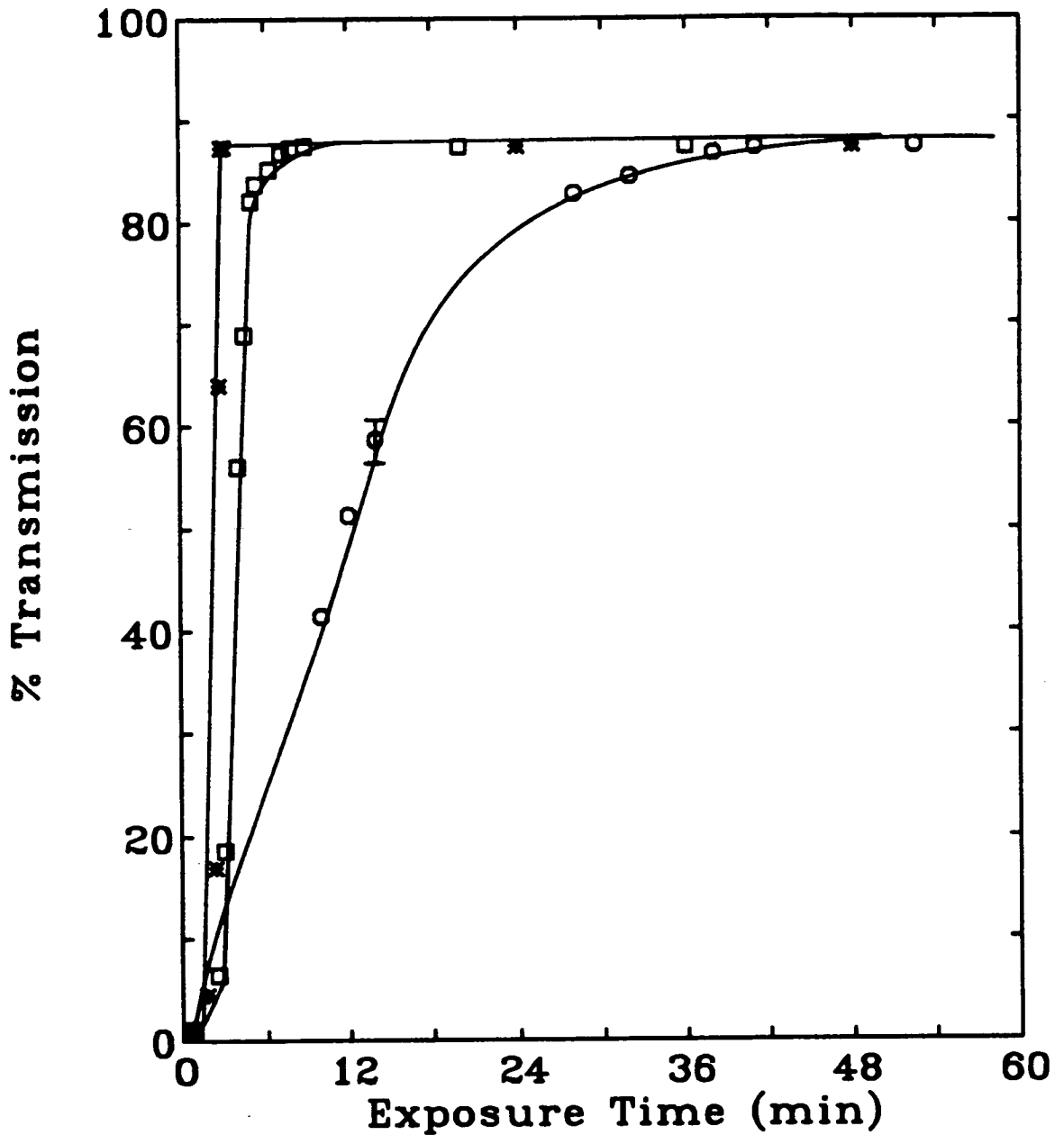


Figure 7.8. Increase of transmission through a $\text{Ag}/\text{As}_{40}\text{S}_{60}$ film combination during exposure for different sample temperatures: room temperature (o), 338 K (\square) and 383 K (*). This transmission was monitored at 1400 nm. The $\text{As}_{40}\text{S}_{60}$ and Ag film thicknesses were 603 and 67 nm respectively. (Light intensity = $70 \text{ mW}/\text{cm}^2$).

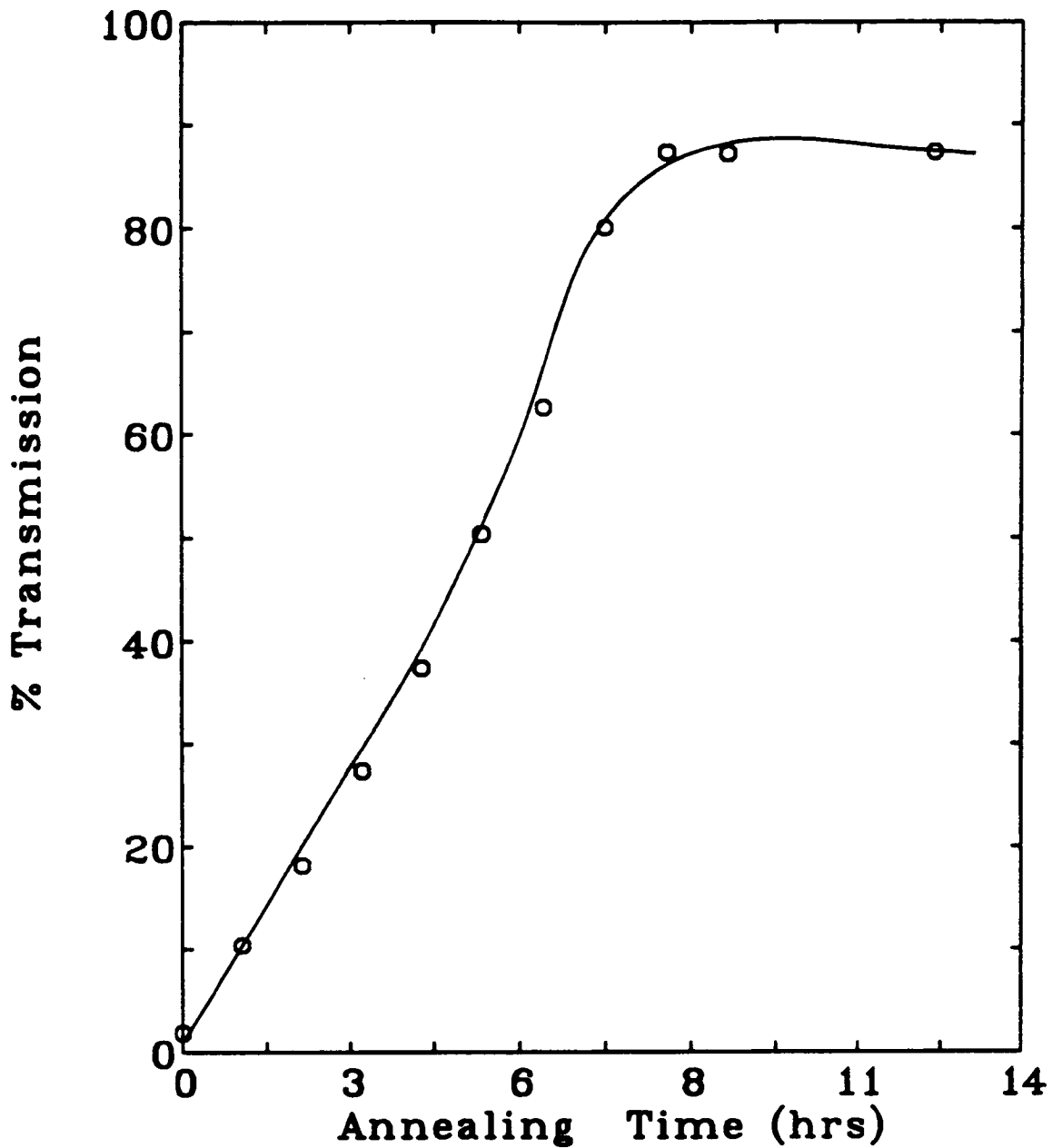


Figure 7.9. Increase of transmission through a Ag/As₄₀S₆₀ film combination during sample heating at 383 K. This transmission was monitored at 1400 nm. The As₄₀S₆₀ and Ag film thicknesses were 602 and 46 nm respectively.

~1.2 nm/min.

In order to compare the above saturation time to that of photodissolution at room temperature, the first three points of figure 7.9 were replotted in figure 7.10, together with the corresponding data for photodissolution at room temperature and combined photo/thermal dissolution at 383 K. This figure shows clearly that for photodissolution the transmissivity, both at room temperature and 383 K, reaches saturation far sooner than in the case of thermal dissolution. The time required for the transmissivity during photodissolution to saturate is about 4 min at 383 K and 40 min at room temperature. These values indicate that the time to reach saturation at 383 K is a factor of 12 smaller for photodissolution than for thermal dissolution. This result suggests that the extent of lateral dissolution during photodoping at 383 K is negligible. In support of this, figure 7.11 shows a phase-contrast micrograph of a grating pattern (12 μm period) produced in a $\text{Ag/As}_{40}\text{S}_{60}$ film at 383 K. Some image degradation is apparent, possibly due to over exposure (the exposure time was > 4 min) or to the temperature exceeding 383 K. Nevertheless, a clear pattern has been produced and this would not be expected if significant lateral dissolution occurred.

A temperature dependence such as that observed in photodissolution, may be due to a variety of reasons. In a solid-state chemical reaction it is usually indicative of a diffusion-controlled process, with the diffusion constant being a function of temperature. In the case of a doped semiconductor the conductivity rises with temperature (over certain temperature ranges), not due to a diffusion effect, but due to thermal promotion of charge carriers. Alternatively, in a system which is in thermodynamic equilibrium the value of the equilibrium constant, and hence various properties of the system, may vary exponentially with temperature. The Arrhenius plot of the rate versus reciprocal temperature, shown in figure 7.6, exhibited an activation energy of ~ 0.24 eV. This value is in accordance with the values obtained in other studies and is also comparable to the activation energy for Ag diffusion in Ag_2S (0.11 eV).⁷ The fact that the photodissolution process has such a low activation energy, indicates that this process is not thermally activated, so that the nature of the

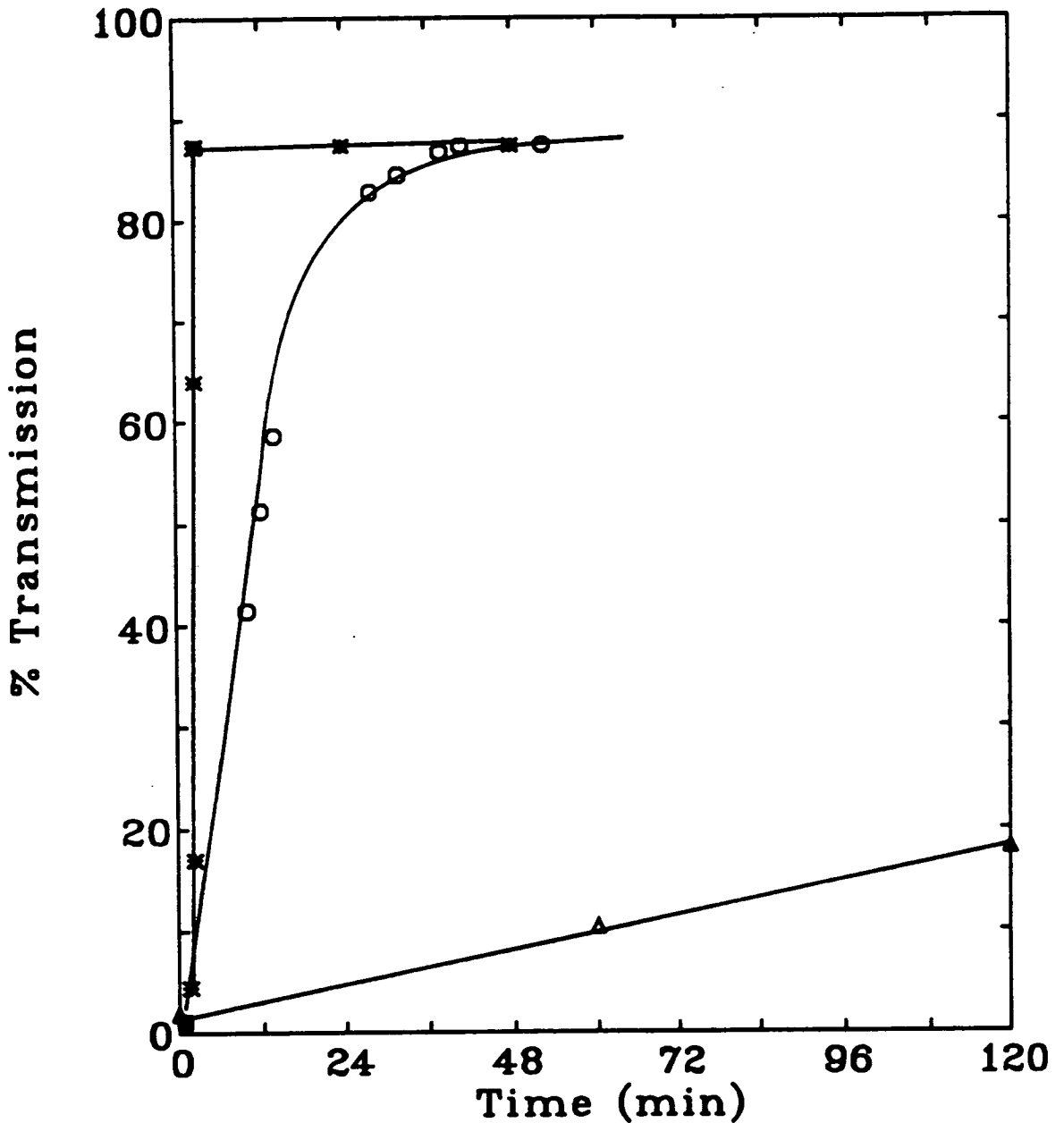


Figure 7.10. Increase of transmission through a $\text{Ag}/\text{As}_{40}\text{S}_{60}$ film combination during exposure for two temperatures: room temperature (o) and 383 K (*). The data of figure 7.9, corresponding to thermal doping, is also shown (Δ). This transmission was monitored at 1400 nm. The $\text{As}_{40}\text{S}_{60}$ and Ag film thicknesses are given in figures 7.8 and 7.9.



Figure 7.11. Phase-contrast micrograph of a grating made at 383 K (110 °C) using white light exposure through a mask of 12 μm period. The $\text{As}_{40}\text{S}_{60}$ and Ag film thicknesses are 600 and 67 nm respectively.

photodoping process is rather different from the typical diffusion-controlled solid-state reaction.

7.3.3. The effect of light intensity

The investigation of the effect of light intensity on the photodissolution rate provides useful information about the mechanism of the photodissolution process. In addition, the study of this parameter at room temperature and above will determine its importance in obtaining an increase in the photodissolution rate. The effect of light intensity was therefore investigated at room temperature and at 373 K, the intensity being varied by changing the slit width separating the illumination source and the sample, as described in Chapter 5. The intensity range studied was from 3.5 to 70 mW/cm². A review of other studies concerned with the effect of intensity on the photodissolution rate was presented in Chapter 4.

Figure 7.12 shows typical results for the dependence of photodissolution rate on light intensity at room temperature and at 373 K. This figure shows that the rate at room temperature is increased by a factor of 6 as a result of increasing the light intensity from 3.5 to 70 mW/cm². The same intensity increase at 373 K resulted in an 8-fold increase in the rate, so at higher temperatures the rate appears to be more sensitive to intensity. Illumination with 70 mW/cm² at 373 K yields the highest increase in rate. Analysis of this data also shows that the difference between the rates at room temperature and at 373 K increases as the light intensity increases. This observation implies that the maximum increase in the rate cannot be achieved at 373 K unless a high light intensity is used (70 mW/cm²).

The above results are replotted in log-log form in figure 7.13. Both sets of data can be fitted with a straight line. The gradient at 373 K is about 0.68 and that at room temperature is about 0.6. Most of the previous studies showed a gradient ~ 1 , which is significantly

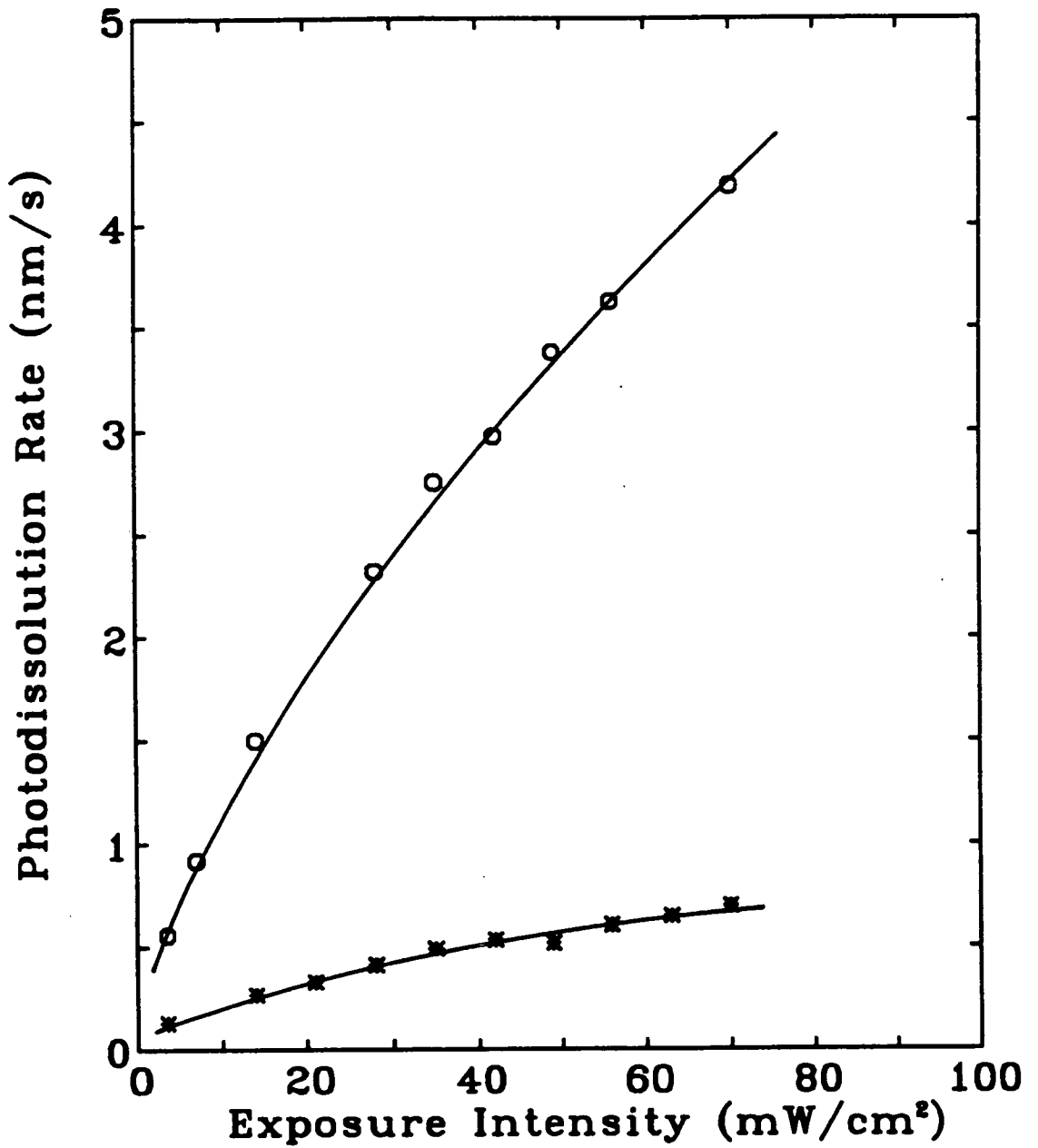


Figure 7.12. Ag photodissolution rate versus light intensity at room temperature (*) and 373 K (o). The $As_{40}S_{60}$ and Ag film thicknesses are 254 and 108 nm respectively

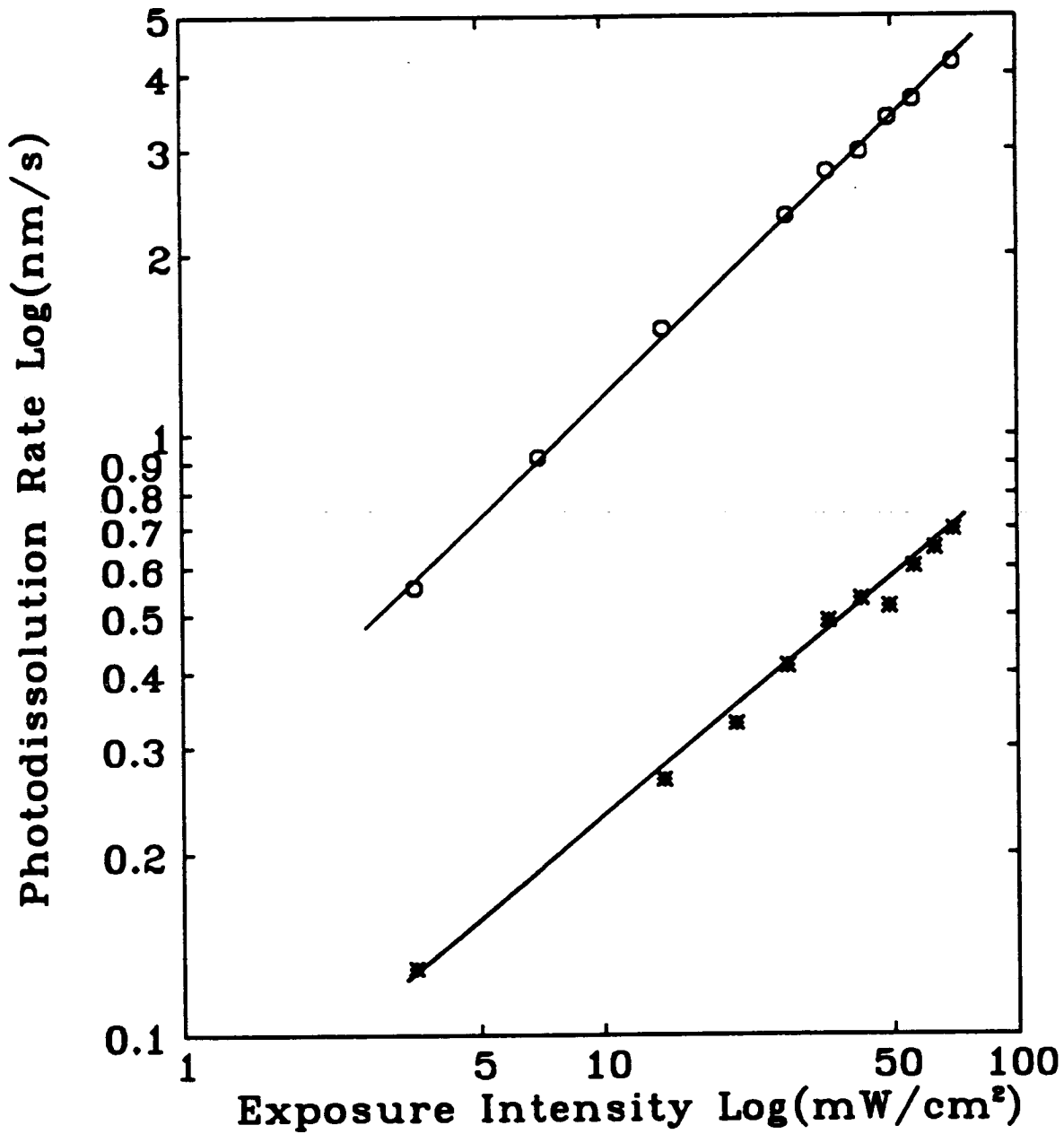


Figure 7.13. A log-log plot of Ag photodissolution rate versus light intensity at room temperature (*) and 373 K (o). The data is derived from that of figure 7.12.

higher than that obtained in the present study. This difference might be due to several parameters: chalcogenide composition, the type of metal ion source, the type of illumination, the As-S/Ag thickness ratio, the technique used to measure the rate, and finally the intensity range investigated.⁸⁻¹³ The common feature of most of these earlier studies is the technique used to investigate the kinetics (the resistance monitoring technique) which only measures the amount of Ag remaining on the surface of the chalcogenide layer. However, the technique used in the present study measures the changes in the chalcogenide layer. The resistance technique cannot be used to monitor the complete photodissolution process unless the initial As-S/Ag thickness ratio is less than or equal to about three, otherwise the Ag layer will be exhausted before the process finishes. Therefore, the authors who used this technique were looking at the rate for the case where Ag is present on the surface, which might have a linear dependence on intensity. Although Buroff¹³ did not use the resistance technique he used a chemical method which was also based on measuring the remaining Ag. In addition, the fact that his technique is relatively complicated and does not measure the rate in situ might introduce many experimental errors. Since the absolute values of the light intensity used were not given, exact comparison of Buroff's results with other studies is not possible. In those cases where a similar technique to that of the present work was employed, there were differences in the composition⁸ or in the light intensity range¹⁰ used.

In contrast to a linear intensity, the gradient of ~ 0.6 observed in the present work clearly indicates that the photodissolution process, whether at room temperature or 373 K, has a weak dependence on light intensity over the intensity range investigated.

7.3.4. The effect of Cu as the metal ion source

It is known from previous work, as reviewed in Chapter 4, that Cu dissolves into the As-S structure faster than Ag. The essential

problem with Cu dissolution is that it proceeds even in the dark, which makes it uncontrollable. A solution to this problem is to evaporate a thin Ag film sandwiched between the Cu and $As_{40}S_{60}$ films to act as an initial barrier layer against thermal dissolution at room temperature. It is expected that from this arrangement a faster and more controllable Cu photodissolution process might be obtained.

Typical kinetics results obtained from this novel arrangement are plotted in figure 7.14, which shows data corresponding to two film combinations: Cu/Ag/ $As_{40}S_{60}$ and Ag/ $As_{40}S_{60}$. The $As_{40}S_{60}$, Ag and Cu film thicknesses are 414, 24 and 154 nm respectively. These results show that the rate corresponding to the Cu/Ag/ $As_{40}S_{60}$ film combination is three times faster than that for the Ag/ $As_{40}S_{60}$ combination, so that with this new arrangement it may be possible to exploit Cu photodissolution in applications. The increase in the rate is not as large as expected but this may be due to the high $As_{40}S_{60}$ /Ag thickness ratio used ($d_{As_{40}S_{60}}/d_{Ag} = 17$). An attempt was made, therefore, to study the effect of the Ag thickness on the rate improvement for this new arrangement.

The rate for the two combinations is plotted as a function of Ag thickness in figure 7.15. This figure shows clearly that the rate enhancement for the Cu films vanishes as the Ag film thickness increases. The ratio of the rate for the Cu/Ag combination to that for Ag alone versus Ag film thickness is shown in figure 7.16. This figure shows that Cu films will yield a significant increase in rate only for Ag thicknesses less than 120 nm (which is approximately one third of the As-S thickness used in these experiments). This observation might be due to the fact that as the Ag film thickness increases, the extent to which the Cu can participate in the photodissolution process decreases, eventually becoming negligible. The data of figures 7.15 and 7.16 were obtained for constant values of the As-S and Cu film thicknesses (these are given above).

A further experiment was carried out to investigate the effect of Cu thickness on the rate of the Cu/Ag/As-S combination. In contrast to the previous experiments, the As-S and Ag film thicknesses, (414 and 180 nm respectively) were kept constant and the rate for the

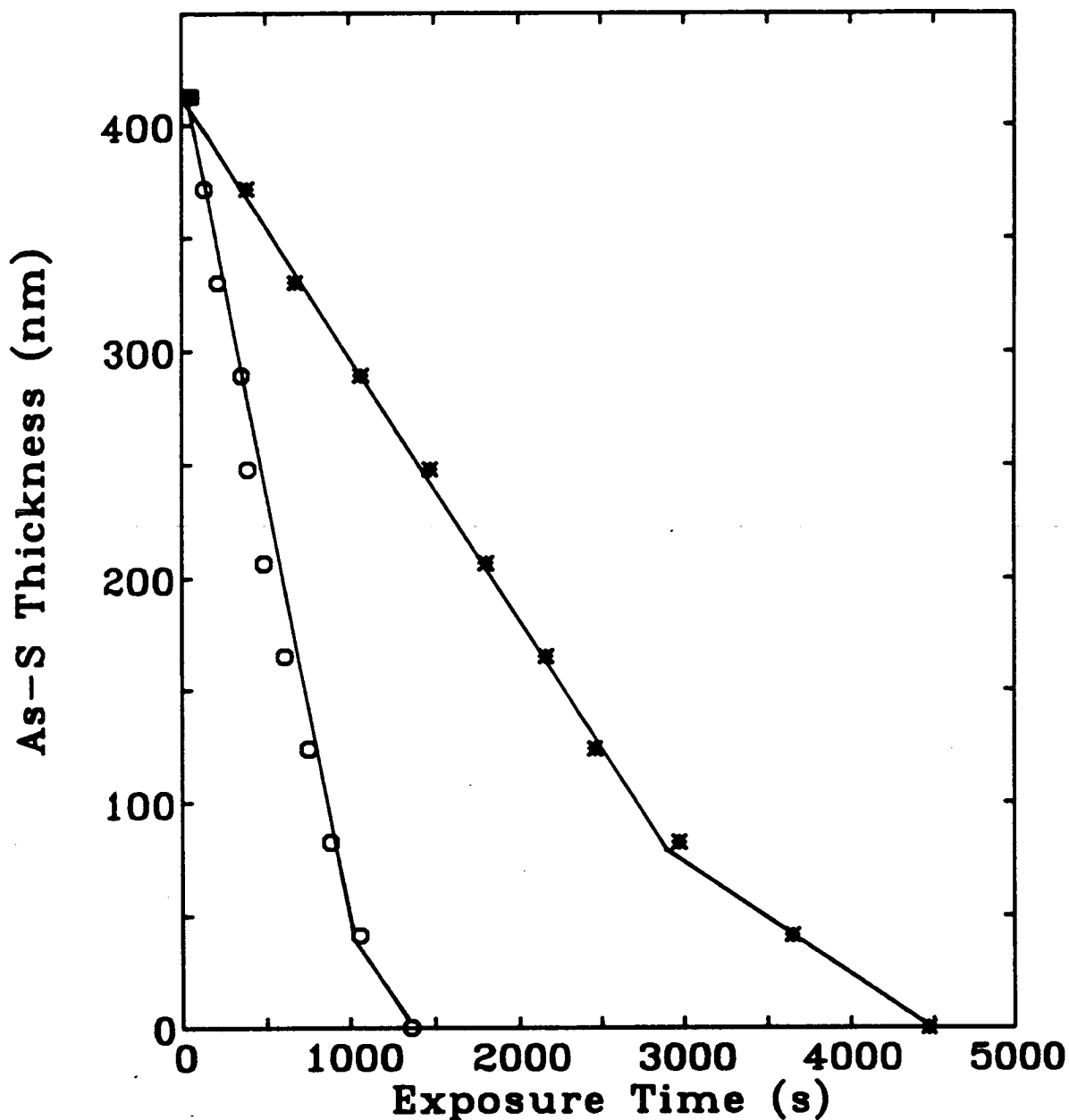


Figure 7.14. Decrease of the $As_{40}S_{60}$ film thickness during Ag photodissolution for two film combinations: Cu/Ag/ $As_{40}S_{60}$ (o) and Ag/ $As_{40}S_{60}$ (*). The $As_{40}S_{60}$, Ag and Cu film thicknesses are 414, 24 and 154 nm respectively.

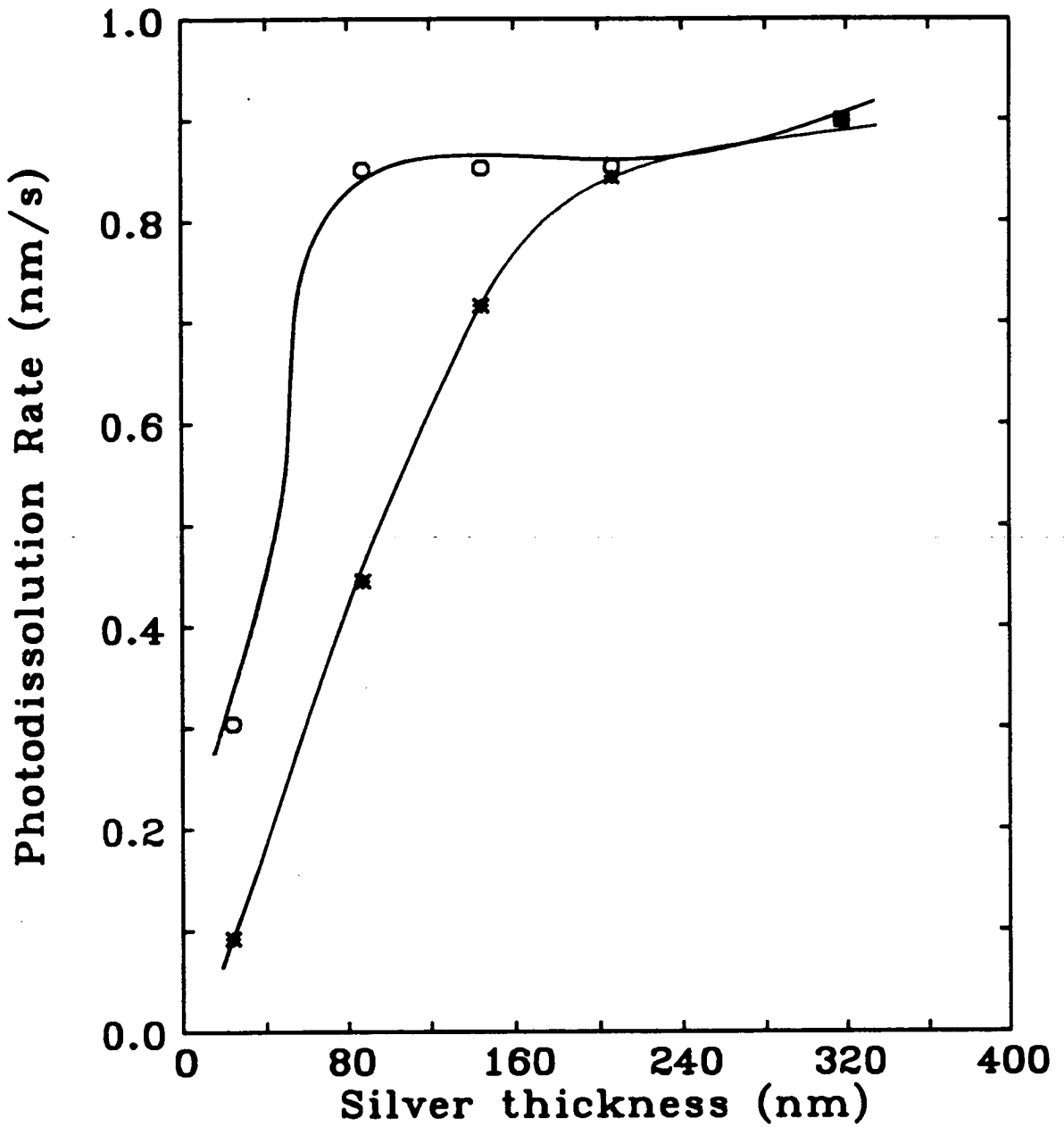


Figure 7.15. Dependence of the photodissolution rate on Ag film thickness for two film combinations Cu/Ag/As₄₀S₆₀ (o) and Ag/As₄₀S₆₀ (*). The As₄₀S₆₀ and Cu film thicknesses are similar to those of figure 7.14.

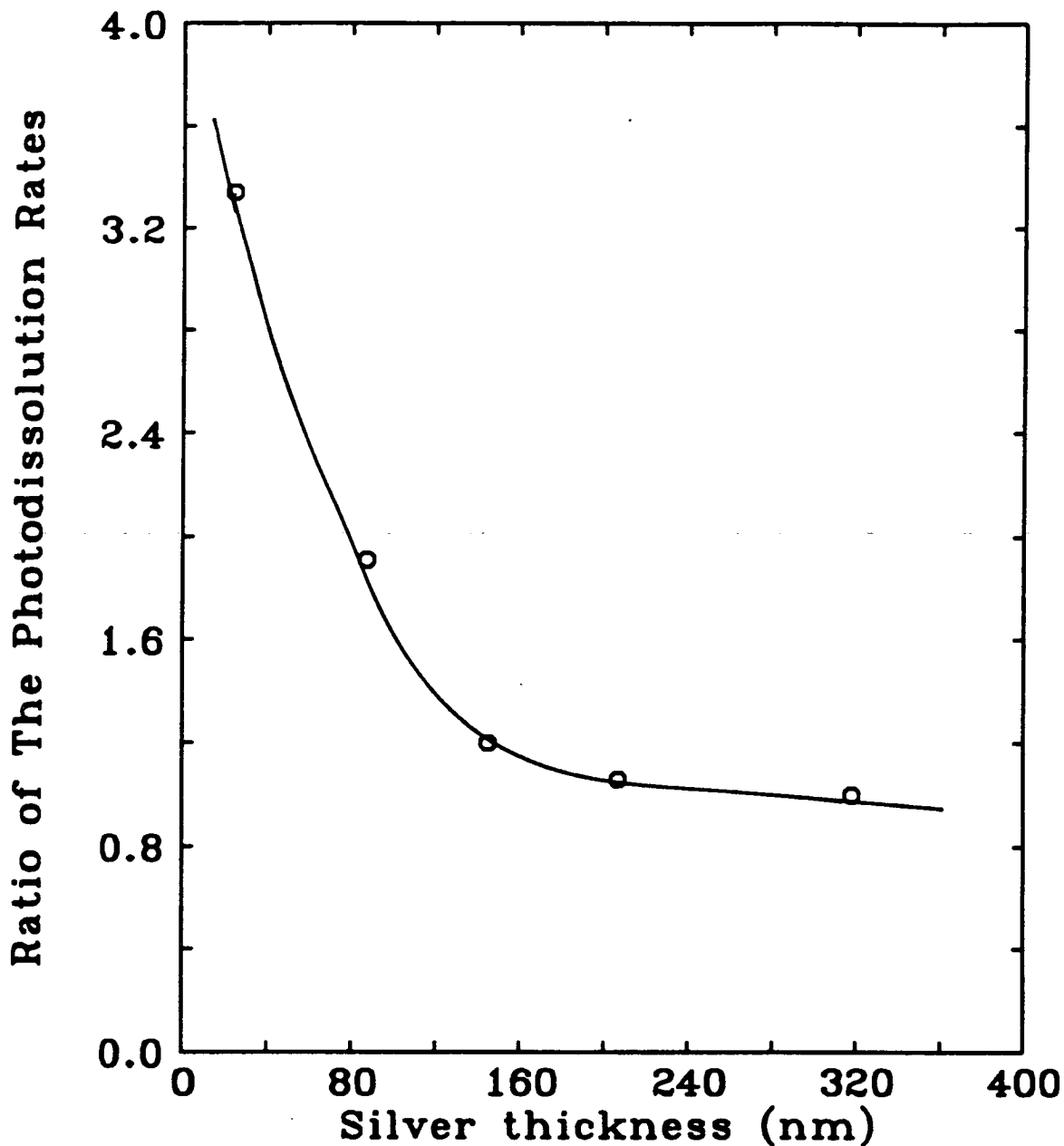


Figure 7.16. Dependence of the ratio of the photodissolution rates on Ag film thickness. This ratio is defined as the rate for the Cu/Ag/As₄₀S₆₀ combination rate divided by that for Ag/As₄₀S₆₀. The data is derived from that in figure 7.15.

Cu/Ag/As-S combination was monitored as a function of Cu film thickness over the range 23 to 400 nm. The Ag film thickness was chosen to be above 120 nm because above this value, Cu films of thickness ~ 150 nm appears to have negligible effect on the rate for the Cu/Ag/As₄₀S₆₀ combination. Therefore examining a range of Cu film thicknesses might lead to an improvement in the rate for these samples. However, the photodissolution rate did not show any dependence on the Cu film thickness. This result might be explained by the fact that the Ag layer, which initially acts as a barrier between the As-S and Cu films, is so thick that once it is exhausted there is no As-S layer left to be photodoped by the Cu film.

The effect of temperature on the rate for the Cu/Ag/As₄₀S₆₀ combination was also investigated and compared with the corresponding results for Ag/As₄₀S₆₀. The Cu and As-S film thicknesses used were similar to those used previously and the Ag film thickness was 180 nm. Again, the Ag film thickness was chosen to be above 120 nm because above this value the Cu film thickness has negligible effect on the rate for the Cu/Ag/As₄₀S₆₀ combination at room temperature. Thus for Ag thicknesses ≥ 120 nm any difference between the rates for the Cu/Ag/As₄₀S₆₀ and Ag/As₄₀S₆₀ at higher temperatures must be due to the Cu film. The results are presented in figure 7.17, which shows that the Cu/Ag/As₄₀S₆₀ combination at 393 K exhibits a rate higher than that at room temperature by a factor of 12, whereas the Ag/As₄₀S₆₀ rate at this temperature is only 10 times faster than at room temperature. This shows that the Cu film can have an effect on the rate for the Cu/Ag/As₄₀S₆₀ combination even though the Ag thickness is greater than 120 nm. This figure also shows that the difference in rates between the two film combinations increases with temperature. The fact that the rate for the Cu/Ag/As₄₀S₆₀ combination is more affected by temperature than that for Ag/As₄₀S₆₀ might be connected with the fact that Cu is known to have a higher thermal dissolution rate than Ag in the As-S structure.¹⁴ It can be concluded, therefore, that this new arrangement yields a faster yet controllable rate at high temperature.

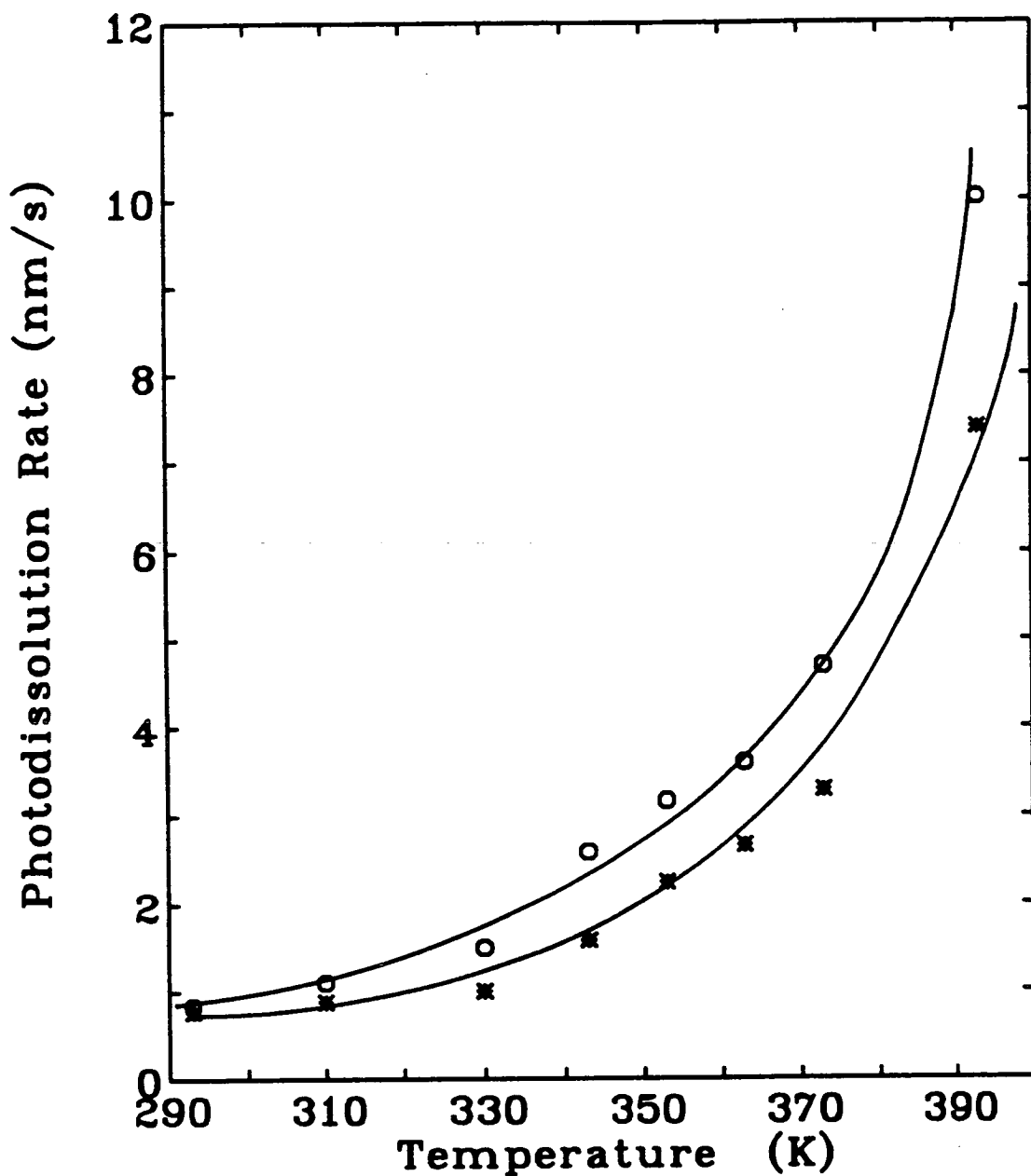


Figure 7.17. Temperature dependence of the photodissolution rate for two film combinations: Cu/Ag/As₄₀S₆₀ (o) and Ag/As₄₀S₆₀ (*). The Ag film thickness is 180 nm and the As₄₀S₆₀ and Cu film thicknesses are similar to those of figure 7.14.

7.4. Compositional dependence of the Ag-photodissolution rate

In the As-S system it was found, as shown in Chapter 4, that the maximum Ag photodissolution rate is achieved around the composition $As_{30}S_{70}$. The purpose of the work described in this section is to find out if pre-annealing or increased temperature have an effect on the compositional trend found previously.

7.4.1. The effect of pre-annealing

The effect of composition on photodissolution rate was investigated for both as-deposited and annealed films. This work revealed that the compositional trend of the photodissolution rate, described earlier, is unchanged as a result of the pre-annealing treatment. This is shown clearly in figure 7.18 which compares the compositional trend of the rates for as-deposited and annealed films. This figure also shows that the annealing has decreased the rate for all the compositions investigated. It is also noticeable that the magnitude of the decrease due to annealing has a maximum at $As_{30}S_{70}$. This maximum, like the peak in the photodissolution rate, is probably due to the homogeneous morphology of the photodoped product for compositions around $As_{30}S_{70}$.

The fact that $As_{30}S_{70}$ was the composition to be the most affected by the annealing treatment, as far as the rate is concerned, suggests that its structure in the as-deposited form is very sensitive to external factors which cause structural changes. Because the structural changes produced lead to a decrease in the photodissolution rate, as-deposited $As_{30}S_{70}$ films require careful handling in order to achieve the optimum rate for the photodissolution process. It should be noted here that even the breaking of the vacuum between the Ag and $As_{30}S_{70}$ film depositions causes a decrease in the photodissolution rate. In the present case, the breaking of the vacuum during deposition was

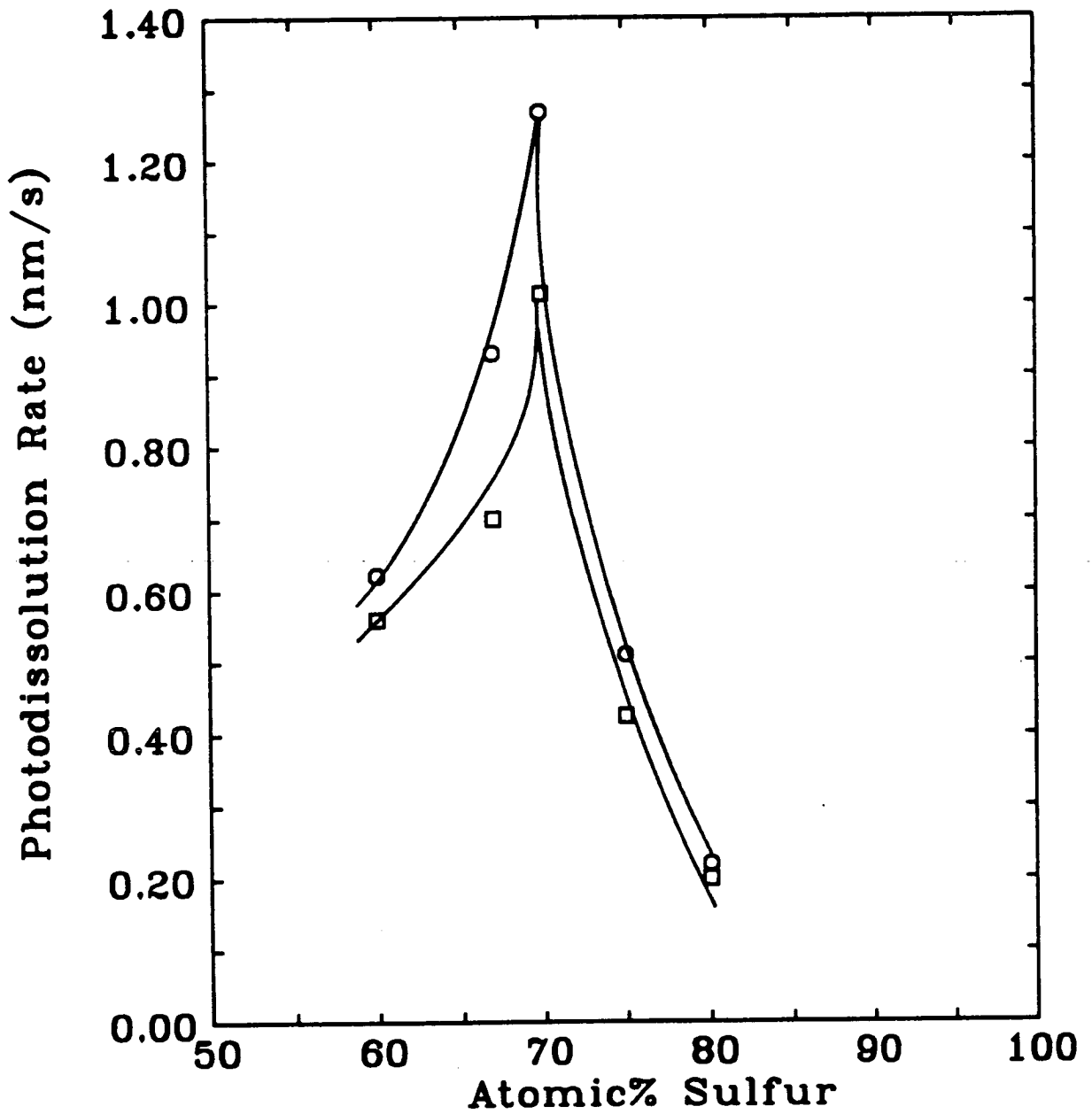


Figure 7.18. The dependence of the Ag photodissolution rate on As-S composition for annealed (□) and as-deposited (*) films. The As-S film thickness is similar to that of figure 7.3 and the Ag film thickness is 148 nm.

necessary in order to anneal the $As_{30}S_{70}$ films.

7.4.2. The effect of temperature

For these experiments, the investigation was limited to as-deposited samples of the $As_{30}S_{70}$ composition, since it is expected that above room temperature this composition will exhibit a higher rate than $As_{40}S_{60}$. Surprisingly, the opposite behaviour was observed. Figure 7.19 shows the photodissolution rate versus temperature for $As_{30}S_{70}$: as the temperature increases, the rate increases slightly, peaking at 293 K, and then decreases sharply. This result might be due to the structural difference between the two compositions (see Chapter 2). In addition this result is in agreement with the result of the previous section (7.4.2) and therefore the explanation given in that section might also be applicable here.

The opposite behaviour was found in a recent study¹⁵ investigating the composition $As_{33}S_{67}$, which is near to $As_{30}S_{70}$. This difference might be due to the higher values of light intensity ($> 70 \text{ mW/cm}^2$) and/or the As-S/Ag thickness ratio (15) used in that study together with the slight difference in composition. These conflicting results show that a more extensive study of the compositional dependence of the effect of temperature on the rate is required.

7.5. Characteristics of the Ag-photodissolution process

From the experimental results of the previous sections, it is possible to extract some information which is of use in understanding the nature of the photodissolution process. As pointed out earlier (Chapter 3), several aspects of the photodissolution process are the

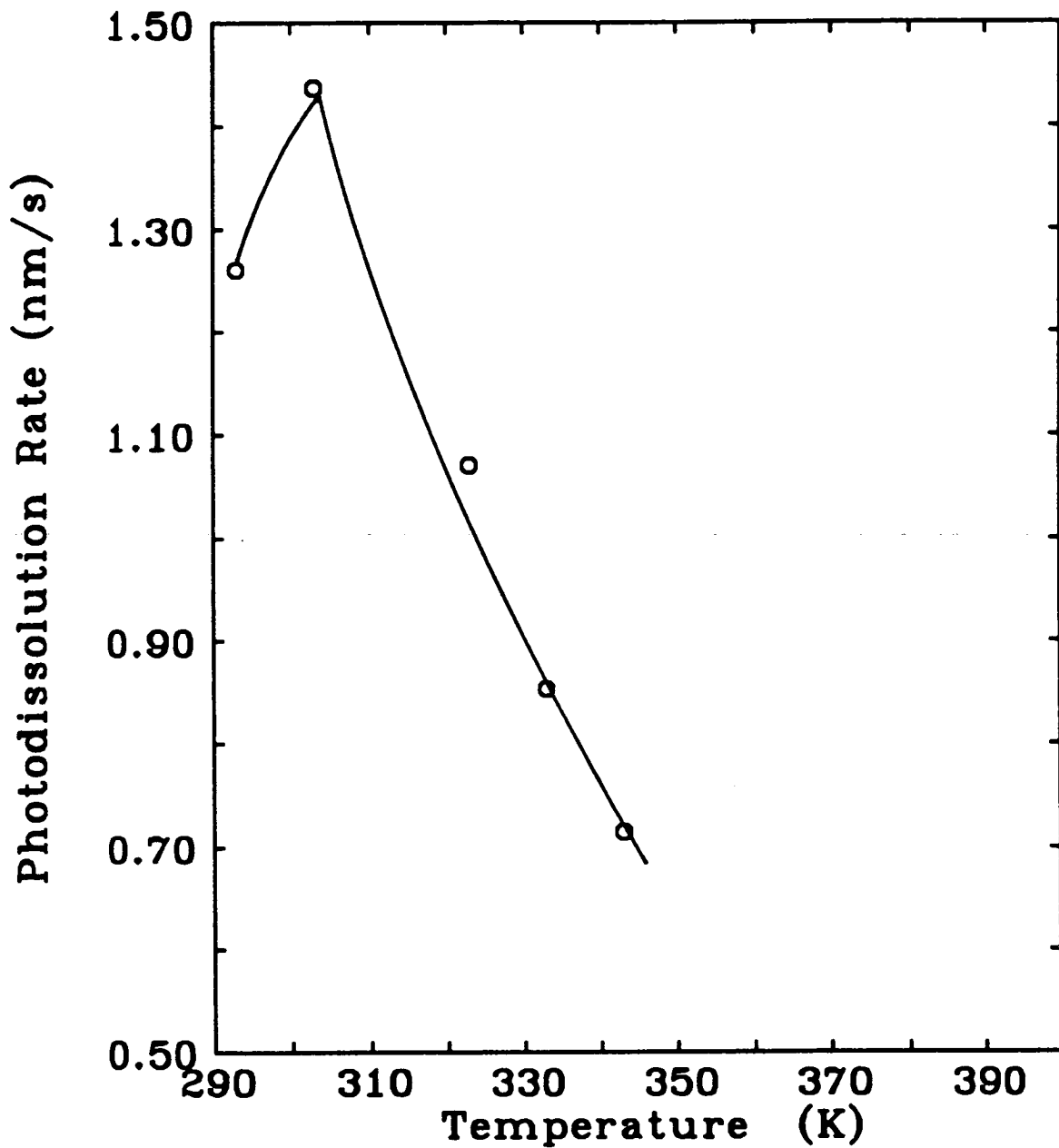


Figure 7.19. Temperature dependence of the Ag photodissolution rate for the composition $As_{30}S_{70}$. The $As_{30}S_{70}$ and Ag film thicknesses are 1220 and 370 nm respectively.

subject of controversy. It is generally accepted that the kinetics is governed by an S-shaped curve consisting of three regions: an initial induction period where the photodissolution rate increases slowly from zero; then a second region with a significant (sometimes constant) dissolution rate; and finally a third region during which the photodissolution rate decreases slowly.^{11, 16} One of the principal areas of controversy is the second stage. While some investigators report that the propagation distance depends on the square root of time,¹⁷ which implies that diffusion of the ions or electrons through the photodoped layer is the rate-limiting step, others observe a linear time dependence,^{11, 12} which indicates that the speed of the process is controlled by the chemical reaction. In one study the form of the time dependence was also found to depend on the silver layer thickness, a square-root-time dependence being found for thinner films and a linear time dependence for thicker ones.¹⁸

The kinetics results of the present work indicate that, for the conditions used, the time dependence of the photodissolution process is definitely linear. A typical plot of the decrease in As-S thickness versus time is shown in figure 7.20, and the same data is plotted against square-root-time in figure 7.21. A good straight line fit is obtained in the first case but not the second, showing clearly that there is a linear time dependence under these conditions.

The number of stages in the photodissolution process was found to depend on the magnitude of the rate. A single linear stage is found for high rates and three stages for lower rates. Since the magnitude of the rate depends on the As-S/Ag thickness ratio and the temperature, the number of stages in the process also depends on these two parameters.

The effect of the As-S/Ag thickness ratio is clearly shown in figure 7.22 where three sets of data corresponding to three different thickness ratios are plotted. As the ratio increases from 3.6 to 11.7, the number of stages increases from one to three: for ratios of 6 and 11.7 the process has three stages, the first one being shorter and faster than the second, and the last one forming a tail. It is also noticeable that both the first and the second stage are linear.

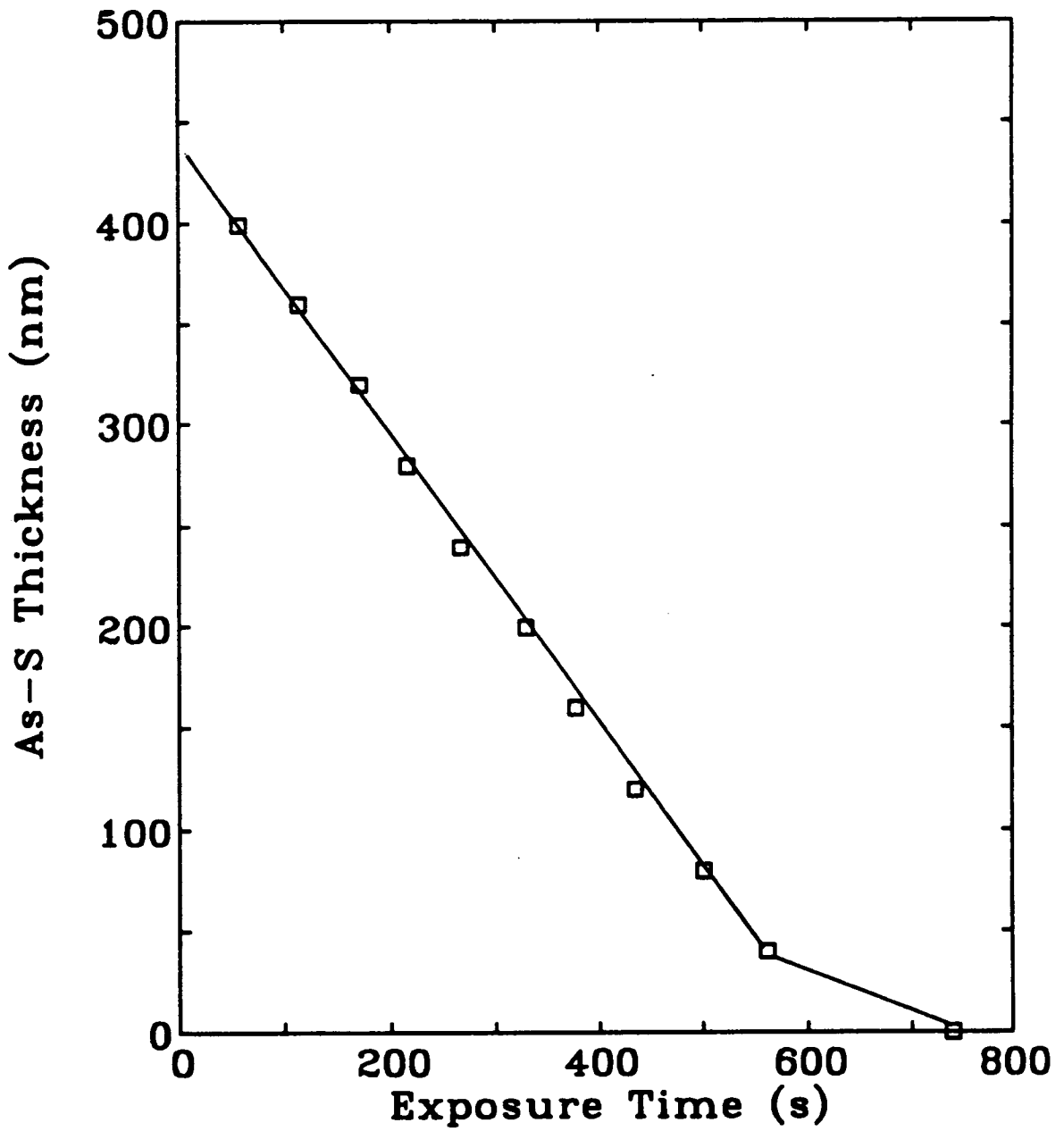


Figure 7.20. The decrease in thickness of an annealed $\text{As}_{40}\text{S}_{60}$ film plotted versus a linear time scale. The $\text{As}_{40}\text{S}_{60}$ and Ag film thickness are given in figure 7.2.

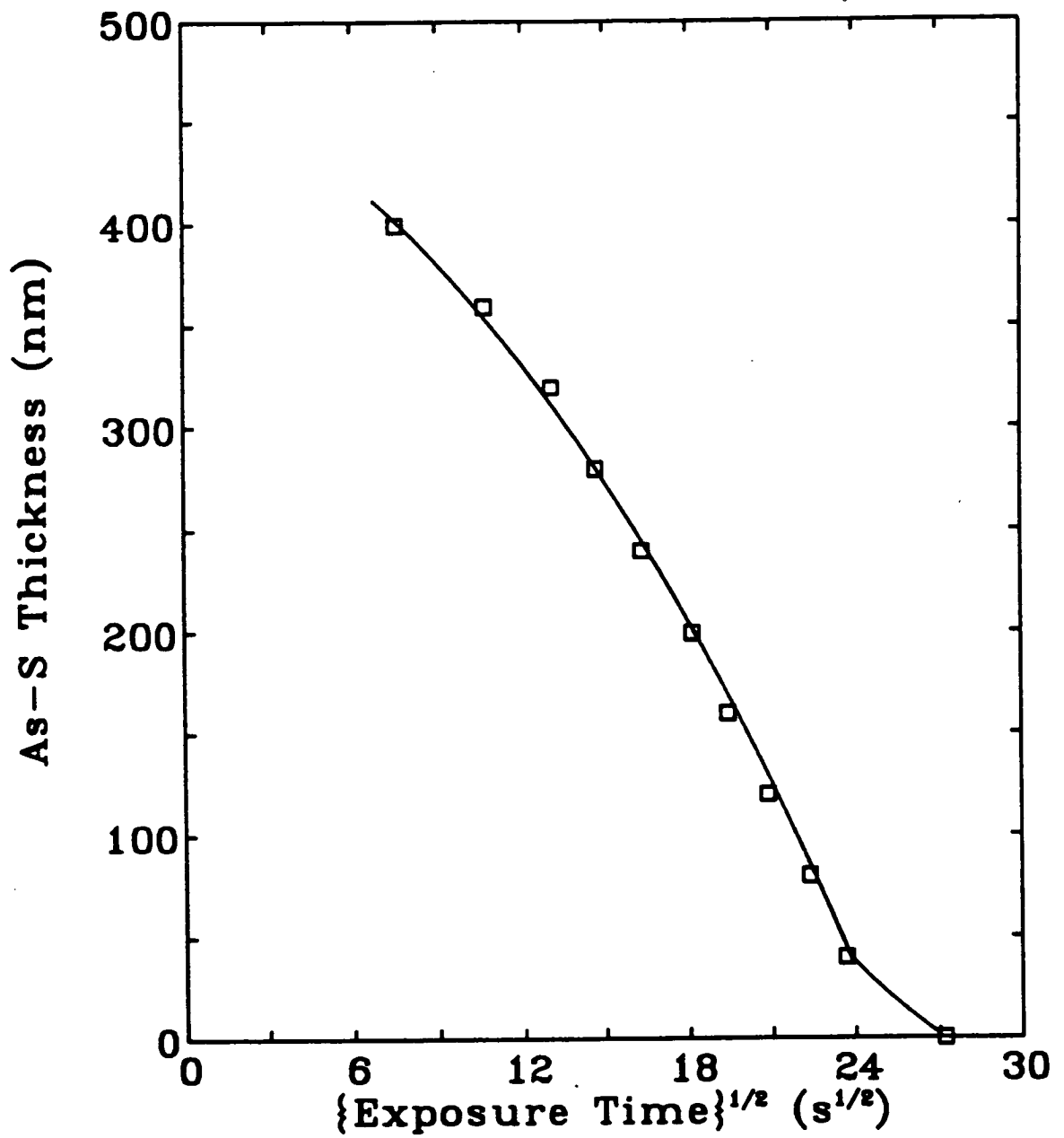


Figure 7.21. The data of figure 7.20 plotted versus the square root of exposure time.

The effect of temperature was to reduce the number of stages in the photodissolution process, as illustrated in figure 7.7 (section 7.3.3.) which shows that the first stage and the tail present at room temperature disappear at 393 K where the rate is almost 10 times that at room temperature. The effect of temperature on the change in the slope might be due to an increase in the diffusivity of the Ag ions and electrons or in the rate of the chemical reaction.

It is also found that the transition from the first to the second stage occurs when the As-S thickness consumed is about 3 times the initial Ag thickness. In figure 7.22 this transition is apparent in the data corresponding to thickness ratios of 6 and 11.7, which were obtained for initial As-S film thicknesses of ~ 500 and 700 nm respectively. For these curves the transition occurs when the As-S thickness consumed is 3.1 and 3.6 times the initial Ag thicknesses respectively. In figure 7.23, where the initial $As_{40}S_{60}$ film thickness is 1120 nm and the ratio is 7, the transition occurs when the As-S thickness consumed is 2.6 times the initial Ag thickness. These results suggest that the transition is occurring at the point where the Ag becomes exhausted so that in the second stage of the photodissolution process the Ag is provided by the photodoped layer generated in the first stage. A visual check was made to confirm that the Ag had disappeared from the surface of these samples. Therefore it can be concluded that the photodissolution process does not stop once the Ag is exhausted. This finding is in agreement with a previous study¹⁹ and shows that the assertion of Kolwicz and Chang²⁰ that the process stops when the Ag is exhausted is incorrect. The change in the photodissolution process from a faster stage to a slower one was also reported previously¹⁰ for the composition $As_{30}S_{70}$, but in that case the change in slope was present even before the exhaustion of the silver. This difference might be due to the different As-S compositions used or more likely the difference in film thicknesses.

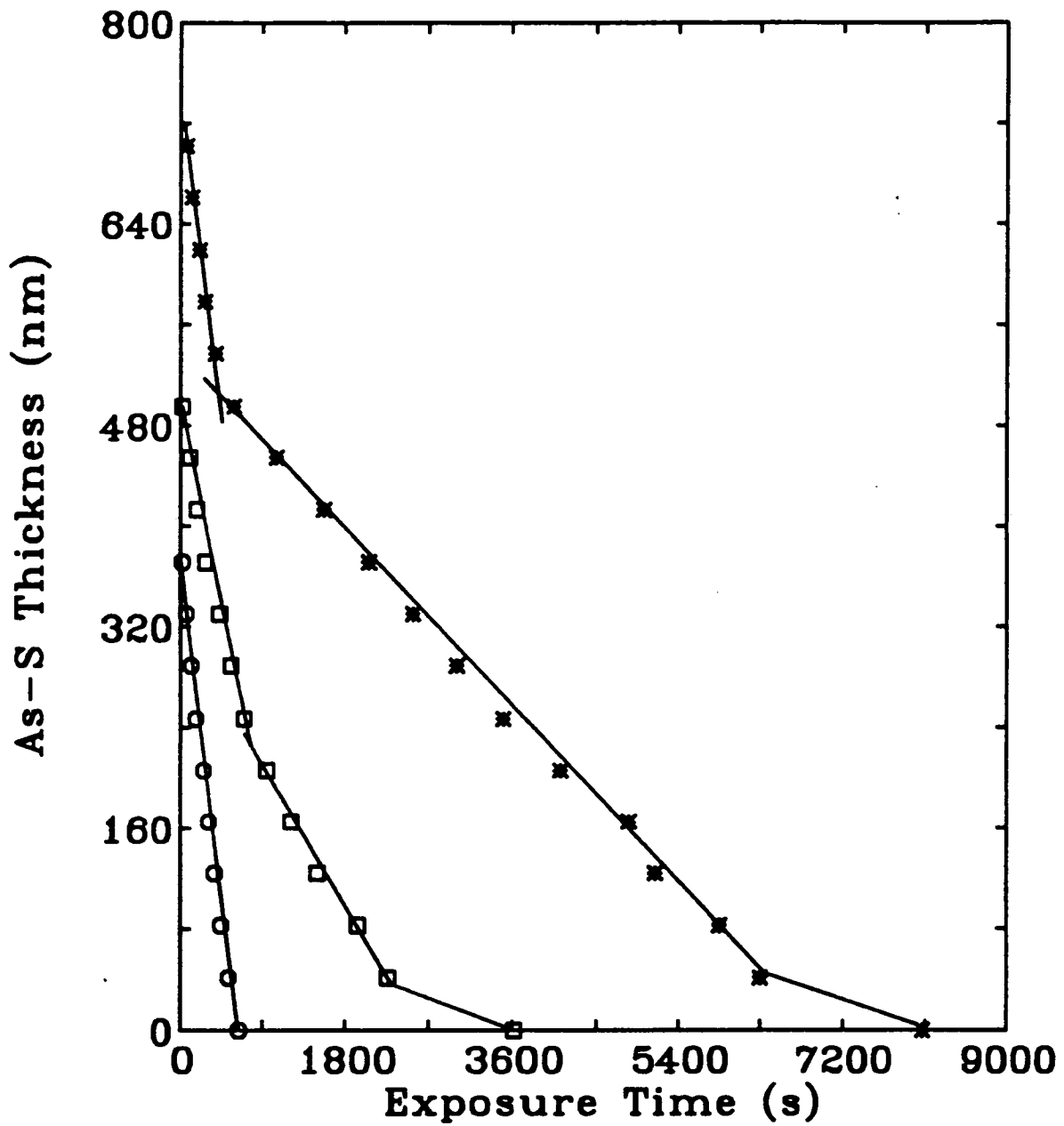


Figure 7.22. Decrease in $As_{40}S_{60}$ film thickness during Ag photodissolution for different ratios of $As_{40}S_{60}$ to Ag thicknesses: 3.6 (o), 6 (\square) and 11.7 (*). The $As_{40}S_{60}$ film thicknesses are 372 nm (o), 496 nm (\square) and 702 nm (*).

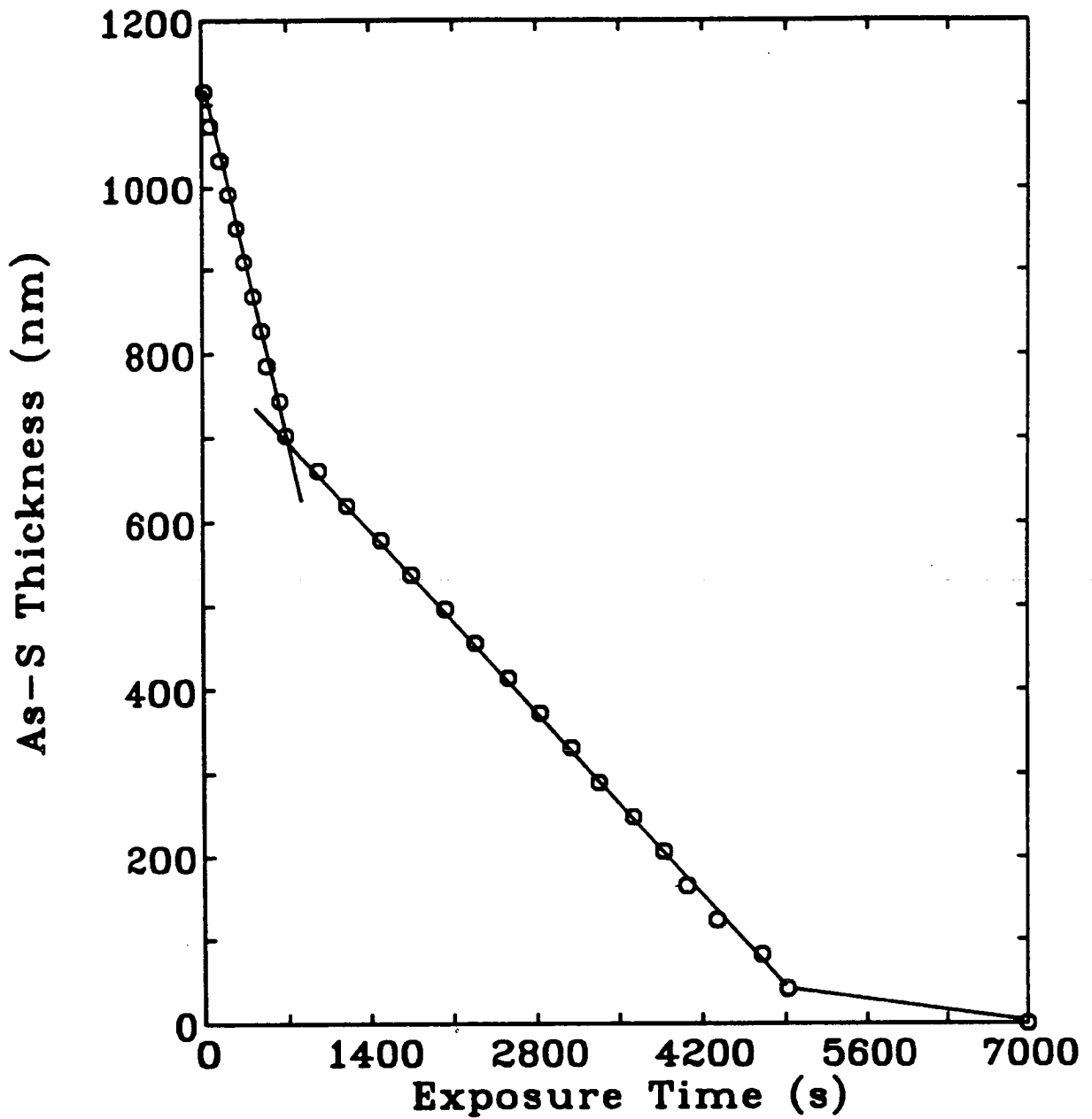


Figure 7.23. The decrease in $As_{40}S_{60}$ film thickness during Ag photodissolution, showing the kink separating the first and second stages. The $As_{40}S_{60}$ and Ag film thicknesses are 1120 nm and 149 nm respectively.

7.6. The mechanism of the photodissolution process

On the basis of the experimental results obtained the following model of the photodissolution process can be proposed. A weak activation energy and a linear time dependence suggest that the photodissolution process is a solid state chemical reaction and not a straightforward diffusion process. The fact that photodissolution continues even when the metallic Ag is exhausted emphasises the importance of the doped/undoped interface in the photodissolution process. In the absence of metallic Ag the photodoped product takes on the role of the Ag^+ reservoir, thereby ensuring the continuation of the process. The fact that the photodissolution before the Ag exhaustion is much faster than that afterwards (at least at room temperature) demonstrates also the importance of the Ag/doped interface in the photodissolution process.

The increase in the photodissolution rate with increasing temperature might be explained by the temperature dependence of the conductivities of both the photodoped and undoped material, since it is well known that the conductivity of these materials increases with temperature due to an increase in the free electron concentration. As electrons are essential to the chemical reaction occurring their concentration may have an important effect in increasing the rate of photodissolution. This proposal is consistent with the results of experiments on lateral photodissolution,²¹ which only occurs when the chalcogenide is in contact with a conducting layer that can transport electrons to the reaction front. In addition, the ionic conductivity of the photodoped material will also be increased as a result of temperature and this will act in conjunction with the change in the electronic conductivity.

7.7. Conclusions

From the results reported above, several points should be noted:

- 1- Pre-annealing decreases rather than increases the rate of Ag-photodissolution for all the As-S composition investigated.
- 2- The effect of pre-annealing on the photodissolution rate increases slightly as the thickness ratio $d_{As_{40}S_{60}}/d_{Ag}$ decreases and is a maximum at $As_{30}S_{70}$.
- 3- The weak activation energy and linear time dependence observed shows that the process is not diffusion controlled but reaction controlled.
- 4- The maximum improvement (by a factor of 12) in the rate of photodissolution was obtained with the film combination Cu/Ag/ $As_{40}S_{60}$ at 393 K. The improvement in the rate for the Ag/ $As_{40}S_{60}$ film combination, obtained at 393 K, was a by factor of 10.
- 5- The thermal dissolution rate for Ag was shown to be negligible in comparison to that for Ag photodissolution.
- 6- A grating pattern was fabricated at high temperature using photodissolution, confirming that lateral dissolution at high temperature is not significant.
- 7- A sublinear dependence of photodissolution rate on light intensity was observed rather than a linear relation as obtained by most authors.
- 8- The compositional dependence revealed that the maximum rate is obtained at $As_{30}S_{70}$ for both annealed and as-deposited films. However, with increasing temperature the photodissolution rate for the

As₃₀S₇₀ film showed a small increase, peaking at 314 K, and then decreased.

9- Ag photodissolution was found to continue even when the metallic Ag source is exhausted.

10- The number of stages in the photodissolution process was found to depend on the magnitude of the rate, and therefore on the thickness ratio $d_{\text{As}_{40}\text{S}_{60}}/d_{\text{Ag}}$ and the temperature. In the case of fast rates, a single linear stage is found but in the case of slow rates three stages are observed.

11- The results are consistent with a mechanism based on a light-induced solid state reaction between the metal and the chalcogenide.

References

1. Chatani K., Shimizu I., Kokado H. and Inoue E., *Jap. J. Appl. Phys.*, vol. 16, p. 389, 1977.
2. Tamaki Y. and Shoichi K., *J. Appl. Phys.*, vol. 54(2), p. 647, 1983.
3. Kluge G., *Phys. Stat. Sol. (a)*, vol. 101, p. 105, 1987.
4. Kostyshin M.I., Krashnojonov E.P., Makeev V.A. and Solobov G.A., *Application of Holography*, 1970. Eds.: Vienot J.C., Bulabois J. and Pasteur J. paper 11.7
5. Plochanski J., Przulski J. and Teodorczyk M., *J. Non-Cryst. Solids*, vol. 93, p. 303, 1987.
6. Chang M.S., Hou T.W., Chen J.T., Kolwicz K.D. and Zemel J.N., *J. Vac. Sci. Technol.*, vol. 16, p. 1973, 1979.

7. Kolobov A.V., Elliot S.R., *Advances in Physics*, vol. 40, p. 625, 1991.
8. Firth A.P., *Ph.D. Thesis*, University of Edinburgh, 1985.
9. Oldale J.M., Rennie J.H.S. and Elliot S.R., *Thin Solid Films*, vol. 164, p. 467, 1988.
10. Zakery A., *Ph.D. Thesis*, University of Edinburgh, 1991.
11. Goldschmidt D. and Rudman P.S., *J. Non-Cryst. Solids*, vol. 22, p. 229, 1976.
12. Yaji T. and Kurita S., *Jap. J. of Appl. Phys.*, vol. 22, p. 400, 1983.
13. Buroff A. and Baeva R., 1976. Proc. 6th Int. Conf. Amorph. Liquid
14. Mizuno H., Tanaka K. and Kikuchi M., *Sol. Stat. Commun.*, vol. 12, p. 999, 1973.
15. Wagner T., Vlck M., Smrcka V., Ewen P.J.S. and Owen A.E., *To be published in J. Non-Cryst. Solids*, 1993.
16. Malinowski J. And Buroff A., *Contemp. Phys.*, vol. 19, p. 99, 1978.
17. Inoue E., Kokado H. and Shimizu I., in *Proc. 5th Int. Conf. on Solid State Devices (Suppl. to J. Japan Soc. of Appl.Phys. pp. 101 Vol. 43 1974)*, Tokyo, 1973.
18. Ewen P.J.S., Zakery A., Firth A.P. and Owen A.E., *Phil. Mag. B*, vol. 57, p. 1, 1988.
19. Kasyarum O.P. and Kudryavtsev A.A., in *Proc. of the Int. Conf. on Non-Cryst. Semiconductors, Part 2*, p. 227, Uzhgorod, 1989.
20. Kolwicz K. D. and Chang M.S., *J. Electrochem. Soc. Solid State*, vol. 127, p. 135, 1980.

21. Owen A.E., Firth A.P. and Ewen P.J.S., *Phil. Mag.*, vol. B52, p. 347, 1985.

CHAPTER 8

SECONDARY ION MASS SPECTROSCOPY ANALYSIS OF PHOTODOPED As-S FILMS

8.1. Introduction

The kinetics of the photodissolution process and the optical constants of the photodoped and undoped material have been investigated in previous chapters. Another aspect of the process which is important, both for fundamental reasons and as far as applications are concerned, is the distribution of Ag with depth into the photodoped film. In the case of grating applications, any change in Ag concentration with depth will be accompanied by a change in refractive index and hence in the modulation. This chapter reports an investigation of the depth profile of the Ag photodissolved in the As-S structure using the Secondary Ion Mass Spectroscopy (SIMS) technique. The previous depth profile studies of the Ag/As₂S₃ system^{1, 2} have revealed a step-like profile while in systems like Ag₂Se/GeSe₂ and Ag₂Se/GeSe₉, where the silver is initially present as a compound, the silver distribution is more like that expected from thermal diffusion.³

The SIMS method has been shown by Polasko's study⁴ to give useful information about Ag profiles in Ge-Se glasses. In this chapter, two types of results, obtained from the SIMS method, will be shown: the nature of the Ag depth profile within the photodoped layer, and the effect of exposure time on the Ag depth profile. The latter will be compared to the results obtained from the optical reflectivity technique.

8.2. The SIMS technique

The interaction of energetic ions with a solid results in the ejection of subsurface atoms and molecules in both neutral and charged states. This moderately efficient production of charged particles (secondary ions) coupled with higher sensitivity mass spectrometric techniques forms the basis of the SIMS method. The general procedure for producing a SIMS depth profile is to monitor the secondary ion signal of the element of interest as a function of sputter time. A typical SIMS profile of an As-S photodoped layer is shown in figure 8.1. For a uniform matrix, time can be translated into depth by a suitable calibration experiment (which involves using a film of known thickness and measuring crater depth and sputter yield.)

It is virtually impossible to extract meaningful depth profile information from SIMS data unless one maintains constant primary ion intensity and uniform primary ion current density over the secondary ion extraction area of the sample. In a stationary focused beam, the ion current density on the sample is not constant over the beam diameter, therefore surface layer removal cannot be uniform. If the information zone for secondary ions extends over the total area of the incident beam, the contribution of ions from the crater edges will distort the profile of the subsurface layer. The broadening or skewing of a profile might also be caused by the diffusion of elements brought on or enhanced by ion damage to the solid, an increase in the local temperature of the bombarded area, or high electric field gradients produced from primary ion beam charging of the surface. The degree of surface charge buildup depends on the primary ion species, charge, energy and current density, the dimensions of the bombarded area and the conductivity and the thickness of the insulating layer.

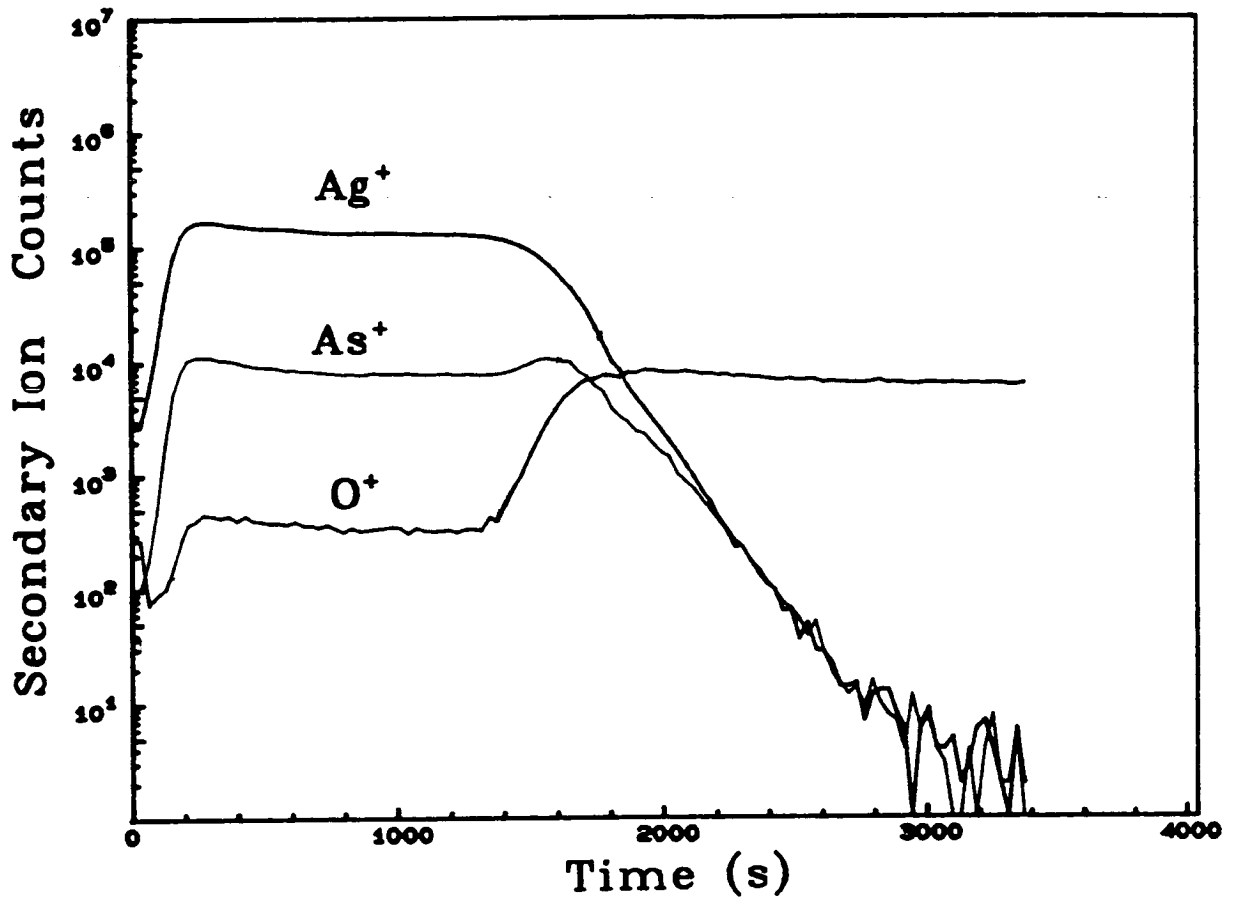


Figure 8.1. Typical SIMS depth profiles for an As-S photodoped layer. The photodoped layer thickness is about 490 nm.

8.3. Experimental procedure

The SIMS analysis was performed with a Cameca IMS-3f ion microanalyser using different primary beams, namely Cs^- , O_2^- and O_2^+ . This analysis was carried out to obtain the concentration depth profile for Ag and As in photodoped As-S films. The secondary ion species analysed were Ag_{109}^+ , As_{75}^+ and O_{16}^+ . The SIMS parameters such as raster size, primary beam species and depth resolution were varied in order to optimize the profiles, the best results being obtained, using an O_2^- beam with a bombardment energy of 10.6 keV and a raster size of 150 μm . The surface area investigated was about $8.9 \times 10^{-4} \text{ cm}^2$.

The samples were prepared in a similar way to that described in Chapter 5. For these experiments the As_2S_3 film being evaporated first on microslide glasses and subsequently a silver film was evaporated on top. This double layer sample was then coated with a thin gold layer to avoid beam charging effects. The As-S and Ag film thicknesses were respectively 370 nm and 120 nm. Photodoping of the films was achieved by illuminating samples with a halogen lamp, the power density was about 70 mW/cm^2 . In order to follow the evolution of the Ag profile as a function of exposure time the samples were illuminated for different periods. A SIMS profile and a reflectivity interference plot were recorded immediately after each exposure.

8.4. Quantitative analysis of SIMS data

Since the secondary ion yield is sensitive to the state of the surface, the matrix and the effects induced by the primary ion beam,⁵ the variation of the secondary ion intensity is not always a measure of a relative difference in element concentration. Therefore, care must be exercised in the interpretation of depth profiles, especially for depth profiles very near to the surface, or of films composed of dissimilar

layered phases, or of matrices with a non-homogeneous distribution of trace elements that have a major influence on the secondary emission characteristics of the matrix. In fact, it can be seen in figure 8.1 that the SIMS profiles suggest that the Ag concentration is higher than that of As in the As-S photodoped matrix, whereas the reverse is true.

The system investigated in this work is initially composed of three parallel matrices: the first is an Ag layer; the second is an As-S layer; and the third is the SiO₂ substrate. After partial photodoping of the As-S layer, a fourth matrix, the photodoped layer, is generated between the Ag and As-S matrices. A total photodoping of the As-S layer generates a system composed only of two matrices: the photodoped layer and the substrate. It is expected that, in these circumstances, the depth profile will show separate regions corresponding to different matrices.

The ability of ion beam bombardment to cause Ag dissolution into the As-S matrix, as reported previously,^{6, 7} and the contribution of Ag ions from the crater edges during the SIMS process, represent the essential instrumental effects. These instrumental effects influenced the element distribution, and therefore it was not possible to detect in the raw data a Ag-containing region distinct from the undoped region. The influence of the ion beam on the Ag distribution is shown in figure 8.2, which shows the final profiles obtained for a partially exposed sample. In this case the Ag has been pushed completely through the As-S layer and to reach the As-S/substrate interface. To obtain meaningful results in this situation, procedures for quantifying the secondary ion intensities must be applied to the profile data. If this is not possible, one must attempt, as a minimum, to reference the profiled element to the secondary ion intensity of one or more uniformly distributed constituent of the film. Profile data for the O₁₆⁺ element was intentionally collected for this purpose. The O₁₆⁺ profiles obtained were approximately uniform within each matrix.

The O₁₆⁺ profile provides a useful means for quantifying the SIMS profiles of interest because it can be used as a zero level for the Ag and As-S matrices since they do not contain O₂, and can also be used as an indicator of the interface between the Ag/As-S system and the

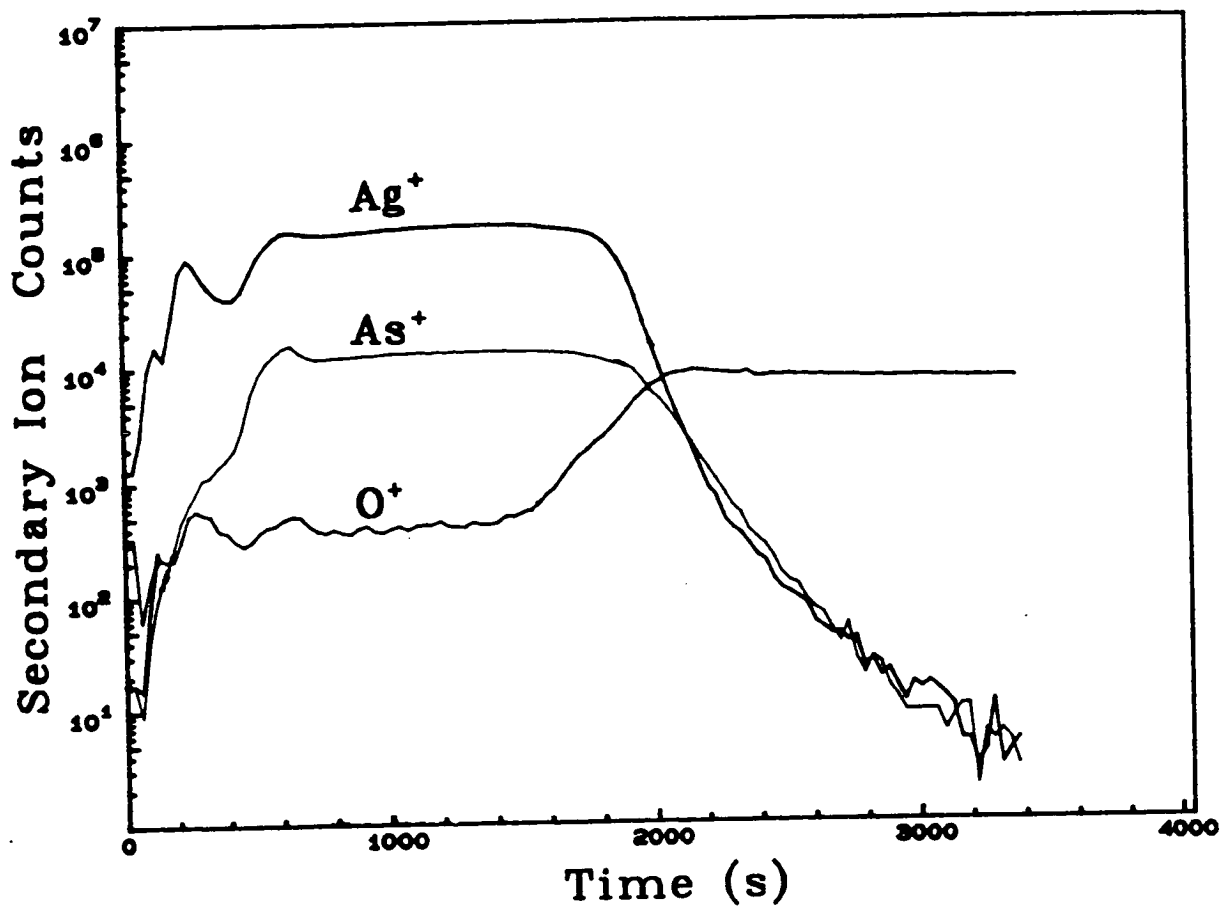


Figure 8.2. The effect of the ion beam on the Ag distribution in a partially exposed Ag/As-S sample.

substrate, which contains O_2 but not Ag or As. Therefore, the Ag^+/O^+ and As^+/O^+ profile ratios will be used to determine the Ag and As depth profiles. The analysis of these profile ratios showed a clear difference between the different matrices and particularly between the Ag and As-S layers. Typical plots of these profile ratios are shown in figure 8.3. This figure corresponds to the Ag/As-S system before photodoping. The narrow profile is for the Ag layer, which is on top of the As-S layer, and the wide profile corresponds to the As-S layer. The abscissa of figure 8.3 represents the sputtering time and the ordinate, which is on a logarithmic scale, represents the ratio of the Ag_{109}^+ or As_{75}^+ ion count to that for O_{16}^+ .

8.5. Ag depth profile in the photodoped layer

Figure 8.3 shows the Ag and As profile of the Ag/As-S system before it undergoes any exposure. The Ag profile is narrower than that of As due to the fact that the As-S layer is thicker than the Ag layer. Starting from the origin, the Ag profile occurs first and is followed by the As profile. This is because the Ag is on top of the As-S, and the primary beam therefore sputters the Ag layer first and then the As-S layer. The Ag/As-S interface is marked by the fall in the Ag profile and the subsequent increase in the As profile.

This system was then exposed for a period of 580s which corresponds to the time required for fully photodoping the As-S layer. This period of time is obtained from the reflectivity data which will be seen later (figure 8.11). The resulting photodoped layer was then analysed using the SIMS probe and yielded the plots shown in figure 8.4. The upper profile corresponds to the Ag content and the lower to the As content. The difference in level between the two profiles is not due to the difference in concentrations but to the difference in the secondary ion yield. These results show that the Ag has a uniform profile within the photodoped layer. The Ag profile is behaving similarly to that of As, which shows that the photodoped layer is

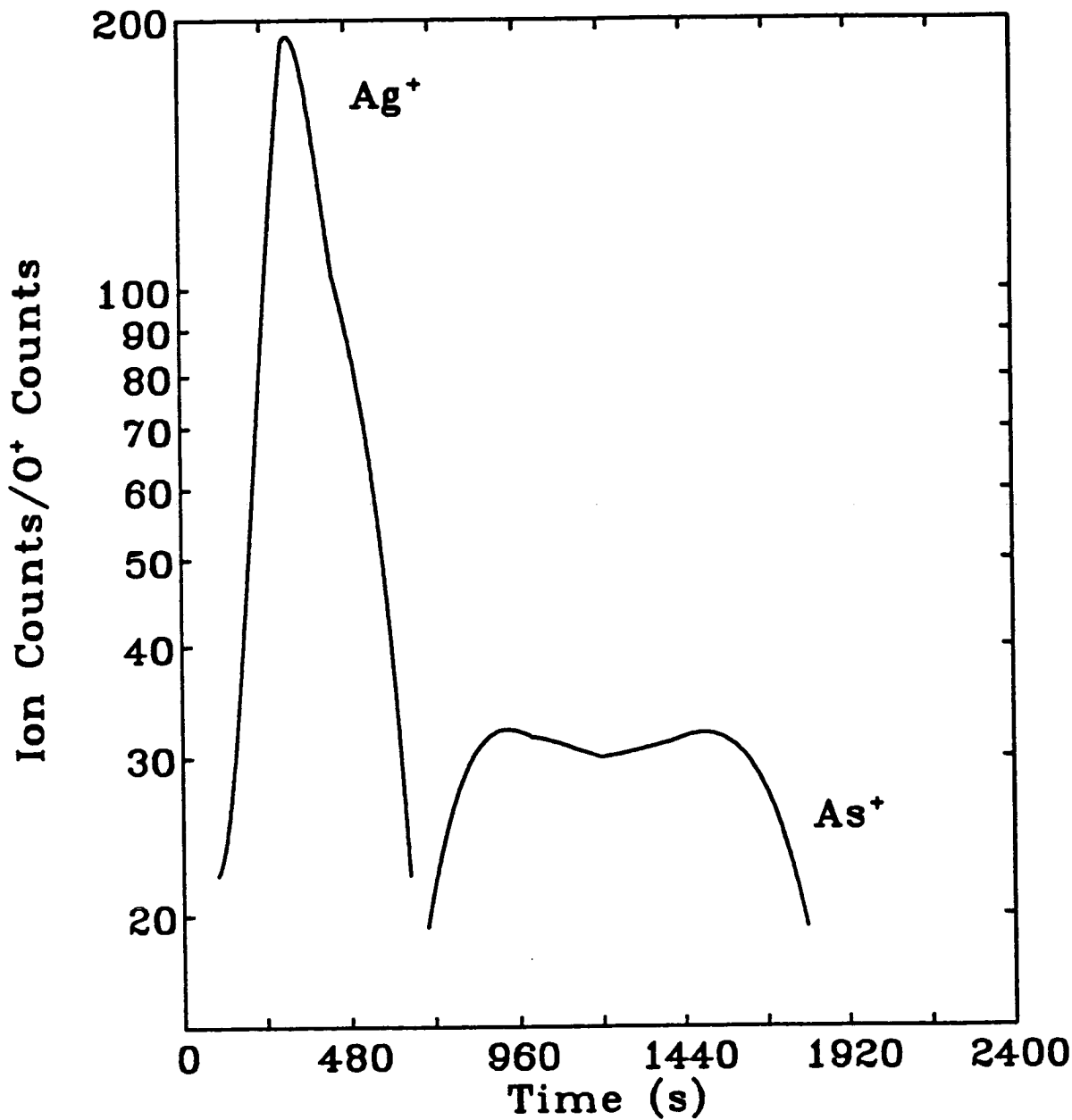


Figure 8.3. Typical SIMS depth profiles for Ag and As in an Ag/As₂S₃ double layer before light exposure. The Ag profile corresponds to the Ag layer on the top and the As profile is for the As-S layer beneath. The y-axis is the ratio of Ag₁₀₉⁺ or As₇₅⁺ ion counts to O₁₆⁺ counts.

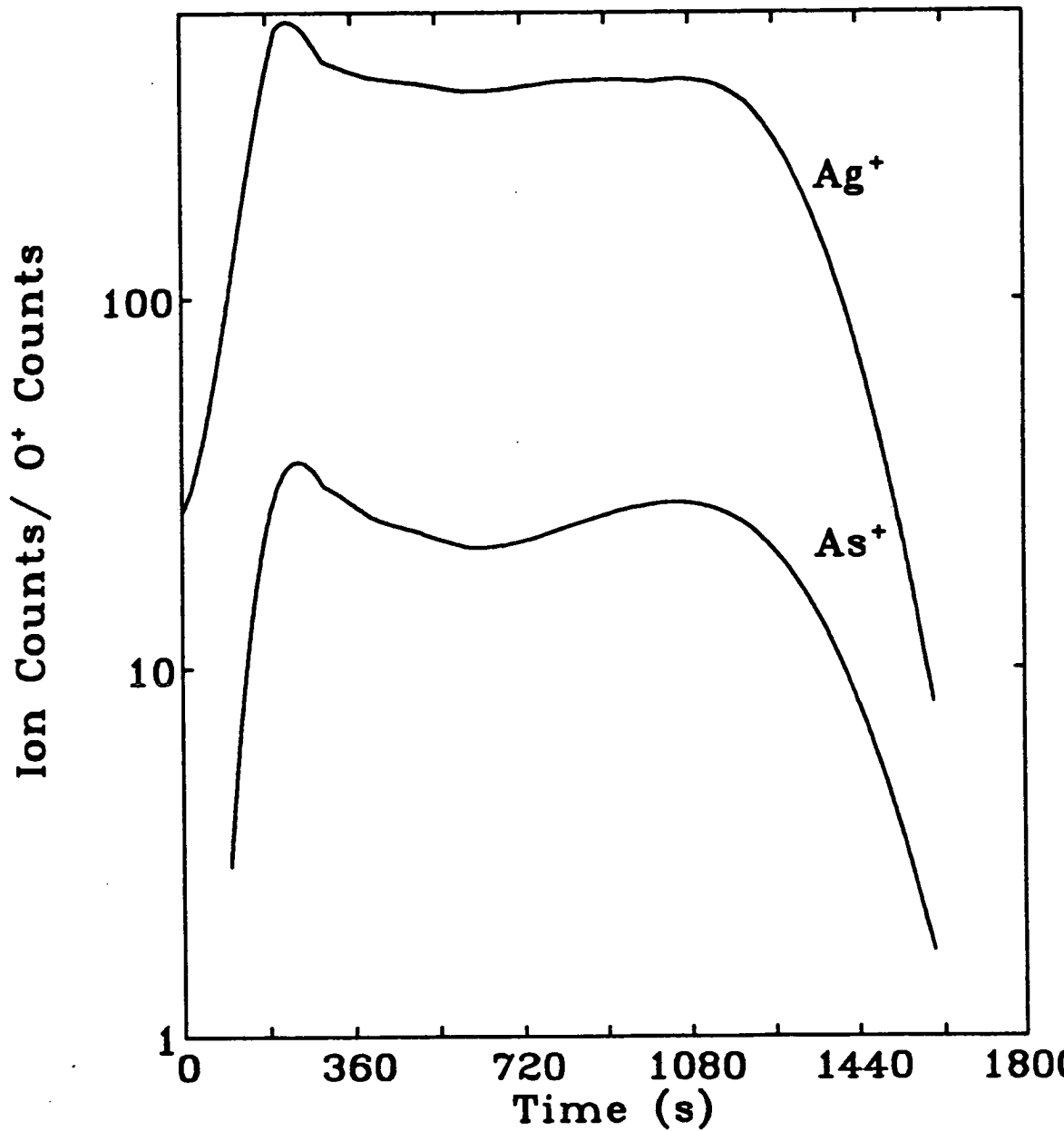


Figure 8.4. SIMS depth profile for Ag and As after prolonged light exposure of the Ag/As-S system. The Ag depth profile here is that of the photodoped layer.

homogeneous.

Figures 8.5 and 8.6 show the Ag and As profiles before and after exposure. In figure 8.5 the Ag profile is a narrow peak before exposure but then spreads out considerably as a result of illumination. Although the profiles in figure 8.5 are of the same element there is a difference in the magnitude of these profiles due to the difference in the matrices in which the Ag was sputtered. The secondary ion yield depends on the matrix containing the ions being sputtered. In this case the yield of Ag in the photodoped matrix is higher than for the Ag matrix.

The As profiles before and after exposure are shown in figure 8.6. The profile which is the nearest to the y-axis is the one obtained after exposure, i.e. it is that of the photodoped layer. It is expected that transformation of the undoped to the photodoped layer will lead to a decrease of the As concentration in the photodoped layer compared to that in the undoped layer. For a single matrix, a decrease in the concentration of an element is usually accompanied by a decrease in the element's SIMS profile. In the case of figure 8.6, the two As profiles are for different matrices (undoped and photodoped) and therefore the heights of the profiles do not reflect the true As concentrations. For the same reason, the widths of these two profiles also do not reflect the actual thicknesses of the undoped and photodoped layers. The sputtering rate of an element depends on the matrix containing the element being sputtered.

8.6. Time development of the Ag depth profile

This experiment was carried out in order to determine how the Ag depth profile is affected by different periods of exposure. Besides zero exposure and the final long exposure, a 100 and 300 second exposure time was used. The profile for the 300s exposure was very similar to that for the final exposure but the 100s profile could be distinguished from those for the zero and final exposures. This shows clearly that

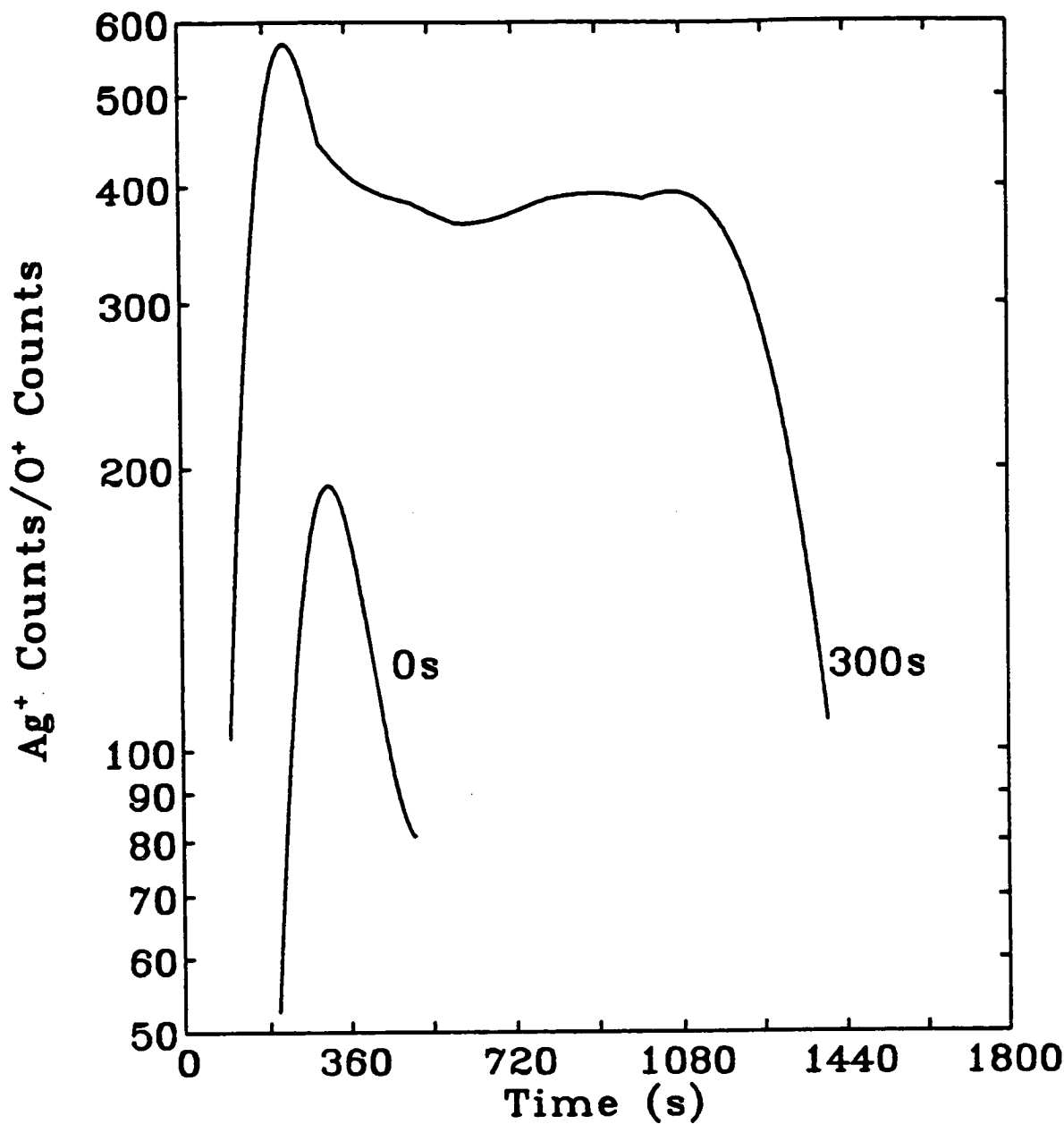


Figure 8.5. SIMS depth profile for Ag before (0s exposure) and after exposure (300s or prolonged light exposure). The narrow profile corresponds to the Ag layer before photodissolution and the wide profile to the Ag layer after the As-S film has been fully photodoped.

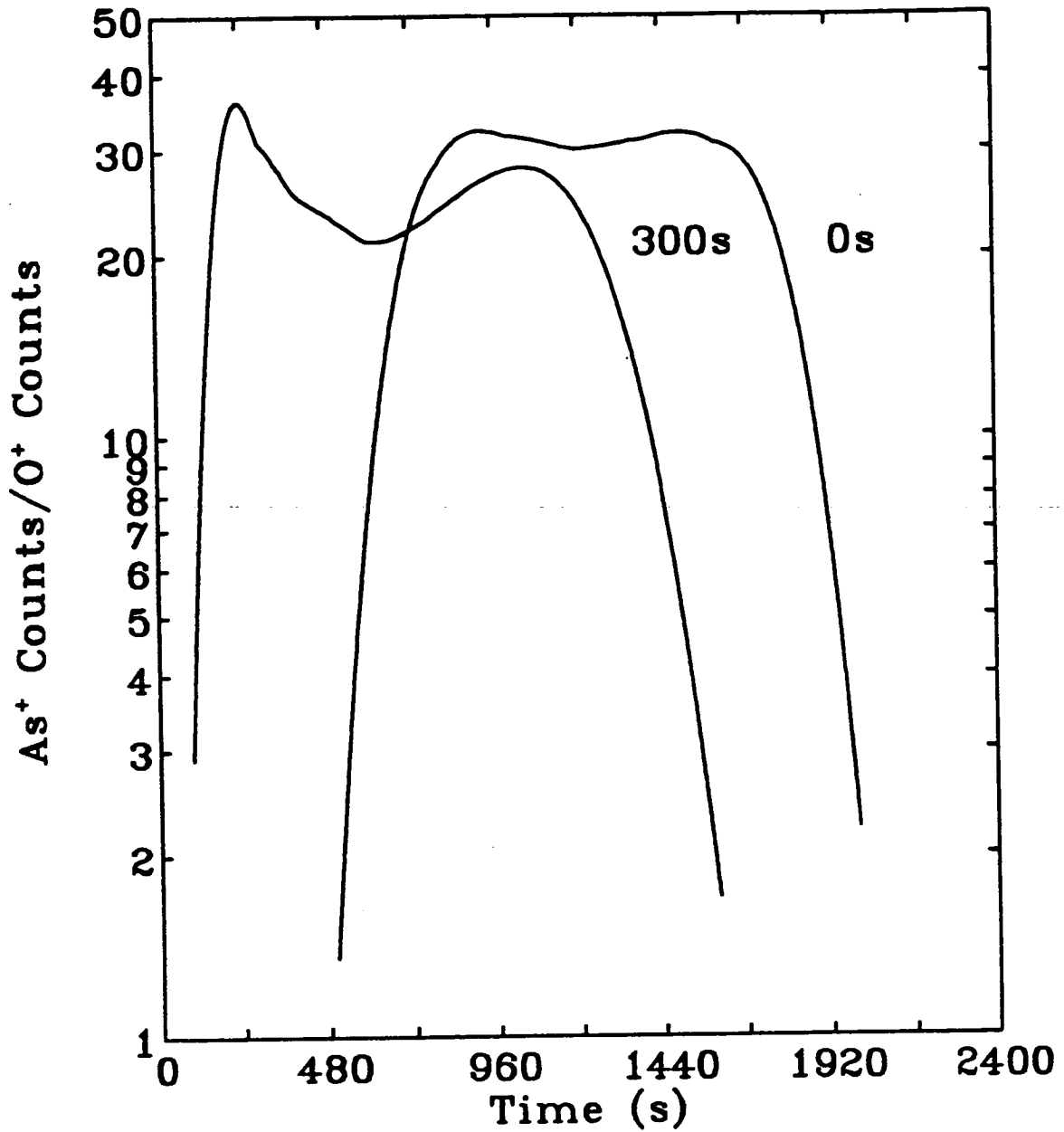


Figure 8.6. SIMS depth profile for As before (0s exposure) and after exposure (300s or prolonged light exposure).

poor time resolution may be a disadvantage of the SIMS technique. Figure 8.7 shows three Ag profiles corresponding, from the lower to the upper, to the 100s, 0s and 300s (or final) exposure. The magnitude of the 0s and 100s profile can be compared since the sputtering is carried out in the same matrix, namely the Ag layer, so the decrease in the magnitude of the 100s profile can be interpreted as the decrease in the Ag thickness. The highest profile cannot be compared to the other two in terms of magnitude since the matrices are different.

Analysis of the SIMS data suggests that, in view of the problems with the Ag profile, the best way to study the time development of the Ag concentration is to monitor the As profile, which shifts towards the y-axis as the exposure time increases. These shifts are clearly seen in figure 8.8, which shows the initial part of three of the As profiles. The nearest profile to the y-axis corresponds to the 300s exposure (or the fully photodoped film), the next is that for the 100s exposure, and the final one corresponds to the unexposed system. Only the initial part of the profiles is shown because this corresponds to the region nearest to the Ag layer and also to the top surface, therefore any changes in this part might reflect the changes in the silver thickness. The points corresponding to the "edge" of each profile were determined by drawing two tangents along the profile, as shown in the figure, and finding their intersection. These points were then plotted against exposure time, as shown in figure 8.9, which shows that the shift of the As profile towards the y-axis is approximately linear in time.

These points mark the interface between the Ag and the As-S layers, hence it is possible to determine from them the Ag layer thickness at the corresponding times. The conversion is based on the sputtering rate of the Ag within the Ag matrix, which is equal to the ratio of the initial Ag thickness to the total sputtering time. The initial thickness for these experiments was 120 nm and the total sputtering time for this thickness was 690s, which implies a sputtering rate of about 0.17 nm/s. The Ag thicknesses obtained from this conversion are plotted as a function of exposure time in figure 8.10. This data is consistent with a linear time dependence for the Ag photodissolution process in As-S films.

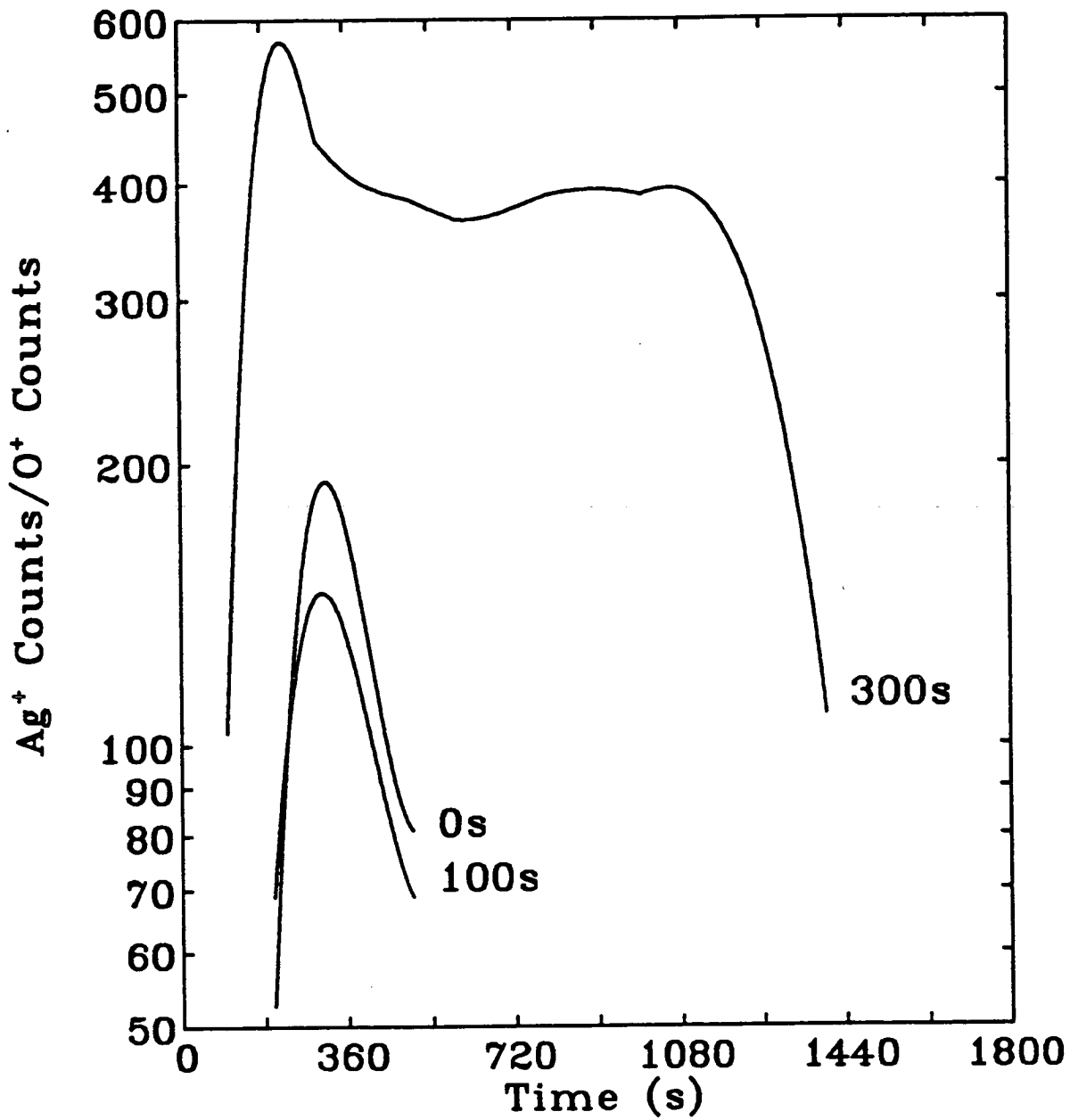


Figure 8.7. SIMS depth profile of Ag for different periods of exposure: 0s; 100s; 300s (and complete photodoping).

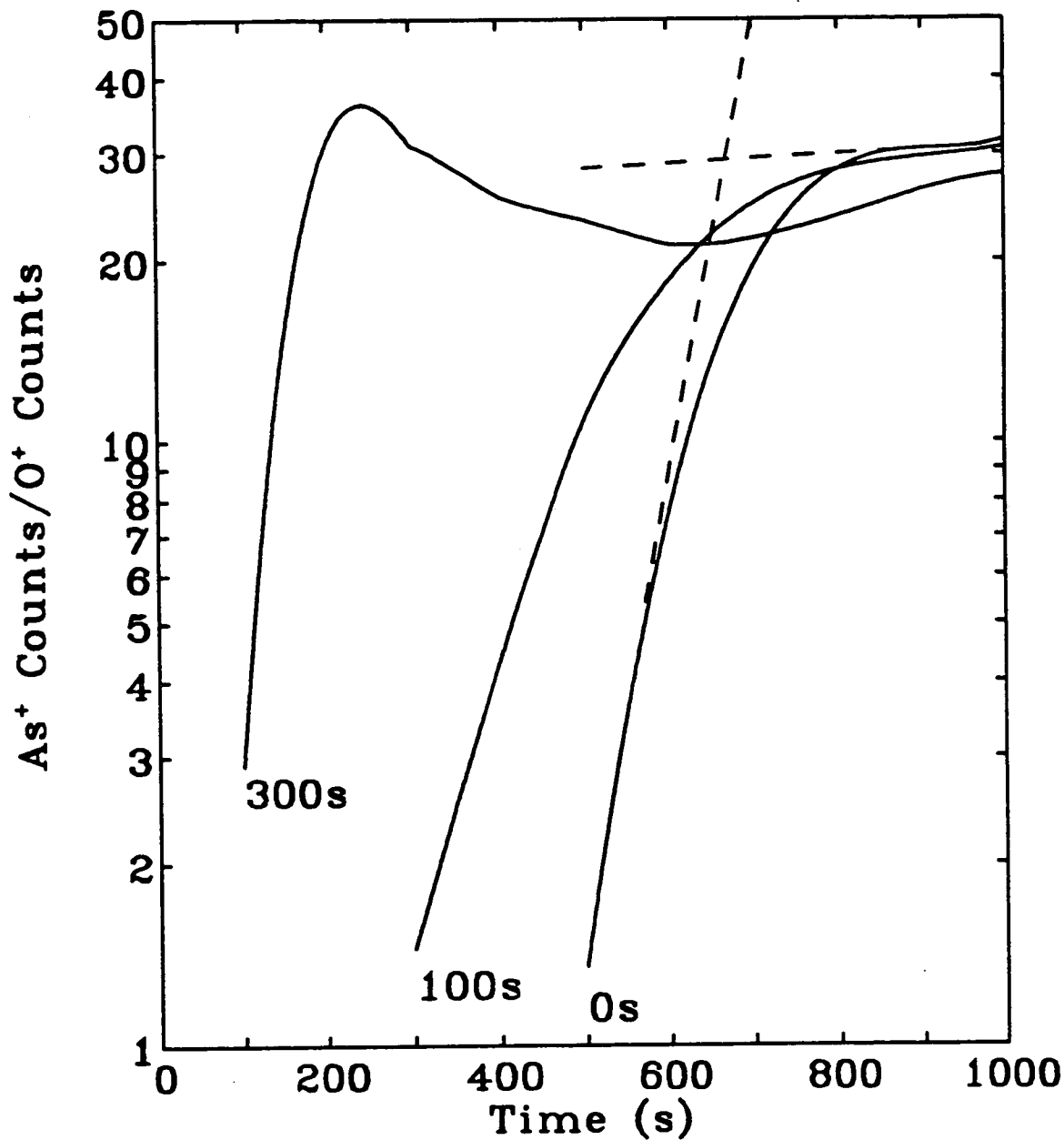


Figure 8.8. The initial part of the SIMS depth profile of As for different periods of exposure: 0s; 100s; 300s (and complete photodoping). The intersection of the two tangents drawn on the profile for the unexposed system is taken to mark the "edge" of the profile.

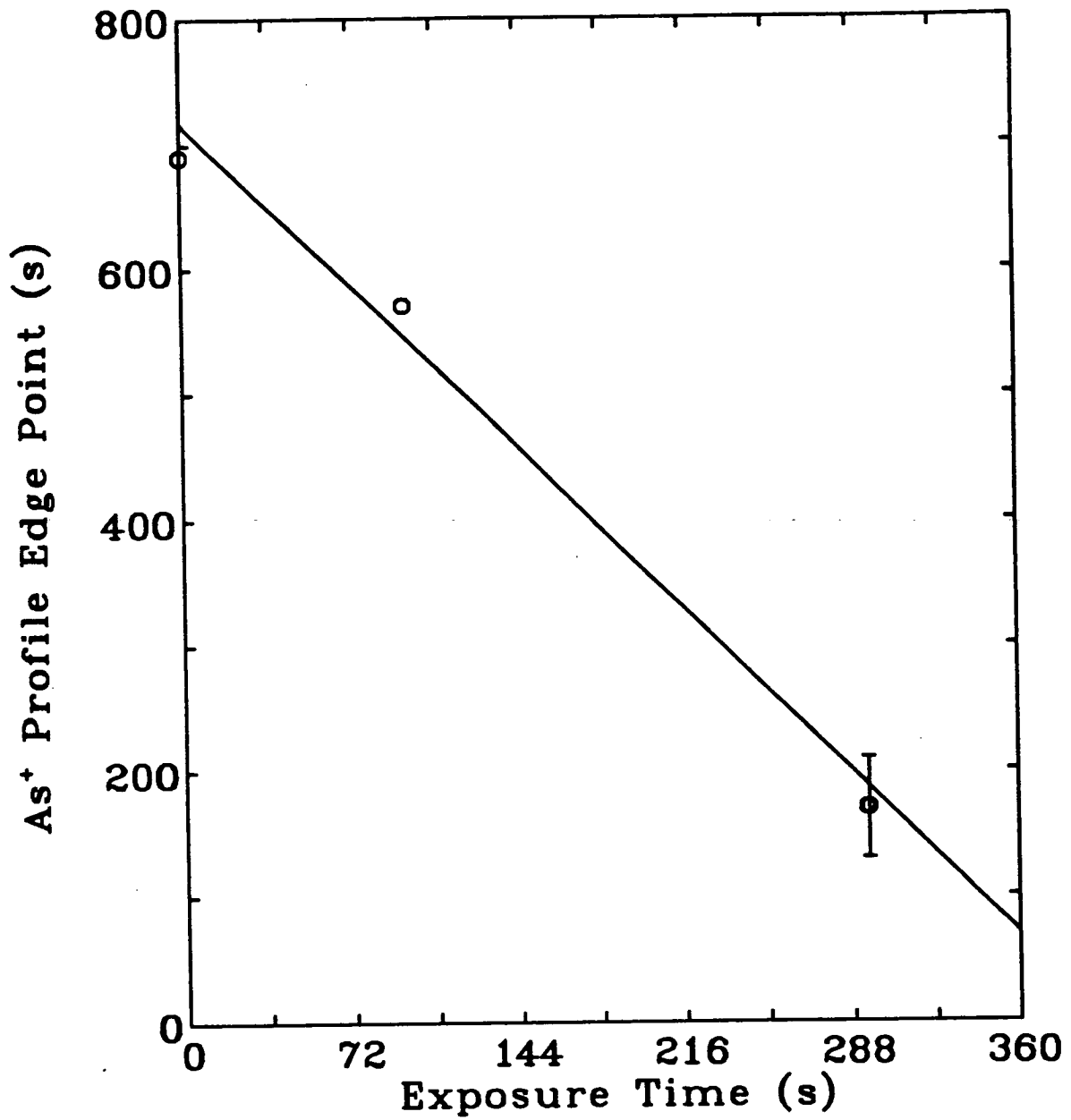


Figure 8.9. The "edge" points extracted from the As profiles of figure 8.8 plotted as a function of light exposure time.

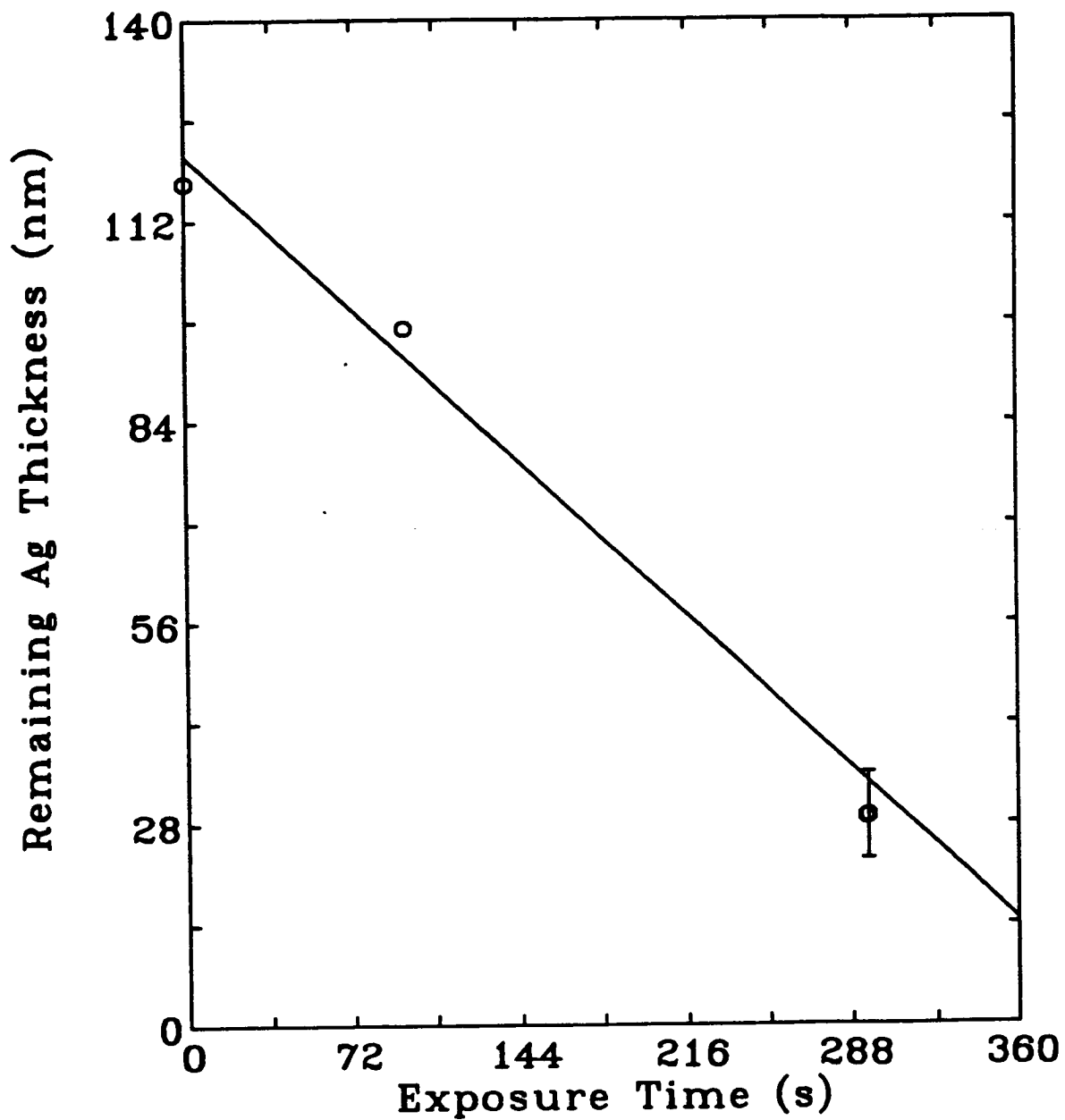


Figure 8.10. The Ag thickness remaining as calculated from figure 8.7, plotted as a function of exposure time.

The Rutherford Back Scattering (RBS) method used by Rennie also revealed a linear time dependence for the growth of the photodoped layer generated in the Ag/GeSe₂ system.⁸ In comparison to the SIMS technique, the RBS method was shown to be more reliable. The SIMS work carried out by Polasko et al. on the Ag₂Se/GeSe₂ combination confirmed that it is possible to extract reliable information on these systems from the SIMS data. However, they reached the conclusion that the Ag distribution is Fickian rather uniform as observed in the present case. The difference in the nature of the Ag distributions might be due to the difference in the material system investigated, particularly the fact that the Ag source in his case was a compound (Ag₂Se) rather than elemental Ag.

8.7. Comparison of the SIMS and optical reflectivity kinetics results

As was mentioned in the section on experimental procedure, the optical reflectivity was also monitored along with the SIMS experiments. The reflectivity monitoring technique as explained in Chapter 7, can be used to measure accurately the decrease of As-S thickness with exposure time. In the chapter on kinetics it was shown from results obtained using this technique, that photodissolution in the Ag/As-S system has a linear time dependence. Because optical reflectivity monitoring is an indirect technique, an important objective of making reflectivity measurements together with the SIMS experiments was to compare the kinetics results for the two techniques. The decrease in As-S thickness versus time obtained from the reflectivity results is plotted in figure 8.11. These results correspond to those of figure 8.10 obtained using the SIMS technique. The data in figure 8.11 exhibits a linear dependence on time, which supports the SIMS finding that the photodissolution of Ag in As-S is a linear process. In addition, the similarity of the two sets of results confirms that the method used to analyse the SIMS data is correct. The ratio of the slopes obtained from figures 8.11 and 8.10 is ~2.3, which suggest that the As-S is used up 2.3 times faster than the Ag.

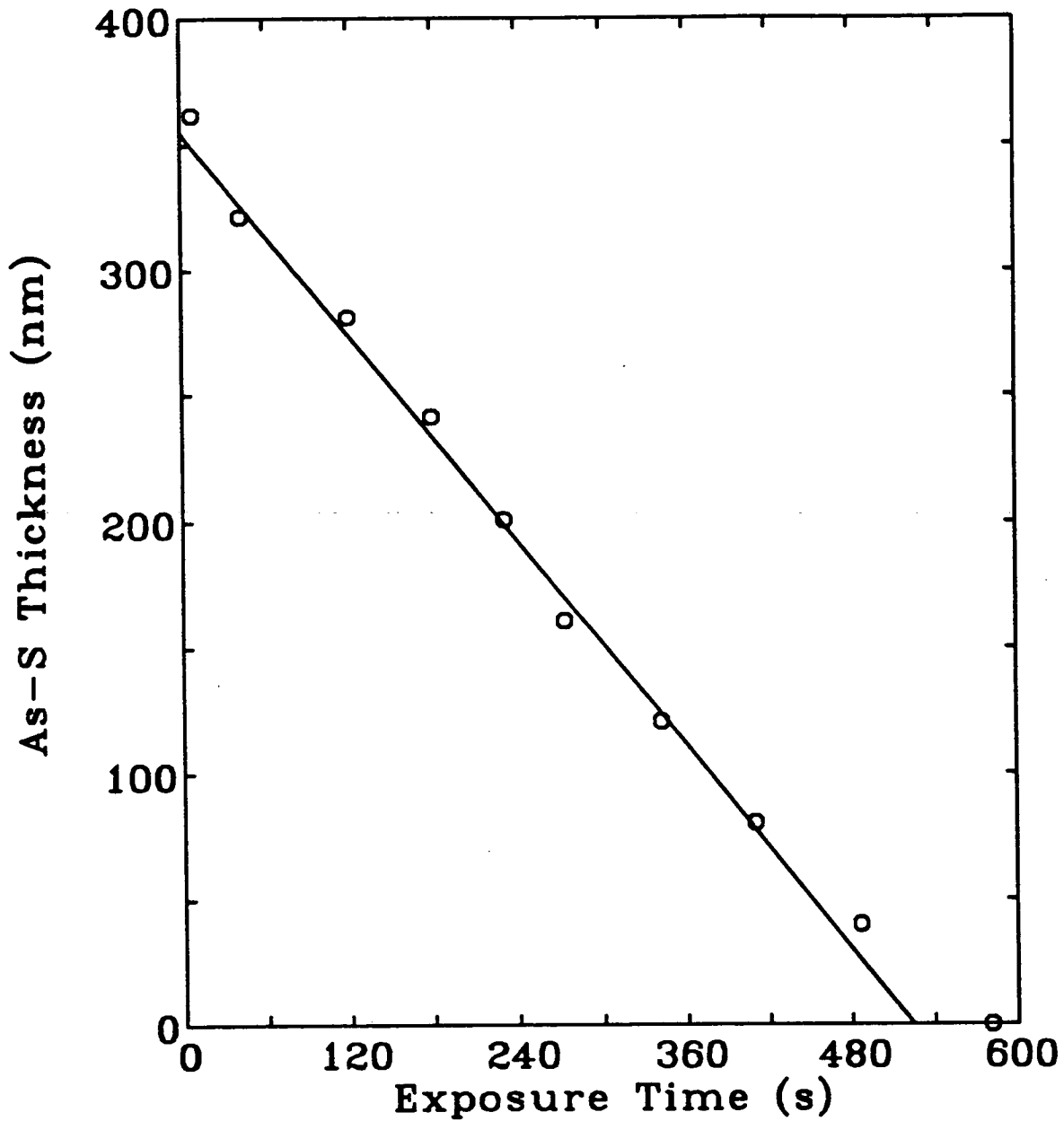


Figure 8.11. The decrease in As-S thickness as a function of exposure time, derived from optical reflectivity data obtained along with the SIMS experiments.

8.8. Conclusions

The Ag concentration in photodoped As-S as measured by the SIMS analysis, has a uniform depth profile, that is, the photodoped layer has a uniform distribution of Ag. It has also been found that the decrease in the Ag layer thickness at the surface of the double layer sample has a linear time dependence, which was confirmed by the optical reflectivity results. These SIMS results are consistent with the kinetics data obtained in Chapter 7. It was also found that the As-S layer is used up 2.3 times faster than the Ag layer.

As far as the study of the photodissolution effect is concerned, it is clear that the SIMS data requires careful analysis in order to extract meaningful results. Better results for the kinetics of the process might be obtained from the SIMS technique using films thicker than 1000 nm. This is because the photodissolution process for thicker films is very slow, and hence the number of intermediate data points obtainable will be higher than in the present case (figure 8.10).

References

1. Yamamoto Y., Itoh T., Hirose Y. and Hirose H., *J. Appl. Phys.*, vol. 47, p. 3603, 1976.
2. Goldschmidt D., Bernstein T. and Rudman P.S., *Phys. Stat. Sol. A*, vol. 41, p. 283, 1977.
3. Wagner A. and Barr D., *Proc. Electrochem. Soc.*, vol. 82, p. 281, Symp. Inorg. Resist. Syst., 1982.
4. Polasko K.J., Tsai C.C., Cagan M.R. and Pease R.F.W., *J. Vac. Sci. Technol.*, vol. B4, p. 418, 1986.
5. Benninghoven A and Muller A, *Phys. Lett. A*, vol. 40, p. 169, 1972.

6. Wagner A., Barr D., Venkatesan T., Crane W.S., Lamberti V.E., Tai K.L. and Vadimsky R.G., *J. Vac. Sci. Technol.*, vol. 19, p. 1363, 1981.
7. Singh B. and Chopra K.L., *J. Appl. Phys.*, vol. 52, p. 428, 1981.
8. Rennie J.H.S., Ph.D. Thesis, Jesus College, Cambridge, 1986.

CHAPTER 9

CONCLUSIONS AND SUGGESTIONS FOR FURTHER WORK

9.1. Introduction

The present work was concerned mainly with those fundamental aspects of the photodissolution effect relevant to its application in the fabrication of gratings for operation in the IR. Of the various light-induced changes exhibited by chalcogenide glasses, the metal-photodissolution effect is probably the most important as far as applications are concerned because it produces the largest change in the properties of the chalcogenide, particularly the etch resistance and the refractive index. The metal-photodissolution effect has been observed in many chalcogenide systems, but most investigations of this effect have been carried out on As-based chalcogenides or on Ge-Se glasses, using Ag metal as the source for photodoping.

Although the metal-photodissolution effect has been under investigation for more than twenty years, no completely satisfactory explanation of the process has been put forward and there are many inconsistencies in the published results. For example, there is still controversy over the fundamental issue of where the light which effectively stimulates the process is absorbed. Some investigators have suggested that this light is absorbed in the metal layer, stimulating a solid-phase chemical reaction¹ or photoemission of electrons from the metal into the chalcogenide glass.^{2, 3} However, a number of experimental results obtained using different methods point to the active role of light absorbed in the doped region,^{4, 5} or near the interface between the doped and undoped chalcogenide.⁶⁻⁹ The

different experimental results obtained have lead to a variety of models for the metal-photodissolution effect, which were described in Chapter 3.

The present study has dealt exclusively with the As-S system and has used Ag as the source for photodoping. This combination of materials was chosen because it is the most widely studied, although despite extensive investigations the process is not fully understood. This study has examined three main areas: the optical constants of Ag-photodoped and undoped As-S films, the kinetics of the photodissolution process, and finally the Ag depth profile in Ag-photodoped As-S films.

9.2. Optical constants of undoped and photodoped As-S films

As stated earlier in Chapter 6, a knowledge of the optical constants (absorption coefficient and refractive index) of both Ag-photodoped and undoped As-S films is important for both fundamental reasons and from the point of view of applications. In particular, the optical constants are necessary for measuring the kinetics of the photodissolution process using optical techniques and for detailed modelling of grating performance.

Although many reports have been published on the optical properties of the As-S system very few have investigated the effect of pre-treatment¹⁰⁻¹² (e.g. pre-annealing) and Ag photodoping^{13, 14} on the optical characteristics of As-S films. In addition, these studies were either limited to one As-S composition (e.g. As₄₀S₆₀) or to a single wavelength. Because chalcogenide diffractive elements may have applications throughout the IR region, particularly in either of the commonly used IR spectral bands (3-5 μm and 8-12 μm), it is important to obtain information on their optical properties over a wide range of wavelengths.

The general conclusion which can be drawn from the work of other authors¹⁵⁻¹⁸ on the effect of annealing is that annealing of an as-deposited film near the glass transition temperature, T_g , causes a structural compaction and densification. This is due to the fact that the as-deposited film consists of molecules of the vapour species (particularly As_4S_4) embedded in a continuous random network, and annealing allows the molecular component to polymerise and combine with the original network to form a structure similar to that of the bulk glass.¹⁹ Annealed films may have advantages over as-deposited films as far as grating fabrication is concerned since they should have better adhesion to the substrate and should produce elements which are more stable under illumination. They will also produce a more controllable fabrication process. Pre-annealing is also known to affect the Ag-photodissolution rate and thus a knowledge of the optical constants of annealed As-S films is needed for the analysis of the photodissolution kinetics and for modelling the performance of gratings made using annealed films.

The present study of the optical constants has therefore extended this investigation over a wider wavelength range (from the visible to the far-IR regions) and a wider range of As-S compositions. The effect of pre-annealing and Ag-photodoping on the optical properties of As-S films is compared and the dependence of the optical properties on the amount of Ag photodoped into the glass is also examined. This investigation of the optical constants of undoped and photodoped As-S films, and the effect of annealing on these, revealed the following:

1- Pre-annealing

The pre-annealing treatment of undoped As-S films produced an overall increase of about 3% in their refractive index from the visible to the IR region. The single oscillator energy, E_o , for the undoped material was found to decrease by 3.9% as a result of annealing, and the dispersion energy, E_d , to increase by 2%. The magnitude of the pre-annealing effect was found to increase with increasing As content, being most pronounced at $As_{40}S_{60}$. The optical gap or the optical

absorption edge were not altered significantly by the pre-annealing treatment. It was also found that pre-annealing did not alter the optical constants of photodoped films containing more than 12 atomic % Ag.

2- Photodoping with Ag

The photodoping of both as-deposited and annealed As-S films with Ag produced a much greater increase in the refractive index compared to annealing. The maximum, overall increase, which extended from the visible to the IR, was found to be about 20%. The refractive index, the single oscillator energy, E_o , and the dispersion energy, E_d , were all found to depend on the Ag content in the As-S structure. E_o and the optical gap were found to decrease and E_d and the refractive index to increase with increasing Ag content. As far as the dependence on the As-S composition is concerned, for the most heavily doped films there is a peak around 30 atomic% As for the refractive index and the single oscillator and dispersion energies. However, the dependence of the optical gap on As-S composition for the most heavily doped films was similar to that of the undoped films.

9.3. Kinetics of the Ag-photodissolution process in the As-S system

A knowledge of the kinetics of the photodissolution process is essential both to understanding the mechanism of the effect and to exploiting its application, since the speed of image formation in the Ag/As-S system is mainly governed by the photodissolution rate. The photodissolution rate was found to be influenced by many factors as reviewed in Chapter 4. The influence of these factors on the speed of image formation in the As-S system was examined and it was shown that they could lead to a much more significant improvement in the rate than suggested by previous studies. The factors investigated were: temperature, pre-annealing treatment, Ag film thickness, light

intensity, As-S composition and the use of Cu films as the metal ion source. The thermal dissolution kinetics of Ag in $\text{As}_{40}\text{S}_{60}$ films was also investigated. These results were also used to elucidate the nature of the Ag-photodissolution process in the As-S system.

As pointed out earlier (Chapter 3), several aspects of the photodissolution process are the subject of controversy. It is generally accepted that the kinetics follows an S-shaped curve consisting of three regions: an initial induction period where the photodissolution rate increases slowly from zero; a second region with a significant (sometimes constant) dissolution rate; and finally a third region in which the photodissolution rate decreases slowly.^{20, 21} One of the principal areas of controversy is the second stage: while some investigators report that the propagation distance depends on the square root of time,²² which implies that diffusion of the ions or electrons through the photodoped layer is the rate-limiting step, others observe a linear time dependence,^{11, 20} which indicates that the speed of the process is controlled by the chemical reaction. The form of the time dependence was also found in one study to depend on the Ag layer thickness, a square-root-time dependence being found for thinner films and a linear time dependence for thicker ones.¹³

The kinetics results obtained in the present work indicate that, for the conditions used, the time dependence of the photodissolution process is definitely linear. The number of stages in the photodissolution process was found to depend on the magnitude of the rate. A single linear stage is found for high rates and three stages for lower rates. Increasing the temperature was found to reduce the number of stages in the photodissolution process. The first stage and the tail present at room temperature disappear at 393 K, where the rate is almost 10 times that at room temperature. The photodissolution process is very sensitive to temperature because it affects the diffusivity of the Ag ions and electrons and also the rate of the chemical reaction.

It is also found that the photodissolution process does not stop once the Ag is exhausted. This observation is in agreement with a previous study²³ and shows that the assertion of Kolwicz and Chang²⁴ that the process stops when the Ag is exhausted is incorrect. A change

in the photodissolution process from a fast stage to a slower one, is found to occur when the Ag becomes exhausted. This was reported previously²⁵ for the composition $As_{30}S_{70}$, but in that case the change in slope was present even before the exhaustion of the Ag. This discrepancy might be due to the different As-S compositions or film thicknesses used.

On the basis of the experimental results obtained in the present study the following model of the photodissolution process was proposed. A weak activation energy and a linear time dependence suggest that the photodissolution process is a solid state chemical reaction and not a straightforward diffusion process. The fact that photodissolution continues even when the metallic Ag is exhausted emphasise the importance of the doped/undoped interface in the photodissolution process. In the absence of metallic Ag the photodoped product takes on the role of the Ag^+ reservoir, thereby ensuring the continuation of the process. The fact that the photodissolution before the Ag exhaustion is much faster than that afterwards (at least at room temperature) may indicate that the Ag/doped interface is also important in the photodissolution process under some circumstances. Alternatively, this may be due to the fact that a different chemical reaction - with a different reaction rate - is occurring after Ag exhaustion. Whichever is true, it appears that the presence of the Ag/photodoped interface is necessary for a fast photodissolution rate.

The increase of the photodissolution rate with increasing temperature might also be connected with the temperature dependence of the conductivities of both the photodoped and undoped material, since it is well known that the conductivity of these materials increases with temperature due to an increase in the free electron concentration. As electrons are essential to the chemical reaction occurring their concentration may have an important effect in increasing the rate of photodissolution. This proposal is consistent with the results of experiments on so called lateral photodissolution,⁹ which only occurs when the chalcogenide is in contact with a conducting layer that can transport electrons to the reaction front. In addition, the ionic conductivity of the photodoped material will also be increased as a

result of temperature and this will act in conjunction with the change in the electronic conductivity.

The main points arising from the kinetics experiments of the present work can be summarised as follows:

- 1- Pre-annealing decreases rather than increases the rate of Ag-photodissolution for all the As-S compositions investigated.
- 2- The effect of pre-annealing on the photodissolution rate increases slightly as the thickness ratio $d_{As_{40}S_{60}}/d_{Ag}$ decreases and is a maximum at $As_{30}S_{70}$.
- 3- The weak activation energy and linear time dependence observed shows that the process is not diffusion controlled but reaction controlled.
- 4- The maximum improvement (by a factor of 12) in the rate of photodissolution was obtained with the film combination Cu/Ag/ $As_{40}S_{60}$ at 393 K. The improvement in the rate for the Ag/ $As_{40}S_{60}$ film combination, obtained at 393 K, was by a factor of 10.
- 5- The thermal dissolution rate for Ag was shown to be negligible in comparison to that for Ag photodissolution.
- 6- A grating pattern was fabricated at 383 K using the photodissolution process, confirming that lateral dissolution at temperatures up to this value is not significant.
- 7- A sublinear dependence of photodissolution rate on light intensity was observed rather than the linear relation obtained by most authors.
- 8- The study of the compositional dependence revealed that the maximum rate is obtained at $As_{30}S_{70}$ for both annealed and as-deposited films. However, with increasing temperature the photodissolution rate for the $As_{30}S_{70}$ film showed a small increase,

peaking at 314 K, and then decreased.

9- Ag photodissolution was found to continue even when the metallic Ag source is exhausted.

10- The number of stages in the photodissolution process was found to depend on the magnitude of the rate, and therefore on the thickness ratio $d_{\text{As}_{40}\text{S}_{60}}/d_{\text{Ag}}$ and the temperature. In the case of fast rates, a single linear stage is found but in the case of slow rates three stages are observed.

11- The results are consistent with a mechanism based on a light-induced solid state reaction between the metal and the chalcogenide.

9.4. Secondary ion mass spectroscopy analysis

Another aspect of the process which is important, both for fundamental reasons and as far as applications are concerned, is the distribution of Ag with depth into the photodoped film. In the case of grating applications, any change in Ag concentration with depth will be accompanied by a change in the refractive index and hence in the modulation. Therefore an investigation of the depth profile of the Ag photodissolved in the As-S structure, using the Secondary Ion Mass Spectroscopy (SIMS) technique, was carried out in this work. The previous depth profile studies of the Ag/As₄₀S₆₀ system^{26, 27} have revealed a step-like profile while in systems like Ag₂Se/GeSe₂ and Ag₂Se/GeSe₉, where the Ag is initially present as a compound, the Ag distribution is more like that expected from thermal diffusion.²⁸

The SIMS technique has been shown by Polasko's study²⁹ to give useful information about Ag profiles in Ge-Se glasses. In the present study, two types of information were obtained from the SIMS analysis: the nature of the Ag depth profile within the photodoped layer and the development of this profile with exposure time. The latter was

compared to the results obtained using the optical reflectivity technique.

The reflectivity monitoring technique, as explained in Chapter 7, can be used to measure accurately the decrease in the As-S thickness with exposure time and has been used along with the SIMS experiments. In the chapter on the kinetics it was shown from results obtained using reflectivity monitoring, that the photodissolution process in the Ag/As-S system has a linear time dependence. Because optical reflectivity monitoring is an indirect technique, an important objective of making reflectivity measurements together with the SIMS experiments was to compare the kinetics results for the two techniques.

From the SIMS investigation it can be concluded that the Ag concentration in photodoped As-S has a uniform depth profile, and hence the photodoped layer has a uniform distribution of Ag. It has also been found that the decrease in the Ag layer thickness at the surface of the double layer sample has a linear time dependence, which was confirmed by the optical reflectivity results. These SIMS results are consistent with the kinetics data obtained in Chapter 7. It was also found that the As-S layer is used up ~ 2.3 times faster than the Ag layer.

9.5. Suggestions for further work

As far as research into the applications of the photodissolution effect is concerned, it might be advantageous in future work to study the fundamental and applied aspects in parallel, since a thorough understanding of the applications will enable one to identify the relevant fundamental aspects that need to be addressed and to define exactly the aims of these fundamental studies. For example, sensitivity is an important parameter both for the photolithographic applications and the fabrication of IR optical elements. This depends on the kinetics of the photodissolution effect but whereas an improvement in

the rate by a factor of 2-5 would be sufficient to make chalcogenide resists compatible with commercial resists, an improvement by at least an order of magnitude is necessary for the IR applications, which is a much more difficult problem. Clearly, a detailed knowledge of the applications is required in order to set the boundary conditions for the fundamental study.

9.5.1. Kinetics measurements

The techniques used so far to study the kinetics of the process measure either the change in the Ag or the As-S film thickness and therefore the information obtained is limited to a single layer and tells us only indirectly what is happening in the photodoped layer. A procedure which combined both measurements of the Ag and As-S layer thickness at the same time might give a more complete picture of the photodissolution process. For example, the optical reflectivity and the resistance monitoring techniques could be combined to measure simultaneously the changing thickness of these two layers.

9.5.2. Sensitivity

Sensitivity is one of the most important parameters in the photodissolution process both from the point of view of application and fundamental studies and therefore a more extensive investigation is required. Improving the sensitivity of the photodissolution process is important for both photoresist technology and for the fabrication of IR devices. Several possibilities exist to increase the sensitivity or the speed of the photodissolution process but the most promising appears to be the simultaneous illumination/heating procedure used in the present work. The procedure was only applied to samples of two As-S

compositions with thicknesses less than 2000 nm and for a maximum light intensity of 70 mW/cm². Therefore this procedure needs to be extended to thicker films (> 2000 nm) since deep structures are required for optical elements operating in the IR region. This procedure should also be studied in other As-S compositions to obtain a complete picture of the compositional dependence. Finally, more systematic work needs to be done on enhancing the photodissolution rate by the application of electric fields and pre-doping the chalcogenide with elements which increase the electrical or ionic diffusivity or conductivity.

9.5.3. Photoconductivity of the photodoped layer

The photoconductivity of the photodoped layer is also an important parameter both for fundamental reasons and from the point of view of applications. Investigation of the photoconductivity will enable the identification of the type of electronic charge carrier (electrons or holes) dominant in the photodoped layer. This information will provide useful insight into how to increase the photoconductivity of the doped layer and hence increase the speed of the photodissolution process. The type of electronic charge carrier in the photodoped layer also effectively determines where the actinic light is absorbed.³⁰ It is therefore worthwhile investigating the photoconductivity of the photodoped layer for a range of Ag concentrations since it will depend strongly on the amount of Ag in the photodoped layer. It is also important to investigate the dependence of the photoconductivity of the photodoped layer on the composition of the initial chalcogenide layer.

9.5.4. Ag distribution in the photodoped layer

The distribution of Ag with depth into the photodoped film is again important, both for fundamental reasons and as far as applications are concerned. As far as the SIMS study of the photodissolution effect is concerned, it is clear that the SIMS data requires careful analysis in order to extract meaningful results. Better results might be obtained from the SIMS technique using films thicker than 1000 nm. This is because the photodissolution process for thicker films is very slow, and hence the number of intermediate data points will be numerous and more quantitative results can be obtained.

9.6. Summary

The aim of the present work was to investigate certain fundamental aspects of the metal photodissolution effect relevant to the fabrication of IR diffractive optical elements. In particular, the optical constants of these materials were measured to assess their suitability for producing IR grating structures and to enable the diffraction efficiency of such structures to be predicted; the kinetics of the process were investigated with a view to improving the speed of image formation; and the Ag depth profile was measured to assess the uniformity of these structures once they are produced. The main conclusions which can be drawn from the present study are that, for the conditions used:

- 1- The difference in optical constants between the Ag photodoped and undoped As-S films is sufficiently large to be used in optical image recording.
- 2- The photodoped Ag in the As-S modifies the structure of the As-S films.

3- A 3% change in the refractive index from the visible to the infra-red occurs as a result of annealing.

4- The time dependence of the photodissolution process is found to be linear.

5- The number of stages in the photodissolution process was found to depend on the magnitude of the rate, and therefore on the thickness ratio $d_{As_{40}S_{60}}/d_{Ag}$ and the temperature. In the case of fast rates, a single linear stage is found but in the case of slow rates three stages are observed.

6- The simultaneous illumination/heating procedure resulted in an improvement of the photodissolution rate by a factor of 12.

7- The kinetics results are consistent with a mechanism based on a light-induced solid state reaction between the metal and chalcogenide.

8- The SIMS measurements revealed that the Ag concentration in photodoped As-S films has a uniform depth profile.

References

1. Janai M., *Phys. Rev. Lett.*, vol. 47, p. 726, 1981.
2. Kostyshin M.T. and Minko V.I., *Fiz. Tekh. Poluprov.*, vol. 13, p. 809, 1979.
3. Lis S.A. and Lavine J.M., *Appl. Phys. Lett.*, vol. 42, p. 675, 1983.
4. Yamaguchi M., Shimizu I. and Inoue E., *J. Non-Cryst. Solids*, vol. 47, p. 341, 1982.
5. Kostyshin M.T., Kasyarum O.P. and Kudryavtsev A.A., *Ukrain. Fiz. Zh.*, vol. 29, p. 981, 1984.

6. Rennie J.H.S. and Elliot S.R., *J. Non-Cryst. Solids*, vol. 97/98, p. 1231, 1987.
7. Leung W., Cheung N. and Neureuther A.R., *Appl. Phys. Lett.*, vol. 46, p. 543, 1985.
8. Ewen P.J.S., Firth A.P., Zakery A. and Owen A.E., *J Non-Cryst Solids*, vol. 97/98, p. 1127, 1987.
9. Owen A.E., Firth A.P. and Ewen P.J.S., *Phil. Mag.*, vol. B52, p. 347, 1985.
10. Matsuda A. and Kikuchi M., *Proc. 4th Conf. on Solid State Devices (Suppl. to J. Japan Soc. of Appl. Phys. Vol.42 p.239 1973)*, Tokyo, 1972.
11. Yaji T. and Kurita S., *J. Appl. Phys.*, vol. 54, p. 647, 1983.
12. Chatani K., Shimizu I., Kokado H. and Inoue E., *Jap. J. Appl. Phys.*, vol. 16, p. 389, 1977.
13. Ewen P.J.S., Zakery A., Firth A.P. and Owen A.E., *Phil. Mag. B*, vol. 57, p. 1, 1988.
14. Zakery A., Zekak A., Ewen P.J.S., Slinger C.W. and Owen A.E., *J Non-Cryst Solids*, vol. 114, p. 109, 1989.
15. DeNeufville J.P., Moss S.C. and Ovschinsky S.R., *J. Non-Cryst. Solids*, vol. 13, p. 191, 1974.
16. Apling A.J., Leadbetter A.J. and Wright A.C., *J. Non-Cryst. Solids*, vol. 23, p. 369, 1977.
17. Leadbetter A.J., Apling A.J. and Daniel M.E., *J. Non-Cryst Solids*, vol. 21, p. 47, 1976.
18. Solin S.A. and Papatheodorou G.N., *Phys. Rev. B*, vol. 15, p. 2084, 1979.

19. DeNeufville J.P., Seguin R., Moss, S.C. and Ovshinsky S.R., *Proc. 5th Int. Conf. on Amorp. and Liquid. Semicond.*, p. 737, Garmish-Partenkirchen, Taylor and Francis, London, 1973.
20. Goldschmidt D. and Rudman P.S., *J. Non-Cryst. Solids*, vol. 22, p. 229, 1976.
21. Malinowski J. And Buroff A., *Contemp. Phys.*, vol. 19, p. 99, 1978.
22. Inoue E., Kokado H. and Shimizu I., in *Proc. 5th Int. Conf. on Solid State Devices (Suppl. to J. Japan Soc. of Appl.Phys. pp. 101 Vol. 43 1974)*, Tokyo, 1973.
23. Kasyarum O.P. and Kudryavtsev A.A., in *Proc. of the Int. Conf. on Non-Cryst. Semiconductors, Part 2*, p. 227, Uzhgorod, 1989.
24. Kolwicz K. D. and Chang M.S., *J. Electrochem. Soc. Solid State*, vol. 127, p. 135, 1980.
25. Zakery A., Ph.D. Thesis, University of Edinburgh, 1991.
26. Yamamoto Y., Itoh T., Hirose Y. and Hirose H., *J. Appl. Phys.*, vol. 47, p. 3603, 1976.
27. Goldschmidt D., Bernstein T. and Rudman P.S., *Phys. Stat. Sol. A*, vol. 41, p. 283, 1977.
28. Wagner A. and Barr D., *Proc. Electrochem. Soc.*, vol. 82, p. 281, Symp. Inorg. Resist. Syst., 1982.
29. Polasko K.J., Tsai C.C., Cagan M.R. and Pease R.F.W., *J. Vac. Sci. Technol.*, vol. B4, p. 418, 1986.
30. Elliot S.R., *J. Non-Cryst. Solids*, vol. 130, p. 85, 1991.

APPENDIX

LIST OF PUBLISHED WORKS

- 1- Zakery A., Zekak A., Ewen P.J.S., Slinger C.W. and Owen A.E., J. Non-Cryst. Solids, vol. 114, p.109, 1989.

- 2- Zakery A., Ewen P.J.S., Slinger C.W., Zekak A. and Owen A.E., J. Non-Cryst. Solids, vol. 134/138, p.1333, 1991.

- 3- Ewen P.J.S., Slinger C.W., Zakery A., Zekak A. and Owen A.E., SPIE Proc., vol. 1512, p.101, 1991.

- 4- Ewen P.J.S., Zekak A., Slinger C.W., Dale G., Pain D.A. and Owen A.E., to be published in J. Non-Cryst. Solids, 1993.